5th Proceedings of the International Students Conference "Modern Analytical Chemistry"

Prague, 21–22 September 2009

Edited by Karel Nesměrák

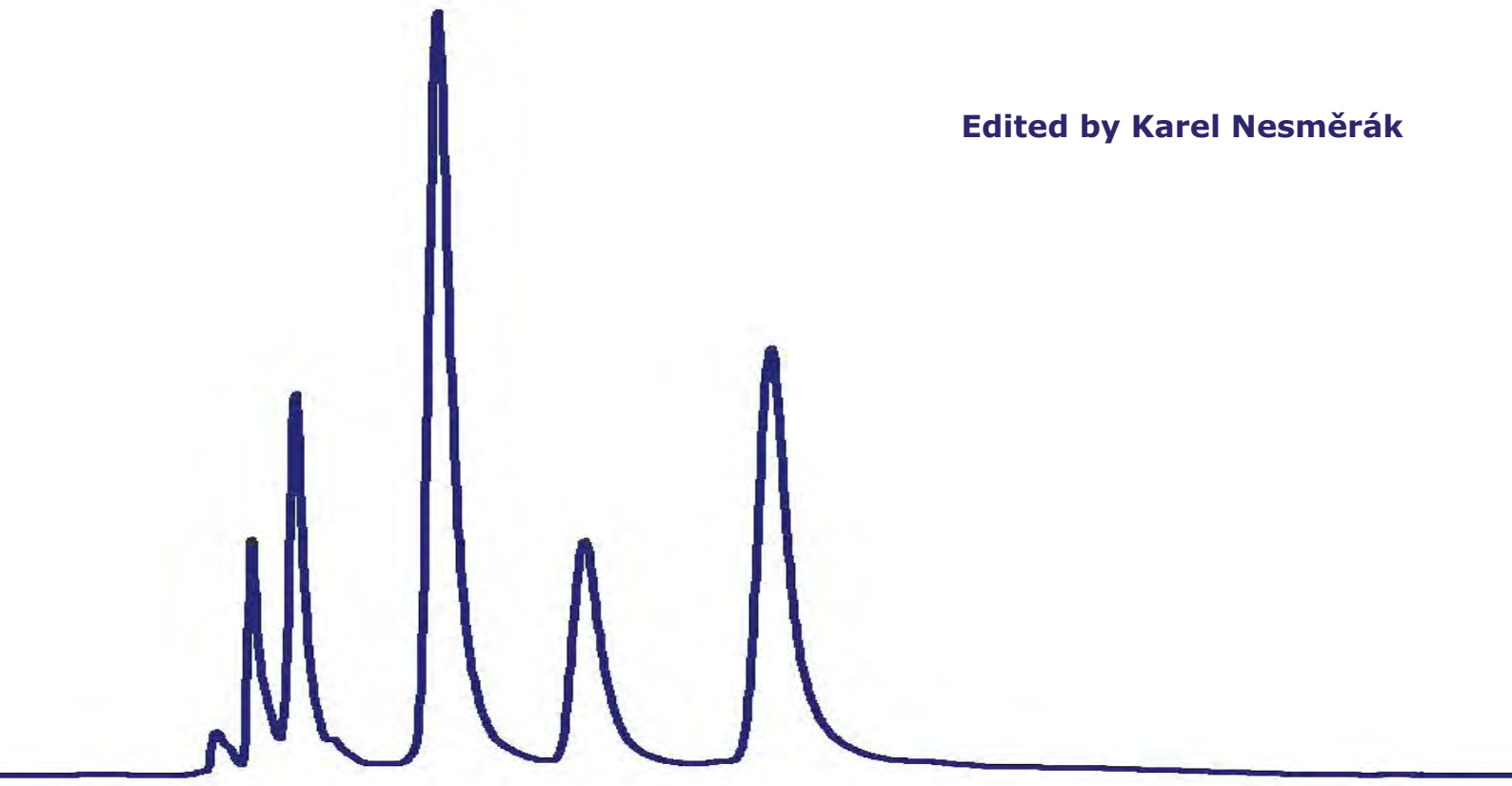

Charles University in Prague – Faculty of Science
Prague 2009

The 5th International Students Conference "Modern Analytical Chemistry" was held at the Institute of Chemistry, Faculty of Science, Charles University in Prague, on 21 and 22 September 2009.

The Proceedings publication was supported by research project MSM0021620857 of the Ministry of Education of the Czech Republic.

ISBN 978-80-86561-41-7

Preface

Dear friends and colleagues,

We are very pleased that the number of you, the participants in the already 5th International Conference of PhD Students of Analytical Chemistry in the English Language, is so large. This Conference is aimed at supporting creativity and research activities of PhD students, helping them in development of capabilities connected with the presentation of research results to the wide scientific public, providing the floor for discussions and exchange of experience, and laying the ground for long-term mutual cooperation. It should also contribute to mastering of the English language and possibly of some other languages.

The growth of the Conference is quite impressive – from nine PhD students in the beginning in 2005, to twenty eight of them in the past year and twenty four of you this year, from all the participants coming merely from our Faculty of Science of Charles University in Prague in 2005, to PhD students of the Faculty of Science of the Comenius University in Bratislava, the Slovak Technical University in Bratislava, the University of Pardubice, the Palacký University in Olomouc and the Southern Bohemian University in České Budějovice joining our students this year. The Conference presentations are added a further value, as they are included in the Proceedings with the appropriate ISBN code.

We would be unable to organize this Conference without the kind support from our sponsors. The companies Shimadzu GmbGH, Zentiva k.s., Quinta Analytica s.r.o., HPST s.r.o, and Sigma-Aldrich s.r.o. are cordially thanked, not only for their financial contributions on this occasion, but for their continuous cooperation and help in many of our activities.

We wish you successful presentation of your contributions, rich discussions with your colleagues from all the participating universities, pleasant social encounters and nice stay in Prague. We are happy that you have come.

Prof. RNDr. Věra Pacáková, CSc.
chair of the organizing committee

Sponsors

The organizing committee of 5th ISC Modern Analytical Chemistry gratefully acknowledges the generous sponsorship of following companies:

SHIMADZU
Solutions for Science
since 1875
http://www.shimadzu.cz/

ZENTIVA
http://www.zentiva.cz/

Quinta - Analytica
http://www.quinta.cz/

HPST
High Performance
Separation Technologies
http://www.hpst.cz/

SIGMA-ALDRICH
http://www.sigmaaldrich.com/

Table of Contents

Selected Endocrine Disrupting Chemicals and Their Analysis by Capillary GC-MS

Mária Andraščíková, Svetlana Hrouzková, Eva Matisová

Department of Analytical Chemistry, Faculty of Chemical and Food Technology Slovak University of Technology in Bratislava, Radlinského 9, 812 37 Bratislava, Slovak Republic, ✉ maria.andrascikova@stuba.sk

Keywords
alkylphenols
GC-MS analysis
endocrine disruptors
PAHs
pesticides
phenols
phthalates

Abstract
Endocrine disrupting chemicals are of global concern due to their widespread occurrence, persistence, bioaccumulation and potential adverse effects on human health and ecosystem functioning. The adverse effect of endocrine disruptors are relevant at low concentration level (often down to ppb and ppt region), thus screening these compounds requires more sensitive and selective instrumental analytical techniques that are able to reach sufficiently low limits of detection. The aim of the presented work was overview methods used for screning and determination compounds of different chemical classes acting as endocrine disrupting chemicals or suspected to be potential endocrine disruptors. Pesticides, polycyclic aromatic hydrocarbons, phtalates, phenols and alkylphenols were selected as endocrine disrupting chemicals of interest, the focus was given so the analysis of these compounds from various matrices and their analysis by GC-MS. The special stress to fast GC of pesticides was given.

1. Introduction

In the last decade a great deal of concern has been expressed worldwide over the increasing levels of endocrine disrupting chemicals (EDCs) found in the environment. This anxiety is caused by the adverse effects of these pollutants on the hormone systems of humans and wildlife even when present at levels under ppb [1]. Therefore, highly sensitive methods are needed to evaluate the potential risks posed by these substances.

Analytical techniques as gas chromatography combined with MS or tandem MS can reach satisfactory selectivity and sensitivity analyzing EDC in complex food matrices mainly of food and environmental origin. Especially fast GC technique satisfies the present day demands on faster and cost-effective analysis. Nowadays, fast GC can be performed on commercial gas chromatographs, which are standardly equipped with high-speed injection systems, electronic gas pressure control, rapid oven heating/cooling and fast detection [2].

2. Endocrine disrupting chemicals and their influence on endocrine system

Human endocrine system is a complex mechanism that regulates and controls intercell communication. Endocrine system releases hormons which act as chemical information agents. Hormone interaction with cell receptor and so the appeal for natural biological function as grow, reproduction and fetus development is executed [3].

The endocrine system consists of a set of glands, such as the thyroid, gonads, adrenal and pituitary glands. Hormones they produce, such as thyroxine, oestrogen, testosterone and adrenaline, help to guide the development, growth, reproduction, and behaviour of animals and human beings.

Endocrine disrupters interfere with the functioning of the endocrine system, in at least three possible ways:

1. by mimicking the action of a naturally-produced hormone, such as oestrogen or testosterone, and thereby setting off similar chemical reactions in the body;
2. by blocking the receptors in cells receiving the hormones (hormone receptors), thereby preventing the action of normal hormones; or
3. by affecting the synthesis, transport, metabolism and excretion of hormones, thus altering the concentrations of natural hormones [4].

Endocrine disrupting chemicals according to European Commision are defined as "an exogenous substance or mixture that alters function(s) of the endocrine system and consequently causes adverse health effects in an intact organism, or its progeny, or (sub)populations" [5]. Endocrine disrupting chemicals are of global concern due to their widespread occurrence, persistence, bioaccumulation and potential adverse effects on ecosystem functioning and human health. These chemicals may originate from natural processes and industrial activities. Natural hormones such as 17β-estradiol and estrone are derived from excreta of humans and livestock, and 16α-hydroxyestrone from the hepatic metabolite of the natural estrone. Man-made substances include

synthetically produced hormones, *e. g.* 17β-ethynylestradiol and industrial chemicals, *e. g.* bisphenol A, 4-nonylphenol and 4-*tert*-octylphenol associated with plastics, household products and industrial processes. In recent years, there has been increasing attention toward the potential effects of EDCs in aquatic environments on human and wildlife endocrine systems, *e. g.* the feminisation of male fish, abnormal reproductive processes and the development of testicular and prostate cancer [6].

A wide variety of substances have been classified as potential EDCs; most of these are pesticides, polycyclic aromatic hydrocarbons (PAHs), phthalates, chlorophenols, alkylphenols, polychlorinated biphenyls (PCBs), organotins, as well as other classes of compounds have also been found to be potential EDCs. Agricultural activities as well as urban and industrial effluents are the main sources of man-made EDCs in the environment and marine ecosystems such as estuaries are particularly badly affected, since most of the discharges flow into such systems. The broad range of the EDCs known and the very low EDC concentrations that occur in the environment make it necessary to devise analytical strategies that can easily screen contaminated samples.

The state-of-the-art analytical methodologies that are currently used to screen for EDCs are limited and are often based on both biological assays and chromatographic or hyphenated techniques. Besides biomonitoring environmental pollutants worldwide, relatively quick and straightforward tests can be used to detect EDCs, but these cannot be used to identify the actual EDC compounds involved and thus their potential to interact with the endocrine system. Moreover, biological tests are sometimes too specific to cover a wide range of different EDCs and they do not present enough sensitivity at the ultratrace level. Currently, high-resolution gas chromatography and liquid chromatography coupled to mass spectrometry or tandem MS (GC-MS, LC-MS, LC-MS/MS) are the standard methodologies for monitoring most of semi-volatile EDCs, due to the versatility, high selectivity and the unequivocal spectral evidence of the individual analytes it affords [7]. In this contribution we will focus on GC-MS methodology.

3. Pesticides

The extensive use of pesticides to improve agricultural productivity played an important role in the last century. These compounds have been applied for decades in preventing, repelling or mitigating the effects of pests. Important aspects of the safe use of pesticides are the occurrence and the persistence of the residues of these compounds and their metabolites in the food chain. Some of them are proved carcinogens and mutagens. Thus, regulation and environmental monitoring programmes have been adopted to control the risks to human health.

In 1999 the European commission published a list of chemicals that are presumably responsible for damaging of human health by interference with hormones [8]. This list was based on the studies of these chemicals and was divided into categories according to documentated/potential endocrinal effect. For some chemicals the production and usage was already forbidden and others are still under testing. Also pesticides are registered in this list of chemicals [9]. This list of chemicals divides compounds in to four categories according to their impact on endocrine system:

- Category 1 – endocrinal effect recorded at least on one type of animal.
- Category 2 – a record of biological activity *in vitro* leading to disruption.
- Category 3 – there is not enough evidence or no evidence data to confirm/disconfirm endocrinal effect of tested chemicals.
- Category 4 – endocrinal effect was not confirmed.

Some pesticides and alkylphenols cause to disrupt the chemical messengers system in the body. For the general population, the greatest exposure to EDCs is from food and from drinking water [10].

In GC analysis of pesticide residues, selective detectors have progressively been replaced by MS, mainly using EI and CI. Moreover, in recent years, the use of ion-trap tandem MS has allowed improvement in the selectivity and the sensitivity of GC-MS methods for analysis of pesticides in environmental samples [11]. The use of EI and NCI technique for analysis of endocrine disrupting pesticides by PTV-GC-MS was compared by Húšková *et al.* [12], and also fast GC-MS was applied to the analysis of EDCs from fruit and vegetables matrices [13, 14]. An example of chromatogram of overlapped target ions of pesticides in matrix-matched standard (apple matrix) analyzed by GC-MS in SIM mode at the concentration level of 50 ng mL^{-1} (50 μg kg^{-1}) is shown in Fig. 1. The separation of pesticides was performed on narrow-bore column CP-SIL 8 CB (15 m × 0.15 mm × × 0.15 μm) under temperature controlled condition. Electron ionization and mass spectrometric quadrupole analyzer was utilized.

Solid phase extraction was applied to the extraction of EDCs pesticides from drinking, river and coastal waters and also human plasma, SBSE was used for liquid sample with in situ derivatization, microwave assisted extraction was used for extraction pesticides from sediment samples.

Samples were analysed using GC-MS, GC-MS/MS both using either electrone ionization, negative chemical ionization or electrone capture detector.

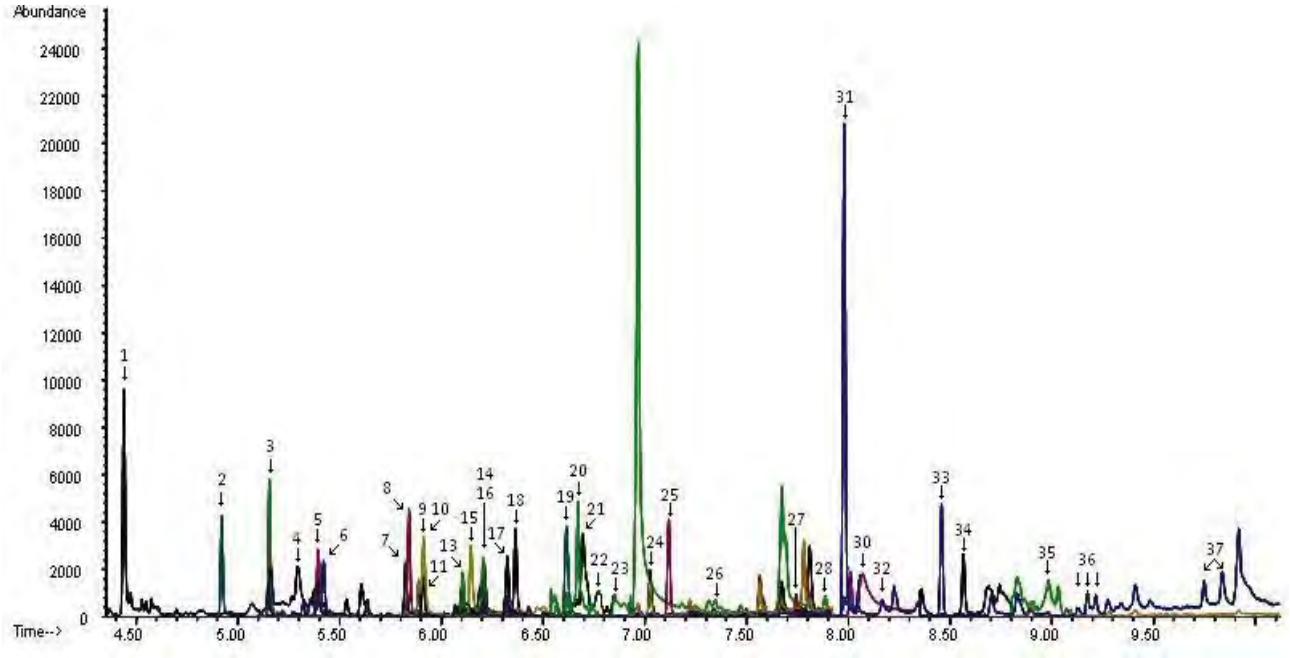

Fig. 1. Chromatogram of overlapped target ions of pesticides in matrix-matched standard (apple matrix) analyzed by GC-MS in SIM mode at the concentration level of 50 ng mL^{-1} (50 μg kg^{-1}). The peaks numbers are the following (where IS is internal standard): (1) *o*-phenylphenol, (2) trifluralin, (3) hexachlorobenzene, (4) dimethoate, (5) atrazine, (6) lindane, (7) acetochlor, (8) chlorpyrifos-methyl, (9) vinclozolin, (10) parathion-methyl, (11) metribuzin, (12) heptachlor (IS), (13) fenitrothion, (14) linuron, (15) malathion, (16) chlorpyrifos, (17) triadimefon, (18) dicofol, (19) fipronil, (20) procymidone, (21) triadimenol, (22) folpet, (23) endosulfan-α, (24) imazalil, (25) myclobutanil, (26) endosulfan-β, (27) chlordecone, (28) tebuconazole, (29) triphenylphosphate (IS), (30) iprodione, (31) bifenthrin, (32) fenoxycarb, (33) mirex, (34) fenarimol, (35) prochloraz, (36) cypermethrin, (37) deltametrin.

4. Polycyclic aromatic hydrocarbons

Polycyclic aromatic hydrocarbons (PAHs) represent an impor-tant class of hazardous organic chemicals that are ubiquitous in the environment and there are released from natural or anthropogenic sources [11].

Polycyclic aromatic hydrocarbons are known for their carcinogenic and mutagenic properties and for being responsible of background level contamination in environmental matrices. They are formed from anthropogenic (*e. g.,* emissions in the environment as a result of vehicle exhausts, asphalt pavements, unvented radiant and convective kerosene space heaters, heating appliances) and natural sources (all incomplete combustion at high temperature and pyrolytic processes involving fossil fuels such as peat, coal and petroleum). Diffuse contamination of these compounds is generalized due basically to atmospheric transport, deposition and dispersion in the environment and residues levels have been found in domestic, industrial and rain water.

Due to the low water solubility and high hydrophobicity, PAHs have a high affinity for the organic fraction of the sample and in water; they are adsorbed on particulate matter, which can be deposited as sediments. In addition, PAHs are accumulated in the fat tissue of filtrating organisms such as mussels, oysters, clams, *etc.*

Since year 2000 PAHs are legislated in the New Framework Water directive (2000/60/CE) which includes all those compounds those demonstrate carcinogenic, mutagenic, estrogenic properties or affect endorine functions of the organisms. Directives 75/440/CE and 80/778/CEE indicate maximum residue levels of 0.2 μg/L in surface water directed to produce drinking water for human consumption [15].

European Commision assigned six PAHs to the priority list as EDCs from them five (3,9-dihydroxybenz[*a*]anthracene, 3-methylcholanthrene, 5,6-cyclopento-1,2-benzanthracene, 7,12-dimethyl-1,2-benz[*a*]anthracene, benzo[*a*]pyrene) are in category 1 and one (benz[*a*]anthracene) in category 2 [9].

Liquid-liquid extraction (LLE), solid phase extraction (SPE) and solid phase microextraction (SPME), stir bar sorptive extraction (SBSE) were the most frequently used extraction methods for isolation of PAHs from liquid matrix. Soxhlet extraction, ultrasonic extraction (UE) and pressurized liquid extraction (PLE) were used for isolation of PAHs from solid matrix.

Liquid-liquid extraction, SPE and SBSE with polydimethylsiloxane were used for extraction of PAHs from environmental water samples, which was subsequently analysed by GC-MS. Other authors used

for extraction of PAHs from sediment Soxhlet and ultrasonic extraction and ultrasonic assisted extraction and from mussels pressurized liquid extraction Soxhlet and ultrasonic extraction. Ultrasonic assisted extraction was also used for extraction of PAHs from solid soil. Further, sediments were extracted using accelerated solvent extraction and cleaned with gel permeation chromatography and finally analysed with GCxGC-MS. Samples from control source combustion were prepared using microwave extraction and samples from non--control source combustion were prepared using Soxhlet extraction and analysed by multidimensional gas chromatography-mass spectrometry (MDGC-MS).

Capillary GC was first applied to analyse PAHs in the early 1960s, and its use has progressed to the point that it now comprises one of the standard methods for the determination of these compounds in environmental matrices. A flame ionization detector (FID) is normally adequate for sensitive detection, but coupling GC with MS affords greater selectivity through the application of selected ion monitoring (SIM). LC is still widely used but it is being replaced by GC-MS, mainly for identification and confirmation purposes. Electron ionisation (EI) has been successfully employed for the analysis of these compounds, but PAH isomers are almost always indistinguishable. Positive chemical ionisation (CI) with methane, a mixture of methane/argon or dimethyl ether as reagent can be used to differentiate between PAH isomers [11].

5. Phthalates

Phthalate esters (PAEs) are synthetic compounds commonly used as pesticide carries or insect repellents, in cosmetics, fragrances, lubricants and defoaming agent. However, by far they are mostly utilized as additives in plastic products. Today, the total global annual output is estimated to be around several million tons and will continue to increase. Since they are only physically bound to the plastic structure, PAEs can leach out from the plastic products during use and after disposal. As a result, PAEs have become ubiquitous contaminants and are often found in water, soil, air and biological fluids/tissues [16].

Phthalate esters have several degradation pathways and they are therefore not considered to be persistent chemicals, but a number of studies have shown their potential health impact on humans due to their carcinogenic and endocrine-disrupting effects [17].

Metabolic breakdown of phthalate esters for phthalate from microorganisms is considered to be one of the major ways of environmental degradation of these widespread pollutants. A number of studies have reported on the biodegradation of phthalates in natural water, wastewater, and soil. Many bacteria have been isolated from rivers, soil, and even marine regions for their ability to degrade phthalate aerobically or anaerobically. To date, it is well known that phthalic acid esters (PAEs) with shorter alkyl chains are very easily biodegraded, while PAEs with longer alkyl chains are poorly degraded under aerobic and anaerobic conditions; and it also confirmed that a correlation exists between increasing length of the ester side-chain and decreasing biodegradability [18].

Concern about the health implications and ubiquitous presence of phthalates has prompted an increasing demand for reliable analytical methods that allow their detection and quantification at very low levels in many different environmental, biological and food matrices [6].

Liquid-liquid extraction and SPE with various columns and discs were used for extractions of phtalates from liquid matrices, additionaly LLE was used for extractions phthalate from medically used PVC tubes, “head space” SPME with various fibers was specially used for extraction of wines, Soxhlet extraction of solid samples was widely used.

Determination of PAEs from water, sediment and biota was carried out with GC equipped with flame ionization detector (FID), PAEs from sewage sludge were determined using high resolution gas chromatography (HRGC) with quadrupole mass spectrometer in EI mode. Quantification of other water sample was carried out using GC-MS and GC-MS in combination with PTV or TD.

Degradation of *n*-butyl benzyl phthalate (BBP) by bacterium *Pseudomonas fluorescens* B-1 that was isolated from mangrove sediment by SPE extraction; degradation of di-2-etyl hexyl phthalate (DEHP) by bacterium *Bacillus subtilis* that was isolated from soil and the photocatalytic degradation with subsequent SPE discs was studied. The degradation products were identified by GC-MS.

6. Phenols

Alkylphenols are most widely known EDCs from the group of phenols. Alkylphenols have been widely used in the chemical industries as herbicides, detergents and synthetic resin products. Also, bisphenol A has been widely used as a material for the production of epoxy resins, phenol resins, polycarbonates, polyesters and lacquer coatings on food cans [19].

Alkylphenols occur in the environment mainly as degradation products from the non-ionic surfactants alkylphenol ethoxylates [20].

Liquid-liquid extraction and SPE extraction techniques for extraction of phenols from liquid samples are mostly used methods, additionaly SBSE with or without derivatization and SPE followed by derivatization with bis(3-methylsilyl)3-fluoroacetamide (BSTFA) were used. For extractions of waste, river and tap water SBSE technique combined with liquid desorption and LVI GC-MS were used. Sediment samples were extracted using microwave-assisted extraction (MAE) technique. Phenols were also analysed in paper sample by MAE followed by headspace (HS) solid phase microextraction (SPME), coupled with GC-MS. Phenols can also be detected in cereal samples by pressurized liquid extraction (PLE) with SPE preconcentration, in sediment samples by LLE and in human plasma by SPE GC-MS technique.

Analysis of phenols were carried out mainly with the use of GC-MS and GC-MS/MS techniques but liquid chromatography-electrospray ionization mass spectrometry (LC-ESI-MS) was also applied.

7. Conslusions

This contribution was focused on analysis of endocrine disrupting compounds by gas chromatography-mass spectrometry. It gives an overview of the most often used techniques for sample isolation and pre-concentration of EDCs in various matrices and their separation and detection. It can be seen that LLE, SPE, SPME and SBSE are the most common sample preparation techniques for liquid matrices and Soxhlet extaction, UE and PLE for solid matrices. The use derivatisation of some analyts before analysis, especially for analysis of phenols and other basic or acidic analyts is required. Analysis of these EDCs was done using GC-MS, GC-MS/MS, GCxGC--MS or HRGC-MS eventually in combination with LVI or TD. Example of fast GC-MS with EI method developed and validated for analysis of 35 endocrine disruptors from the group of pesticides was shown.

Acknowledgements. *This work was supported by the Slovak Research and Development Agency under the contract No. 20-000705 and the Slovak Grant Agency (project no. 1/0390/09).*

References

[1] Jobling S., Casey D., Rodgers-Gray T., Oehlmann J., Schulte-Oehlmann U., Pawlowski S., Baunbeck T., Turner A.P., Tyler C.R..: *Aquat. Toxicol.* **66** (2004), 207–222.
[2] Dömötörová M., Matisová E.: *J. Chromatogr. A* **1207** (2008), 1–16.
[3] Environment Canada: *Endocrine Disrupting Substances in Environment* (1999).
[4] http://ec.europa.eu/research/endocrine/background_system_en.html
[5] http://ec.europa.eu/environment/endocrine/definitions/endodis_en.htm
[6] Liu R., Zhou J.L., Wilding A.: *J. Chromatogr. A* **1038** (2004), 19–26.
[7] Almeida C., Serôdio P., Florêncio M. H., Nogueira J.F.M.: *Anal. Bioanal. Chem.* **387** (2007), 2569–2583.
[8] Commission of the European Communities: Community Strategy for Endocrine Disrupters (1999), 706.
[9] Commission of the European Communities: Commission staff working document on the implementation of the "Community Strategy for Endocrine Disrupters" (2007), 1635.
[10] Nagel S.C., vom Saal F.S., Thayer K.A., Dhar M.G., Boechler M., Welshons W.V.: *Environ. Health Persp.* **105** (1997), 70–76.
[11] Santos F.J., Galceran M.T.: *Trends Anal. Chem.* **21** (2002), 9–10.
[12] Húšková R., Švorc Ľ., Matisová E., Mocák J.: *J. Chromatogr. A* **1216** (2009) 4927.
[13] Hrouzková S., Horváth M., Andraščíková M., Húšková R., Matisová R. In: *13th Österreichische Chemietage, August 24–27, 2009.* Vienna University of Technology, Vienna 2009, PO 103.
[14] Húšková R., Matisová R., Hrouzková S., Švorc Ľ.: *J. Chromatogr. A* **1216** (2009) 6326.
[15] Martinez E., Gros M., Lacorte S., Barcelo D.: *J. Chromatogr. A* **1047** (2004) 181–188.
[16] Li X.H., Ma L.L., Liu X.F., Fu S., Cheng H.X., Xu X.B.: *Bull. Environ. Contam. Toxicol.* **77** (2006) 252–259.
[17] Virtanen H.E., Rajpert-De Meyts E., Main K. M., Skakkebaek N.E., Toppari J.: *Toxicol. Appl. Pharmacol.* **207** (2005) S501–S505.
[18] Quan C.S., Liu Q., Tian W.J., Kikuchi J., Fan S.D.: *Appl. Microbiol. Biotechnol.* **66** (2005) 702–710.
[19] Brossa L., Marce R.M., Borrull F., Pocurull E.: *J. Chromatogr. A* **963** (2002) 287–294.
[20] *Organic Pollutants in the Water Cycle.* T. Reemtsma, M. Jekel (Eds.). Wiley-VCH, Weinheim 2006.

Preparation of DNA-Nanostructured-Chitosan Modified Electrochemical Sensor and Its Application for Evaluation of DNA Damage by Malondialdehyde and Oxidized Edible Oils

Katarína Beníková, Adriana Ferancová, Ľudmila Sirotová, Ján Labuda

Institute of Analytical Chemistry, Faculty of Chemical and Food Technology, Slovak University of Technology in Bratislava, Radlinského 9, 812 37 Bratislava, Slovakia, ✉ *katarina.benikova@stuba.sk*

Keywords
carbon nanotubes
cyclic voltametry
DNA biosensor
DNA sensing
electrochemical impedance spectroscopy
malondialdehyde
oxidized edible oils

Abstract
Significant progress in the development and application of electrochemical sensors and biosensors based on deoxyribonucleic acid has been achieved. We report preparation of DNA biosensor and electrochemical sensor for sensing of DNA with additional modification of sensing surface by carbon nanotubes and conducting biopolymer chitosan. We report comparison of three types of carbon nanotubes, singlewall carbon nanotubes, multiwall carbon nanotubes and carboxylated singlewall carbon nanotubes and their chitosan mixtures used for surface modification. We report application of such sensor for evaluation of DNA damage by malondialdehyde in various concentrations and DNA damage by oxidized edible oils in various incubation times. Individual electrode surfaces were characterized by cyclic voltammetry and electrochemical impedance spectroscopy with $[Fe(CN)_6]^{3-}/[Fe(CN)_6]^{4-}$ indicator.

1. Introduction

Biosensors based on deoxyribonucleic acid and other nucleic acids (including aptamers and peptide nucleic acids) are today of great interest as an effective tool for nucleic acids (NA) research as well as testing of wide range of compounds that interact with NA. We distinguish strictly between the NA biosensors and NA sensing. While at the electrochemical NA biosensor, the NA has to be in an intimate contact with the electrode prior to and during the NA interaction with an analyte, the NA electrochemical sensing is of broader meaning when the interaction of any NA with an analyte or NA itself in bulk solution is detected/measured electrochemically, even after the accumulation of the product onto the electrode surface.

Screen-printed electrodes (SPCE) consisting of carbon paste working electrode, silver auxiliary and silver reference electrodes has shown good electrochemical properties and stability for preparation of DNA biosensors or for electrochemical sensing of DNA. Additional modification of carbon surface by various carbon nanotubes (CNTs) and conducting polymers or biopolymer such as chitosan (CHIT) are well known. Each type of CNTs differs in structure, mechanical and electronical properties [1], conductivity and have different disperse ability in solvents. Most types of CNTs are commercially available and thus present relatively simple mean to improve electrochemical properties of carbon surface or to enlarge the active surface of the sensor. Chitosan films are used by immobilisation of proteins, carbon structures and by electoanalysis of DNA [2]. Chitosan or CNTs-CHIT mixtures were previously used to prepare DNA biosensor and sufficient results such as great improvement in carbon surface conductivity and so the ability to evaluate DNA damage was acquired [3].

Lipid oxidation is closely connected with ageing of cells, chronic diseases such as cancer and cardiovascular disease. By lipid oxidation reactive oxygen species react with polyunsaturated fatty acid's double bonds forming lipid hydroperoxides. Studies of the interaction of hydroperoxides with DNA show that these compounds are reactive and cause cleavage of double-stranded DNA or formation of hydroperoxide-induced DNA adducts. Malondialdehyde (MDA) presents one of the most considerable secondary oxidation product, it exhibits great mutagenic and cytotoxic properties and it is used as a marker by lipid oxidation [4, 5].

The anion mixture $[Fe(CN)_6]^{3-}/[Fe(CN)_6]^{4-}$ is frequently used as a redox probe in cyclic voltammetry for its electro-chemical reversibility and up to day also in electroche-mical impedance spectroscopy (EIS). By DNA sensing it can be used as simple redox probe in the solution phase where its voltammetric signal decreases comparing to bare electrode due to electrostatic repulsion by the present negatively charged DNA backbone. Electrochemical impedance spectroscopy is a method

used to characterise properties of solutions and surfaces, it is used in analytical applications such as characterisation of electrode surfaces with immobilized proteins, detection of antigen-antibody interactions, detection of DNA hybridization. Electrochemical impedance spectra are commonly evaluated according to Nyquist diagram as a dependence between imaginary part of impedance *Z''* and relative part of impedance *Z'*. Each dot presents measurements of *Z' vs. Z''* by specific frequencies. Spectra consist of semicircle in area of high frequencies and from straight line in area of low frequencies. The semicircle describes Faradic electron transfer on electrode surface and the line describe diffusion transport of redox ions close to the electrode. Evaluation of spectra repose in searching of adequate model of equivalent circuit, Randles circuit is commonly used. It consists of double layer capacitance C_d, charge transfer resistance R_p, solution phase resistance R_s and Warburg impedance Z_w [6].

The aim of this work is to prepare suitable electrode for evaluation of DNA by modification with CNTs and CHIT. Three types of CNTs were investigated for this purpose. Individual surfaces were studied by CV and EIS of $[Fe(CN)_6]^{3-}/[Fe(CN)_6]^{4-}$ indicator.

2. Experimental

2.1. Apparatus

Voltammetric measurements were performed using the potentiostat Autolab and the software GPEs version 4.9.005 (Eco Chemie, Netherland). Electrochemical impedance spectroscopy measurements were carried out on the Autolab using FRA module, version 4.9.006. SPCE assembly with working carbon electrode (21 mm^2 geometric surface area) was obtained from Food Research Institute, Biocentrum, Modra Slovakia. KCl electrode were used as external reference electrode.

2.2. Chemicals

Multiwall carbon nanotubes (MWCNT; OD 40–60 nm, ID 5–10 nm, length 0.5–500 μm) and singlewall carbon nanotubes (SWCNT; OD 0.7–1.2 nm, length 2–20 μm) were obtained from Sigma-Aldrich Chemie (Germany) and without additional cleaning were used to prepare suspensions with sodiumdodecylsulphate (SDS) or dimethylformamide (DMF) in following ratio 2 mg MWCNT resp. SWCNT to 1 mL SDS (DMF), 30 min. of sonification was used for suspension homogenisation. SWCNT-COOH (OD 4–5 nm, length 0.5–1.5 μm) were obtained from Sigma-Aldrich Chemie (Germany) and without additional cleaning was used to prepare suspension using deionised water as disperse solvent in ratio 2 mg SWCNT-COOH to 1 mL H_2O. Chitosan (M = 600 000 g mol^{-1}, degree of deacetylation 85%) was obtained from Fluka. Its 0.5% (w/w) solution was prepared in 1% (v/v) acetic acid (Lachema, Czech Republic) and filtered through a single paper strip. The final CHIT solution was of pH = 5.0 [3]. Calf thymus double stranded DNA (dsDNA) was obtained from Merck. Its stock solution (5 mg mL^{-1}) was prepared in 1×10^{-2} M Tris-HCl and 1×10^{-3} M EDTA solution of pH = 8.0 and stored at 2 °C. Malondialdehyde was prepared by the hydrolysis of tetraethoxypropane in 0.1 M HCl at 40 °C for 40 min and subsequent neutralization. Edible oils (Oliol, Amphor, Heliol, Forte and olive oil) were purchased from a local store. Samples of oxidized oils were prepared as follows: oil was resuspended in 0.1 M phosphate buffer (PBS, pH = 7.0) and oxidized at 85 °C during 24 hours. Mixture of $[Fe(CN)_6]^{3-}/[Fe(CN)_6]^{4-}$ with concentration of 1×10^{-2} M was used as electrochemical DNA indicator Phosphate buffer (0.1 M) of pH = 7.0 was used as the supporting electrolyte. Other chemicals used were of analytical grade purity.

2.3. Isolation of DNA samples after its interaction with malondialdehyde and oxidized oils

DNA solution (0.1 mg mL^{-1}) was incubated with MDA of different concentration (1×10^{-3} M, 1×10^{-4} M, 1×10^{-5} M, 1×10^{-6} M) in 0.1 M phosphate buffer (pH = = 7.0) at 37 °C during 72 h. After incubation, DNA was isolated using precipitation with ethanol. Briefly, ethanol was added to sample of DNA (2.5 times of sample volume) after the addition of 3 M sodium acetate (pH = = 5.5, tenth of sample volume). The mixture was left at – 18 °C for 2 h and subsequently washed with 70 % ethanol. DNA extracted was dried at room temperature, resolved in ultra-pure water and stored at – 18 °C. DNA (0.1 mg mL^{-1}) was incubated with oxidized oil (0.01 g mL^{-1}) during 24 h and 48 h at 37 °C was isolated from reaction mixture by using the precipitation with ethanol (the procedure described above) [7].

2.4. Preparation of modified electrodes

The CNTs-CHIT mixtures were prepared in the 1 : 1 ratio (v/v) followed by sonification. The 5 μL of mixture was put onto the electrode surface and let to evaporate to dryness. Then 5 μL of DNA sample was added and let to evaporate to dryness.

2.5. Cyclic voltammetry and electrochemical impedance spectroscopy of $[Fe(CN)_6]^{3-}/[Fe(CN)_6]^{4-}$

The cyclic voltammograms of 1×10^{-3} M $[Fe(CN)_6]^{3-}$ and $[Fe(CN)_6]^{4-}$ in 0.1 M phosphate buffer were recorded from –650 mV to +700 mV using a scan rate of 50 mV s^{-1} and evaluated against the CV record obtained in blank phosphate buffer. Electrochemical impedance spectroscopy measurements were carried out in presence of 1×10^{-3} M $[Fe(CN)_6]^{3-}$ and $[Fe(CN)_6]^{4-}$ in 0.1 M phosphate buffer (pH = 7.0) at ambient temperature and at the potential of 0 V within the frequency range of 0.1–10^4 Hz and amplitude of 10 mV.

3. Results and discussion

3.1. Carbon nanotubes and carbon nanotubes-chitosan mixture measurement for preparation of DNA sensor

Cyclic voltammograms of 1×10^{-3} M $[Fe(CN)_6]^{3-}$ and $[Fe(CN)_6]^{4-}$ redox probe are shown in Fig. 1 aquired on SPCE modified with MWCNT, SWCNT, SWCNT--COOH. According to increased current signal of $[Fe(CN)_6]^{3-}/[Fe(CN)_6]^{4-}$against unmodified SPCE current signal it can be seen that CNTs increase the electrode surface effectively. Reversibility of electrochemical process has also improved what can be seen from decrease of peak and antipeak potencial separation (ΔE_p). Current signal values as well as peak potencial separation values of all three types of CNTs are approximately the same. Fig. 2 shows impedance spectra, as it can be seen SPCE again shows faradic transport in high frequency values and diffusion transport in low frequency values. Modification of SPCE by CNTs caused loss of semicircle in spectrum and so the whole transport of electrones was due to diffusion. Conductivity of SWCNT/SPCE, SWCNT-COOH/SPCE and MWCNT/SPCE was alike. Advantage of SWCNT--COOH lies in its ability to disperse simply in aqueous solutions, what is very usefull in preparation of DNA biosensors. This way use of organic solvents that could damaged DNA can be avoided. SWCNT-COOH created homogenic and stabile suspension with deionized water without sonification.

Consequently with this suspension carbon surface of SPCE could be covered more uniformly than by using other two CNTs. Considering this adventages SWCNT--COOH was used in additional measurements.

Fig. 3 shows cyclic voltamograms aquired on SPCE, CHIT-SWCNT-COOH/SPCE a DNA/CHIT-SWCNT--COOH/SPCE. The ΔE_p, decrease from 454 mV (SPCE) to 152 mV after CHIT-SWCNT-COOH modification.

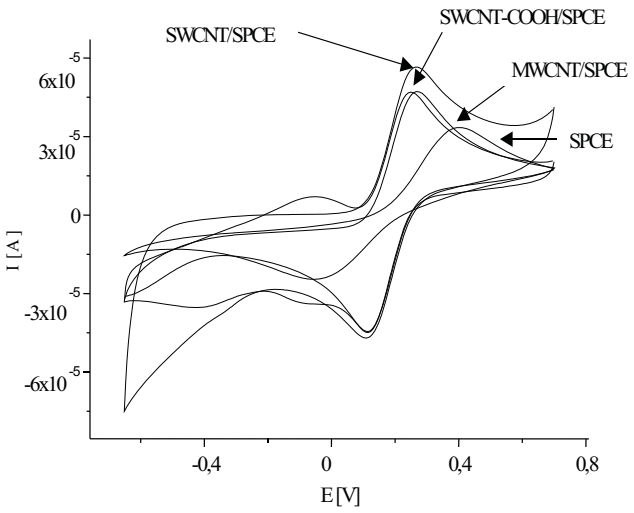

Fig. 1. Cyclic voltammograms of 1×10–3 M $[Fe(CN)_6]^{3-}$ and $[Fe(CN)_6]^{4-}$ measured on screen-printed electrode with carbon nanotubes modification in 0.1 M phosphate buffer, scan rate 50 mV s^{-1}.

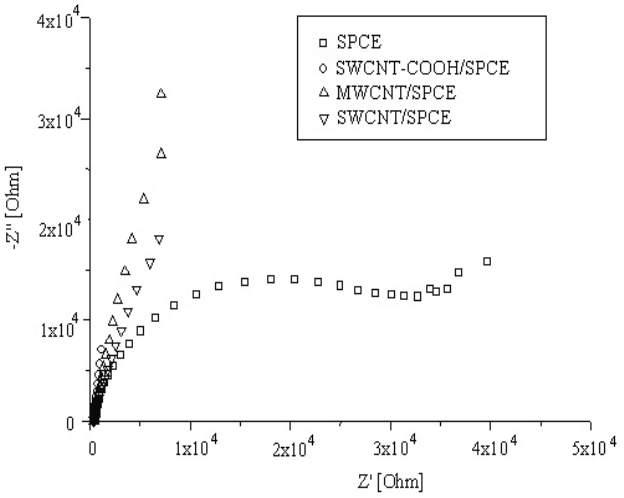

Fig. 2. Electrochemical impedance spectra of 1×10–3 M $[Fe(CN)_6]^{3-}$ and $[Fe(CN)_6]^{4-}$ in 0.1 M phosphate buffer, amplitude 10 mV.

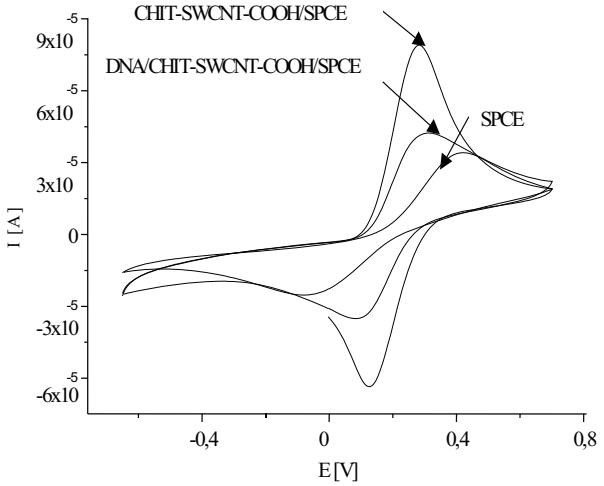

Fig. 3. Cyclic voltammograms of 1×10–3 M $[Fe(CN)_6]^{3-}$ and $[Fe(CN)_6]^{4-}$ measured on modified electrodes in 0.1 M phosphate buffer, scan rate 50 mV s^{-1}.

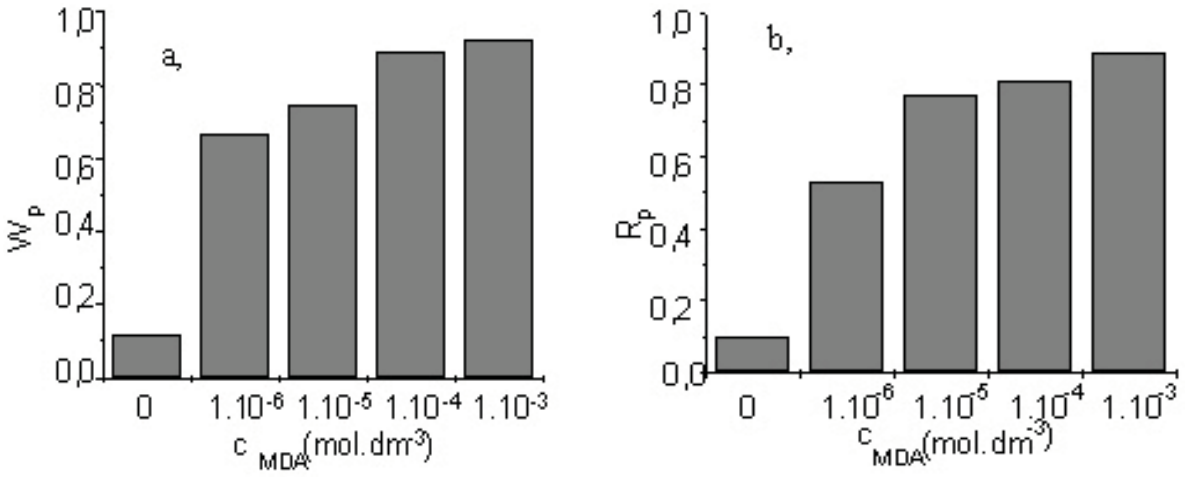

Fig. 4. Dependance (a) relative Warburg impedance signal, and (b) relative charge transfer signal, on malondialdehyde concentration.

Additional modification with dsDNA caused increase in ΔE_p value to 188 mV. Differences in current values were more significant. Oxidation peak current increased three times by SWCNT-COOH modification and then 52% decrease was observed due to additional modification with dsDNA. This difference creates sufficient space for evaluation of DNA damage. DNA/CHIT-SWCNT-COOH/SPCE biosensor or CHIT-SWCNT-COOH/-SPCE sensor can be used for sensing and evaluating of DNA damage.

3.2. Evaluation of DNA damage by malondialdehyde and oxidized edible oils

Cleavage solution producing free radicals according to Fenton reaction was used for model damage of DNA. It consists of H_2O_2, $CuSO_4$ and ascorbic acid. DNA/CHIT--SWCNT-COOH/SPCE was incubated in cleavage solution for 10 min. Cyclic voltamograms as well as EIS of $[Fe(CN)_6]^{3-}/[Fe(CN)_6]^{4-}$ redox probe were measured before and after biosensor incubation in cleavage solution. Measured values were compared. For evaluation of DNA damage with DNA biosensor relative signal (S_{rel}) was used. It helped to eliminate difference between electrodes, effect of non uniform modification and it evaluated DNA layer changes only. The equation

$$S_{rel} = \frac{S_1 - S}{S_0 - S} \qquad (1)$$

was used to calculate relative signal, where S_0 and S_1 were values measured before and after DNA damage (incubation in cleavage solution) and S was value measured with SPCE without DNA layer. Current signals are most common valued but ΔE_p values, charge transfer Q values (acquired from CV peak integration), charge transfer resistance R_p (from impedance spectra) or Warburg impedance W_p (if strong diffusion element is present in spectra) can be evaluated too. In our case shapes of CV peaks were different and so charge transfer seemed to be the most efficient for evaluation. The 63% damage of surface bound DNA was acquired using cleavage solution. This value is relative and shows rate of DNA damage. Similar results were acquired using EIS method, in this case Warburg impedance values were evaluated. By DNA sensing 5 μL of predamaged DNA was placed onto CHIT-SWCNT-COOH/SPCE and let to evaporate to dryness. DNA damage was evaluated as relative signal. Fig.4a shows column diagram dependence of Q_{relat} to MDA concentration in which DNA was incubated. With increasing MDA concentration increase in DNA damage and increase in relative signal can be seen. It is caused by increasing damage in DNA layer and so the accessibility of electrode surface for $[Fe(CN)_6]^{3-}/[Fe(CN)_6]^{4-}$ electrochemical marker is enabled. Similar results were acquired using EIS. Warburg impedance (Fig. 4b) that increase with increasing DNA damage, because of the increasing of marker diffusion in porous layer of modificator and more simple charge transfer, was evaluated.

Column diagram dependance of relative signal (Q and W) on oil type in which DNA was incubated is shown in Fig. 5. Fig. 5a shows 24 h incubation and Fig. 5b shows 48 h incubation time. It can be seen that longer time of incubation caused bigger DNA damage, what led to increase of relative signal in both cases. Although results acquired by both methods are not similar they are same for all oils and it can be seen that Amphor and Heliol caused the biggest DNA damage, probably because highest amount of free radicals is created by oxidation in these two edible oils.

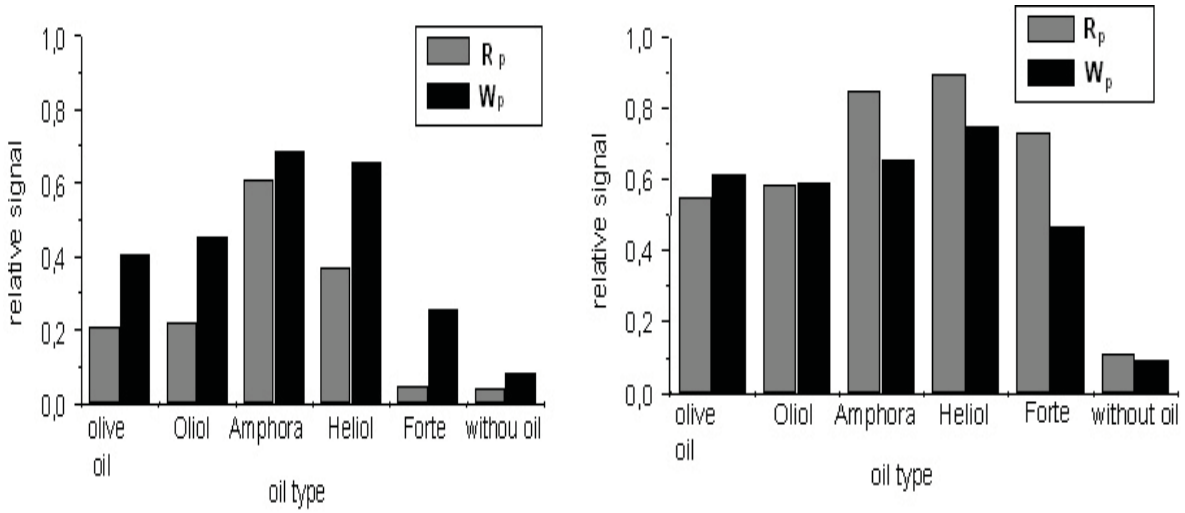

Fig. 5. Dependence of R_p a W_p on DNA damage incubated (a) for 24 hours, or (b) 48 hours in oxidized edible oils.

4. Conclusions

Chitosan-carboxylated singlewall carbon nanotubes/-screen-printed electrodes sensor for sensing of DNA damage was created. DNA/CHIT-SWCNT-COOH/-SPCE biosensor was created. Increase in the DNA damage by increasing malondialdehyde concentration and time of DNA incubation in oxidized edible oils was found.

Acknowledgement. *This work was supported by the Scientific Grant Agency VEGA (Project No. 1/0852/08)*

References

[1] Rubianes M.B., Rivas G.A.: *Electochim. Commun.* **5** (2003), 689.
[2] Rassaei L., Sillanpää M., Marken F.: *Electrochim. Acta.* **53** (2008), 5732.
[3] Ziyatdinova G., Galandova J., Labuda J.: *Int. J. Electrochem. Sci.* **3** (2008), 223–235.
[4] Suttnar J., Cermak J., Dyr E.: *Anal. Biochem.* **249** (1997), 20.
[5] Yeo H.C., Helbock H.J., Chyn D.W., Ames B.N.: *Anal. Biochem.* **220** (1994), 391.
[6] Zhang W., Yang T., Huang D.M., Jiao K.: *Chin. Chem. Letters* **19** (2008), 589.
[7] Ferancova A., Benikova K., Galandova J., Sirotova L., Labuda J.: *Acta Chimica Slovaca* **1** (2008), 58–71.

HPLC of Aminonitrophenols Using Electrochemical Detection on Boron-Doped Diamond Electrode

Hana Dejmková, Jiří Zima, Jiří Barek

UNESCO Laboratory of Environmental Electrochemistry, Department of Analytical Chemistry, Faculty of Science, Charles University in Prague, Hlavova 2030, 128 43 Prague 2, Czech Republic, ✉ *hdejmkova@natur.cuni.cz*

Abstract

The work is linked to the previous measurements and concerns the applicability of boron-doped diamond electrode (BDDE) for an amperometric detection in HPLC and the comparison with both amperometric detection on carbon paste electrode and UV spectrophotometric detection. The conditions of determination were as follows: Gemini 3μm C18 110A, 150 × 4.6 mm column, 0.01 M phosphate buffer pH = 9:methanol = 3:1 (v/v) mobile phase, spectrophotometric detection at the wavelength λ = 216 nm, detection potential +0.4 V when using CPE and +0.8 V when using BDDE. Stability of the BDDE response was proven. The results show similar performance of both electrodes concerning the linearity of calibration dependences and reached limits of quantification.

Keywords

aminonitrophenol
amperometric detection
boron-doped diamond electrode
carbon paste electrode
HPLC-ED

1. Introduction

Aminonitrophenols used to be employed as ingredients to hair dyes, particularly for obtaining light and red tones. However, these substances are suspected mutagens and carcinogens [1–3], they are also proven or suspected sensitizers, causing skin dermatitis [4] and their presence in cosmetics is now banned. They can be easily oxidized, which offers to employ electrochemical methods for their analysis.

Boron-doped diamond (BDD) is nowadays an expanding electrode material for its exceptional properties: wide potential window, low and stable background current, both mechanical and chemical robustness and resulting resistance to passivation [5–7]. Applications of BDDE for detection in flow systems are also described. Wide range of analytes is covered, including derivatives of phenol [8], antibiotics [9] and aromatic amines [10]. Obtained results are usually better in comparison to glassy carbon electrode.

Some of the favourable properties of diamond electrodes are being ascribed to carbon paste electrodes (CPE) as well, namely the broad potential window and the low background current [11]. Carbon pastes based on glassy carbon spherical microparticles are compatible with high contents of organic modifiers in mobile phase [12] and therefore, it can be used in HPLC as well.

The aim of this work was to compare the properties of CPE and BDDE when used as working electrodes for amperometric detection of 2-amino-3-nitrophenol, 2-amino-4-nitrophenol, 2-amino-5-nitrophenol, 4-amino-2-nitrophenol and 4-amino-3-nitrophenol.

2. Experimental

2.1. Chemicals

Studied substances were 2-amino-3-nitrophenol (2A3NP, CASN [603-85-0]), 2-amino-4-nitro-phenol (2A4NP, CASN [99-57-0]), 2-amino-5-nitrophenol (2A5NP, CASN [121-88-0]), 4-amino-2-nitrophenol (4A2NP, CASN [119-34-6]), 4-amino-3-nitrophenol (4A3NP, CASN [610-81-1]), all purchased from Sigma-Aldrich. The stock solutions (c = 1×10^{-3} M) were prepared by dissolving the exact amount of the substances in methanol and were kept at laboratory temperature. It was observed spectrophotometricaly, that the solutions are stable for at least three months.

Solution of phosphate buffer was prepared from 0.01 M sodium dihydrogenphosphate. Its pH was adjusted to the desired value by 0.2 M sodium hydroxide (all Lachema Brno, Czech Republic). Other used chemicals were methanol (for HPLC, Merck, Germany) and deionized water (Millipore).

2.2. Apparatus

An HPLC system consisted of degasser, high-pressure pump Beta 10, injector valve with 20 μL loop, Gemini 3μm C18 110A, 150 × 4.6 mm column (Phenomenex, USA) with chemically bonded C18 phase, UV/VIS detector Saphire 800 (all Ecom, Czech Republic) and amperometric detector ADLC 2 (Laboratorní přístroje, Czech Republic) connected in series. The HPLC system was controlled via Clarity 2.3 software (DataApex,

Czech Republic) working under Windows XP. The three--electrode wall-jet system was used for electrochemical detection with an Ag/AgCl (3 M KCl) reference electrode, a platinum wire auxiliary electrode and a boron-doped diamond working electrode (Adamant Technologies, Switzerland) adjusted against the outlet capillary.

The pH measurements were performed with the combined glass electrode using 3510 pH Meter (Jenway, UK).

2.3. Procedures

Samples for injection were prepared by exact dilution of the stock solutions to contain the required concentration of the analyte in 50% methanol (v/v in water). The detection wavelength of 216 nm for the spectrophotometric detection was selected from UV spectra of the analytes. Mobile phase flow rate of 1 mL min^{-1} was used throughout the measurements.

Calibration dependences were evaluated by the least squares linear regression method. The quantification limits were calculated as the concentration of the analyte which gave the signal ten times the background noise ($S/N = 10$).

3. Results and discussion

The optimal separation conditions were based on previous work [13] and adapted. An RP-HPLC column Gemini 3µm C18 110A, 150 × 4.6 mm with stability in a wide pH range and the mobile phase consisting of phosphate buffer pH = 9 and methanol in proportion of 3:1 (v/v) was employed. Overall analysis time was 7 min, with resolution exceeding value 2.0 when using UV spectrophotometric detection.

The behaviour of BDD electrode is highly dependent on the state of the surface carbon atoms. Strong electrochemical oxidation or reduction can change the termination groups and enhance the accessibility of the surface for the analyte. In the same time, electrochemical cleaning is the most common way of removing possible passivating layer. The procedure successfully employed for the determination of the analytes was used both for cleaning and activation [14]. It consisted of applying the potential of +3.0 V for a period of 20 s, followed by applying the potential of –3.0 V for 20 s in 1 M nitric acid. To make sure that the electrode response is stable, the mixture of analytes containing 1×10^{-4} M of each compound was injected for twenty times in the periodes of five minutes and the response of the electrode was measured. Working potential of the electrode was +0.8 V. Relative standard deviations of the results vary in the range from 2% to 8% when using spectrophotometric detection and from 3% to 9% when using amperometric detection. Thus, the electrode signal is considered stable and the activation was further repeated once a day.

Hydrodynamic voltammograms were measured in anodic potential range, taking advantage of good oxidizability of the analytes (Fig. 1). Besides the differences in peak heights, caused by the larger area of the BDDE, we can also note the potential shift of the waves. The optimal potential for the detection using CPE is +0.4 V, on the other hand, working potential of +0.8 V was chosen for BDDE. Nevertheless, the noise is not increasing markedly and the higher potential is compensated by wider potential window, allowing to measure above the potential of +1.2 V.

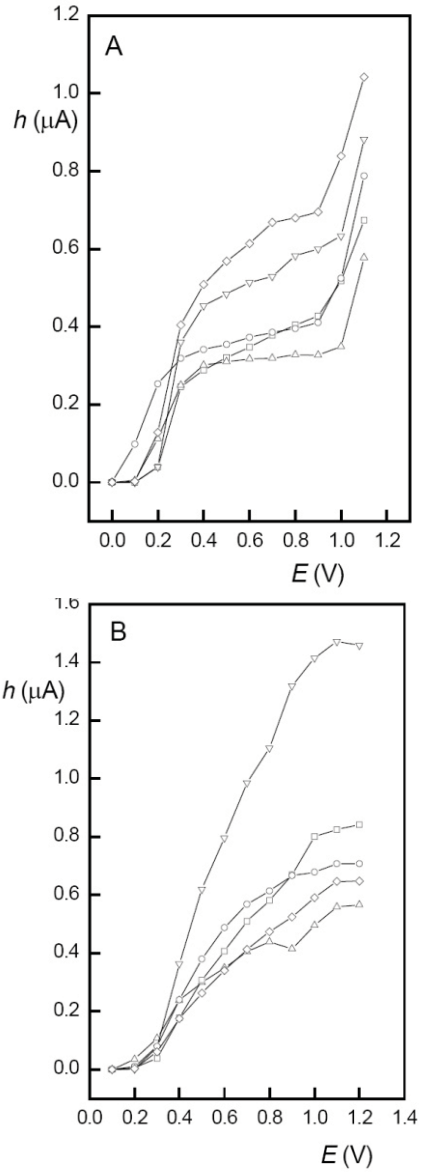

Fig. 1. Hydrodynamic voltammograms of 2A3NP (◇), 2A4NP (□), 2A5NP (▽), 4A2NP (△) and 4A3NP (○) obtained using CPE (A) and BDDE (B) as the working electrode. Gemini 3µm C18 110A, 150 × 4.6 mm column, 0.01 M phosphate buffer pH = 9:methanol = = 3:1 (v/v) mobile phase, injected 20 µL of a solution with $c = 1\times10^{-4}$ M of each analyte. (A) adopted from [13].

Table 1. Correlation coefficients of calibration dependences (R) and limits of quantification (LOQ) of the tested analytes, obtained by spectrophotometric detection and amperometric detection using CPE and BDDE.

Analyte	Detection					
	Spectrophotometric		Amperometric, CPE[a]		Amperometric, BDDE	
	R	LOQ (10^8 M)	R	LOQ (10^8 M)	R	LOQ (10^8 M)
2A3NP	0.9984	5.7	0.9977	3.7	0.9976	4.7
2A4NP	0.9993	3.0	0.9922	4.7	0.9983	2.7
2A5NP	0.9993	3.0	0.9990	4.0	0.9986	1.8
4A2NP	0.9968	3.5	0.9971	2.9	0.9957	2.7
4A3NP	0.9973	5.0	0.9944	2.9	0.9980	3.3

[a] Adopted from [13]

To evaluate the linearity and sensitivity of the electrodes, calibration dependences were measured in the range from 1×10^{-5} to 4×10^{-8} M. Table 1 summarizes some of the results, including the data from the earlier work with CPE [13]. Linearity of the calibration dependences increases in the sequence: amperometric on CPE – amperometric on BDDE – spectrophotometric detection. Limits of quantification increase in reversed order. However, the differences between the detection methods are surprisingly small. Similar signal to noise ratio as well as peak shape and height can also be observed in Fig. 2. Other aspects can thus be considered, particularly low selectivity of spectrophotometric detection and low price together with more demanding preparation of CPE in comparison with BDDE.

4. Conclusions

Optimal conditions were found for electrochemical detection of five isomers of aminonitrophenol on boron-doped diamond electrode. Regeneration of the electrode consisted of oxidation and reduction step, *e. g.* application of potential + 3 V for 20 s and – 3 V for 20 s in 1 M nitric acid. Working potential of the electrode was + 0.8 V in mobile phase consisting of phosphate buffer pH = 9 and methanol in ratio of 3:1 (v/v). Performance of CPE and BDDE is similar with respect to linearity and sensitivity, reached limits of quantification for BDDE are between 2.7×10^{-8} and 4.7×10^{-8} M.

Acknowledgements. *Financial support of the Czech Ministry of Education, Youth and Sports (projects No. MSM 0021620857, RP14/63 and LC06035) is gratefully acknowledged.*

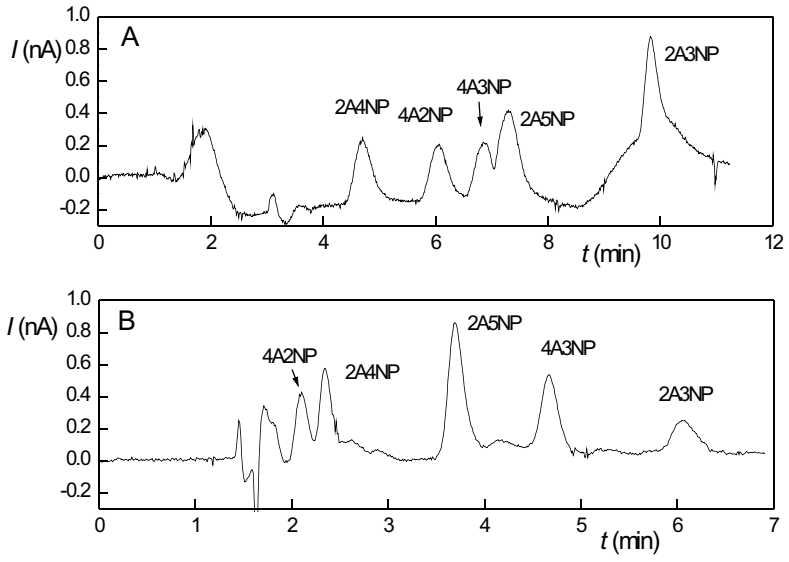

Fig. 2. Chromatograms of equimolar mixture of 2A3NP, 2A4NP, 2A5NP, 4A2NP and 4A3NP of $c = 1\times10^{-7}$ M obtained using CPE (A) and BDDE (B) as working electrode for amperometric detection. Gemini 3μm C18 110A, 150 × 4.6 mm column, 0.01 M phosphate buffer pH = 9:methanol = 3:1 (v/v) mobile phase, E_{det} = +0.8 V). (A) adopted from [13].

References

[1] Shahin M.M., Bugaut A., Kalopissis G.: *Chem. Mutagens* **8** (1983), 151–181.

[2] *IARC Monographs on the Evaluation of the Carcinogenic Risks to Humans, Vol 57.* IARC, Lyon 1993, p. 167.

[3] *National Toxicology Program,* http://ntp.niehs.nih.gov-/ntp/htdocs/LT_rpts/tr339.pdf (28.1.2009)

[4] Sorsted H., Basketter D.A., Johansen E.D., Patlewicz G.Y.: *Contact Dermatitis* **51** (2004), 241–254.

[5] Compton R. G., Foord J. S., Makren F.: *Electroanal.* **15** (2003), 1349– 1363.

[6] Pleskov Y. V.: *Russ. J. Electrochem.* **38** (2002), 1275–1291.

[7] Kraft A.: *Int. J Electrochem. Sci.* **2** (2007), 355–385.

[8] Codognotoa L., Zuinb V.G., de Souzaa D., Yariwakeb J.H., Machadoa S.A.S., Avacaa L.A.: *Microchem. J.* **77** (2004), 177–184.

[9] Charoenraks T., Chuanuwatanakul S., Honda K., Yamaguchi Y., Chailapakul O.: *Analyt. Sci.* **21** (2005), 241–245.

[10] Pecková K., Jandová K., Maixnerová L., Swain G. M., Barek J.: *Electroanal.* **21** (2009), 316–324.

[11] Švancara I., Vytřas K., Barek J., Zima J.: *Crit. Rew. Anal. Chem.* **31** (2001), 311–345.

[12] Barek J., Muck A., Wang J., Zima J.: *Sensors* **4** (2004), 47–57.

[13] Dejmková H., Zima J., Barek J.: HPLC-ED Determination of Aminonitrophenols. In: *Proceedings of 3rd International Student Conference of Modern Analytical Chemistry.* Červený V. (ed.). Praha, Czech Chemical Society 2007, p. 40–48.

[14] Dejmková H., Fischer J., Zima J., Barek J.: Voltammetric determination of aminonitrophenols using boron-doped diamod electrode. In: *Proceedings of 7th Meeting of Serbian Chemical Society.* Markovic R., Dunjic B., Dekanski A. (edits.). Beograd, Serbian Chemical Society 2009, p. 15–17.

Voltametric Determination of 4-Nitrophenol and 5-Nitrobenzimidazole on Different Amalgam Electrodes

Dana Deýlová[a], Jiří Barek[a], Bogdan Yosypchuk[b]

[a] *UNESCO Laboratory of Environmental Electrochemistry, Department of Analytical Chemistry, Faculty of Science, Charles University in Prague, Hlavova 2030, 128 43 Prague 2, Czech Republic,* ✉ *d.deylova@centrum.cz*
[b] *J. Heyrovský Institute of Physical Chemistry, v.v.i., Academy of Sciences of the Czech Republic, Dolejškova 3, 182 23 Prague 8, Czech Republic*

Keywords
differential pulse voltammetry
4-nitrophenol
5-nitrobenzimidazole
solid amalgam electrode

Abstract
Optimal conditions were found for the determination of 4-nitrophenol and 5-nitrobenzimidazole by direct current voltammetry and differential pulse voltammetry in the concentration range 1×10^{-4} to 1×10^{-7} M at a polished silver solid amalgam electrode, meniscus-modified silver solid amalgam electrode and mercury film modified silver solid amalgam electrode.

1. Introduction

Nitrophenols coming from pesticide degradation products, car exhausts, and industrial wastes are listed as priority pollutants by the US Environmental Protection Agency [1, 2]. Pesticides based on simple nitrophenols are generally not approved today but some of them are still used as growth stimulators in agriculture [3]. They are potential carcinogens, teratogens, and mutagens [4]. Because of their toxicity and vast scale distribution in the environment, their determinations have become one of the important goals of environmental analysis.

5-nitrobenzimidazole (5-NBIA) belongs to the group of genotoxic nitrated heterocyclic aromatic compounds. It can damage natural biological functions of living organisms. The occurrence of 5-NBIA in environment is expected in connection with fossil fuels combustion [5]. 5-nitrobenzimidazole was polarographically determined as a part of photographic processing solutions [6] and its properties have been studied in the area of metal corrosion protection [7]. 5-nitrobenzimidazole is proven carcinogen and mutagen [8].

Table 1. Experimentally found optimal values of regeneration potentials of p-AgSAE, m-AgSAE and MF-AgSAE in Britton-Robinson buffer.

Electrode		pH = 6	pH = 8
p-AgSAE	$E_{reg,\,1}$ (mV)	0	–100
	$E_{reg,\,2}$ (mV)	–1200	–600
m-AgSAE	$E_{reg,\,1}$ (mV)	–100	–100
	$E_{reg,\,2}$ (mV)	–900	–600
mf-AgSAE	$E_{reg,\,1}$ (mV)	–100	–100
	$E_{reg,\,2}$ (mV)	–600	–600

Both substances were determined using practically non-toxic polished silver solid amalgam electrod (p-AgSAE), meniscus-modified silver solid amalgam electrode (m-AgSAE) and mercury film modified silver solid amalgan electrode (MF-AgSAE). All electrodes have a good mechanical stability, simple handling and regeneration including an electrochemical pre-treatment of their surface.

2. Data

5-nitrobenzimidazole and 4-nitrophenol (4-NP) were determined by diferential pulse voltametry (DPV) a DC voltametry (DCV) at three above mentioned electrodes in Britton-Robinson buffer at pH = 8 (5-NBIA) and pH = 6 (4-NP).

Mercury film at a large area p-AgSAE was deposited in a special vessel with mercury bottom containing mercuric chloride solution. Into this solution we placed p-AgSAE and deposited mercury film for required period of time.

Before starting the work, as well as in the case of electrode passivation, the electrochemical activation of electrodes was carried out in 0.2 M KCl at –2200 mV under stirring of the solution for 300 seconds followed by rinsing with distilled water.

The regeneration was carried out by periodical swit/-ching every 0.1 s between potentials 100 mV more negative than the potential of amalgam dissolution ($E_{reg,\,1}$) and 100 mV more positive than the potential of hydrogen evolution ($E_{reg,\,2}$) in the given base electrolyte, for optimal values see Table I. Regeneration always ended at more negative potential.

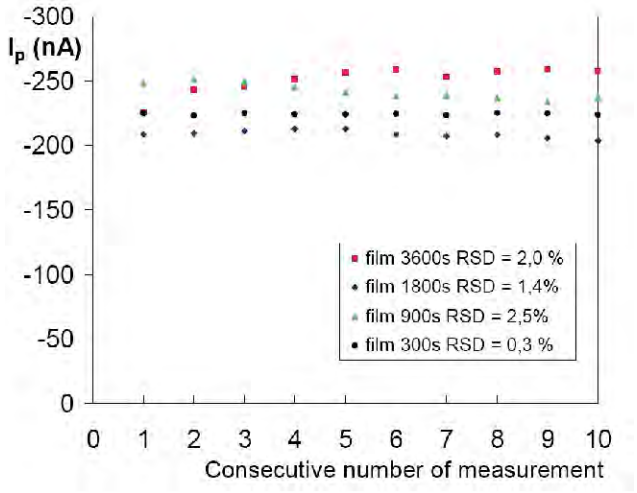

Fig. 1. Repeatability of diferential pulse voltametry determination of 4-nitrophenol (c = 1×10^{-5} M) in Britton-Robinson buffer pH = 6 on MF-AgSAE with different deposition times.

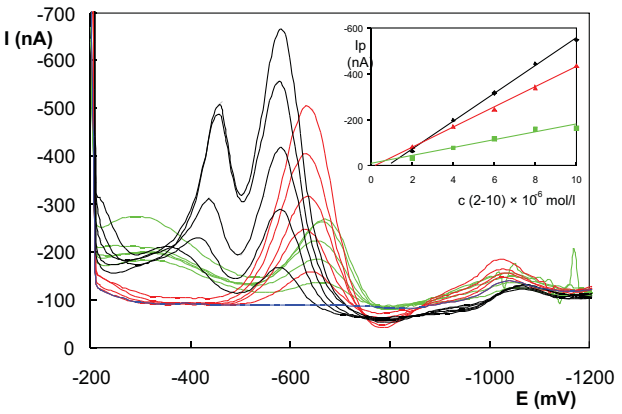

Fig. 2. Calibration curves of diferential pulse voltametry determination of 5-nitrobenzimidazole (c = (0–10)×10^{-6} M) in Britton-Robinson buffer pH = 8 on MF-AgSAE (3600), p-AgSAE, and m-AgSAE electrode.

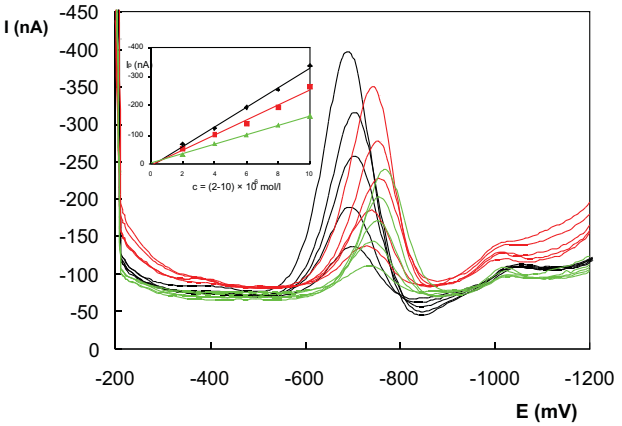

Fig. 3. Calibration curves of diferential pulse voltametry determination of 4-nitrophenol (c = (2–10)×10^{-6} M) in Britton--Robinson buffer pH = 6 on MF-AgSAE (3600), p-AgSAE, and m-AgSAE electrode.

Repeatability of determination of 4-NF on MF-AgSAE was very good on film deposited for 300 s to 3600 s (Fig. 1). Optimal regeneration potentials are listed in Table 1.

Linear calibration curves were obtained in the concentration range 2-1000 μmol/l (Figs. 2, 3). Their parameters for the lowest concentration range are summarized in Table 2. The determination limit was calculated as ten times the standard deviation for ten determinations of the analyte at a concentration corresponding to the lowest point of the appropriate calibration graph. It can be seen than MF-AgSAE gives the highest peak (slopes of calibration curves). However the repeatability is worse then for p-AgSAE.

Table 2. Parameters of the calibration straight lines for the determination of 4-nitrophenol (4-NP) and 5-nitrobenzimidazole (5-NBIA) in the concentration range of (2–10)×10^{-7} M using DC voltametry (DCV) and diferential pulse voltametry (DPV) at m-AgSAE p-AgSAE, and MF-AgSAE (deposition time 3600 s) in a Britton-Robinson buffer pH = 6 (4-NP) and pH = 8 (5-NBIA).

Electrode	Substance	Method	Slope (10^{-7} nA.mol L^{-1})	Intercept (nA)	*R*	*LOQ* (10^{7} mol L^{-1})
p-AgSAE	4-NP	DCV	–1.17	1.1	0.9987	3.7
		DPV	–2.19	1.7	0.9990	3.2
	5-NBIA	DCV	–1.95	0.5	0.9904	7.7
		DPV	–2.09	1.2	0.9969	4.7
m-AgSAE	4-NP	DCV	–1.25	–1.3	0.9636	1.4
		DPV	–2.68	–1.3	0.9997	8.0
	5-NBIA	DCV	–4.94	5.6	0.9993	3.2
		DPV	–4.91	–0.8	0.9930	6.0
MF-AgSAE	4-NP	DCV	–3.02	3.6	0.9899	8.8
		DPV	–3.47	3.1	0.9986	3.7
	5-NBIA	DCV	–4.48	9.3	0.9897	9.7
		DPV	–4.71	9.3	0.9954	7.0

3. Conclusions

It has been shown that DPV at m-AgSAE gives reliable results for 4-NP. For 5-NBIA the results are less reliable probably because of complex formation of 5-NBIA with mercury ions. Lowest achievable concentration range for DCV and DPV determination of both substances at all tested electrodes was 10^{-7} M. Optimized deposition time for MF-AgSAE was 300s.

Acknowledgements. *This research was supported by the Ministry of Education, Youth and Sports of the Czech Republic (projects LC 06035 and MSM 0021620857, and RP 14/63) and Grant Agency of the Czech Republic (no. 203/07/1195)*

References

[1] U.S. Environmental Protection Agency, *Federal Register 52* (1989), p. 131
[2] Luttke J., Scheer V., Levsen K., Wunsch G., Cape J.N., Hargreaves K.J., StoretonWest R.L., Acker K., Wieprecht W., Jones B.: *Atmos. Environ.* **31** (1997), 2637
[3] *List of the Registered Plant Protection Products 3*. The State Phytosanitary Administration, Brno 2006.
[4] *Toxicological Profile for Nitrophenols.* Agency for Toxic Substances and Disease Registry, Atlanta 1992.
[5] Barek J., Cvacka J., Muck A., Quaiserova V., Zima J., *Electroanalysis* **13** (2001), 779.
[6] Canterford D.R.: *J. Photogr. Sci.* **26** (1978), 65.
[7] Popova A., Christov M., Raicheva S., Sokolova E.: *Corros. Sci.* **46** (2004), 1333.
[8] Rosenkranz H.S., Karol M.H.: *Mutat. Res.* **431** (1999), 81.
[9] Fischer J., Vanourkova L., Danhel A., Vyskocil V., Cizek K., Barek J., Peckova K., Yosypchuk B., Navratil T.: *Int. J. Electrochem. Sci.* **2** (2007), 226.

Fast Derivatization Method for Analysis of Perfluorinated Organic Acids by GC

Veronika Dufková, Radomír Čabala

Department of Analytical Chemistry, Faculty of Science, Charles University in Prague, Albertov 2030, 128 43 Prague 2, Czech Republic, ✉ *dufkova.k.v@volny.cz*

Keywords
derivatization
gas chromatography
isobutyl chloroformate
perfluorinated organic acids
water samples

Abstract
A rapid and simple derivatization procedure has been developed for gas chromatographic determination of perfluorinated organic acids (PFCAs, C_6–C_{12}), using isobutyl chloroformate (IBCF) to convert the acids into the more volatile isobutyl esters, under catalysis by pyridine. Eight different capillary columns have been tested for separation of PFCAs isobutyl esters. The derivatization reaction has been optimized in acetonitrile medium and in aqueous phosphate buffer, with a pH = 2.5 and concentration of 50 mM. The reaction in aqueous phosphate buffer had yield higher by almost 10% compared to that in the acetonitrile medium. The LOD (LOQ) values obtained when using the aqueous phosphate buffer are in the ranges, 0.2–0.7 (0.5–2.4) μg/ml for GC-ECD and 0.03–0.31 (0.10–1.05) μg/ml for GC-EI-MS. The practical applicability was tested on Vltava river water samples.

1. Introduction

Perfluorinated organic acids (PFCAs) have recently received much attention because they belong among ubiquitous environmental contaminants [1, 2]. PFCAs with a typical structure of F–$(CF_2)_n$– COOH, where n = 1–13, have unique physical, chemical and biological properties, closely related to their high-energy carbon--fluorine bonds [3]. They are resistant to hydrolysis, photolysis, biodegradation and to metabolic processes in living organisms [4]. These properties make them both water- and fat-repellent ("supersurfactants") and thus they have been used for treatment of textiles and paper, in paints, lubricants, polishes, PTFE precursors, food packages, insecticide formulations, fire-fighting foams, and in the photographic and the semi-conductor industries [5–8]. The emissions of PFCAs over the period from 1951 to 2004 have been estimated to amount to 3200–7300 tons [9]. They are globally distributed, environmentally persistent, bioaccumulative and potentially harmful [10]. In 2005, EPA's science advisory board recommended that the agency classify perfluorooctanoic acid (PFOA) as a "likely" human carcinogen [11].

Analyses for PFCAs are now mostly carried out by means of HPLC-MS(-MS) to meet the requirements of high sensitivity and selectivity [12, 13]. However, many laboratories are not equipped for this method and would prefer readily available GC techniques. PFCAs should theoretically be directly determinable by GC because they are sufficiently volatile, but their chromatographic peaks exhibit pronounced tailing, owing to their high polarity. Consequently, the analytes are converted into more volatile and less polar derivatives using various procedures. The published works describe their derivatization to the methyl esters by the reactions with diazomethane [14, 15], methyl iodide [16] and with a methanolic solution of BF_3 [17]. Alzaga and Bayona [18] published a GC-NCI-MS technique for PFCAs determination employing an ion-pair extraction of their tetrabutylammonium salts, followed by their thermal decomposition on a SPME fiber producing the appropriate butyl esters. This approach has an advantage in the combination of the preconcentration and derivatization steps. Scott *et al.* [19, 20] describe a less common procedure for the PFCAs derivatization, involving the conversion of C_2 to C_9 acids into the corresponding 2,4-difluoroanilides by the reaction with 2,4-difluoroaniline in the presence of N, N-dicyclohexylcarbodiimide, followed by their GC-MS determination.

The proposed procedure employs esterification of PFCAs due to the reaction with alkyl chloroformates, which has not yet been published for PFCAs derivatization. The works of Hušek *et al.* [21–23] describe conversions of various acids, *e. g.,* fatty, oxo-, amino-, or phenolic acids, into various alkyl esters, using the acid reactions with alkyl chloroformates. A great advantage of these reactions lies in the possibility of performing them in aqueous media, which makes it possible to use them for direct derivatization of biological samples, *e. g.,* those of blood plasma or urine. The alkyl is first bound to the acid, with liberation of hydrochloric acid and the formation of the labile acid anhydride which rapidly decarboxylates and provides the

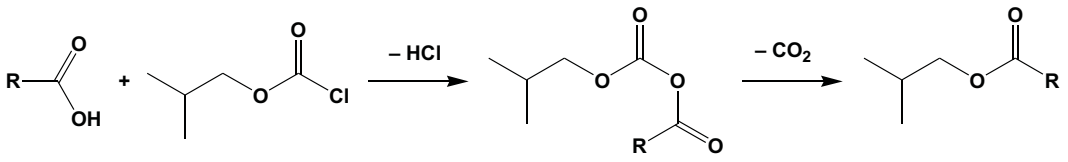

Fig. 1. Reaction scheme of derivatization of perfluorinated acid by isobutyl chloroformate; R is the perfluorinated alkyl chain.

ester and carbon dioxide. Pyridine is used as the catalyst and the corresponding alkyl alcohol sometimes serves as an auxiliary agent. For isobutyl chloroformate and a perfluorinated acid, the reaction scheme is depicted in Fig. 1. In addition to the isobutyl esters, small amounts of several volatile compounds are formed which, however, do not interfere in the following analytical procedure. Isobutyl esters have been selected because of their optimum volatility. For example, the methyl esters of PFCAs with shorter chains are too volatile and elute too rapidly from GC columns.

The present work aims at development of a very rapid, simple and reliable derivatization procedure based on the above reaction scheme, to be followed by a GC determination of the PFCA isobutyl esters. The method operates with micro liter samples and thus can be considered as an economically and ecologically advantageous micromethod. In combination with an efficient preconcentration technique, it should be suitable for PFCA determination in environmental samples; the development of suitable preconcentration and extraction techniques is the subject of our further research.

2. Experimental

2.1. Chemicals

The following substances were used as the analytical standards: perfluorohexanoic acid (PFHxA, <95%, Fluka), perfluoroheptanoic acid (PFHpA, <95%), perfluorooctanoic acid (PFOA, 95%), perfluoroonanoic acid (PFNA, 97%), perfluorodecanoic acid (PFDA, 98%), perfluoroundecanoic acid (PFUnA, 95%), and perfluorododecanoic acid (PFDoA, 95%), all from Aldrich. All the other chemicals, acetonitrile (< 99.5%, Fluka), hexane (99%, Mallinckrodt Baker B.V., Netherlands), isobutyl chloroformate (98%, Aldrich), pyridine (99%, Aldrich), hydrochloric acid (35%, Lach-Ner, Czech Republic), ammonium acetate, isobutylalcohol, phosphoric acid, sodium hydroxide, sodium carbonate (all p.a., Penta, Czech Republic) and water (Milli-Q Plus, Millipore) were used as received.

The standard substances were dissolved in acetonitrile to prepare standard stock solutions of 10000 μg mL^{-1} PFCA. The buffer solutions (50 mM) were prepared as follows: the pyridine buffer by dissolving the appropriate amount of pyridine in water; the phosphate buffer by adjusting the pH value of the aqueous H_3PO_4 with 2 M NaOH; the carbonate buffer by adjusting the pH of the aqueous Na_2CO_3 with 1 M HCl.

2.2. Instruments

AGC-ECD analyses were performed using a PU 4600 GC instrument (Unicam Analytical Systems, UK), equipped with a 15 m × 0.25 mm i. d., 0.25 μm film thickness SPB-5 column (Supelco, USA). Splitless-mode injection (sample volume, 1μL) at 250 °C (split valve closed for 1 min) and nitrogen carrier gas (flow rate, 0.44 mL min^{-1}) were used. The oven temperature was held for 1 min at 50 ºC, ramped at 10 ºC min^{-1} to 170 ºC and then held for 5 min (total run time, 23 min). The detector temperature was maintained at 300 ºC. The pressure of make-up nitrogen was 25 kPa.

GC-EI-MS analyses were performed using a GCMS-GP5050A instrument (Shimadzu, Japan), equipped with a 30 m × 0.25 mm i. d., 0.25 μm film thickness DB-5MS column (Agilent Technologies, USA). Helium (99.999%, Linde) was used as the carrier gas with a flow rate of 1.0 mL min^{-1}. Splitless-mode injection (sample volume, 1μL) at 250 °C was employed (split valve closed for 1 min). The oven temperature was held at 40 ºC for 3 min, ramped at 10 ºC min^{-1} to 170 ºC and then held for 3 min (total run time, 19 min). The mass spectrometer was operated in the selected ion monitoring (SIM) mode at *m/z* values 69, 131, 169 and 181 and the transfer line maintained at 300 °C.

2.3. Derivatization procedure

The reaction mixture for derivatization in the acetonitrile medium was prepared in a polypropylene vial by mixing 20 μL sample, 161 μL of reaction medium (acetonitrile or buffer), 8 μL of isobutylalcohol, 1 μL of pyridine and 10 μL of isobutyl chloroformate (IBCF). The total volume of the reaction mixture was 200 μL with the resultant PFOA concentration equal to 10 μg mL^{-1}. The mixture was stirred for 20 s in an ultrasonic bath, 200 μL of hexane were added and the isobutyl ester formed was extracted into hexane for 1 min in a shaker. The upper hexane phase was separated into a clean polypropylene vial and injected onto the gas chromatographic column.

2.4. Sample preparation

Three real samples of river water, denoted as Vltava 1 to 3, were collected from the Vltava river at a site close to the Prague centre, at a depth of 50 cm, into 1 L polypropylene vessels and filtered through a nylon membrane filter (47 mm in diameter, 0.45 μm, Whatman, England). Their volume was decreased from 500 to 5 ml in a Rotavapor EL 130 (Büchi, Switzerland) rotary evaporator and concentrated phosphoric acid was added to the concentrate to attain a concentration of 50 mM. The pH was then adjusted to a value of 2.5 by adding a 2 M NaOH solution and the solution was centrifuged. The volume, 181 μL, of this solution was subjected to the derivatization procedure, adding the appropriate amounts of isobutyl alcohol, pyridine and IBCF. The mixture was extracted with 200 μL of hexane and injected into the GC-EI-MS system.

3. Results and discussion

3.1. Development of the derivatization procedure

The derivatization reaction in the acetonitrile medium was optimized in several steps, in order to improve its efficiency and increase the sensitivity of analytical measurements. The duration of the reaction was varied within an interval from 0 to 50 min., finding the optimum value at 8 min. The volume of pyridine was optimized within a range from 0 to 20 μL per 200 μL of the reaction mixture, which corresponds to the pyridine concentration range, 0.000 to 1.238 M. Variations in the volumes of the other components of the reaction mixture had negligible effects on the reaction course. Finally, the reaction temperature was optimized in the range, 20 to 60 ºC, finding the lower limit to be suitable. This optimization improved the derivatization procedure efficiency by more than 60%, expressed in terms of the areas under the analyte chromatographic peaks.

Figs. 2 and 3 depict examples of GC-ECD and GC-EI--MS chromatograms of PFCAs (C_6–C_{12}) standards derivatized to the isobutyl esters in acetonitrile under the optimum conditions. The large peak of IBCF in Fig. 2 obscures the coeluting ibu-PFHxA peak.

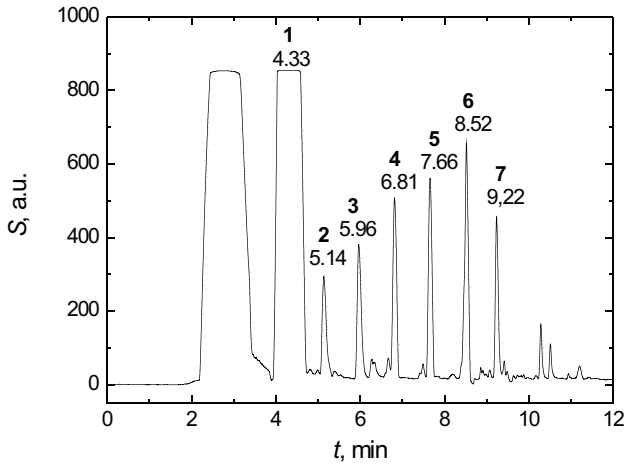

Fig. 2. A GC-ECD chromatogram of a mixture of perfluorinated acid standards (10 μg mL^{-1} of each) derivatized to isobutyl esters. An SPB-5 column (15 m × 0.25 mm i. d., 0.25 μm); a 1 μL sample injected (splitless, 1 min); detector temperature, 300 °C; injector temperature, 250 °C; column temperature, 50 ºC (1 min) to 170 ºC (5 min) in 10 ºC min^{-1}; make-up gas pressure, 25 kPa, nitrogen flow rate, 0.44 mL min^{-1}; (1) IBCF, (2) ibu-PFHpA, (3) ibu-PFOA, (4) ibu-PFNA, (5) ibu-PFDA, (6) ibu-PFUnA, (7) ibu-PFDoA.

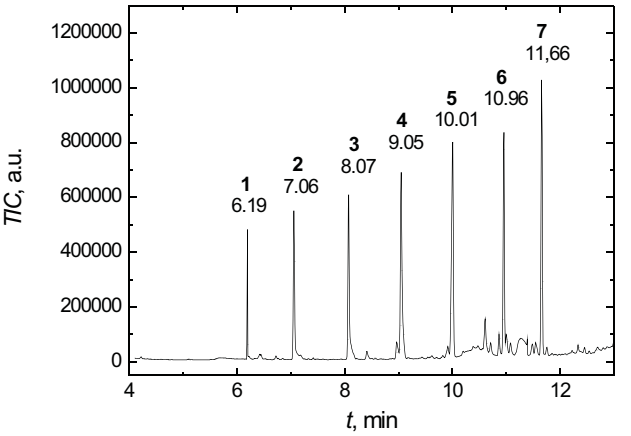

Fig. 3. A GC-EI-MS chromatogram of a mixture of perfluorinated acid standards (10 μg mL^{-1} of each) derivatized to the isobutyl esters. A DB-5MS column (30 m × 0.25 mm i. d., 0.25 μm); a 1 μL sample injected (splitless, 1 min); MS interface temperature, 300 °C; injector temperature, 250 °C; temperature program: 40 ºC (3 min) to 170 ºC (3 min) in 10 ºC min^{-1}; constant helium flow rate, 1.0 mL min^{-1}; SIM mode: *m/z* = 69, 131, 169 and 181; (1) ibu-PFHxA, (2) ibu-PFHpA, (3) ibu-PFOA, (4) ibu-PFNA, (5) ibu-PFDA, (6) ibu--PFUnA, (7) ibu-PFDoA.

3.2. Column selection

The mechanism of interactions of PFCAs derivatives with stationary phases used for their separations in GC were not studied in detail yet. Therefore, separation of PFCAs isobutyl esters on eight different stationary phases was performed and compared. The highest retention was found on RTX-200MS column (trifluoropropyl methyl polysiloxane) followed by SPB-5 (5% phenyl methyl polysiloxane) and SPB-1 (100% methyl polysiloxane) columns. RTX-200MS is relatively new column on the market and was purchased at the end of the study. As a compromise between the retention and the analysis time, SPB-5 column was selected for further investigations. The advantage of this selection is that the majority of common GC-MS data are collected on this

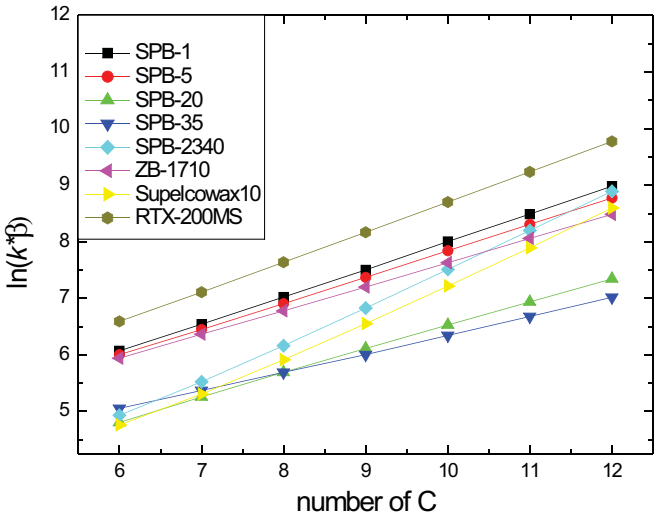

Fig. 4. Dependence of retention factor corrected to β on number of carbons in PFCAs in semi logarithmic scale for eight different columns by GC-ECD, isothermal analysis (60 ºC). Columns: SPB-1 (Supelco, 30 m, 0.25 mm i. d. , film 0.25 µm, dimethyl polysiloxane), SPB-5 (Supelco, 15 m, 0.25 mm i. d., film 0.25 µm, 5% diphenyl, 95% dimethyl polysiloxane), SPB-20 (Supelco, 15 m, 0.25 mm i. d., film 1 µm, 20% diphenyl, 80% dimethyl polysiloxane), SPB-35 (Supelco, 30 m, 0.25 mm i. d., film 1 µm, 35% diphenyl, 65% dimethyl polysiloxane), ZB-1701 (Phenomenex, Torrance, USA, 15 m, 0.25 mm i. d., film 0.25 µm, 14% cyanopropyl-phenyl, 86% dimethyl polysiloxane), Supelcowax 10 (Supelco, 30 m, 0.25 mm i. d., film 0.25 µm, polyethylenglykol), RTX-200MS (Restek, Bellefonte, USA, 30 m, 0.25 mm i. d., film 0.25 µm, trifluoropropylmethyl polysiloxane), SP-2340 (Supelco, 30 m, 0.32 mm i. d., film 0.2 µm 100% poly(bis-cyanopropyl siloxane)).

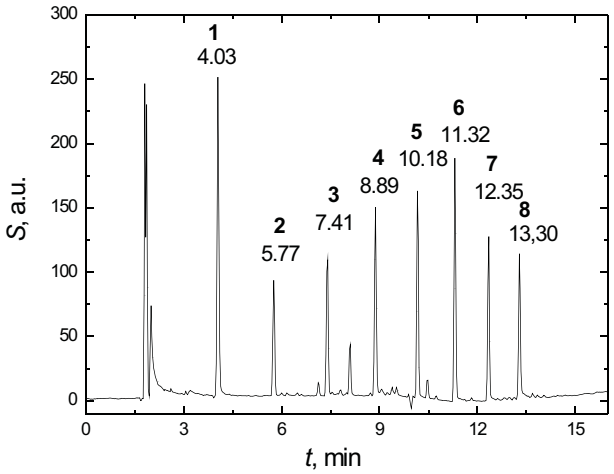

Fig. 5. A GC-ECD chromatogram of a mixture of perfluorinated acid standards (10 µg mL^{-1} of each) derivatized to isobutyl esters. An RTX-200MS column (30 m × 0.25 mm i. d., 0.25 µm); a 1 µL sample injected (split, 1 min); detector temperature, 300 °C; injector temperature, 250 °C; column temperature, 60 ºC (5 min) to 170 ºC (5 min) in 10 ºC min^{-1}; make-up gas pressure, 25 kPa, nitrogen flow rate, 0.44 mL min^{-1}; (1) IBCF, (2) ibu-PFHxA, (3) ibu-PFHpA, (4) ibu-PFOA, (5) ibu-PFNA, (6) ibu-PFDA, (7) ibu-PFUnA, (8) ibu-PFDoA.

stationary phase and allow an easy comparison. Fig. 4 shows the dependence of β-corrected values of separation factor on the number of carbon atoms in PFCA molecule for the columns under test. Two columns, Supelcowax 10 (polyethylenglycol) and SP-2340 (non-bonded 100% bis-cyanopropyl polysiloxane) have higher slope which fact reflects probably a higher fraction of polar interactions of the retention mechanism compared to the less polar polysiloxane-based stationary phases. Detailed analysis of these data will be presented in separate publication. A GC-ECD chromatogram of a mixture of perfluorinated acid standards separated on column RTX-200MS are given in Fig. 5.

3.3. Derivatization reaction in aqueous medium

Preliminary measurements indicated that PFCAs derivatization in aqueous media needs optimization. One of the principal parameters is the pH value of the medium and thus various buffers were tested, within a pH range from 1 to 11, at a concentration of 50 mM (to adjust the lowest pH values, 100 mM HCl was used). These aqueous buffers, pH = 1.0 (HCl), pH = 2.0, 2.5, and 3.0 (a phosphate buffer), pH = 5.0 (a pyridine buffer), pH = 7.0, 9.0, and 11.0 (a carbonate buffer), replaced acetonitrile in the reaction mixture. The phosphate buffer with a pH = 2.5 provided the best results. The phosphate buffer concentration exerts no significant effect on the deriva-tization reaction; therefore, of the tested values, 1, 10, 50 and 100 mM, the concentration equal to 50 mM was further used. The amount of pyridine, as the reaction catalyst, was most important for the reaction yield in the acetonitrile medium. Therefore, the effect of the pyridine concentration was also investigated in the aqueous medium, within a range of 0.00–1.98 M, corresponding to the additions of 0–32 µL of pyridine to obtain the total volume of the reaction mixture, 200 µL.

When comparing the optimized PFCA derivatization in acetonitrile and in water, it can be seen that the area under the PFOA isobutyl ester GC-EI-MS peak, for the PFOA concentration, 10 µg mL^{-1}, equals 417000 ± ± 30800 a. u. in the acetonitrile medium and 460000 ± ± 46400 a .u. in the 50 mM aqueous phosphate buffer with a pH = 2.5. Therefore, the yield of the derivatization reaction is higher, by almost 10%, in the aqueous medium. Another advantage of the aqueous medium lies in the fact that the overall analytical procedure is much simpler, compared to the use of the non-aqueous system.

The LOD and LOQ values for the perfluorinated acid isobutyl esters obtained after derivatization in the aqueous phosphate buffer are given in Table 1. LOD (LOQ) was computed as three-times (ten-times) the standard deviation of the calibration line divided by its slope. Higher LOD and LOQ values for GC-EI-MS were

Table 1. The limits of detection (LOD) and quantitation (LOQ) in μg mL^{-1} for the PFCAs isobutyl esters after derivatization in the aqueous phosphate buffer obtained by the GC-ECD and GC-EI-MS techniques (without preconcentration).

	GC-ECD		GC-EI-MS	
	LOD	LOQ	LOD	LOQ
PFHxA	–	–	0.15	0.49
PFHpA	0.3	1.1	0.06	0.19
PFOA	0.6	1.9	0.04	0.12
PFNA	0.2	0.5	0.03	0.10
PFDA	0.2	0.5	0.26	0.86
PFUnA	0.5	1.7	0.23	0.77
PFDoA	0.7	2.4	0.31	1.05

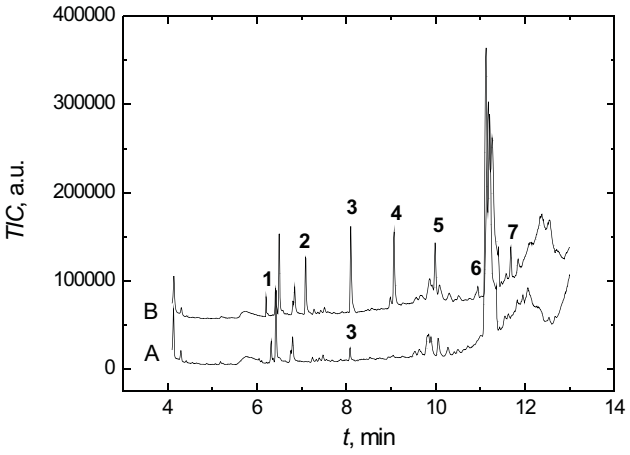

Fig. 6. GC-EI-MS chromatograms of the Vltava 2 sample (A) and of the Vltava 2 sample with PFCAs standards added (B) (the PFCAs concentration, 2 μg mL^{-1}, for the measuring conditions see Fig. 3).

observed with acids containing higher numbers of carbon atoms (C_{10}–C_{12}), probably due to the noise gradually increasing during the temperature gradient of the GC procedure.

3.4. Testing of the application of the procedure

The optimized derivatization procedure in the aqueous medium was tested on three real samples of river water. A sample of distilled water spiked with a PFOA standard was analyzed in parallel. The GC-EI-MS method was used and the yield of the derivatization reaction was found equal to 64%. This preconcentration step is the simplest possible approach and does not require any sample purification. However, it represents only a preliminary step. The use of more sophisticated methods, *e. g.*, solid-phase extraction, will probably yield better results.

In two samples (Vltava 1, Vltava 3), no perfluorinated acid was detected. The PFOA peak was found in the Vltava 2 sample, corresponding to the concentration, 0.20 μg mL^{-1} in 200 μL hexane, or 3.4 ng mL^{-1} in the sample. The chromatograms of the Vltava 2 sample prior (A) and after (B) the addition of PFCAs standards are given in Fig. 6.

4. Conclusions

A rapid and simple micromethod has been developed for determination of perfluorinated acids (C_6–C_{12}) by gas chromatography, after the analyte conversion into the isobutyl esters by the reaction with isobutyl chloroformate. Eight different capillary columns have been tested for separation of PFCAs isobutyl esters and SPB-5 column selected as optimum. The derivatization reaction has been optimized in the acetonitrile medium and in the medium of an aqueous phosphate buffer, with a pH = 2.5 and a concentration of 50 mM, catalyzed by 0.06 M pyridine. The reaction in the aqueous phosphate buffer had a yield higher by almost 10%, compared to that in the acetonitrile medium.

The LOD (LOQ) values obtained when using the aqueous phosphate buffer are in the ranges, 0.2–0.7 (0.5–2.4) μg mL^{-1} for GC-ECD and 0.03–0.31 (0.10–1.05) μg mL^{-1} for GC-EI-MS. These techniques have been applied to the determination of the PCFAs concentrations in three samples of the Vltava river water. None of these acids was found in two samples, while the third sample contained PFOA at a concentration of 3.4 ng mL^{-1} of the river water.

Acknowledgements. *The financial support of this work by the Ministry of Education, Youth and Sports of the Czech Republic (the project No. VZ MSM 0021620857), by the Grant Agency of Charles University in Prague (the project No. 40908) and by the Norwegian Financial Mechanism (the project No. CZ0116) is gratefully acknowledged.*

References

[1] Hori H., Nagaoka Y., Murayama M., Kutsuna S.: *Environ. Sci. Technol.* **42** (2008) 7438–7443.
[2] Yamashita N., Kannan K., Taniyasu S., Horii Y., Okazawa T., Petrick G., Gamo T.: *Environ. Sci. Technol.* **38** (2004) 5522–5528.
[3] de Voogt P., Sáez M.: *Trends Anal. Chem.* **25** (2006) 326–342.
[4] Tseng C.L., Liu L.L., Chen C.M.: W.H. Ding, *J. Chromatogr. A* **1105** (2006) 119–126.
[5] González-Barreiro C., Martínez-Carballo E., Sitka A., Scharf S., Gans O.: *Anal. Bioanal. Chem.* **386** (2006) 2123–2132.
[6] Villagrasa M., López de Alda M., Barceló D.: *Anal. Bioanal. Chem.* **386** (2006) 953–972.
[7] Weremiuk A.M., Gerstmann S., Frank H.: *J. Sep. Sci.* **29** (2006) 2251–2255.

[8] Mawn M.P., McKay R.G., Ryan T.W., Szostek B., Powley C.R., Buck R.C.: *Analyst* **130** (2005) 670–678.
[9] van Leeuwen S.P.J., de Boer J.: *J. Chromatogr. A* **1153** (2007) 172–185.
[10] Li M.H.: *Environ. Toxicol.* **24** (2009) 95–101.
[11] Renner R.: *Environ. Sci. Technol.* **42** (2008) 648–650.
[12] Washington J.W., Henderson W.M., Ellington J.J., Jenkins T.M., Evans J.J.: *J. Chromatogr. A* **1181** (2008) 21–32.
[13] Furdui V.I., Helm P.A., Crozier P.W., Lucaciu C., Reiner E.J., Marvin C.H., Whittle D.M., Mabury S.A., Tomy G.T.: *Environ. Sci. Technol.* **42** (2008) 4739–4744.
[14] Belisle J., Hagen D.F.:, *Anal. Biochem.* **101** (1980) 369–376.
[15] Henderson W.M., Weber E.J., Duirk S.E., Washington J.W., Smith M.A.: *J. Chromatogr. B* **846** (2007) 155–161.
[16] Moody C.A., Field J.A.: *Environ. Sci. Technol.* **33** (1999) 2800–2806.
[17] Alzaga R., Bayona J.M.: *J. Chromatogr. A* **1042** (2004) 155–162.
[18] Alzaga R., Salgado-Pentinal C., Jover E., Bayona J.M.: *J. Chromatogr. A* **1083** (2005) 1–6.
[19] Scott B.F., Moody C.A., Spencer C., Small J.M., Muir D.C.G., Mabury S.A.: *Environ. Sci. Technol.* **40** (2006) 6405–6410.
[20] Scott B.F., Spencer C., Mabury S.A., Muir D.C.G.: *Environ. Sci. Technol.* **40** (2006) 7167–7174.
[21] Husek P.: *J. Chromatogr. B* **717** (1998) 57–91.
[22] Husek P., Simek P., Matucha P.: *Chromatographia* **58** (2003) 623–630.
[23] Husek P., Simek P.: *Curr. Pharm. Anal*. **2** (2006) 23–43.

Comparison of Generation Efficiency of H_2Se in Newly Constructed Electrolytic Cells Using ^{75}Se Radiotracer

Jakub Hraníček, Václav Červený, Petr Rychlovský

Department of Analytical Chemistry, Faculty of Science, Charles University in Prague, Albertov 2030, 128 43 Prague 2, Czech Republic, ✉ *hranicek@natur.cuni.cz*

Abstract

One of the most important characteristics of flow-through electrolytic cells for electrochemical hydride generation used in atomic absorption spectrometry is the hydride generation efficiency which depends mainly on the cell construction parameters (shape and volume of electrode chambers) and working parameters (*e. g.* electrolyte flow rate). Six different types of flow-through electrolytic cells were constructed and its generation efficiency of H_2Se was studied. This group of electrolytic cells included except of the classical thin-layer electrolytic cell also compact tubular electrolytic cell and cells without typical ion-exchange membrane. The hydride generation efficiency of H_2Se was preliminary found out by comparison of sensitivity of selenium determination among chemical generation and electrochemical generation. Finally the detailed experiments with ^{75}Se radiotracer were realized. The maximal generation efficiency which was obtained by one of the newly constructed cell was 96%. For another two cells the generation efficiency was approximately 90%.

Keywords

atomic absorption spectrometry
electrochemical generation
electrolytic cell
generation efficiency
radiotracer
selenium hydride

1. Introduction

The electrochemical generation (EcHG) is an alternative method of generation of volatile compound [1]. This method eliminates many complications coupled with classical chemical generation (CHG). The electrochemical generation of volatile compound technique is possible to use as a derivatization technique in connection of separation techniques (HPLC) with detection by element selective spectroscopic method. This experimental connection is often applied in the speciation analysis to determine individual form of hydride-forming element [2]. The important requirement for this formation is minimal inner volume, especially minimal cathode chamber of electrolytic cell. On the other hand, the efficiency should not be declined with decreasing inner volume. However, both of these requirements, high efficiency and minimal inner volume are contradictory and it is necessary to find out compromise.

Nowadays the thin-layer model of electrolytic cell [3, 4], usually designed from plexiglass, teflon or polypropylene, is often used and therefore they is sufficiently examined and exist in various modifications [5–7]. There are ion-exchange Nafion membranes used to separate cathode and anode chamber and electrolyte. In the separated compartments there are electrodes of different types, shapes and materials (lead, carbon or platinum).

The process of electrochemical generation of volatile compounds contains several steps. The analyte is converted to the gaseous hydride form in the electrolytic cell and it is release from the liquid matrix into the gaseous phase and finally transported in to the atomizer by carrier gas. The overall generation efficiency is arithmetic product of partial efficiency of each previous step. The generation efficiency of volatile compound depends on many significant factors such as chemical form and oxidation state of analyte, experimental conditions (composition and flow rate of both electrolyte, generation current, carrier gas flow rate), cathode parameters (material, shape, size of active surface), inherence of interfering elements.

In this work there are described two ways how to find out the generation efficiency. For these experiments selenium in a standard solution was used as a model analyte. The hydride generation efficiency of H_2Se was preliminary found out by sensitivity comparison of selenium determination among chemical generation and electrochemical generation. The efficiency of the chemical generation of H_2Se is practically 100 %. The detailed experiments were realized with a radiotracer. This way enable find out overall distribution of the analyte (radiotracer) in the electrolytic cell and it is possible to determine percent fraction converted to the hydride form.

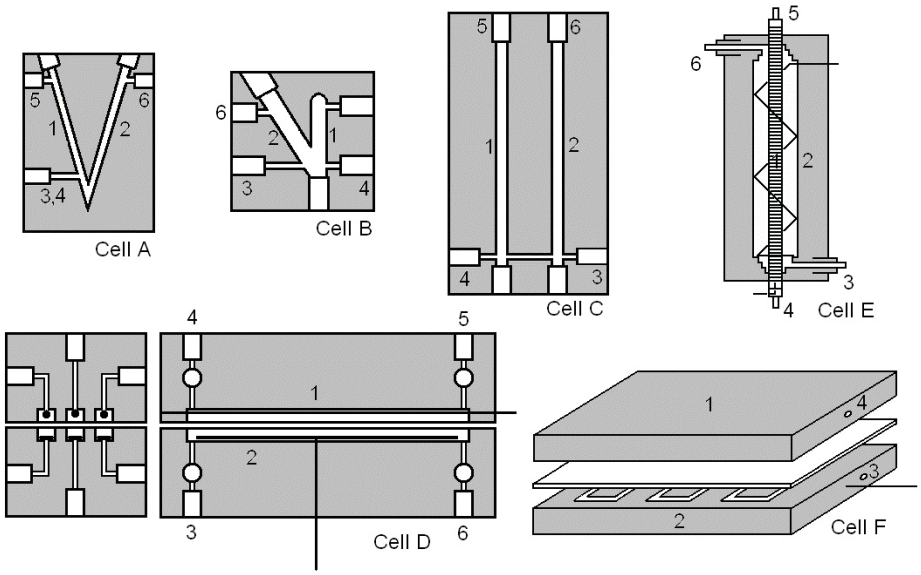

Fig. 1. Comarison flow-through electrolytic cells; (1) cathode chamber, (2) anode chamber, (3) anolyte inlet, (4) catholyte inlet, (5) outlet to gas-liquid separator, (6) waste outlet.

2. Experimental

2.1 Newly constructed electrolytic cells

The generation efficiency was investigated for newly constructed cells which are shown in the Fig. 1. The common characterization of cells A, B and C is absence of the ion-exchange membrane between the cathode chamber and the anode chamber. Both of these chambers are filled by the same electrolyte. Electrolyte flow rate is controlled by two or three peristaltic pump sited before the electrolyte inlets and behind the anolyte outlet. The cell D is the similar as classical thin-layer electrolytic cell but this contains three cathode and three anode chambers and the electrolyte stream is uniformly divided. The cell E is one version of tubular electrolytic cell with concentric cathode and anode chambers. The cathode chamber is put inside of the anode chamber (in the Fig. 1). Cell F is characterized by all-metal cathode chamber in which there is groove for catholyte with minimal inner volume and maximal length. The cells A, B and C were primarily constructed to achieve minimal inner volume of the cathode chamber. Cells D, E, F were constructed afterwards to increase generation efficiency. The generation efficiencies of H_2Se for each newly constructed cell were compared with classical thin-layer electrolytic cell (cell TL) and with chemical generation (CHG).

All the parameters of the electrochemical hydride generation of selenium hydride (gas and electrolyte flow rates, electric current, *etc.*) used in the radiotracer study were the same as in all previously performed optimization studies by AAS making the results fully comparable. These parameters are shown in Tab. 1. The experimental setup used in the radiotracer study was very similar as previous experiment with the same cells. The connecting tube between gas-liquid separator and atomizer placed in the optical axis in the atomic absorption spectrometer was exchanged for two columns with active charcoal to adsorb gaseous selenium hydride with radiotracer (Fig. 2, *see next page*). All the radiometric experiments were carried out in the exhaust hood of a radiochemical laboratory. The working parameters of classical chemical generation were set up corresponding with the electrochemical generation. The flow rate of solution containing analyte (in CHG) was adjusted that amount of selenium per unit of time flowing into the reaction cell was the same as amount flowing into the electrolytic cell.

2.2. Instrumentation

Atomic absorption spectrometer Solaar 939AA (Unicam, UK) with Se hollow cathode lamp (8 mA, 196.0 nm and spectral width 1.0 nm) was used for working parameters optimization and determination of basic characteristics (sensitivity). Programmable eight

Table 1. Working parameters for each cell used in the radiotracer study (catholyte 1 M HCl, anolyte 2 M H_2SO_4, electrolyte flow rate 2.5 mL min^{-1}).

Cell	A	B	C	D	E	F	TL
Electric current (A)	0.4	0.7	0.5	1.2	0.75	0.2	1.2
Carrier gas flow rate (mL min^{-1})	10	20	10	40	60	80	20

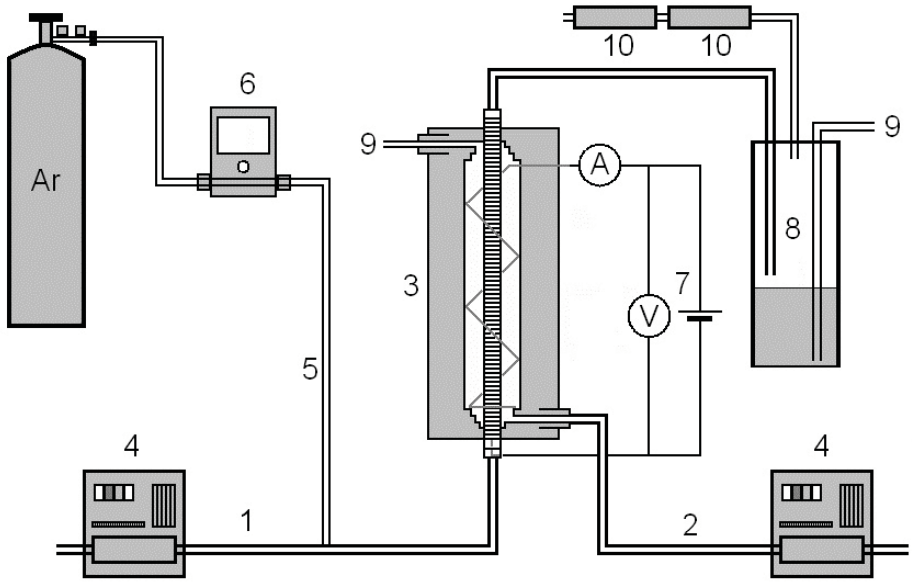

Fig. 2. Instrumental setup for radiometric experiments EcHG with cell E; (1) catholyte, (2) anolyte, (3) flow-through electrolyte cell, (4) peristaltic pump, (5) carrier gas, (6) flow meter, (7) electric current supply, (8) gas-liquid separator, (9) waste, (10) column with active charcoal.

channel peristaltic pumps MasterFlex® L/S with mini-cartridge pump head (Cole-Parmer, USA) and Tygon tubes were used for electrolytes transport. Constant electric current supply LPS 303 (American Reliance, Taiwan) with maximal current 3.0 A and maximal voltage 30 V was used for generation of volatile compounds. Teflon tubes (1.0 mm i. d.) with minimal length were used for connection of all components. Mass flow controller 0–100 mL min^{-1} (Cole-Parmer, USA) was used for control of carrier gas flow rate.

The radioactivity was quantified employing an auto-gamma counting system equipped with the scintillation NaI(Tl) well-type crystal detector (Minaxi 5000, Packard) with 1 min counting time and using the window in the energy range from 60 to 450 keV. The spatial distribution of ^{75}Se radioactive indicator in the electrolytic cells was investigated by image plate autoradiography. A Fuji BAS 5000 laser scanner was employed to measure phosphorescence induced by radioactivity present in the individual parts of the cell. The radiograms were further evaluated using the Aida software.

2.3. Reagents

All working non-radioactive selenium (Se (IV)) solutions of required concentration were prepared from the standard solution (1.000 ± 0.002 g dm^{-3} Se; Analytika, Czech Republic). Electrolytes (H_2SO_4 and HCl) were of research grade quality (Merck, Germany). Deionized distilled water prepared with a Milli-QPLUS (Millipore, USA) system was used for all dilution. Argon of the 99.998% purity was used as the carrier gas. The working radiotracer solutions of required analyte concentration used in this work were prepared to dilute radiotracer solution at the specific activity of 1 kBq mL^{-1} in 1 M HCl by adding appropriate amount of the (non-radioactive) selenium working standard in 1 M HCl. Radionuclide ^{75}Se was prepared by educated personal in radiochemical laboratory.

2.4. Radioactive balance measurement

At the beginning of each experiment, the radioactivity of the sample solution of exact volume was counted. Consequently this volume of radioactive sample solution (12.5 mL) was delivered by the pump (at the flow rate of 2.5 mL min^{-1}) into the electrolytic cell exchanging the incoming tubes between non-radioactive and radioactive selenium solution. After all radioactive solution was delivered the incoming tubes was replaced back to the non-radioactive selenium solution and after about ten minutes the electrolytic cell was disassembled and each part and both columns and waste catholyte and anolyte solution was measured. The radioactivity of each part was expressed as a percent part of overall activity of the sample solution at the beginning.

3. Results and discussion

3.1. Sensitivity comparison

The first way to investigate generation efficiency of selenium hydride was comparison of sensitivity of selenium determination. These sensitivities accordant with each newly constructed electrolytic cell were compared together with sensitivity achieved by classical thin-layer

Table 2. Sensitivity for electrochemical and chemical generation

	CHG	TL	A	B	C	D	E	F
Sensitivity (10^3 dm^3 μg^{-1} of Se)	16.2	5.32	1.86	4.46	8.30	15.6	14.2	14.9
% of CHG	100.0	32.8	11.5	27.5	51.2	96.3	87.7	92.0

electrolytic cell. The efficiency of electrochemical hydride generation was obtained comparing sensitivity of selenium determination with classical chemical hydride generation whose efficiency is nearly one hundred per cent. For individual sensitivity for electrochemical and chemical generation see Table 2.

The results from previous experiments are that only cell D, E and F able to offer high generation efficiency of selenium hydride. The cell D was constructed primary to increase generation efficiency but its inner volume due to three cathode chambers is not suitable for practical applications. On the other hand the cell E and F are characterized, except of high generation efficiency, by minimal inner volume and thanks to this they are suitable for more application in AAS.

3.2. Radiometric experiments

The radiometric experiments were realized for each of six newly constructed electrolytic cells and for classical thin-layer electrolytic cell. On the basis of previous experiments the cells E and F were studies with more attention. The results only about the cell E are presented in this text. The similar results and trends were obtained by another cell F.

To get overall distribution of selenium (presented by different radioactive chemical forms) one replicate experiment was realized. After this experiment the electrolytic cell was disassembled and each part of it was measured. The catholyte, anolyte and two columns packed with active charcoal were measured to. Activities of each part were expressed as the percent part of activity of initial radioactive solution. It is important that summation of all percentage gave together one hundred percent – it means all parts, which were in contact with radioactive selenium, were measured. According these results the activity of waste catholyte solution outside of the cell was about 30 %. This fraction of analyte was not in contact with cathode material or the rising selenium hydride was by return dissolved in catholyte. More then 50% of radioactivity were detected in the first column with active charcoal. The second column contained minimal radioactive selenium (< 0.01%) in every case. The capacity of the first column was sufficient and every gaseous selenium hydride was adsorbed on the surface of active charcoal. The rest of activity (about 20 %) was detected on different parts of apparatus (cathode: 15%, connecting material plus transporting tubes: 4%, nafion membrane: 1%). Incoming tubes for analyte and catholyte, anolyte chamber and anolyte waste solution contained minimal (< 0.1%) selenium in any form.

After this first experiment two and three replicates experiments were gradually realized. The sense of this was to find out the reproducibility of previous radiometric experiments data. In the first case two replicates were realized with time interval about 10 minutes and in the second case three replicates were realized with the same time delay. The results were very similar and the percent distribution of the selenium radiotracer was minimally modified. For example the radioactivity of waste catholyte solution outside of the cell in previous cases was 29.09%, 29.01%, and 30.21%. In series of last three replicates there was observed trend of moderate increasing activity in the first column. This can be explain that at the beginning the cathode surface was not saturated by selenium / selenium hydride and the generation efficiency was lower than during the third replicate when the cathode surface was more saturated. This premise can be confirmed by the cathode radioactivity during the same three consecutive replicates when the activity was increased and then stayed the same.

4. Conclusions

In this work the hydride generation efficiency for six newly constructed electrochemical cells was investigated. Selenium in aqueous solution was used as a model analyte. At the beginning comparison of sensitivity of chemical and electrochemical (with different types of electrolytic cells) selenium determination showed that only for cell D, E and F the generation efficiency is about 90%. But only cell D and E are suitable for further analytic application because of its minimal inner volume. For each six cells (and for comparison cell TL) the radiotracers studies were realized. On the basis of these experiments the spatial distribution of selenium in the each cell were investigated.

Acknowledgements. *The authors are obliged to Jan Kratzer from Institute of Analytical Chemistry AS CR for help with radiotracer experiments. The authors thank also to the Grant Agency of the ASCR (project: A400310507/2005) and MSMT CR (research project: MSM0021620857 and RP 14/63) for the financial support.*

References

[1] Dědina J., Tsalev D.: *Hydride Generation Atomic Absorption Spectrometry.* Wiley, Chichester 1995.

[2] Červený V., Válková Z., Rychlovský P.: The application of electrochemical hydride generation as a derivatization step for HPLC-QFAAS determination of selected arsenic species. In: *Book of Abstracts of Colloquium Spectroscopicum Internationale XXXIV.* University of Antwerp 2005, p. 232.

[3] Lin Y.H., Wang X.R., Yuan D.X., Yang P.Y., Huang B.L., Zhuang Z.X.: *J. Anal. Atom. Spectrom.* **7** (1992) 287.

[4] Brockmann L., Nonn C., Golloch A.: *J. Anal. Atom. Spectrom.* **8** (1993) 397.

[5] Šíma J., Rychlovský P.: *Chem. Listy* **92** (1998) 676.

[6] Hraníček J., Červený V., Rychlovský P.: *Chem. Listy* **102** (2008) 200.

[7] Červený V., Rychlovský P., Hraníček J., Šíma J.: *Chem. Listy* **103** (2009) 652.

New Electrochemical Cell For Studies of Phthalocyanines

Věra Hudská[a], Pavel Janda[b], Karel Nesměrák[a]

[a] *Department of Analytical Chemistry, Faculty of Science, Charles University in Prague, Albertov 6, 128 43 Prague 2, Czech Republic,* ✉ *hudska1@natur.cuni.cz*
[b] *J. Heyrovský Institute of Physical Chemistry, v.v.i., Academy of Sciences of the Czech Republic Dolejškova 3, 182 23 Prague 8, Czech Republic*

Abstract

We have developed a new type of electrochemical cell for electrochemical studies of phthalocyanines. The cell employs a HOPG as a working electrode covered by a thin layer of dichlorobenzene with dissolved phthalocyanine. The layer of dichlorobenzene solution is overlaid by aqueous supporting electrolyte solution where the reference and counter microelectrodes are immersed. The volume of phase where electrochemical reaction of phthalocyanine takes place is typically less than 10^2 μL. Thus the cell allows performing electrochemistry of new synthesized phthalocyanines, available usually in mg-amounts, as well as a "bulk" spectroelectrochemistry in relatively short time scale. With the same arrangement, phthalocyanine-mediated reactions with reactants residing in adjacent immiscible phases and phase transfer processes can be examined. Low amounts of studied compounds allow performing also stability measurements usually not feasible in common (bulk) arrangement of the cell.

Keywords
cyclic voltrammetry
electrochemical cell
HOPG
liquid-liquid interfaces
phthalocyanines

1. Introduction

Phthalocyanines, for the first time synthesised by Braun and Tcherniac in 1907, became useful as inexpensive pigments and dyes in textile industry a few years later. Nowadays, their stability and properties tunable by modifications of skeleton and changes of central metal respectively, attract attention in (electro) catalysis, photochemistry as well as in sensor development. Due to their tunable photosensitivity, phthalocyanines appeared to find their application also in medicine in photodynamic therapy [1, 2].

Liquid-liquid interfacial processes namely so called phase transfer catalysis are of great interest in different fields, because they allow bringing mutually insoluble reagents in sufficient concentrations to attain conveniently rapid reaction rates. Besides, many biological processes occur just at liquid-liquid interfaces, accompanied with phase separation or transport of electrons, ions, and molecules. Basic simulation models and experiments were performed by Samec's group [3, 4] who published a series of papers about the topic.

The liquid-liquid interface system was used to investigate the electrochemical behaviour of new phthalocyanine compounds, synthesized by Kobayashi's group [5].

The highly oriented pyrolytic graphite (HOPG) is a special type of graphite, with very large differences between basal plane and edge surfaces. In spite of the fact that carbon surfaces are prone to adsorption, the adsorption of oxygen on HOPG basal plane is minimal (as distinguished by low chemical reactivity), on contrary the HOPG edge surface is prone to absorption of oxygen. One of the next benefits is HOPG semimetal character, which predestines its employment in electrochemistry. HOPG has well defined surface, which could be cleaned very easily by peeling off using adhesive tape. The main problem of electrode, where HOPG is sealed in epoxy or in Teflon housing [6], is the damage of HOPG surface after several cleaning cycles (the surface has more edge defects, the electrode area is poorly defined and not reproducible).

The aim of our work was the construction of new type of electrochemical cell, where HOPG electrode can retain its advantage of simple, effective and well defined cleaning, with the option to detach the electrode reversibly for ex-situ examination by XPS, AFM, STM and other ex-situ techniques.

The cell was employed in electrochemical study of newly synthesised phthalocyanines. This model of electrochemical cell allows performing both the electrochemistry on the electrode with immiscible liquid-embedded interface as well as on solid supported films.

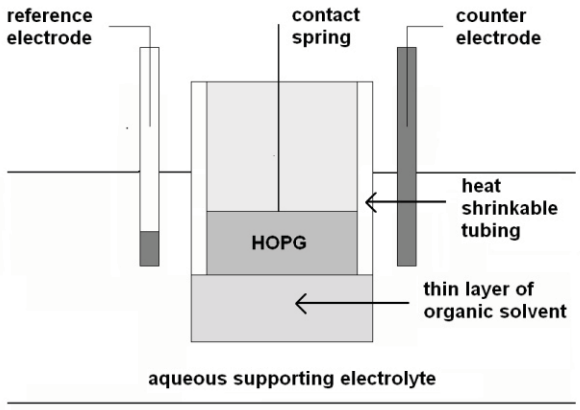

Fig. 1. The scheme of the electrode used in primary experiments.

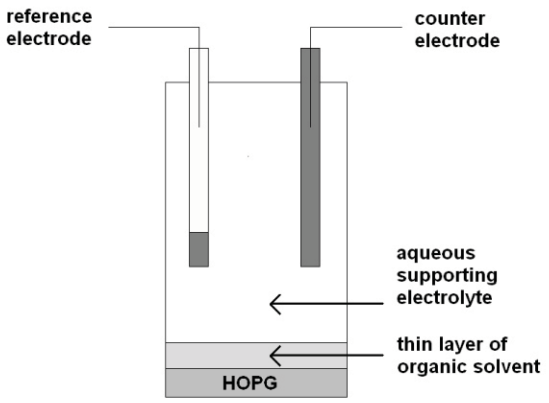

Fig. 2. The schematic view of the proposed cell.

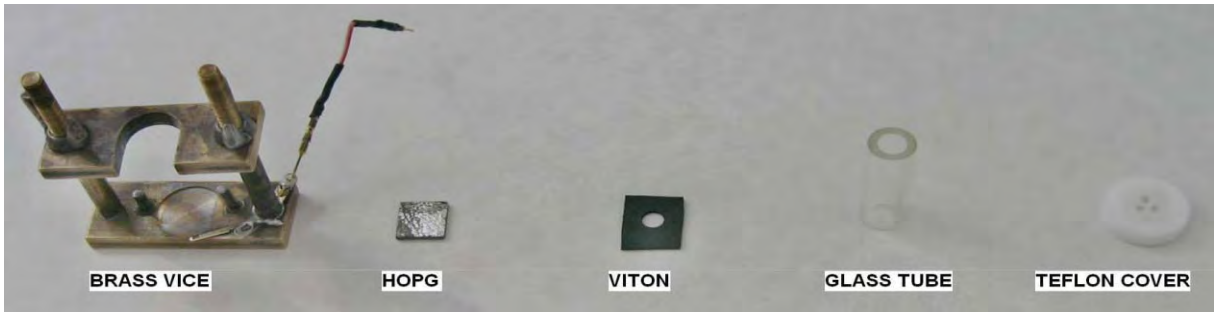

Fig. 3. The detailed view of the parts of the proposed cell.

2. Experimental

2.1. HOPG electrode housing, a construction of new electrochemical cell

Firstly, we employed conventional type of HOPG electrode (Momentive Performance Materials Quartz, Inc., ZYB grade) utilizing circular HOPG with surface area 50 mm^2 housed in a shrinkable Teflon tubing (Fig. 1). This electrode construction did not allow convenient HOPG surface cleaning using adhesive tape due to formation of concave shape of the electrode surface and solvent leaking into interspace between HOPG and Teflon holder. Thus, we proposed new type of electrochemical cell, which can utilize virtually any shape of HOPG specimen and allows unrestricted conventional peal-off cleaning. The HOPG wafer is placed on the brass support and sealed by the slice of viton (DuPont Performance Elastomers S.A.) which is pressed by thick-walled glass tube on HOPG basal plane. This arrangement forms an electrochemical cell with HOPG working electrode bottom, capped by Teflon cover from which counter and reference electrode protrude. The cap contains gas input capillary and optionally can accommodate fiber optic spectroscopic probe respectively. Whole assembly is clamped firmly in the support. The schematic view is shown in Fig. 2 and individual parts of cell are shown in Fig. 3. Area of HOPG electrode is determined by the area of opening in the viton sealing. In our case the area of viton opening is 28 mm^2 and 10 × 10 × 2 mm block of HOPG was employed. Nonaqueous liquid-embedded HOPG electrode is formed by placing o-dichlorobenzene layer with dissolved electrolyte (TBAP) and studied water-insoluble redox system (PC I, PC II or ferrocene) on the basal plane surface of HOPG. The nonaqueous phase in a form of thin layer is in fact embedded to the surface of basal plane HOPG thanks to graphite/o-dichlorobenzene hydrophobic interfacial forces. The nonaqueous layer was then overlaid by aqueous bulk phase containing 0.1 M electrolyte solution.

2.2. Instrumentation

Voltammetric measurements were performed using the potentiostat/galvanostat Wenking POS 2 (Bank Elektronik, Germany) controlled by the CPC-DA software (Bank Elektronik, Germany). A three-electrode system was used for all measurements with a saturated calomel electrode (SCE) or silver wire (Ag) was used as a reference and quasi-reference electrode respectively. Platinum wire served as an auxiliary electrode. The ferrocenium/ferrocene (Fc^+/Fc) redox couple was used

as an internal standard. All experiments were performed at room temperature in solution deoxygenated by bubbling with argon for five minutes. Stock solutions were kept in glass vessels in dark at laboratory temperature.

2.3. Chemicals

Nonaqueous solvent *o*-dichlorobenzene (99%, Aldrich), tetrabutylammonium perchlorate (TBAP, Fluka electrochemical grade, > 98%) and lithium perchlorate ($LiClO_4$, Fluka, p.a.) were used as received. Ferrocene (98%) were purchased from Sigma-Aldrich. Purified water (Milli-Q system Gradient, Millipore, resistivity 18.2 MΩcm) was used for preparation of aqueous electrolytes.

Cobalt tetraneopentoxy phthalocyanine (PC I, Fig. 4) and nickel hexabutyloxy phthalocyanine-C_{60} (PC II, Fig. 4) were synthetized in the laboratory of Tohoku University, Japan, by Kobayashi's group.

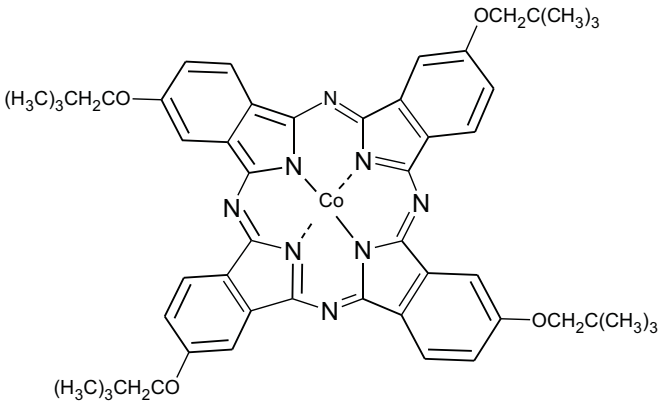

PC I

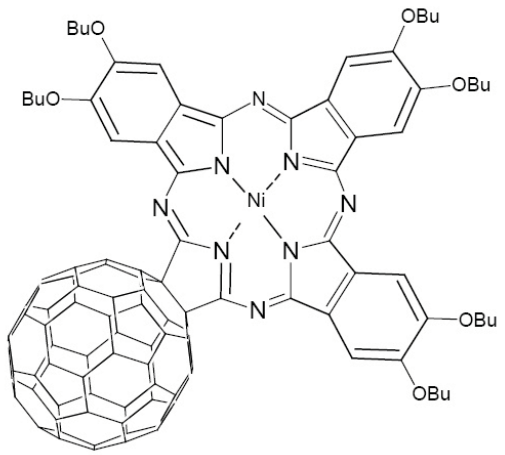

PC II

Fig. 4. Structures of the studies compounds (PC I) cobalt tertaneopentoxy phthalocyanine, and (PC II) nickel hexabutyloxy phthalocyanine-C_{60}.

3. Results and discussion

3.1. Comparison of electrode arrangements

The new electrochemical cell was tested on *o*-dichlorobenzene/water system. The HOPG electrode was covered by the solution of 1×10^{-3} M PC I and 0.1 M tetrabuthylammonium perchlorate in *o*-dichlorobenzene. The aqueous phase contained 0.1 M of lithium perchlorate. The difference between voltammograms acquired in conventional bulk cell and in the new thin-layer cell respectively is illustrated in Fig. 5. Although HOPG mounted in Teflon holder had larger area of electrode surface than that in our new cell, the corresponding peak currents are lower. This effect can be explained by difference in the effective interface area. At HOPG electrode mounted in Teflon, situated upside down in the cell, the interface tends to shrink to the centre of the electrode, uncovering margins of the electrode surface, while our new arrangement allows spreading *o*-dichlorobenzene phase evenly on the basal plane.

3.2. Comparison of ferrocene electrochemical behavior in bulk and thin-layer liquid system

Fig. 6 shows the cyclic voltammograms of ferrocene in *o*-dichlorobenzene measured in the new cell with either the TBAP (curve 1) or in addition it was covered by aqueous phase of 0.1 M $LiClO_4$ (curve 2). We employed

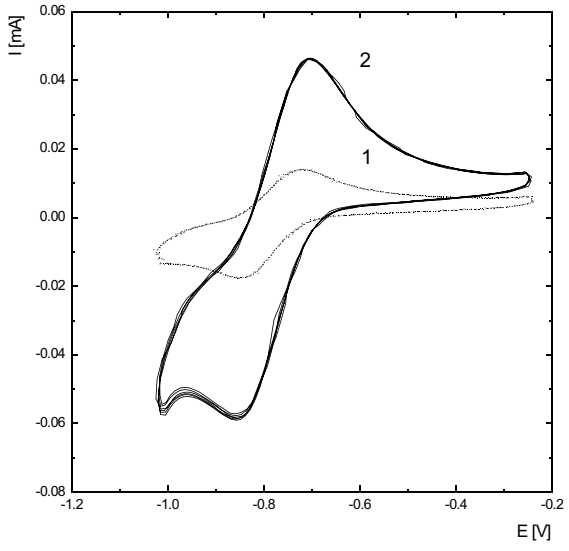

Fig. 5. Cyclic voltammograms of PC I in *o*-dichlorobenzene obtained by (1) HOPG mounted in Teflon (A = 50 mm^2), and (2) HOPG in a new cell arrangement (A = 28 mm^2). Organic phase: c(PC I) = 1×10^{-3} M, c(TBAP) = 0.1 M in *o*-dichlorobenzene; water phase: $c(LiClO_4)$ = 0.1 M, reference electrode SCE, scan rate 100 mV s^{-1}.

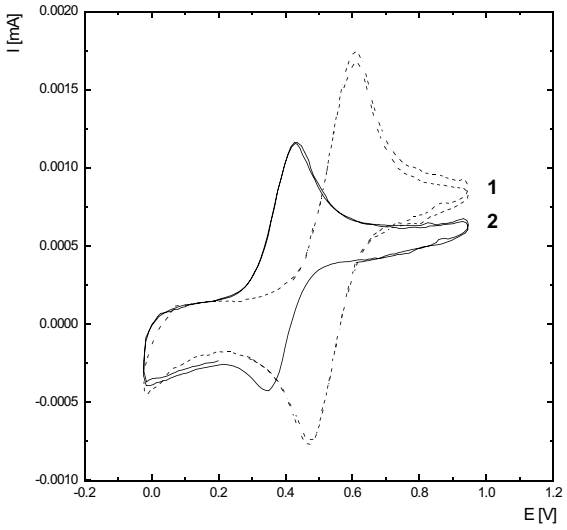

Fig. 6. Cyclic voltammograms of ferrocene in bulk, measured against silver quasi-reference electrode (1) and thin-layer o-dichlorobenzene/water system, measured against SCE in aqueous phase (2). Organic phase: c(ferrocene) = 1×10^{-3} M, *c*(TBAP) = 0.1 M in *o*-dichlorobenzene; water phase: *c*($LiClO_4$) = 0.1 M, reference electrode SCE, scan rate 10 mV s^{-1}.

corresponding reference electrode, silver wire quasi-reference electrode for bulk *o*-dichlorobenzene system and SCE immersed in aqueous phase for thin-layer system respectively. The E_p of ferrocene/ferrocenium couple was found to be higher for bulk *o*-dichlorobenzene system, which indicates a slow electron transfer as was observed by other researches [7]. The peak current ratio of the reverse and the forward scans is equal to unity ($I_{p,a}/I_{p,c}$ = 1.0). The half-wave potential ($E_{1/2}$) of the ferro-cene/ferrocenium couple was determined according to the following equation:

$$E_{1/2} = E_{p,a} - \Delta E_p/2 \quad (1)$$

where $E_{p,a}$ is the anodic peak potential and E_p is the potential difference between the anodic and cathodic peaks ($E_p = E_{p,a} - E_{p,c}$). The values of the half-wave potential were found 542 mV for bulk *o*-dichlorobenzene system and 387 mV for thin-layer *o*-dichlorobenzene/water system. A plot of the anodic ($I_{p,a}$) and the cathodic peak ($I_{p,c}$) against the square root of the scan rate ($v^{1/2}$) results in a straight line confirms that the oxidation process of ferrocene is reversible and diffusion controlled in the *o*-dichlorobenzene.

3.3. Phthalocyanines

The new electrochemical cell has been designed preferentially for electrochemistry of new synthesized phthalocyanines, available often in mg quantities only. As a model compound PC I was chosen. The redox behaviour of this compound was observed in two experimental settings: The first was Nonaqueous Liquid-Embedded Electrode (NLEE) where the interface *o*-dichlorobenzene/water interface was used. At the second experimental setting only *o*-dichlorobenzene solution was employed. The comparison of cyclic voltammograms is shown in Fig. 7. Potential shifts are ascribed to different reference electrodes used, while characteristic PC I redox peaks [8] can be identified in both voltammograms.

According to our best knowledge [9] the electrochemistry of PC I has been performed only in bulk nonaqueous solution yet, where conventional measurements consumed orders of magnitude higher amounts of phthalocyanines.

Thanks to NLEE PC II have been investigated and Fig. 8 displays cyclic voltammograms of PC II in thin-layer o-dichlorobenzene/water system. The half-wave potentials of the couples are listed in Tab. 1, and were determined on the basis of the cyclic voltammograms. The mostly observed processess belong to C_{60}-centered as shown in Tab. 1.

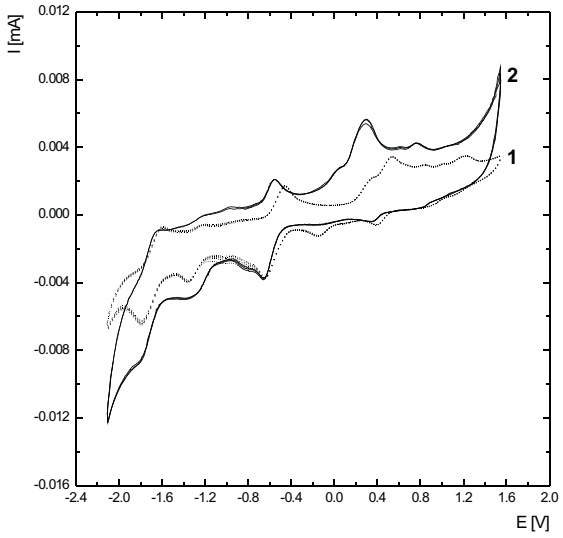

Fig. 7. Cyclic voltammograms of PC I in bulk, measured against silver quasi-reference electrode (1) and thin-layer *o*-dichlorobenzene/water system, measured against SCE in aqueous phase (2). Organic phase: c(PC I) = 1×10^{-3} M, *c*(TBAP) = 0.1 M in *o*-dichlorobenzene; water phase: *c*($LiClO_4$) = 0.1 M, reference electrode SCE, scan rate 10 mV s^{-1}.

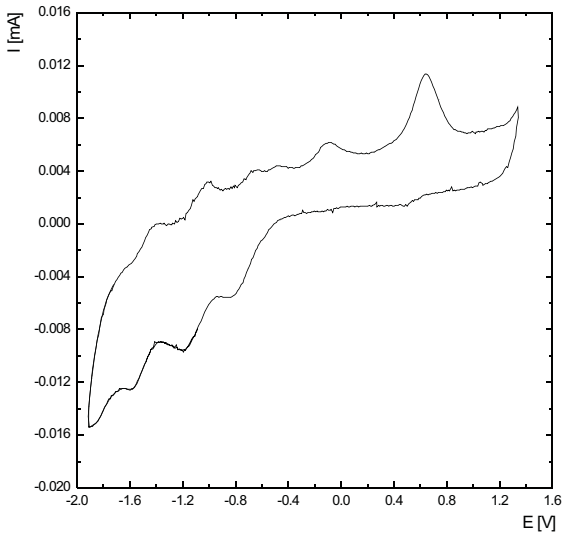

Fig. 8. Cyclic voltammograms of PC II in *o*-dichlorobenzene measured against SCE. c(PC II) = 1×10^{-3} M, *c*(TBAP) = 0.1 M, scan rate 10 mV s^{-1}.

Table 1. Redox potentials PC II *vs.* (Fc^+/Fc) in thinlayer *o*-dichlorobenzene/water system, measured against SCE in aqueous phase. Organic phase: c(PC II) = 1×10^{-3} M, *c*(TBAP) = 0.1 M in *o*-dichlorobenzene; water phase: *c*($LiClO_4$) = 0.1 M, scan rate 10 mV s^{-1}.

E_p, V	compound	
	PC II	C_{60} [a]
4th red.	–1.92	–2.36
3rd red.	–1.52	–1.90
2nd red.	–1.16	–1.46
1st red.	–0.54	–1.07
1st ox.	–0.14	–

[a] Reference [5]

4. Conclusions

In this article, we have presented new design of an electrochemical cell allowing simple mounting of a HOPG electrode virtually of variety of shapes and thicknesses allowing conventional cleaning by the adhesive tape, but other electrode materials can be used as well. The cell arrangement is suitable for electrochemical experiments utilizing mg-amounts of compounds soluble in nonaqueous solvents, though also surface electrochemistry and aqueous solutions can be employed. Low residual currents reached thanks to quality viton sealing, large surface area of the electrode, fast response as well as fast bulk electrolysis option is among its advantages. As it was presented here, electrochemical measurements of model compounds soluble in nonaqueous solvents including phthalocyanines and ferrocene respectively, yielded data consistent with those obtained in classical (bulk) single-phase electrochemical cell arrangement.

The redox activity of PC II showed four reversible reduction and one oxidation peak. Three reduction peaks belongs to C_{60}.

Acknowledgements. *We are grateful to N. Kobayashi, Tohoku University, Japan for supplying phthalocyanines used in this work. This work was supported by the research project MSM0021620857 and the development project RP 14/63 of the Ministry of Education Youth and Sports of the Czech Republic.*

References

[1] Ke M. S., Xue L., Feyes D. K., Azizuddin K., Baron E. D., McCormick T. S., Mukhtar H., Panneerselvam A., Schluchter M. D., Cooper K. D., Oleinick N. L., Stevens S. R.: *Photochem. Photobiol.* **84** (2008), 407–414.
[2] Mir Y., Houde D., van Lier J. E.: *Lasers Med. Sci.* **23** (2008), 19–25.
[3] Samec Z., Mareček V., Koryta J., Khalil M. W.: *J. Electroanal. Chem.* **83** (1977), 393–397.
[4] Samec Z., Mareček V., Homolka D.: *Faraday Discuss. Chem. Soc.* **77** (1984), 197–208.
[5] Fukuda T., Masuda S., Kobazashi N.: *J. Am. Chem. Soc.* **129** (2007), 5472–5479.
[6] Shi Ch., Anson F. C.: *Anal. Chem.* **70** (1998), 3114–3118.
[7] Tsierkezos N. G.: *J. Solution Chem.* **36** (2007), 289–302.
[8] Lever A. B. P., Hempstead M. R., Leznoff C. C., Liu W., Melnik M., Nevin W. S., Seymour P.: *Pure Appl. Chem.* **58** (1986), 1467–1476.
[9] Yu B., Lever A. B. P., Swaddle T. W.: *Inorg. Chem.* **43** (2004), 4496–4504.

Separations of Biologically Active Peptides on Zirconia-Based Columns

Lucie Janečková[a], Jana Sobotníková[a], Eva Tesařová[b], Zuzana Bosáková[a]

[a] *Department of Analytical Chemistry,* [b] *Department of Physical and Macromolecular Chemistry, Faculty of Science, Charles University in Prague, Albertov 6, 128 43 Prague 2, Czech Republic,* ✉ *lucie.janeckova@t-email.cz*

Abstract

In this work, RP-HPLC methods using zirconia-based columns have been developed for the separation of biologically active nonapeptides from the group of vasopressins. Zirconium dioxide is an alternative carrier to silica gel and apart from its excellent stability it offers additional interactions, which are helpful in the separation of ionizable compounds. Chromatographic behavior of the analytes was studied on two zirconia reversed phases, zirconium dioxide modified with polybutadiene and polystyrene. The influence of mobile phase composition (namely pH, concentration of the buffer and buffer-to-acetonitrile ratio) and temperature on chromatographic parameters (retention, separation efficiency, resolution and symmetry of peaks) was investigated in detail.

Keywords

biologically active peptides
optimization of separation
RP-HPLC
zirconium dioxide carrier

1. Introduction

Research and analysis of biologically active compounds represents an important part of science, especially biochemistry, analytical chemistry, molecular biology, pharmacology and medicine. Modern analytical chemistry aims at development of selective and efficient separation methods such as high performance liquid chromatography (HPLC), which provides fast, efficient separations with high resolution [1]. This technique can be successfully applied to the separation of biologically active peptides, compounds of weak or strong basic character [2].

Reversed separation mode (RP) has dominant position in HPLC [3] due to its versatility and applicability to a wide range of analytes. Commonly used carrier of stationary phases in RP-HPLC is silica gel. Its particles are mechanically stable and have large surface, which can be easily modified. The major disadvantage of silica gel is its low chemical and thermal stability. Restriction in pH ranges of mobile phases is a limiting factor especially in the separations of basic compounds. Siloxane bond (Si-O-Si) is unstable in acidic solutions (pH below 2) while at higher pH values (above pH 8) silica gel hydrolyses [4, 5]. Increased separation temperature leads to gradual loss of the bonded phase. Moreover, residual silanol group activity affects negatively retention and peak symmetry of the analytes [6]. These are the reasons to replace silica-based phases with phases of higher stability.

In an effort to develop alternatives to silica-based stationary phases, other support materials have been investigated. Research of some metal oxides (ZrO_2, TiO_2, Al_2O_3) led to interesting results [7]. Among these oxides, zirconium dioxide has shown the most promising quality [8–10]. Zirconium dioxide is an amphoteric oxide providing cation- or anion-exchange interactions, which depend on solution pH and nature of the buffer used. Compounds of ionic character can interact with the carrier surface by secondary (ion-exchange) interactions, which can significantly affect selectivity and retention of the analytes. Atom of zirconium in the structure Zr-O-Zr has free *d*-orbitals and can accept free electron pairs. It acts as Lewis acid and thus it can interact with Lewis bases, such as phosphate, fluoride, acetate, carboxyl ions or hydroxyl groups [11]. These components of mobile phases strongly adsorb on ZrO_2 surface, which is being dynamically modified. Adsorbed Lewis base acts as an ion-exchange group and can take part in ion-exchange interactions with ionizable analytes. Fig. 1 shows the described interaction mechanism on ZrO_2 surface.

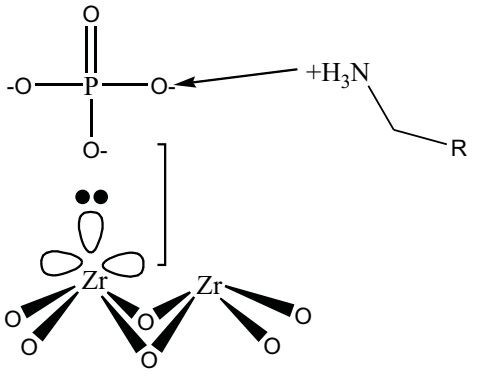

Fig. 1. Interaction mechanism on zirconium dioxide surface.

Some organic polymers were used for modification (hydrophobization) of ZrO_2 surface and thus decrease of its polarity. There are commercially available zirconia--based stationary phases, such as polybutadiene (PBD) and polystyrene (PS), which are stable in the whole pH range (1–14) and at temperatures up to 200 °C and which can be used in the reversed mode of HPLC. Separation is based on hydrophobic interactions of analytes with stationary phase and on ion-exchange interactions with adsorbed Lewis base. This mixed retention mode can be successfully applied to the separation of peptides [9].

Nonapeptides, vasopressin, oxytocin and other structurally and functionally related peptides show biological activity not only in human body. Table 1 shows amino acid sequences of the peptides studied in this work. Arg-vasopressin (AVP), also known as antidiuretic hormone (ADH), has physiological function in kidneys. It regulates retention of water and increases its reabsorption [12]. Arg-vasopressin also increases blood pressure by inducing vasoconstriction. Decreased AVP level in blood or decreased renal sensitivity to AVP leads to disease called diabetes insipidus. Oxytocin (OXY) is a mammalian hormone that also acts as a neurotransmitter in brain. It affects final period of gravidity, birth and injection of milk. In medical treatment, oxytocin is used to stimulate contractions of the uterus. Arg-vasotocin (AVT) is an evolutional ancestor of the mentioned peptides and can be found in vertebrates such as birds, reptiles, fishes and amphibians. Arg-vasotocin has similar effects to Arg-vasopressin. Another analogue is Lys-vasopressin (LVP), which has lower antidiuretic activity than Arg-vasopressin and which is often used in human therapy. Current research of physiological functions of nonapeptides aims at the processes of learning and memorizing, social and sexual behavior, anxiety, depression and agressiveness [13–15].

In this work, two alternative phases (polybutadiene and polystyrene) based on ZrO_2 were examined and successfully used for the separation of biologically active nonapeptides from the group of vasopressins. The separation conditions were optimized, *i. e.* effect of mobile phase composition (type, concentration and pH of buffer, type and amount of organic modifier) and effect of temperature on separation parameters (retention factor, efficiency, resolution, peak symmetry) of analytes were studied in detail.

2. Experimental

All chromatographic measurements were performed with Ecom chromatographic system (Ecom, Czech Republic), equipped with gradient pump Ecom Beta 10, UV-VIS detector Sapphire 800 and vacuum degasser Ecom DG 3014. Manual injection was performed using a Rheodyne Model 7125 injection valve (Cotati, USA) with 5 μL internal injection loop. Column thermostat LCO 101 (Ecom, Czech Republic) was used to control column temperature. Clarity software (Data Apex, Czech Republic) was used for data collection and evaluation.

Two analytical columns, Discovery Zr-PBD and Discovery Zr-PS (Supelco, Bellefonte, PA, USA) were used for separation. Both columns had the same parameters (25 cm × 4,6 mm; particle size 5 μm; pore size 300 Å).

Acetonitrile Chromasolv for HPLC was obtained from Sigma-Aldrich. Sodium phosphate monobasic and sodium phosphate dibasic were purchased from Penta (Czech Republic), phosphoric acid and sodium hydroxide were obtained from Lachema (Czech Republic). Uracil (99%), used as a dead time marker, was supplied by Sigma-Aldrich. Deionised water was prepared using a Milli-Q water system (Millipore, Milford, USA).

Separated nonapeptides listed in Table 1 were all products of Sigma-Aldrich.

Mobile phases were generally composed of phosphate buffer and acetonitrile as organic modifier, flow rate was 1.0 mL min^{-1}. Detection wavelenght was set at 214 nm.

3. Results and discussion

Separation of a set of four nonapeptides (oxytocin, Arg-vasotocin, Arg-vasopressin, Lys-vasopressin) was studied on two stationary phases based on ZrO_2, *i. e.* Discovery Zr-PBD (polybutadiene modified zirconia) and Discovery Zr-PS (polystyrene modified zirconia). Optimization of the separation was performed by altering separation conditions. Changes of ionic strength, pH and composition of mobile phase and also temperature influence the separation process. Therefore effect of the buffer pH and concentration, the ratio of organic modifier in the mobile phase and separation temperature

Table 1. Amino acid sequences of studied nonapeptides

Peptide	Abbrev.	Sequence of amino acids
Oxytocin	OXY	Cys-Tyr-Ile-Gln-Asn-Cys-Pro-Leu-Gly
Arg-vasotocin	AVT	Cys-Tyr-Ile-Gln-Asn-Cys-Pro-Arg-Gly
Arg-vasopressin	AVP	Cys-Tyr-Phe-Gln-Asn-Cys-Pro-Arg-Gly
Lys-vasopressin	LVP	Cys-Tyr-Phe-Gln-Asn-Cys-Pro-Lys-Gly

were studied in detail. Each optimization step included evaluation of retention factors k, resolution values R_S and factors of asymmetry A_S of the analytes.

Starting conditions on both zirconia-based RP columns were based on previous experiments with pentapeptides [16] that led to the following results. Firstly, a great difference between two common organic modifiers, methanol and acetonitrile, was observed for the separation of peptides. Acetonitrile provided higher separation efficiency as well as shorter retention times, better peak shapes and lower backpressure than methanol. Secondly, the effect of buffer type was studied, because the type of buffer strongly affects the interactions between analytes and ZrO_2 surface. Acetate and phosphate buffers were investigated. The results showed that retention of the analytes increased if phosphate buffer was used. It is a stronger Lewis base than acetate and thus it enhances ion-exchange interactions.

Following features that were observed on both columns showed their similarity. Chromatographic behavior of the analytes did not alter much on the both stationary phases; trends in retention of the analytes with altering separation conditions were identical or very similar.

Optimization process started with the variation of buffer pH. Starting mobile phase was composed of acetonitrile and 50 mM phosphate buffer in the ratio 20/80 (v/v). The effect of pH of the phosphate buffer was studied in the range 4–12 on both columns. Higher pH led to lower retention of the analytes. This can be explained by higher deprotonization of the analytes leading to decreased ion-exchange interactions with adsorbed phosphate ions. Lower pH of the buffer led to increased retention and resolution improvement but also peaks symmetry deteriorated. The analytes are more charged in acidic solution and ion-exchange interactions are much stronger than at higher pH. Higher pH was thus found advantageous for separation of nonapeptides; the optimized pH value was 10 and 9 on Discovery Zr-PBD and Discovery Zr-PS, respectively.

Concentration of the buffer is an important factor that affects ion-exchange mechanism on ZrO_2 columns. Therefore, in the next step, the influence of phosphate buffer concentration in the range 10–100 mM was tested. Results showed that increase of buffer concentration led to decreased retention and better peak symmetry. Higher buffer concentration (abundance of phosphate ions) means competition between buffer and analyte molecules for the interaction sites on ZrO_2 surface. Application of lower buffer concentration led to increase of retention, which was accompanied by an improvement of resolution of the analytes. Zirconium dioxide surface mostly interacts with buffer ions. This interaction has positive effect on ion-exchange mechanism. Suppression of the ion-exchange type of interaction makes the hydrophobic interaction a more important contribution to the retention mechanism.

Phosphate buffer concentrations of 40 mM (pH = 10) and 50 mM (pH = 9) were used on Discovery Zr-PBD and Discovery Zr-PS, respectively, in the experiments to assess the effect of organic modifier to buffer ratio. Lower content of acetonitrile in mobile phase means lower elution strength and this was the reason for higher retention of the analytes. They interacted more strongly with non-polar stationary phase. In contrary, higher content of acetonitrile led to lower retention of the analytes, which had then higher affinity to the mobile phase. Application of mobile phase containing only 5% (v) of acetonitrile on Discovery Zr-PS led to efficient separation of the analytes. This result confirmed the manufacturer's specification that this column can be used with nearly aqueous mobile phase.

Discovery Zr columns are designed for work at higher temperatures. Generally, elevated temperature decreases viscosity of mobile phase, it speeds up mass transfer during the separation process and thus it can positively influence the separation. The effect of temperature on separation of nonapeptides was studied in the range 25–75 °C. Higher temperature caused retention decrease, improvement of peak symmetry but resolution of some analytes deteriorated.

Optimized conditions for the separation of nonapeptides on Discovery Zr columns resulted from evaluation of all the optimized data. Discovery Zr-PBD

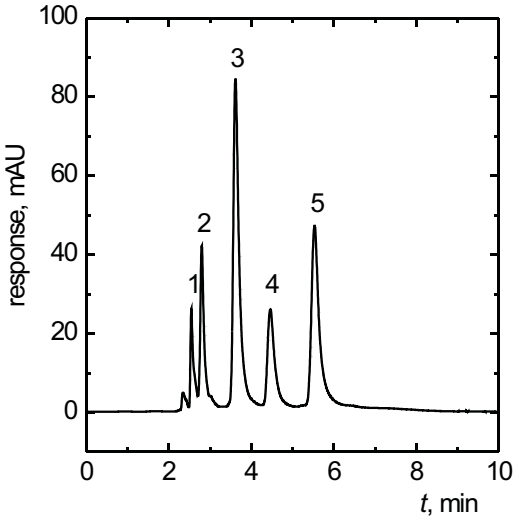

Fig. 2. Optimized separation of nonapeptides on Discovery Zr-PBD; mobile phase acetonitrile/40 mM phosphate buffer, pH = 10, 18/82 (v/v); temperature 45 °C; flow rate 1 mL min^{-1}; injection 5 μL; detection 214 nm. Peak identification: (1) uracil, (2) oxytocin, (3) Arg-vasotocin, (4) Arg-vasopressin, (5) Lys-vasopressin.

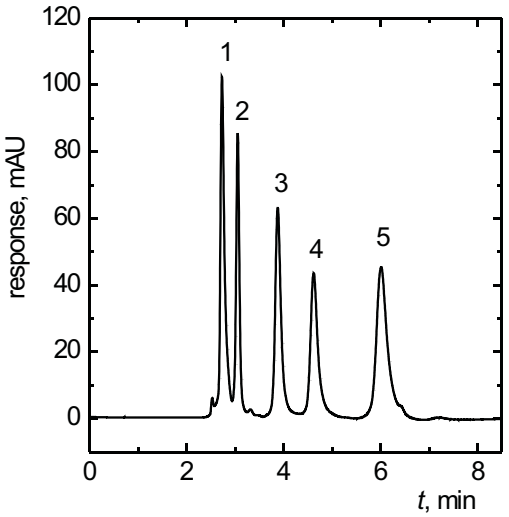

Fig. 3. Optimized separation of nonapeptides on Discovery Zr-PS; mobile phase acetonitrile/50 mM phosphate buffer, pH = 9, 5/95 (v/v); temperature 45 °C; flow rate 1 mL min^{-1}; injection 5 μL; detection 214 nm. Peak identification: (1) uracil, (2) oxytocin, (3) Arg-vasotocin, (4) Arg-vasopressin, (5) Lys-vasopressin.

provided the best separation under these conditions: mobile phase acetonitrile/40 mM phosphate buffer, pH = 10, 18/82 (v/v), temperature 45 °C. The most suitable conditions for the separation of nonapeptides on Discovery Zr-PS were following: mobile phase acetonitrile/50 mM phosphate buffer, pH = 9, 5/95 (v/v), temperature 45 °C. Figs. 2 and 3 show chromatograms obtained under optimized conditions on Discovery Zr-PBD and Discovery Zr-PS, respectively. The separation time did not exceed six minutes.

In order to better understand the interactions that participate in the retention mechanism on these ZrO_2 based reversed phases linear free energy relationship model will be performed.

4. Conclusions

Chromatographic behavior of four biologically active nonapeptides was studied on two alternative reversed phases based on ZrO_2; *i. e.* Discovery Zr-PBD and Discovery Zr-PS with polybutadiene and polystyrene stationary phases, respectively. Experiments showed similar behavior of the both columns for the separation of nonapeptides. Trends in retention of the analytes with altering the separation conditions were almost the same. Efficient separation on column Discovery Zr-PS was achieved using only 5% (v) of acetonitrile in mobile phase. This is the main reason why the polystyrene modified stationary phase is preferable. The separation conditions are gentle and environment-friendly, biological activity of the analytes is maintained and the amount of organic modifier is reduced.

Reversed phases based on ZrO_2 seem to be a good alternative to silica-based columns, especially for separation of basic compounds. Different retention (interaction) mechanism, wide possibility of surface modification, high chemical and thermal stability are the main advantages, which can result in successful separations of other biomolecules.

Acknowledgements. *The research projects MSM 0021620857 and RP14/63 of the Ministry of Education, Youth and Sports of the Czech Republic are gratefully acknowledged for the financial support.*

References

[1] Buszewski B., Kowalska S., Kowalkowski T., Rozpędowska K., Michel M., Jonsson T.: *J. Chromatogr. B* **845** (2007), 253.
[2] Mant C. T., Hogdes R. S.: *High Performance Liquid Chromatography of Peptides and Proteins: Separation, Analysis and Conformation.* CRC Press, Boca Raton 1991.
[3] Claessens H. A., van Straten M. A.: *J. Chromatogr. A* **1060** (2004), 23.
[4] Nawrocki J.: *J. Chromatogr. A* **779** (1997), 29.
[5] Andersen T., Nguyen Q. N. T., Trones R., Greibrokk T.: *J. Chromatogr. A* **1018** (2003), 7.
[6] Trammell B., Ma L., Luo H., Jin D., Hillmayer M. A., Carr P. W.: *Anal. Chem.* **74** (2002), 4634.
[7] Nawrocki J., Dunlap C., McCormick A., Carr P. W.: *J. Chromatogr. A* **1028** (2004), 1.
[8] Zhao J., Carr P. W.: *Anal. Chem.* **71** (1999), 5217.
[9] Sun L., Carr P. W.: *Anal. Chem.* **67** (1995), 2517.
[10] Dunlap C. J., McNeff C. V., Stoll D., Carr P. W.: *Anal. Chem.* **73** (2001), 598A.
[11] Nawrocki J., Rigney M. P., McCormick A., Carr P. W.: *J. Chromatogr. A* **657** (1993), 229.
[12] Lüllmann H., Mohr K., Ziegler A., Bieger D.: *Barevný atlas farmakologie*. 2. vyd. Praha, Grada Publishing 2001, str. 164 a 234.
[13] Do-Rego J.-L., Acharjee S., Seong J. Y. *et al.*: *J. Neurosci.* **26** (2006), 6749.
[14] Keverne E. B.; Curley J. P.: *Curr. Opin. Neurobiol.* **14** (2004), 777.
[15] Storm E. E., Tecott L. H.: *Neuron* **47** (2005), 483.
[16] Soukupová K., Krafková E., Suchánková J., Tesařová E.: *J. Chromatogr. A* **1087** (2005), 104.

The Effect of Natural and Synthetic Entangled Polymers on Separation of Peptides and Proteins by Capillary Electrophoresis

Tomáš Křížek[a], Pavel Coufal[a], Eva Tesařová[b], Zuzana Bosáková[a]

[a] *Department of Analytical Chemistry,* [b] *Department of Physical and Macromolecular Chemistry, Faculty of Science, Charles University in Prague, Albertov 2030, 128 43 Prague 2, Czech Republic,* ✉ *krizek@natur.cuni.cz*

Abstract

Conversion of gel electrophoresis methods to capillary format brings several advantages. These are namely reduced consumption of sample and reagents and shorter analysis time. However, polyacrylamide gel that is traditionally used in slab gel electrophoresis exhibits significant UV-absorption, which negatively influences sensitivity of UV-detection. Two non-absorbing non-cross-linked polymers were tested in this work – polysaccharide dextran as frequently used representative of natural gels and synthetic co-polymer Pluronic F-127. Both gel-forming agents were compared in terms of selectivity, separation power and repeatability of migration times, when used for separation of amino acids, peptides and low-molecular-weight proteins in bare silica capillary under low-pH conditions. Selectivity of both the agents was found to be similar. However, the Pluronic gel provided slightly higher separation power. Repeatability of migration times was greatly influenced by rather difficult removal of dextran from capillary. In this respect, Pluronic F-127 well surpassed dextran.

Keywords

capillary gel electrophoresis
entangled polymers
peptides
proteins
proteomics

1. Introduction

Electromigration separation methods belong to well--established and powerful proteomic tools. Techniques like sodium dodecyl sulphate polyacrylamide gel electrophoresis (SDS-PAGE) or isoelectric focusing (IEF) are capable of efficient separation of proteins and products of their digestion – peptides. Nevertheless, miniaturization, as a general trend in analytical chemistry, does not elude the field of proteomics. In general, conversion of an analytical method to capillary format brings several advantages such as reduced sample and reagents consumption, shortened analysis time or possibility of automated processing of hundreds of samples [1]. It is obvious that miniaturization improves parameters that are important for commercial application of methods and thus it is a matter of great research interest even in proteomics. However, conversion of a gel electrophoresis method to a capillary gel electrophoresis (CGE) method is not a trivial task as the most commonly used polyacrylamide gel exhibits relatively strong UV-absorption which means serious limitation of sensitivity and detection limits when UV-detector is used [2]. Another complication lies in rather short lifetime of gels, which are not reused in slab gel electrophoresis. Instead, they are disposed or stored for further evaluation. Common cross-linked polymers are very difficult to remove from capillary and replacing whole the capillary after each analysis would increase the cost of analysis unacceptably, speaking nothing of technical difficulties and impossibility of automation. Therefore, other gel-forming agents were tested in order to find a suitable substitute for polyacrylamide in CGE [3–5]. These agents should be UV-transparent to allow sensitive detection. The problem of replacement of the gel in capillary can be solved by application of so called physical gels that are not chemically cross-linked. Three--dimensional net of these polymers is formed by physical entanglement of their chains, from which their other name, entangled polymers, originates. These gels possess lower viscosity and can be washed out of capillary easier than the chemical ones because they consist of individual chains and they are not chemically bound to the inner wall of capillary.

Among some other entangled, UV-transparent, natural polymers, dextran was successfully applied for separation of peptides and proteins by several research groups [6–8]. This gel was used usually in a pH range from 8 to 10 for separation of proteins according to their molecular mass. Dextran is a branched glucan that is produced from sucrose by certain bacteria, *e. g. Leuconostoc mesenteroides.* Glucose units in the main chain of dextran are connected with α-1,6 glycosidic bonds while side branches arise from α-1,4 (in some cases even α-1,2 and α-1,3) bonds. Figure 1 shows the above described structure of dextran. Apart from natural polymers, many synthetic ones were tested as potential separation media for CGE of proteins and peptides, among them, polyethyleneglycol [8, 9] and polyvinyl-alcohol [6] play important roles. Also, linear polyacrylamide should be mentioned although it possesses the already mentioned disadvantage of significant

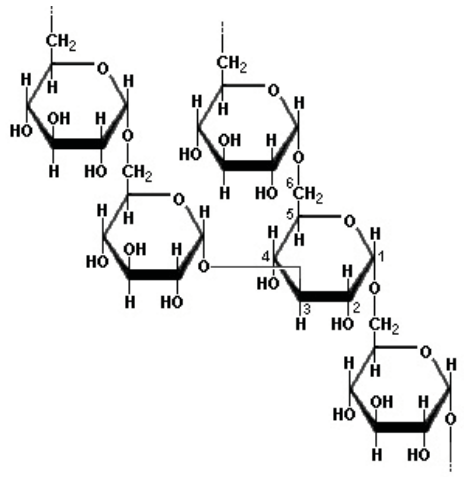

Fig. 1. Structure of dextran.

UV-absorption [2]. Interesting is utilization of thermo--responsive polymers, which change their behaviour according to temperature. Representative of this class of polymers called Pluronic F-127 has been tested as a separation medium for peptides and proteins by research group of Mikšík [10–14]. Pluronic F-127 is a member of Pluronic thermo-responsive co-polymers family. Pluronics are composed of three blocks as can be seen from Figure 2. Outer parts consist of polyethyleneoxide (PEO) while the middle block contains polypropyleneoxide (PPO). It is obvious that the middle part of Pluronic molecule is more hydrophobic than the PEO outer blocks. When a certain concentration level of polymer and certain temperature are reached, PPO blocks of several molecules associate creating core of a micelle-like object and less hydrophobic PEO outer blocks are pointing outside into the surrounding solution in a brush-like manner. Various Pluronic co-polymers differ in size of the three blocks, which alters their "association temperature".

Mikšík et al. added Pluronic F-127 into acid buffers with or without addition of SDS. They reported more or less successful separations of protein digests and some low-molecular-weight proteins. However, certain difficulties with current and signal stability occurred and thus the authors recommended use of wall-coated capillaries with Pluronic gel. In this work, we report a way to overcome this problem even in bare silica capillary. This work also brings a comparison of two gel-forming agents important in CGE separation of proteins and peptides, dextran and Pluronic F-127, in terms of selectivity and repeatability of migration times.

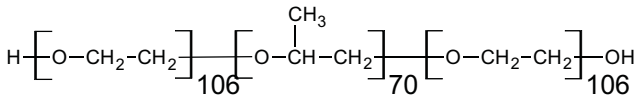

Fig. 2. Structure of Pluronic F-127.

2. Experimental

2.1. Chemicals

Phosphoric acid, 85 %, and sodium hydroxide, p. a., were obtained from Lachema (Czech Republic). Dextran from *Leuconostoc mesenteroides*, M_r ~ 2,000,000; Pluronic F-127; *L*-tyrosine, reagent grade ≥ 98%; *L*-tryptophan, reagent grade ≥ 98%; *L*-histidine, reagent grade ≥ 98%; Val-Tyr-Val, acetate salt; leucine enkephalin, acetate salt; angiotensin I, acetate salt, and angiotensin II, acetate salt, were purchased from Sigma (USA). Aprotinin from bovine lung, cytochrome C from bovine heart and lysozyme from hen egg white were purchased from Fluka (Switzerland). Buffers were prepared using deionised water produced by a Mili-Q system (Millipore, USA).

2.2. Instrumentation and experimental conditions

All experiments were performed on a CE^{3D} instrument (Agilent Technologies, Germany). Undeactivated fused silica capillaries, 75 μm i. d., were purchased from Agilent Technologies (Germany) and cut to 49.0/40.5 cm length. Detection window was burnt with butane flame. Capillary cassette temperature was maintained at 25 °C by air-cooling system, separation voltage was set to 20 kV and a pressure of 1 kPa (2 kPa for gel concentrations higher than 5%) was applied to inlet buffer vial during the run. Samples were injected by a pressure of 5 kPa for 3 s. The diode array detector collected data within the range of 200–400 nm and 200 nm wavelength, exhibiting the highest sensitivity, was used for the data evaluation. 20 mM phosphate buffer, pH = 2.5, was used for all experiments with eventual addition of appropriate amount of dextran or Pluronic F-127. Samples were prepared dissolving amino acids, peptides and proteins in 20 mM phosphate buffer, pH = 2.5.

3. Results and discussion

Dextran and Pluronic F-127 were tested as separation media for CGE separation of peptides and low-molecular-weight proteins. Measurements were carried out in separation buffer of pH = 2.5 so that silanol groups on the inner capillary wall were mostly protonated, which suppressed electroosmotic flow and adverse adsorption of peptides and proteins on the silica surface. All the analytes were positively charged so that they were migrating relatively fast towards cathode. Before Pluronic F-127 could be used for separation of analytes, the problem mentioned in the introduction had to be solved.

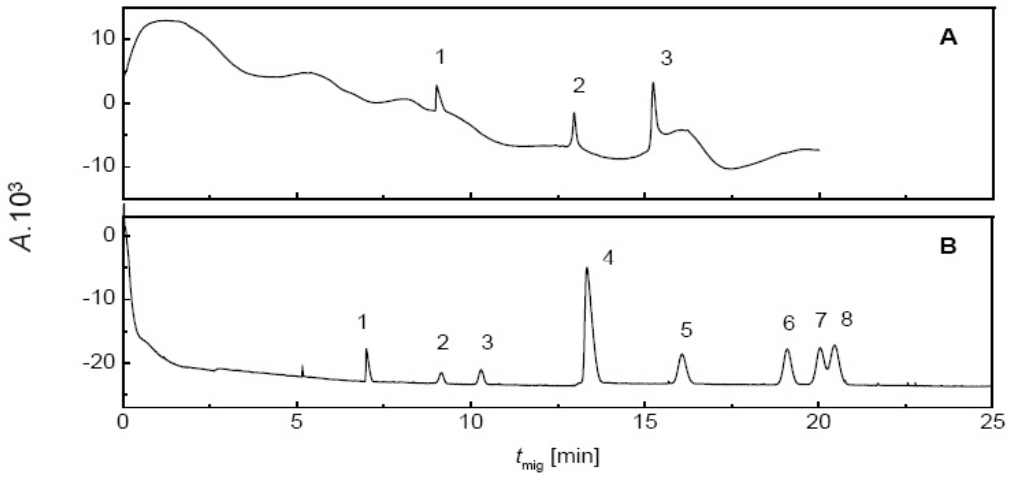

Fig. 3. Separation of amino acids and peptides in 20 mM phosphate buffer, pH = 2.5, with 5 % Pluronic F-127 without (A) and with (B) 1 kPa pressure applied on the inlet buffer vial. Peaks: (1) histidine, (2) angiotensin I, (3) angiotensin II, (4) Val-Tyr-Val, (5) leu enkephalin, (6) tryptophan, (7) phenylalanine, (8) tyrosine. Concentrations: 0.05 mg mL^{-1}, angiotensins 0.025 mg mL^{-1}.

Figure 3 illustrates instabilities of signal during analysis with 5% Pluronic F-127. This adverse effect was suppressed sufficiently when a pressure of 1 kPa was applied to the inlet buffer vial. When concentration of Pluronic was increased to 7.5%, instabilities occurred again which was solved by rising the applied pressure to 2 kPa. The reason for this behaviour is not obvious but it seems that assuring some slow but steady flow in capillary solves the problem effectively.

Figure 4 shows the effect of the additives on mobilities of the testing set of analytes. It is obvious that selectivity of both the gels is very similar. Effect on mobilities of amino acids and peptides is practically the same, which is indicated by nearly collinear curves of these analytes. Histidine represents the only exception. Its mobility is affected less than mobility of other amino acids. This is because histidine is doubly charged under the experimental conditions employed and thus possesses significantly higher charge-to-mass ratio than the other analytes. Rather sharp decrease in relative mobilities of all three proteins at concentrations of gel higher than 5% can be explained by sieving effect beginning to take place in these concentrations. As a measure of the separation power, separation of amino acids phenylalanine and tyrosine and proteins aprotinin, cytochrome C and lysozyme, can be taken. Separation of phenylalanine and tyrosine starts at 5% concentration of both gels. For separation of aprotinin and lysozyme, 5% of dextran is necessary while sufficient concentration of Pluronic is only 2.5%. All three proteins are successfully separated in 10% Pluronic F-127 and cannot be separated by dextran in the tested concentration range. From the above described observations, it is obvious that separation power of Pluronic F-127 is higher.

Both of the gel-forming agents form entangled polymers that should be easy to remove from capillary.

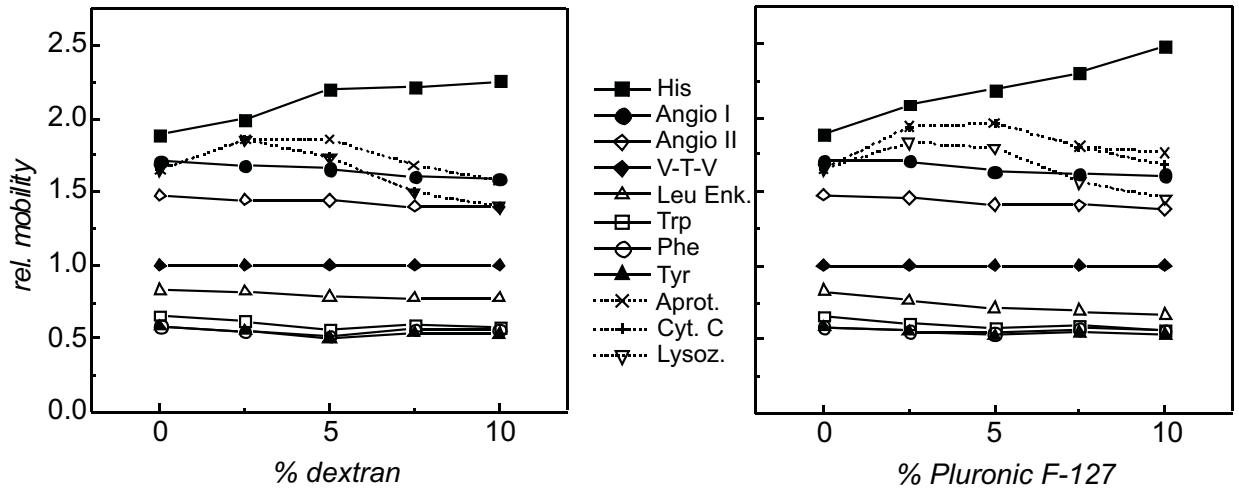

Fig. 4. Effect of dextran and Pluronic F-127 additives on mobility of aminoacids, peptides and proteins. Mobilities are related to mobility of Val-Tyr-Val peptide.

Table 1. Repeatability of migration times (n = 5) with 5% dextran and Pluronic F-127 gels in 20 mM phosphate buffer, pH = 2.5.

Analyte	RSD [%]	
	dextran	Pluronic F-127
L-histidine	1.88	0.43
Angiotensin I	2.83	0.24
Angiotensin II	2.43	0.11
Val-Tyr-Val	3.29	1.14
Leucine enkephalin	3.82	0.74
L-tryptophan	4.59	0.33
L-phenylalanine	2.95	0.37
L-tyrosine	5.06	0.34
Aprotinin	1.35	0.14
Cytochrome C	1.35	0.14
Lysozyme	1.35	0.19

However, replacement of dextran gel proved to be more problematic than it was expected. To remove dextran properly, approx. 40 minute-long flushing procedure, including flush with sodium hydroxide and hydrochloric acid solutions, was necessary. According to the work published by Ganzler et al. [8], dextran can be used also for dynamic coating of capillary walls. This can explain its tendency to remain in the capillary and to modify its electrophoretic properties probably due to accumulation of dextran on the walls. Even if aforementioned time-consuming rinsing procedure was employed the repeatability of migration times was rather unsatisfactory, as can be seen from Table 1. On the other hand, separation buffer containing Pluronic F-127 provided acceptable repeatability with only short flushes of capillary with water between consecutive runs. The repeatability of migration times for all testing analytes is summarized in Table 1.

4. Conclusions

An addition of Pluronic F-127 into separation buffer can cause certain signal and current instabilities. However, this problem can easily be solved by applying a low pressure to the inlet buffer vial during the analysis. On the other hand, buffers containing Pluronic F-127 as the additive possess lower viscosity than buffers with dextran, which results in easier manipulation. Pluronic F-127 shows similar selectivity and higher separation power for the peptides and proteins tested than dextran. There are also no problems with repeatability of migration times or with proper replacement of the gel after each run. In this respect, dextran proved to be rather problematic under the experimental conditions employed. From the above mentioned facts, we can conclude that Pluronic F-127 can successfully compete with dextran as the separation medium for capillary gel electrophoretic separations of peptides and proteins.

Acknowledgements. *This work was financially supported by the Czech Science Foundation, project No. 203/070392, and by the Ministry of Education, Youth and Sports of the Czech Republic, project No. MSM0021620857.*

References

[1] Mermet J. M., Otto M., Kellner R. A., Widmer M. M.: *Analytical Chemistry A Modern Approach to Analytical Science,* 2nd Ed., Weinheim, Wiley 2004, p. 1023–1034.
[2] Werner W. E., Demorest D. M., Stevens J., Wiktorowicz J. E.: *Anal. Biochem.* **212** (1993) 253–258.
[3] Weinberger R.: *Practical Capillary Electrophoresis*. Chapter 5, San Diego, Academic Press 1993.
[4] Mikšík I., Sedláková P., Mikulíková K., Eckhardt A., Cserhati T., Horváth T.: *Biomed. Chromatogr.* **20** (2006) 458–465.
[5] Hsieh M. M., Chiu T. C., Tseng W. L., Chang H. T.: *Curr. Anal. Chem.* **2** (2006) 17–33.
[6] Simo-Alfonso E., Conti M., Gelfi C., Righetti P. G.: *J. Chromatogr. A* **689** (1995) 85–96.
[7] Lausch R., Scheper T., Reif O. W., Schlösser J., Fleischer J., Freitag R.: *J. Chromatogr. A* **654** (1993) 190–195.
[8] Ganzler K., Greve K. S., Cohen A. S., Karger B. L., Cooke N. C.: *Anal. Chem.* **64** (1992) 2665–2671.
[9] Benedek K., Thiede S.: *J. Chromatogr. A* **676** (1994) 209–217.
[10] Mikšík I., Deyl Z.: *J. Chromatogr. B* **739** (2000) 109–116.
[11] Mikšík I., Charvátová J., Eckhardt A., Deyl Z.: *J. Chromatogr. B* **800** (2004) 155–160.
[12] Mikšík I., Eckhardt A., Forgács E., Cserháti T., Deyl Z.: *Electrophoresis* **23** (2002) 1882–1886.
[13] Mikšík I., Deyl Z., Kašička V.: *J. Chromatogr. B* **741** (2000) 37–42.
[14] Sedláková P., Svobodová J., Mikšík I.: *J. Chromatogr. B* **839** (2006) 112–117.

Profiling of Biomarkers of Occupational Exposure Using Extractive Derivatization with Chloroformates and GC-MS – Introduction

Lucie Makuderová[a, b], Petr Šimek[a], Jaroslav Mráz[c], Vladimír Stránský[c], Radomír Čabala[b]

[a] *Biology Centre, Academy of Sciences of the Czech Republic, Institute of Entomology, Laboratory of Analytical Biochemistry, Branišovská 31/1160, 370 05 České Budějovice, Czech Republic,* ✉ *makuderova@bclab.eu*
[b] *Charles University, Faculty of Sciences, Department of Analytical Chemistry, Albertov 6, 12840 Prague 2, Czech Republic*
[c] *Centre of Public Health Laboratories, National Institute of Public Health, Šrobárova 48, 100 42 Prague 10, Czech Republic*

Abstract

People in their living and working environments are exposed to large quantities of chemicals that may be potentially harmful. It is necessary to have suitable analytical methods that allow for the control of exposure. One of them is biological monitoring. In the field of occupational hygiene biological monitoring is a recognized tool for assessing occupational exposure. Many important industrial organic pollutants are excreted from an organism in the urine as carboxylic acids, which are determined as biomarkers of exposure. The most common include the metabolites of benzene, toluene, styrene, xylenes and alkoxyethanols and less common are the metabolites of carbon disulfide, fural and *N,N*-dimethylformamide. The determination of the largest possible number of analytes in single analytical procedure (profiling) is an attractive idea. To accomplish this task, derivatization of the target analytes with alkyl chloroformates is tested.

Keywords
biological limits
biological monitoring
metabolites

1. Introduction

People in their living and working environments are exposed to large quantities of chemicals that may be potentially harmful. To maintain the level of exposure to acceptable level appropriate tools (analytical techniques) allowing the exposure control should be developed. There are two basic approaches: *i)* the determination of pollutants directly in the external environment, *ii)* biological monitoring.

Biological monitoring means determining the chemical pollutants or their metabolites directly in the organism, in practice in a defined biological material. Urine and blood are the most easily available human materials; although exhaled air, hair, saliva or faeces can be used in some cases. The substance to be determined – whether an original toxic substance or its metabolic products – is termed as a biomarker of exposure. Chemical toxic substances sometimes can disrupt normal biochemical processes in the exposed organism. Consequently, the physiological levels of metabolites in urine or blood may be altered. The substance of diagnostic importance is then called biomarker of biochemical effect.

The major advantages of biological monitoring is that it takes into account the total amount of pollutants absorbed into the organism irrespective of the route of absorption. The total absorbed amount is affected by physiological parameters such as pulmonary ventilation and retention, work effort, use of protective equipment and compliance with working safety regulations [1].

2. Biological monitoring

2.1. Biological limits and toxicological effects

In the field of occupational hygiene biological monitoring is a recognized tool for assessing occupational exposure. For several tens of chemical pollutants, so-called biological limits (levels of biomarkers in biological material usually urine) have been introduced. Compliance with these limits should guarantee health of persons employed in daily 8-hour exposure.

Biological limits of industrial pollutants are introduced in many states. The most sophisticated and the most respected are published by American Conference of Governmental Industrial Hygienists (ACGIH) and Germany Deutsche Forschungsgemeinschaft, Commission for the Investigation of Health Hazards of Chemical Compounds in the Work Area (DFG). These organizations present the biological limits under specific names *i. e.* ACGIH: Biological exposure indices (BEI) and DFG: Biologische Arbeitsstoff-Toleranz-Werte (BAT). Biological limits for Czech Republic are included in the notice 432/2003Sb. The comparisons of biological limits of CR, USA and Germany for selected metabolites are shown in Tab. 1.

Table 1. The comparisons of biological limits of CR, USA and Germany for selected metabolites

Substrate	Metabolite	Abbrev.	Biological limit		
			CR	USA	Germany
benzene	*t,t*-muconic acid	*t,t*-MA	–	500 μg/g creat.	–
	S-phenylmercapturic acid	S-PMA	50 μg/g creat.	25 μg/g creat.	–
toluene	hippuric acid	HA	1.6 g/g creat.	1.6 g/g creat.	–
	S-tolylmercapturic acid	S-TMA	–	–	–
	S-benzylmercapturic acid	S-BMA	–	–	–
o-, *m*-, *p*-xylenes	*o*-, *m*-, *p*-methylhippuric acids	MHA	1.4 g/g creat.[a]	1.5 g/g creat.[a]	2 g/g creat.[a]
styrene	mandelic acid	MA	400 mg/g creat.	–	–
	phenylglyoxylic acid	PGA	600 mg/g creat.[b]	400 mg/g creat.[b]	600 mg/g creat.[b]
alkoxyethanols	methoxyacetic acid	MAA	–	–	15 mg/g creat.
	ethoxyacetic acid	EAA	50 mg/L urine	100 mg/L urine	50 mg/L urine
	butoxyacetic acid	BAA	100 mg/L urine	200 mg/g creat.	200 mg/L urine
carbon disulfide	2-thiothiazolidine carboxylic acid	TTCA	–	5 mg/g creat.	2 mg/g creat.
fural	furancarboxylic acid	FCA	200 mg/g creat.	200 mg/L urine	–
N,N-dimethylformamide	*S-N*-methylkarbamoylmercapturic acid	AMCC	–	40 mg/L urine	–

[a]Sum of methylhippuric acids. [b]Sum of mandelic and phenylglyoxylic acids.

Many important industrial organic pollutants (solvents, monomers) are excreted from an organism in the urine as carboxylic acids, which are determined as biomarkers of exposure. Their biological limits are ranging from tens μg to hundreds mg per L of urine or g of creatinine. The most common limits include the metabolites of benzene, toluene, styrene, xylenes and alkoxyethanols (2-methoxyethanol, 2-ethoxyethanol and 2-butoxyethanol); less common are the metabolites of carbon disulfide, fural and *N, N*-dimethylformamide.

Benzene is a ubiquitous environmental pollutant arising from motor vehicle emissions. A relevant source of indoor benzene concentrations could be identified in tobacco smoke. Since at high exposure levels benzene causes progressive degeneration of bone marrow, aplastic anemia, and leukemia, it has been classified in group A1 (carcinogen to human) by the International Agency for Research on Cancer (IARC). Common urinary biomarkers of benzene are S-phenylmercapturic acid (S-PMA) and *trans,trans*-muconic acid (*t,t*-MA) [2]. Metabolic pathway of benzene is shown in Fig. 1. The main toluene and xylenes metabolites are hippuric acid (HA) and *o*-, *m*-, and *p*-methylhippuric acids (MHA).

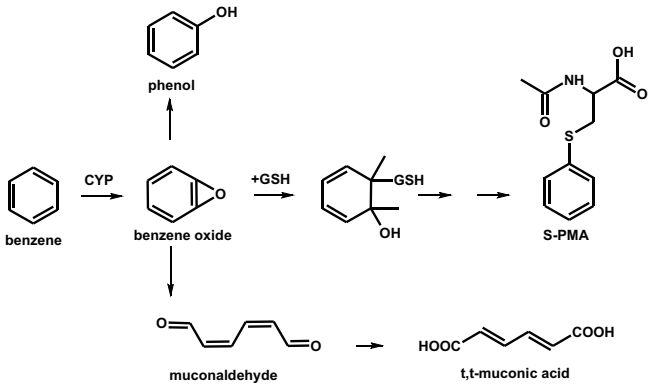

Fig. 1. Metabolic pathways of benzene [3]. CYP – cytochrome P450, GSH – glutathione.

Mandelic acid (MA) and phenylglyoxylic acid (PGA) are the major urinary metabolites of styrene in humans and therefore are used as biological indicators of occupational exposure to styrene Styrene is widely used in plastics industry and has been implicated as reproductive toxicant, neurotoxicant and possible carcinogen [4]. *N*-Acetyl-S-(N-methylcarbamoyl)-cysteine (AMCC), an important metabolite of *N,N*-dimethylformamide is generated during experimental human exposure to this solvent [5]. The metabolite of carbon disulfide is 2-thiothiazolidine carboxylic acid (TTCA). Carbon disulfide is used as a solvent with local anesthetic properties. It is highly toxic with pronounced CNS, hematologic, and dermatologic effects. Fural is used to produce plastics; its metabolite occurring in urine is furancarboxylic acid [6]. Alkoxyethanols are widely used in industry as solvents in the manufacture of lacquers, varnishes, resins, and printing inks owing to their excellent hydrophilic and lipophilic properties. It is well known that alkoxyethanols can cause adverse reproductive, developmental, and hematological effects through inhalation, dermal absorption, and ingestion [7].

2.2. Methods for the analysis of biomarkers of exposure

Currently, the dominant methods for the determination of biomarkers of occupational exposure are HPLC [3, 4, 5, 8–31] and GC [20, 32–48], very often in combination with MS [3, 8, 9, 13, 15–17, 20, 30, 32, 33, 36, 37, 39, 40–42, 46, 48]. HPLC methods have been used for determination of free carboxylic acids. Gas chromatography requires derivatization, the most frequently used is methylation [32, 34–36] or silylation [39, 40, 42]. Other methods used for the determination of these pollutants are for example voltametric determination of PGA by graphite composite electrode [49] or determination of HA by micellar electrokinetic capillary chromatography [50].

Hygiene control usually requires determination of the dominant pollutants; therefore, the established working practices are optimized for determination of the individual biomarkers (while the others are not searched). The laboratory has to maintain and validate a number of methods.

3. Conclusions

The determination of the largest possible number of analytes in a single analytical procedure (profiling) is an attractive idea. To accomplish this task, derivatization of the target analytes with alkyl chloroformates was proposed and became a subject of this work. Derivatization with alkyl chloroformates is simple and fast [51]

Table 2. Relevant published papers dealing with biological monitoring of industrial pollutants using HPLC analysis (references since 2000).

Metabolite	Determination	Ref.
t,t-MA, S-PMA	LC-MS, HPLC	[8]
S-PMA, S-BMA	LC-MS/MS	[3]
S-PMA, S-BMA	HPLC-MS/MS	[9]
PGA, MA, HA	HPLC	[10]
HA	HPLC	[11]
MA, PGA	HPLC	[4]
MA, PGA, HA, MHA	HPLC	[12]
S-PMA	HPLC-MS	[13]
t,t-MA	HPLC	[14]
t,t-MA, HA, MHA, PGA	LC-MS/MS	[15]
S-PMA, S-BMA, t,t-MA	LC-MS/MS	[16]
MA, PGA	LC-MS/MS	[17]
MA, PGA, HA, MHA	HPLC, monolithic column	[18]
MAA, EAA, BAA	HPLC	[7]
HA	HPLC	[19]
MA, PGA	HPLC-MS/MS	[20]
t,t-MA	LC	[21]
t,t-MA	HPLC	[22]
AMCC	HPLC	[23]
S-BMA	HPLC	[24]
MAA	HPLC	[25]
AMCC	HPLC	[5]
t,t-MA	LC-LC	[26]
PGA, MA	HPLC	[27]
TTCA	HPLC	[28]
HA	HPLC	[29]
TTCA	HPLC-MS/MS	[30]
S-PMA	HPLC	[31]

Table 3. Relevant published papers dealing with biological monitoring of industrial pollutants using GC analysis (references since 2000). Abbreviations: BSA: *N,O*-bis(trimethylsilyl)acetamide; TMSC: trimethyl chlorosilane; ECFP: ethylchloroformate; MSTFA: *N*-methyl-*N*-trimethylsilyl-trifluoroacetamide; PFPES:2-(pentafluorophenoxy)ethyl-2-(piperidino)ethanesulfonate.

Metabolite	Derivatization	Detection	Ref.
S-PMA, HA	CH_3OH in HCl	GC-MS	[32]
HA, MHA, t,t-MA, MA, PGA	trimethyloxonium tetrafluoroborate	GC-MS	[33]
HA	CH_3OH in HCl	GC	[34]
Isomers MA	CH_3OH and pentafluoropropionic anhydride	GC	[35]
MA, PGA, HA, MHA	CH_3OH in HCl	GC-MS	[36]
MA, HA, MHA	pentafluorobenzyl bromide	GC-MS	[37]
MAA, EAA, BAA	–	GC	[38]
t,t-MA, S-PMA	Tri Sil reagent	GC-MS	[39]
MA, PGA	–	GC-MS	[20]
HA, MHA	BSA and TMCS	GC-MS	[40]
MA, HA, MHA	ECF	GC-MS	[41]
HA, MHA, PGA, MA	MSTFA	GC-MS	[42]
t,t-MA	PFPES	GC	[43]
HA, MHA	–	GC	[44]
MA, PGA	Isopropyl alkohol in H_2SO_4	GC	[45]
BAA	2,2,2-trichloroethanol in HCl	GC-MS	[46]
MA	Isopropyl alkohol in H_2SO_4	GC	[47]
TTCA	diazoethane/toluene	GC-MS	[48]

and enables efficient transfer of analytes from polar medium into an immiscible organic phase. The derivatization with alkyl chloroformates has been used in a single paper for the determination of MA, HA, MHAs [41] and methodology profiling the pollutants in a single run has not been, to our knowledge, reported.

The aim this work is to evaluate the chloroformate derivatization approach for the determination of common biomarkers of occupational exposure in human urine.

Acknowledgements. *The financial support of this work by the Grant Agency of Charles University in Prague (the project No. 54009), and by the Ministry of Education, Youth and Sports of the Czech Republic, project No. MSM0021620857.*

References

[1] Mraz J., Stransky V.: *Biologické monitorování a biologické expoziční testy*. < http://www.szu.cz/tema/pracovni-prostredi/biologicke-monitorovani-a-biologicke-expozicni-testy?lred=1> [28.8.2009]
[2] Manini P., Andreoli R., Niessen W. M. A.: *J. Chomatogr. A* **1058** (2004), 21–37.
[3] Schettegen T., Musiol A., Alt A., Kraus T.: *J. Chromatogr. B* **863** (2008), 283–292.
[4] Wang J., Wang X. Tang Y., Shen S., Jin Y., Zeng S.; *J. Chromatogr. B* **840** (2006), 50–55.
[5] Perbellini L., Maestri L., Veronese N., Romani S., Bruguone F.: *J. Chromatogr. B* **759** (2001), 349–354.
[6] <http://pubchem.ncbi.nlm.nih.gov> [28.8.2009]
[7] Yoshikawa M., Tani C.: *J. Chromatogr. A* **1005** (2003), 215–221.
[8] Hoet P., De Smedt E., Ferrari M., Imbriani M., Meastri L., Negri S., De Wilde P, Lison D., Houfroid V.: *Int. Arch. Occup. Environ. Health* **82** (2009), 985–995.
[9] Sabatini L., Barbieri A., Indiveri P., Mattioli S., Violante F. S: *J. Chromatogr. B* **863** (2008), 115–122.
[10] Wang J., Lu X., Zhao N., Cheng Y., Zeng S.: *Biomed. Chromatogr.* **21** (2007), 497–501.
[11] Sperlingova I., Dabrowska L., Stransky V., Kucera J., Tichy M.: *Anal. Bioanal. Chem.* **387** (2007), 2419–2424.
[12] Chakroun R., Hedhili A., Faidi F., Nouaigui H., Laiba M. B.: *Anal. Lett.* **39** (2006), 83–97.
[13] Maestri L., Negri S., Ferrari M., Ghittori S., Imbriani M.: *Rapid Commun. Mass Spectrom.* **19** (2005), 1139–1144.
[14] Lee B. L., Ong H. Y., Ong Y. R., Ong C. N.: *J. Chromatogr. B* **818** (2005) 277–283.
[15] Marchese S., Curini R., Gentili A., Perret D., Rocca L. M.: *Rapid Commun. Mass Spectrom.* **18** (2004), 265–272.
[16] Barbiery A., Sabatini L., Accorsi A., Roda A., Violante F.: *Rapid Commun. Mass Spectrom.* **18** (2004), 1983–1988.
[17] Manini P., De Palma G., Andreoli R., Goldoni M., Mutti A.: *Int. Arch. Occup. Environ. Health* **77** (2004), 433–436.
[18] Sperlingova I., Dabrowska L., Stransky V., Tichy M.: *Anal. Bioanal. Chem.* **378** (2004), 536–543.
[19] Cok I., Dagdelen A., Gokce E.: *Biomarkers* **8** (2003) 119–127.
[20] Manini P., Andreoli R., Poli D., De Palma G., Mutti A., Niessen W. M. A.: *Rapid Commun. Mass Spectrom.* **16** (2002), 2239–2248.
[21] Norberg J., Tiruye D., Mathiasson L., Jonsson J. A.: *J. Sep. Sci.* **25** (2002) 351–355.
[22] Panev T., Popov T., Georgieva T., Chohadjieva P.: *Int. Arch. Occup. Environ. Health* **75** (2002), 97–100.
[23] Imbriani M., Maestri L., Marraccini P., Saretto G., Alessio A., Negri S., Ghittori S.: *Int. Arch. Occup. Environ. Health* **75** (2002), 445–452.
[24] Inoue O., Kanno E., Yusa T., Kakizaki M., Ukai H., Okamoto S., Higashikawa K., Ikeda M.: *Int. Arch. Occup. Environ. Health* **75** (2002), 341–347.
[25] Cheever K. L., Swearengin T. F., Edwards R. M., Nelson B. K., Weren D. W., Conover D. L., De Bond D. G.: *Toxicol. Lett.* **122** (2001), 53–67.
[26] Marrubini G., Cociini T., Manzo L.: *J. Chromatogr. B* **758** (2001), 295–303.
[27] Laffon B., Lema M., Mendez J.: *J. Chromatogr. B* **753** (2001), 385–393.
[28] Amarnath V., Amarnath K., Graham D. G., Qi Q., Valentine H., Zhang J., Valentine W. M.: *Chem. Res. Toxicol.* **14** (2001), 1277–1283.
[29] Eisenkraft B. R., Hoffer E., Baum Y., Bentur Y.: *Clinic. Toxicol.* **39** (2001), 73–76.
[30] Kivisto H.: *Int. Arch. Occup. Environ. Health* **73** (2000), 263–269.
[31] Inoue O, Kanno E., Kakizaki M., Watanebe T., Higashikawa K., Ikeda M.: *Industrial Health* **38** (2000), 195–204.
[32] Marrubini G., Terulla E., Brusotti G., Massolini G.: *J. Chromatogr. B* **822** (2005), 209–220.
[33] Pacenti M., Dugheri S., Villanelli F., Bartolucci G., Calamai L., Boccalon P., Arcaugeli G., Vecchione F., Aless P., Kikic J., Cupelli V.: *Biomed. Chromatogr.* **22** (2008), 1155–1163.
[34] Thiesen F. V., Noto A. R., Barros H. M. T.: *Clinical Toxicol.* **45** (2007), 557–562.
[35] Zougagh M., Arce L., Rios A., Valcarcel M.: *J. Chromatogr. A* **1104** (2006), 331–336.
[36] Ohashi Y., Mamiya T., Mitani K., Wang B., Takigawa T., Kira S., Kataoka H.: *Anal. Chim. Acta* **556** (2006), 167–171.
[37] Marais A. A. S., Laurens J. B.: *J. Sep. Sci.* **28** (2005), 2526–2533.
[38] Choi Z. B., Park J. H., Song J. S., Cho Y. B.: *J. Occup. Health* **46** (2004) 260–265.
[39] Waidyanatha S., Rothman N., Li G., Smith M. T., Yin S., Rappaport S. M.: *Anal. Biochem.* **327** (2004), 184–199.
[40] Saito T., Takeichi S.: *J. Pharm. Biomed. Anal.* **30** (2002), 365–370.
[41] Laurens J. B., Mbianda J. B., Spies J. H., Ubbink J. B., Vermaak W. J. H.: *J. Chromatogr. B* **774** (2002), 173–185.
[42] Szucz S., Toth L., Legoza J., Sarvary A., Adany R.: *Arch. Toxicol.* **76** (2002), 560–569.
[43] Lin F., Wu H., Kou H., Lin S.: *Anal. Chim. Acta* **455** (2002), 111–116.
[44] Kongtip P., Vararussami J., Pruktharathikul V.: *J. Chormatogr. B* **751** (2001), 199–203.
[45] Knecht U., Reske A., Woitowitz H.: *Arch. Toxicol.* **73** (2000) 632–640.
[46] Hildenbrand S., Gfrorer W., Schmahl F., Dartsch P.: *Arch. Toxicol.* **74** (2000), 72–78.
[47] Kezic S., Jakasa I., Wenker M.: *J. Chromatogr. B* **738** (2000), 39–46.
[48] Weiss T., Hardt J., Angerer J.: *J. Chromatogr. B* **726** (1999), 85–94.
[49] Navratil T., Senholdova Z., Shanmigam K., Barek J.; *Electroanalysis* **18** (2006) 201–206.
[50] Zuppi C., Rossetti D. V., Vitali A., Vincenzoni F., Giardina B., Castagualo M., Messana I.: *J. Chromatogr. B* **793** (2003) 223–228.
[51] Husek P.; *FEBS Lett.* **2** (1991) 334–336.

Chemometric Deconvolution of Gas Chromatographically Unseparated Conjugated Linoleic Acid Isomers in Ewe and Cow Milks

Beáta Meľuchová[a], Jaroslav Blaško[a], Róbert Kubinec[a], Eva Pavlíková[a], Ján Krupčík[b], Ladislav Soják[a]

[a] *Institute of Chemistry, Faculty of Natural Sciences, Comenius University, Mlynská dolina CH-2, 842 15 Bratislava, Slovakia,* ✉ *meluchova@fns.uniba.sk*
[b] *Institute of Analytical Chemistry, Faculty of Chemical and Food Technology, Slovak University of Technology, Radlinského 9, 812 39 Bratislava, Slovakia*

Abstract

A generally known problem of gas chromatographic (GC) separation of *trans*-7, *cis*-9, *cis*-9, *trans*-11, and *trans*-8, *cis*-10 conjugated linoleic acid (CLA) isomers was studied by GC on a 100 m capillary column coated with a cyanopropyl silicone phase at 160 °C. The resolution of these CLA isomers obtained at given experimental conditions was not high enough for direct quantitative analysis but it was, however, sufficient for the determination of their peak areas by a commercial deconvolution software. Relative retentions and resolution factors of CLA isomers with overlapped peaks determined by the separation of a commercial CLA standard mixture as well as CLA isomer fractions obtained by the HPLC semi-preparation of ewe milk were used as input data in the deconvolution procedure. The milk of pasture-fed ewes with higher *cis*-9, *trans*-11 isomer contents showed higher contents of *trans*-7, *cis*-9 as well as *trans*-8, *cis*-10 CLA isomers in comparison with milk fat of total mixed rations (TMR)-fed ewes. For cow milk samples showing lower CLA contents, no such trends were evident.

Keywords
chemometric deconvolution
conjugated linoleic acid
cow milk fat
ewe milk fat
gas chromatography

1. Introduction

In recent years, there is an increasing interest of the consumers in functional foods that have beneficial effects on human health besides the nutritional values [1]. Such functional food components are also certain isomers of octadecadienoic acid found in milk fat and in meat of ruminants. Conjugated linoleic acid (CLA) isomers are reported to have anti-carcinogenic, atherogenic, diabetic properties and they also improve the immune system, bone metabolism and body composition [2]. Recent reports suggest that each conjugated fatty acid isomer has different physiological functions [3]. The understanding of the biological role of these acids relies on their proper separation, identification and quantitation in complex biological extracts which contain many unsaturated and saturated fatty acids, where the carbon number of 16–20 prevails. There are 14 possible CLA positional isomers and each positional isomer has four geometric isomers *cis, trans*; *trans, cis*; *cis, cis*; *trans, trans,* giving 56 possible isomers. The double bond positions of CLA isomers actually identified in ruminant fat range from 6,8- to 12,14–18:2 in most of the possible geometrical configurations for a total of 20 isomers [2].

The most important analytical task is resolution of *cis*-9, *trans*-11; *trans*-7, *cis*-9; and *trans*-8, *cis*-10 CLA isomers. As it was mentioned, ruminant milk fat is the richest natural common source of CLA, with levels ranging from 0.2% to 5.4% (w/w). The major *cis*-9, *trans*-11 isomer comprises about 75–90% of total CLA in ruminant milk fat [4, 5]. Normally, the *trans*-7, *cis*-9 is the second most abundant CLA isomer in ruminant fat (up to 7% of total CLA). Under special conditions this isomer represents as much as 40% or so little as 1% of the total CLA. In milk fat from cows grazing at high altitude, the second most abundant isomer is the *trans*-11, *cis*-13. The content of other considered *trans*-8, *cis*-10 CLA isomer in milk fat is low, however, high concentrations of this isomer were determined in synthetic CLA products [6] as well as in products of thermal treatment of butterfat (up to 31%) [7]. From these published results follows that content ratio of triplet CLA isomers in various CLA products can be very different. Reporting only the content of the major CLA peak as isomer *cis*-9, *trans*-11, can misses critical information on the correct CLA isomers composition that has a great impact on the understanding and interpretation of CLA content milk fat as well as dietary influences.

For analysis of CLA is used silver-ion high performance liquid chromatography (Ag+HPLC). The main disadvantage of this method is to obtain reproducible results. The sources of errors are variations in silver loadings of the columns; differences in instrument configuration (number of solvent pumps, mixing chambers, and valves); changes in elution volumes and elution orders with sample size, solvent composition

and even storage times; lack of internal standards; and control of column temperature. Further, the HPLC separation of small peak of *trans*-8, *cis*-10 isomer from large peak of *cis*-9, *trans*-11 isomer is very poor in milk fat samples. Analysis of the CLA isomers separated by Ag-HPLC requires the combination with GC. The CLA peaks are quantified by GC analyses of total fatty acids methylesters. [4]

To resolve five distinguish peaks in the CLA region is 100-m capillary GC column coated with cyanopropyl polysilicoxane (CP-Sil 88, Varian, Palo Alto, California, USA) as highly polar stationary phase used. This peaks represent *cis*-9, *trans*-11 + *trans*-7, *cis*-9 + *trans*-8, *cis*-10; *trans*-11, *cis*-13 + *cis*-9, *cis*-11; *trans*-10, *cis*-12; *trans*-11, *trans*-13; and *trans*-9, *cis*-11 CLA isomers. The important *cis*, *trans* isomers of CLA usually elute in a region of the chromatogram that is free from other fatty acids. However, C21:0 and C20:2 elute in the elution range of the *cis*, *cis*- and *trans*, *trans*- CLA isomers. Although the information on CLA isomeric composition provided by GC is incomplete GC is often the only method used in the analysis of fatty acids for CLA.

For resolution of gas chromatographically unseparated peaks various chemometric or mass spectrometric deconvolution procedures can generally be used. In principle, most of them require advanced knowledge, so they are usually not used in an everyday practice. To facilitate deconvolution, an automatic program was developed. Several deconvolution softwares are commercially accessible for computer-assistedsingle-channel-detected chromatograms. PeakFit (Systat Software UK) and Peak Fitting (OriginLab Corporation, USA) belong to the most popular. Mass spectral deconvolution technique for the deconvolution of CLA isomers with overlapped peaks could not be used because mass spectra of *trans*-7, *cis*-9 and *trans*-8, *cis*-10 CLA isomers were not available.

The possibilities and limitations of the use of a commercial Peak Fitting Modul (PFM) inbuilt in Microcal Origin 7.5 software (OriginLab Corporation) for deconvolution of high resolution chromato-graphically unresolved peaks of *trans*-7, *cis*-9, *cis*-9, *trans*-11, and *trans*-8, *cis*-10 CLA isomers in ewe and cow milk products were studied.

2. Experimental

Commercially unavailable standard reference material of *trans*-7, *cis*-9 and *trans*-8, *cis*-10 CLA isomers necessary for obtaining gas chromatographic parameters for deconvolution procedures were investigated in case of *trans*-8, *cis*-10 CLA isomer by using commercial CLA isomers mixture (Nu-Chek Prep, USA). This standard sample does not contain *trans*-7, *cis*-9 isomer. The sample model with increasing content of *trans*-7, *cis*-9 CLA isomer was obtained by HPLC semi-preparative procedure from milk fat sample.

The milk sample of ewes fed by total mixed rations (TMR) as well as fed by pasture with lower and higher CLA content were obtained from Research Institute of Animal Production (Trenčianská Teplá, Slovakia). The winter and summer samples of cow milk were of commercial origin RAJO (Bratislava, Slovakia) and ARO (Kežmarok, Slovakia), respectively. Analysed samples:

- sample No. 1 – milk of pasture-fed ewes containing higher CLA content;
- sample No. 2 – milk of pasture-fed ewes containing lower CLA content;
- sample No. 3 – milk of TMR-fed ewes containing higher CLA content;
- sample No. 4 – milk of TMR-fed ewes containing lower CLA content;
- sample No. 5 – summer cow milk (ARO);
- sample No. 6 – winter cow milk (RAJO).

The lipids from milk samples were extracted using chloroform-methanol mixture (2:1), obtained extracts were filtered through anhydrous sodium sulfate, then dried and stored under nitrogen at 18 °C.

GC-MS measurement of milk extracts were performed on an Agilent Technologies 6890 N gas chromatograph with a 5973 Network mass-selective detector (Agilent, Germany). Fatty acid methyl esters were separated using capillary column 100 m × 0.25 mm I.D. coated with a film thickness of 0.2 μm of cyanopropyl polysilicoxane stationary phase (CP-Sil 88, Varian, USA) at isothermic column temperature of 160 °C with constant flow of carrier gas (helium) of 1,2 mL min^{-1}.

A commercial Peak Fitting Modul (PFM) inbuilt in Microcal Origin 7.5 software (OriginLab Corporation, USA) [12] was used for deconvolution of single peak data from chromatographically unresolved peaks of *trans*-7, *cis*-9, *cis*-9, *trans*-11, and *trans*-8, *cis*-10 CLA isomers.

3. Results and discussion

The procedure for computer assisted deconvolution of overlapped peaks of *trans*-7, *cis*-9, *cis*-9, *trans*-11, and *trans*-8, *cis*-10 CLA isomers obtained by capillary GC-MS separation methyl esters of fatty acids isolated from lipids of ewe milk products started with an import of a chromatogram into the PFM. Sub-range of data containing unseparated methyl esters of *trans*-7, *cis*-9,

cis-9, *trans*-11, and *trans*-8, *cis*-10 CLA isomers were extracted from the whole chromatogram into the PFM. Noisy data were filtered with fast Fourier transform filter. Constant baseline was chosen and Gaussian function was used to fit peak shapes. Since the precision of the fitting procedure for highly overlapped peaks increases with a decrease in the number of optimized parameters, predicted peak widths for three expected overlapped peaks were introduced into the deconvolution procedure. The clusters of overlapped peaks *trans*-7, *cis*-9, *cis*-9, *trans*-11, and *trans*-8, *cis*-10 CLA isomers obtained by the separation of methyl esters of fatty acids isolated from lipids of ewe and cow milk products under various experimental conditions were deconvoluted to find the perspectives and limitations of this method.

The procedure for deconvolution of overlapped peak using commercial PFM software was used to treat chromatograms obtained by the separation of methyl esters of fatty acids by capillary GC-MSD on a 100 m long column at 160 °C. The data obtained for both peaks by deconvolution procedure were used for the determination of resolution factor:

$$R_{s,t8c10/c9t11} = 1.18 \frac{t_{R,t8c10} - t_{R,c9t11}}{w_{h,t8c10} + w_{h,c9t11}} \quad (1)$$

where t_R is retention time, w_h is a half height peak width, *t*8*c*10 are values for *trans*-8, *cis*-10, *and c*9*t*11 are values for *cis*-9, *trans*-11 CLA isomer.

The resolution factor $R_{s,\ t8c10/c9t11}$ were used for the determination of retention time of *trans*-8, *cis*-10 isomer at each analysis of real samples. The part of typical chromatograms for the overlapped *trans*-7, *cis*-9, *cis*-9, *trans*-11, and *trans*-8, *cis*-10 CLA isomers presented in milk of ewes fed pasture containing higher CLA content, as well as in the winter cow milk (RAJO) are shown in Figs. 1 and 2, in left hand side figures. Data corresponding to these chromatograms were exported into the PFM and processed by PFM software similarly as described above for standard CLA mixture sample. Right hand sides of Figs. 1 and 2 depict peaks obtained by deconvolution procedure for *trans*-7, *cis*-9, *cis*-9, *trans*-11, and *trans*-8, *cis*-10 CLA isomers.

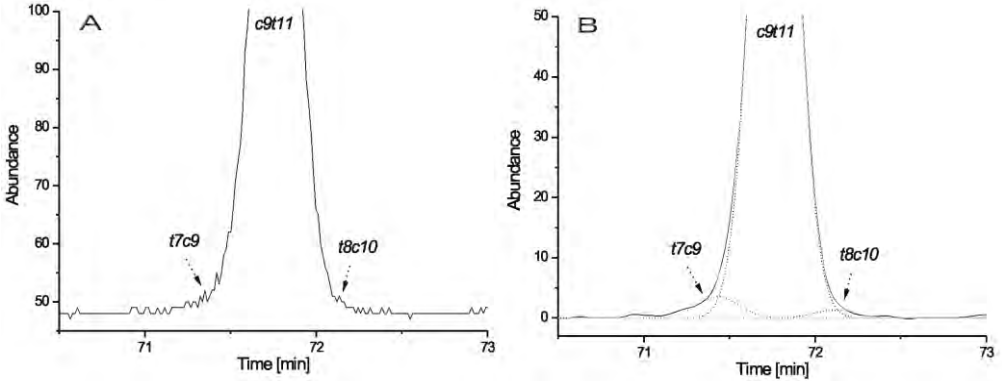

Fig. 1. Separation of methyl esters of *trans*-7, *cis*-9, *cis*-9, *trans*-11, and *trans*-8, *cis*-10-octadecadienoic in the sample of milk fat of ewe milk fed pasture: (A) part of experimental chromatogram, (B) part of chromatogram treated with PFM procedure.

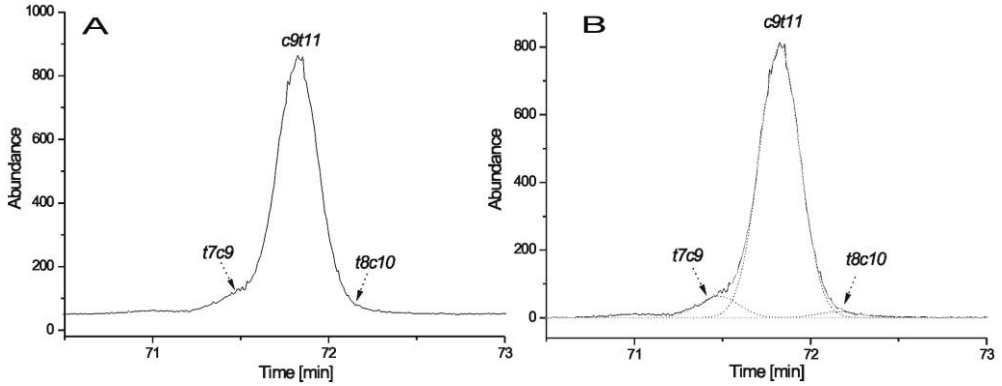

Fig. 2. Separation of methyl esters of *trans*-7, *cis*-9, *cis*-9, *trans*-11, and *trans*-8, *cis*-10-octadecadienoic in the sample of milk fat of winter cow milk: (A) part of experimental chromatogram, (B) part of chromatogram treated with PFM procedure.

Table 1. Deconvoluted peak area ratio (in %) of methyl esters of *trans*-7, *cis*-9, *cis*-9, *trans*-11 and *trans*-8, *cis*-10 isomer of octadecadienoic acids and their standard deviation in the gas chromatographically unseparated CLA peak. Listed values were determined using PFM software, as well as content of CLA determined by GC-MS on 100 m long capillary column at 130 °C in analysed ewe and cow milk samples.

	Sample					
	No. 1 Pasture-fed ewes milk	No. 2 Pasture-fed ewes milk	No. 3 TMR-fed ewes milk	No. 4 TMR-fed ewes milk	No. 5 Summer cow milk (ARO)	No. 6 Winter cow milk (RAJO)
CLA content[a]	2.5	1.1	1.5	0.5	0.9	0.5
trans-7, *cis*-9	2.8 ± 0.01	4.0 ± 0.12	3.5 ± 0.05	7.0 ± 0.13	7.3 ± 0.09	7.2 ± 0.09
cis-9, *trans*-11	96.2 ± 0.01	95.2 ± 0.18	94.7 ± 0.14	91.4 ± 0.35	91.9 ± 0.19	90.9 ± 0.23
trans-8, *cis*-10	1.0 ± 0.02	0.8 ± 0.06	1.8 ± 0.09	1.6 ± 0.22	0.8 ± 0.12	1.9 ± 0.14

[a] CLA content (sum of *trans*-7, *cis*-9, *cis*-9, *trans*-11 and *trans*-8, *cis*-10 isomers as % of total FAMEs determined by GC-MS).

The deconvolution of overlapped peaks in CLA mixture standard on 100 m long capillary at 160 °C was relative simple as the peak area ratio of *cis*-9, *trans*-11, and *trans*-8, *cis*-10 isomers was not too high (~5) in spite of not too high resolution factor (R_s = 0.7196). Deconvolution procedure was working automatically without any interaction. There were, however, problems with the automatic deconvolution of peak clusters in real samples where the peak area ratio of methyl esters of *cis*-9, *trans*-11/*trans*-7, *cis*-9, and *cis*-9, *trans*-11/*trans*-8, *cis*-10 CLA isomers was higher than 10. In these cases prior to finishing deconvolution procedure the peak widths and retention time of *trans*-8, *cis*-10 isomer were fixed using the following conditions:

- the peak width of the *cis*-9, *trans*-11 isomer was used for all peaks overlapped in the cluster,
- the retention time of *trans*-8, *cis*-10 peak predicted from resolution factor of *cis*-9, *trans*-11/*trans*-8, *cis*-10 isomers was used.

The width of the first (*trans*-7, *cis*-9) and third (*trans*-8, *cis*-10) peaks were fixed according to the value found by software for the second peak (*cis*-9, *trans*-11). The retention time of the third peak (*trans*-8, *cis*-10) was calculated from the retention time and fixed, too. Using these fixed values, the optimization in deconvolution procedure was convergent giving the peak data for unseparated CLA cluster. Tab. 1 shows the relative content of methyl esters of *trans*-7, *cis*-9, *cis*-9, *trans*-11, and *trans*-8, *cis*-10 isomers of octadecadienoic acids in various matrices found by capillary gas chromatographic separation on 100 m long capillary column at 160 °C using this simplification in the PFM software.

Taking into account also the CLA contents in samples No. 1–6, the contents of *trans*-7, *cis*-9 isomer in sample No. 1 was 0.070, in No. 2 was 0.044, in No. 3 was 0.053 and in No. 4 was 0.035%. Similarly calculated contents of *trans*-8, *cis*-10 isomer in sample No. 1 was 0.025, in No. 2 was 0.009, in No. 3 was 0.026 and in No. 4 as 0.008%. It is obvious that milk of pasture-fed or TMR-fed ewes with higher CLA contents had higher contents of *trans*-7, *cis*-9 as well as *trans*-8, *cis*-10 CLA isomers. For cow milk samples with lower CLA contents, no such trends are evident.

4. Conclusions

Resolution of *trans*-7, *cis*-9/*cis*-9, *trans*-11, and *cis*-9, *trans*-11/*trans*-8, *cis*-10 CLA isomers with resolution factor $R_{s,\,c9t11/t7c9}$ = 0.6864 and $R_{s,\,t8c10/c9t11}$ = 0.7196 was obtained by gas chromatography on 100 m long capillary column coated with CP-Sil 88 polar stationary phase at 160 °C. The resolution was not sufficient for direct quantitative analysis; but it allowed determination of peak areas by commercial chemometric deconvolution software. The developed deconvolution procedure allowed the determination of the contents of studied CLA isomers in ewe and cow milks. Determined contents of CLA isomers allowed differentiation of the milk from ewes fed by pasture from that fed by total mixture rations, as well as the differentiation between the summer and winter cow milks.

Acknowledgements. *This work was supported by the Slovak Research and Development Agency under the contracts Nos. APVV--0163-06, LPP-0198-06, LPP-0089-06, VEGA-1/0297/08, and VaV 26240220007 and UK/250/2009.*

References

[1] Palmquist D. L., Lock A. L., Shingfield K. J., Bauman D. E.: *Advances in Food and Nutrition Research* **50** (2005), 179–217.

[2] Cruz-Hernandez C., Deng Z., Zhou J., Hill A. R., Yurawecz M. P., Delmonte P., Mossoba M.M., Dugan M.E.R., Kramer J.K.G.: *Journal of AOAC International* **87** (2004), 545–562.

[3] Nagao K., Yanagita T.: *Journal of Bioscience and Bioengineering* **100** (2005), 152–157.

[4] Collomb M., Schmid A., Sieber R., Wechsler D., Ryhänen E.-L.: *International Dairy Journal* **16** (2006), 1347–1361.
[5] Dhiman T. R., Nam S. H., Ure A.: *Critical Reviews in Food Science and Nutrition* **45** (2005), 463–482.
[6] Roach J. A. G., Mossoba M. M., Yurawecz M. P., Kramer J. K. G.: *Analytica Chimica Acta* **465** (2002), 207–226.
[7] Destaillats F., Japiot C., Chovinard P. Y., Arul J., Angers P.: *Journal of Dairy Science* **88** (2005), 1631–1635.

Chemical Vapour Generation of Silver For Atomic Absorption Spectrometry: ^{111}Ag Radiotracer Study of Transport Efficiency and In-Situ Trapping on Quartz Surface

Stanislav Musil[a, b], Jan Kratzer[b], Miloslav Vobecký[b], Tomáš Matoušek[b]

[a] *Department of Analytical Chemistry, Faculty of Science, Charles University in Prague, Albertov 6, 128 43 Prague 2, Czech Republic,* ✉ *stanomusil@biomed.cas.cz*
[b] *Department of Trace Element Analysis, Institute of Analytical Chemistry of the ASCR, v.v.i., Vídeňská 1083, 142 20 Prague 4, Czech Republic*

Abstract

The method of chemical vapour generation (CVG) of silver is presented as a sample introduction technique for analytical atomic spectrometry. Analyte is chemically reduced by sodium tetrahydroborate with the presence of surfactants in reaction mixture (Triton X-100 and Antifoam B emulsion) and permanent Pd deposits as the reaction modifiers, but a special gas-liquid separator is used. Free analyte atoms are detected in an externally heated quartz (multi)atomizer. Our study shows that efficient particles transport to the atomizer is very important step of the CVG. Both transport efficiency and spatial distribution of residual analyte in the apparatus were studied by ^{111}Ag radioactive indicator (half-life 7.45 days) of high specific activity. Nearly 33% of the analyte reached the atomizer when the inlet arm was heated to 300 °C. Relative and absolute *LODs* (3σ, 250µl sample loop) measured with this setup were then improved to: 0.47 ng mL^{-1} and 0.12 ng, respectively. The possibility of in-atomizer collection of volatile silver species on quartz surface in excess of oxygen over hydrogen is also described. The special inlet arm for oxygen supply through the capillary was designed and various possibilities of impleentation including difficuties are discussed.

Keywords
atomic absorption spectrometry
chemical vapour generation
in-situ trapping
radiotracer ^{111}Ag
silver
transport efficiency

1. Introduction

Chemical vapour generation (CVG) of transition and noble metals [1] as a sample introduction method for analytical atomic spectrometry has recently emerged as a powerful alternative to nebulization techniques. Analogously to hydride generation (HG) [2], the same chemical scheme, *i. e.* reduction of analyte by tetrahydroborate in acidic environment, is employed [3]. The practical potential of the CVG of metals lies in separation of analyte from matrix and high analyte introduction efficiency, which substantially increases sensitivity. It enables to achieve low limits of detection (*LODs*) for elements that are toxic already at ppb level (ng mL^{-1}) by means of relatively cheap instrumentation. The further advantage is the possibility of analyte collection and preconcentration prior to the detection by any methods already established for volatile hydrides. Although successful CVG of about 20 transition and noble metals has been described so far including some analytical applications to real samples, the situation is not as simple as in the case of the HG. The generation efficiency [4] is still relatively low reaching only tens of percent compared to efficiencies approaching nearly 100% typical for classical HG. For illustration, by the help of neutron activation analysis Ag generation efficiency was determined to be 7% [5] and other study claims that even over 20% of Ag was found in the gaseous phase [6]. The relatively low efficiency is probably also a source of low stability and reproducibility of the signals. Huge inconvenience is also caused by memory effects. Therefore, the improvement in the CVG efficiency is an essential task before this technique enters a stage of routine analysis. The use of reaction modifiers such as complexing agents: 8-hydroxyquinoline [7] and 1,10-phenantroline [8] or diethyldithiocarbamate [9–11], surfactants [6, 12], finely dispersed metals [13], or, most recently, room temperature ionic liquids [14] have been published with significant enhancement. Very little is still known about the actual reaction mechanism [15] but the crucial question, what the actual identity of volatile metal species is, was answered [16]. Popular belief in "volatile metal hydrides" was not confirmed and silver nanoparticles were detected in the gaseous phase by means of a transmission electron microscope. The results of aerosol study proved that the "volatile" analyte particles are associated with the condensed phase transported by carrier gas.

The former study of generation efficiency and the distribution of the analyte within the whole system using the ^{111}Ag radioactive indicator also determined that although the volatilization efficiency, *i. e.* the fraction of volatilized analyte, was about 23%, the overall CVG efficiency, portion introduced to the atomizer, was only 8%. The 15% of total analyte was found deposited in the conduits and in the spray chamber leading the gaseous phase. The transport efficiency was quite poor as only 35% of the volatilized analyte could reach the atomizer [16]. These results suggest to investigate and minimize transport losses of "volatile species" which have been mentioned in literature very sporadically [17, 18].

The fact that hydrides can be easily preconcentrated makes the HG an extremely valuable tool for ultratrace analysis. To develop an easy and suitable preconcentration technique for the CVG, which could be used on-line, *i. e.* directly in the atomizer, is desired. It would help to achieve *LODs* typical of ultratrace analysis. The most convenient way of preconcentration of transition and noble metal species formed upon reduction by tetrahydroborate is in-situ trapping in graphite furnaces [10, 18]. There is another very recent and much cheaper approach to in-atomizer trapping – in quartz atomizers, hitherto employed only for hydride forming elements [19–22]. This method employs the fact that volatile hydrides can be effectively captured on quartz surface in stochiometric excess of oxygen over hydrogen. The quartz capillary put in the inlet arm is usually used for oxygen supply and the small reaction zone is formed at its tip. Subsequent volatilization of trapped species is realized by the change of gas composition (decrease of oxygen flow and/or increase of hydrogen coming to the atomizer).

The general aims of this work were to minimize and assess transport losses in our system for generation of volatile silver species in order to substantially increase the introduction efficiency. The promising technique of trapping analyte directly in the atomizer in excess of oxygen over hydrogen is described as well.

2. Experimental

2.1. Instrumentation

The detection was performed by the atomic absorption spectrometer Perkin-Elmer 503 with the silver hollow cathode lamp (Perkin-Elmer, 328.1 nm line, 0.7 nm spectral bandpass) operated at 12 mA. Signals from spectrometers' strip chart recorder outputs were AD converted in a PC. Signals were exported as ASCII files into Origin Pro 7.5 (Origin Lab Corp.) software for further processing. Averages from 3–5 replicate measurements of peak areas are shown in figures and tables, error bars represent standard deviation.

2.2. Standards and reagents

Deionized water (<0.2 μS cm^{-1}, ULTRAPURE, Watrex, Czech Rep.) was employed for all solutions. Working standards were prepared by serial dilution of 1000 μg mL^{-1} stock solution (BDH, UK) in 0.6 M HNO_3 (p.p., Lach-Ner, Czech Rep.), which was also used as carrier liquid. A reducing solution containing 2.4% (m/v) $NaBH_4$ (Fluka) and 13 μg mL^{-1} of Antifoam B emulsion (Sigma, USA) in 0.1% (m/v) KOH (p.a., Lachema, Czech Republic) was prepared daily fresh. Bubbles of evolving gas were removed from this solution on-line just before the reaction [5]. The 20 μg mL^{-1} of Triton X-100 (Aldrich) in 0.1 M HNO_3 was used as a reaction modifier. The 0.5 M NaOH solution (Lach-Ner, Czech Republic) served as a waste stabilizer.

2.3. System for flow injection chemical vapour generation

A scheme of the system in flow injection (FI) mode is shown in Fig. 1 (*see next page*). All reagents were pumped by means of peristaltic pump 1 (Reglo Digital 4-11, Ismatec, Switzerland) at the rates of 0.5 mL min^{-1}. The manifold was constructed of PTFE tubing and 1/4-28 threaded PEEK connectors. A sample is injected into a flow of carrier (0.6 M HNO_3) by a six-port injection valve (5020 sample injection valve, Rheodyne, USA) with 250 μL sample loop. In a T-piece, chemical modifier from a separate channel is being mixed with the carrier. The reduction proceeds in a special arrangement at the tip of three concentric capillaries: the two inner ones (non-polar fused silica covered by polyimide, Supelco, USA, i. d. 0.25 mm and 0.53 mm). Innermost capillary leads carrier with a sample plug and chemical modifier, middle one the reductant solution and the outermost (PTFE, 1 mm i. d.) carrier gas Ar. The capillaries end in 1 mm distances and protrude 5 mm inside a gas-liquid separator (GLS, glass, 3 mL volume). The flow rate 50 mL min^{-1} of carrier gas Ar was kept for all experiments. Where stated, the small amount of oxygen was being mixed with carrier gas Ar in a T-piece before entering the PTFE capillary. Gas flows were controlled by mass flow controllers (FMA-2400 or 2600 Series, Omega Engineering). The outlet of the GLS is connected directly to a modified inlet arm of a atomizer (*see* Section 2.4.). A flow of waste stabilizer (0.5 M NaOH) was being pumped to the waste outlet from the GLS to stop the residual H_2 evolution within the waste liquid tubing, the waste liquid was being pumped out at arbitrary rate by the waste pump 2 to assure stable liquid level in the GLS.

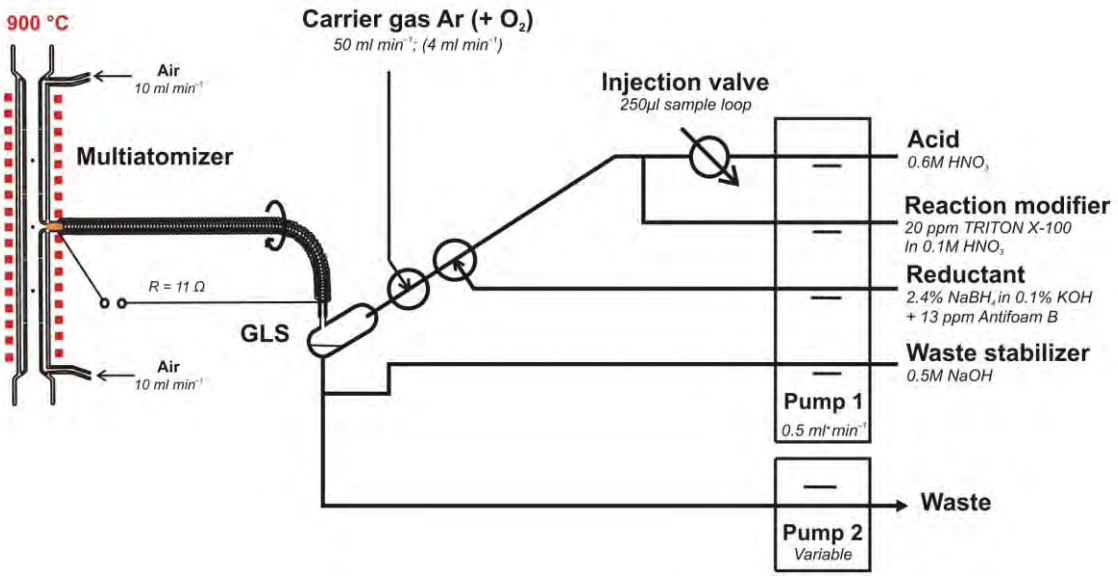

Fig. 1. The FI mode of chemical vapour generator and the modified multiatomizer for efficient transport.

The permanent modification of the generator was carried out by means of 4 mL of 10 µg mL^{-1} Pd solution (BDH, UK) in 0.1 M HNO_3 and 20 µg mL^{-1} Triton X-100 as described earlier [6, 13].

2.4. Atomizers

A modified multiple microflame quartz tube atomizer (model MM4 in Ref. [23]) was employed for atomization (Fig. 1). The horizontal arm of the atomizer was made of two concentric tubes: the inner one (optical, 145 mm long, 7 mm i. d.) was evenly perforated with 14 holes of approximately 0.5 to 1 mm in diameter. A total flow 20 mL min^{-1} of air (outer gas) was introduced from the sides into the cavity between the two tubes of the horizontal arm and then passed through the holes into the optical tube. The atomizer was heated electrically to 900 °C by an in-house made furnace controlled by a REX-C100 controller (Syscon, USA) with a K-type thermocouple sensor (Omega Engineering, USA). The inlet arm was modified because of straight connection to the outlet of the GLS (Fig. 1). The quartz tube (180 mm, 2 mm i. d., 6 mm o. d.) was bent to right angle in three--quarters (*see* Fig. 1) and wrapped with a wire Ni80-Cr20 (0.6 mm o. d., 5.275 Ω m^{-1}, 11 Ω total resistance, Omega Engineering,USA) for constant heating (Laboratory power supply, type EA-PS 3065-10 B, Viersen, Germany). The required temperature in the inlet arm was calibrated by the K-type thermocouple sensor (Omega Engineering, USA) in 6.5 cm distance from the optical path and the proper values of current and voltage were than applied during measurements. For experiments of in-atomizer trapping of silver on quartz surface a special

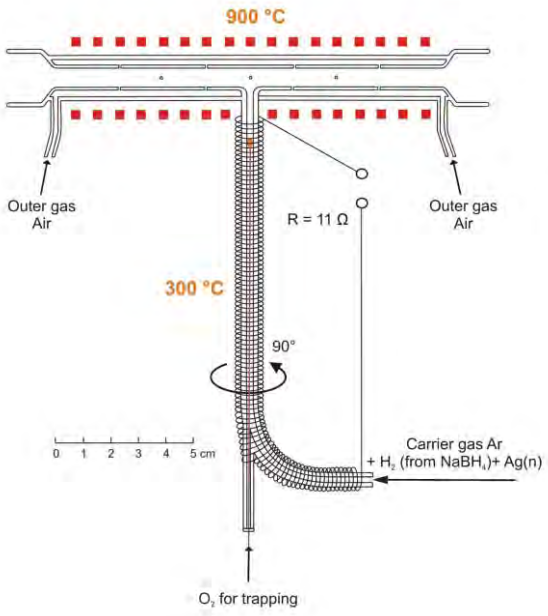

Fig. 2. The multiatomizer with intake for trapping capillary.

intake for capillary (non-polar fused silica covered by polyimide, 0.53 mm i. d.) was added for oxygen supply. The intake was made from a quartz tube (35 mm long, 1 mm i. d., 3 mm o. d.) which was attached in the bend prolonging the inlet arm (*see* Fig. 2). Where stated, the conventional quartz tube atomizer (QTA, 135 mm, 7 mm i. d.) for trapping was employed. In some experiments the end of the capillary (0.8 cm) was covered by THERMOKITT ROTH to prolong its lifetime.

2.5. Preparation of ^{111}Ag *radiotracer*

^{111}Ag radioactive indicator (half-life 7.45 days) of high specific activity (cca 10 MBq ng^{-1} Ag) was prepared by bombarding of target nuclide ^{110}Pd (palladium powder, 5N purity, Aldrich) with high flux of neutrons in a core of research nuclear reactor (LVR-15 Nuclear Research Institute Řež plc, Czech Rep.) at thermal output of 9.5 MW according to the nuclear processes: ^{110}Pd(n,γ) → → ^{111}Pd(β$^-$) → ^{111}Ag. After decaying of ^{111}Pd nuclide it was followed by chemical separation and isolation of ^{111}Ag radionuclide. Irradiated metallic palladium was dissolved in the mixture of concentrated HCl and HNO_3, the solution evaporated, redissolved in a minimum amount of 4 M HCl and applied on the column (2.5 mm diameter, 140 mm) of anion exchanger (Dowex 2, X-8, 200–400 mesh, Biorad) in Cl^- cycle. The ^{111}Ag radionuclide was separated by elution by 7 M HCl from target palladium and ^{192}Ir formed from iridium traces presented in target material. Combined fractions of silver were evaporated, carefully redissolved in 50 μl of 4 M HCl for final isolation of ^{111}Ag by elution by 7 M HCl on the anion-exchanger column (1.8 mm diameter, 50 mm, OSTION LG AT 8003, spheroidal particles 10–15 μm). The final fraction was evaporated and carefully redissolved in 0.6M HNO_3 for the CVG experiments.

2.6. Radiotracer experiments

All the radiometric experiments were carried out in the exhaust hood of a radiochemical laboratory. To establish proper performance of the system, the CVG was performed in CF mode using ^{111}Ag radiolabeled solution (cca 15 kBq per experiment) in 0.6 M HNO_3 with addition of non-active Ag standard solution as carrier to reach the analytical concentration of silver in the sample 50 ng mL^{-1}. The reason for carrier solution addition was to reach the same analyte concentration (or mass) as used in other experiments in this study to make the results fully comparable (contribution of ^{111}Ag, cca 5 pg mL^{-1}, to total analyte concentration is due to its high specific activity negligible). Then, four columns about 40 mm long in series filled with activated charcoal granules and separated by polyurethane foam plugs, followed by the disc syringe filter (FP 30/0.2 CA, 30 mm diameter, 0.2 μm pore size cellulose acetate membrane, Whatman-Schleicher & Schuell), were connected in place of the atomizer to the end of heated or unheated inlet arm in order to collect analyte species from the gaseous phase. The CVG from 300 μL of ^{111}Ag radiolabeled solution followed by blank solution (300 μL) was performed for 420 s to assure complete introduction to the system. At the same time, waste liquid was collected. Without stopping generation, the colums with activated chaircoal and filter were then changed for fresh ones and the CVG of radioactive indicator was repeated in the same way (two times more). Then the system was disassembled and the activity of individual parts of the apparatus was quantified using the auto-gamma counting system equipped with NaI(Tl) well-type detector (Minaxi 5000, Packard) with 2 min counting time. The activity was measured either directly (tubings, waste liquids, columns, PTFE capillary) or aqua regia rinses were made for those parts of the apparatus that could not been fit into the the well-type detector (GLS, inlet arm, quartz capillaries, filters). Obtained count values were corrected for blank counts and radioactive decay. The spatial distribution of the activity was investigated by image plate autoradiography and laser scanner (Fuji BAS 5000) was employed to measure phosphorescence induced by radioactivity present in the sample. Images were further evaluated using the AIDA software (Raytest GmbH, Germany).

3. Results and discussion

3.1. Transport of silver species

When measured with the multiatomizer with the modified inlet arm for efficient transport very noisy signals were sometimes observed. It was discovered that the small addition of oxygen to the carrier gas Ar improves the signal quality. The oxygen flow rate was altered in the range 1–6 mL min^{-1} without significant peak area improvement but it smoothed the shape significantly. The small oxygen-hydrogen flame (1.0–1.5 cm) was formed in the region about 2 cm from the optical path when the inlet arm was heated to 200 °C. At the flow rates higher than 6 mL min^{-1} the flame is unstable and flashes back to the GLS. The 4 mL min^{-1} of oxygen was chosen for futher work.

The optimization of temperature in the inlet arm is presented in Fig. 3 (*see next page*).

The best sensitivity and transport efficiency was achieved in the range of temperatures between 100 and 300 °C. For the unheated inlet arm the signal was only 88% compared with the heated inlet arm to 300 °C. This was caused mainly by condensation of water vapour on the walls near the GLS outlet. At temperatures higher than 300 °C the signal decreased probably becase of decomposition of silver particles. Silver is trapped on the walls and cannot reach the atomizer. 300 °C was found as optimal. The signal measured with the spray chamber (the original setup [16]) is attached for comparison. It can be depicted that the sensitivity increased about 2.7 times. Relative and absolute limits of detection (3σ, 250μL

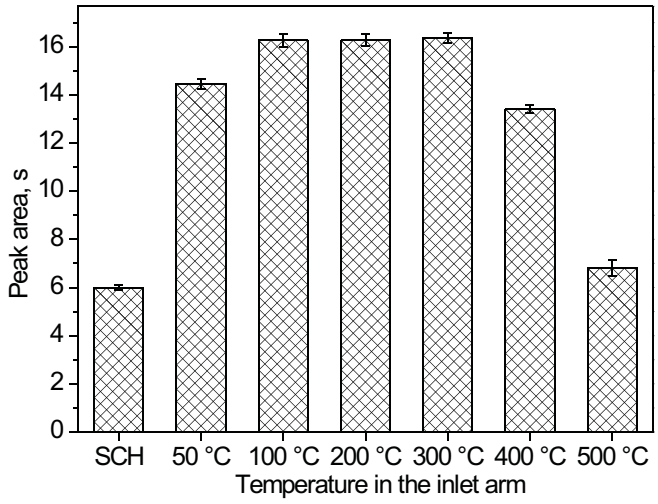

Fig. 3. Temperature in the inlet arm of the multiatomizer, 50 ng mL^{-1} Ag.

sample loop) measured with the new design of atomizer were improved proportionally to values 0.47 ng mL^{-1} and 0.12 ng, respectively.

The ^{111}Ag radiotracer was employed for determination of the CVG efficiency and the spatial distribution of residual ^{111}Ag in the apparatus. Initially, the collection of the volatilized analyte was attempted by two tandem disc filters used in our laboratory for trapping of silver species in previous study [16]. However, the water vapour leaving the heated inlet arm (300 °C) blocked the first filter in a minute and the overpreasure increased dramatically. Afterwards, four colums packed with activated chaircoal were used to remove water vapour and to trap silver species as well. One disk filter was placed at the end as a precaution. It was found out that 34% of analyte was converted to the gaseous phase and 32.5% was found in the columns and filter. The activity value in subsequent columns decreased exponentially and nearly no activity was measured on the filter. About 1.5% remained in the heated inlet arm. The biggest portion of ^{111}Ag was found in the waste liquid (21.9%) and in the waste tubings (18.3%) again. The rest was deposited on the wall of the apparatus: 16.5% on the wall of the GLS and about 5.6% on the tip of the cappilaries, where sample is being mixed with the reductant. Total 96.6% of activity, which entered the system, was recovered. The transport efficiency was also studied at temperatues 25 °C and 700 °C. The portions of analyte in the system were in a good agreement with the previous experiment with exception of activity in the inlet arm and on the columns. Transport losses, *i. e.* the portion of ^{111}Ag found in the inlet arm compared to the portion in the gaseous phase, were 24.4% and 78.3%, respectively. These values are significantly worse than that obtained for the inlet arm heated to 300 °C (4.4%) and so that the need of proper temperature for efficient transport was acknowledged. 300 °C was employed for futher investigations.

3.2. In-situ trapping of silver on quartz surface

A new design was produced for a trapping study so that the capillary could form small oxygen-hydrogen flame at its tip in various positions along the heated inlet arm (Fig. 2). The efficient trapping of hydride forming elements occurs in the excess of oxygen over hydrogen [19–22]. The oxygen flow rate was altered and the dependence of the signal is depicted in Fig. 4. The sudden fall of the signal to zero level was observed between 10 and 15 mL min^{-1} which corresponds to the excess of oxygen over hydrogen in the inlet tube. The flow rate 26 mL min^{-1} of hydrogen, which comes from the tetrahydroborate decomposition, was measured and corresponds to a calculated value.

When doing trapping experiments the CVG is carried out in the same way, only oxygen flow through the capillary (at least 20 mL min^{-1}) is applied over the same time as FIA measurements. It is followed by the volatilization stage. Silver species are evolved by the change of the gas composition, it means oxygen flow is decreased under stochiometric amount in a single step and hydrogen coming from the generator can volatilize trapped analyte. It was discovered that volatilization temperature and the short distance to the optical tube are crucial properties. It appears that 900 °C in the volatilization step is essential in order to minimize the width of the trap signal. For this purpose the tip of the quartz capillary was placed to the optical tube (900 °C both for trapping and volatilization). The quartz tube

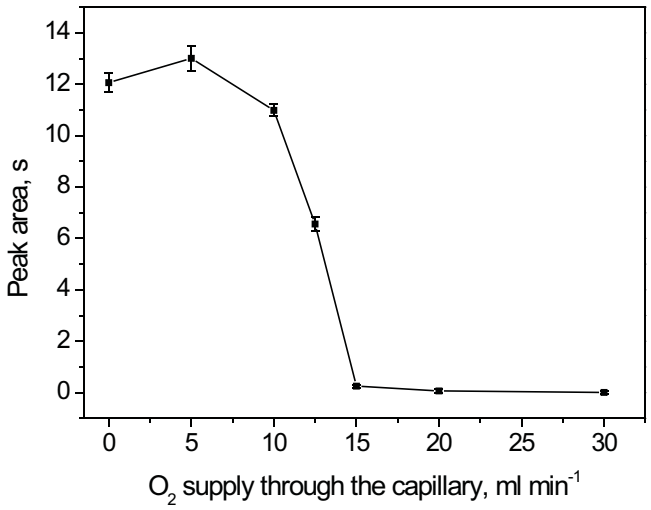

Fig. 4. Influence of oxygen introduced by the capillary on FIA signals, capillary position: 2.5 cm from the optical path of the multiatomizer, 50 ng mL^{-1} Ag.

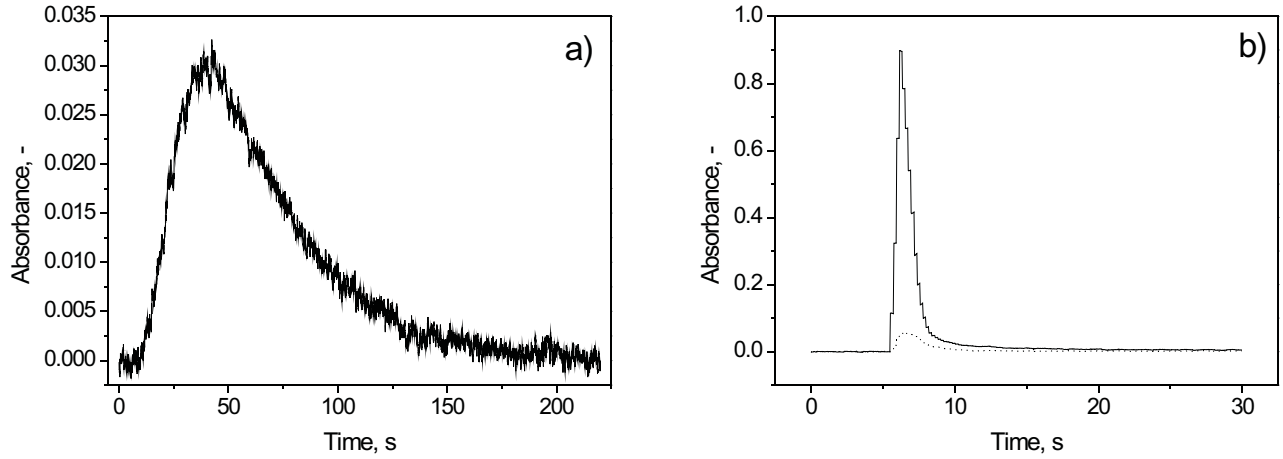

Fig. 5. The comparison of (a) FIA signal, 10 ng mL^{-1} Ag, and (b) trap signal, capillary position: 0 cm; solid line: 10 ng mL^{-1} Ag, dotted line: blank (trapping conditions: 900 °C, 30 mL min^{-1} O_2, 26 mL min^{-1} H_2; volatilization conditions: 900 °C, 26 mL min^{-1} H_2).

atomizer (QTA) with the modified inlet arm for trapping was chosen instead of the multiatomizer to prevent the influence of microflames in the optical tube.

The comparison of FIA and trap signal is displayed in Fig. 5. The trap provides much sharper signals, which can be reflected in the better signal to noise ratio – the important property of *LODs* assessment. However, experimental problems are encountered. The capillary tip is broken very easily after a few measurements of Ag standards. The signal shape is then gradually changed, the peak is decreased and broadened. It is probably caused by interaction of silver atoms with quartz surface at high temperature. The quartz corrosion can be even seen at the end of the inlet arm and junction with the optical tube. The high blank signals are the second relevant problem (*see* Fig. 5b). The reason may lie in the contamination from reagent solutions or silver deposited in the generator and released by the later reaction. To prolong the lifetime of the trapping capillary it was tested to coat its tip by high-temperature resistant material. At the same time some flow of oxygen through the capillary (8 mL min^{-1}) was maintained in the volatilization stage to avoid breaking during ignition. All other experimental conditions were the same. The trap signals were compared with the FIA signals (Table 1.) and the overall preconcentration efficiency (trapping and release) was assessed as 88±4%.

Table 1. Comparison of signals obtained with coated capillary, capillary position: 0 cm; 10 ng mL^{-1} Ag; trapping conditions: 900 °C, 30 mL min^{-1} O_2, 26 mL min^{-1} H_2; volatilization conditions: 900 °C, 8 mL min^{-1} O_2, 26 mL min^{-1} H_2.

Type of signal	Peak area, s
FIA	1.59 ± 0.02
Trap	1.55 ± 0.06
Trap (blank corrected)	1.40 ± 0.06

4. Conclusions

To sum up, the method of silver vapour generation was further developed in order to enhance transport efficiency. The new design of the multiatomizer is presented and the heating of the inlet arm to 300 °C was found to increase the introduction efficiency to more than 30 %. The ^{111}Ag radiotracer experiments have confirmed the AAS results. Yet unpublished possibility of in-atomizer collection of volatile silver species on quartz surface has been found feasible. The capillary position as well as volatilization temperature play a crucial role to gain very sharp signals without tailing. The material difficulties are discussed and will be solved in the near future.

Acknowledgements. *This project is supported by Grant Agency of the ASCR, v.v.i. (Grant No. IAA400310704), Academy of Sciences of the Czech Republic, v.v.i. (Institutional research plan No. AV0Z-40310501) and by the Czech Ministry of Education, Youths and Sports (project MSM 0021620857).*

References

[1] Pohl P., Prusisz B.: *Anal. Bioanal. Chem.* **388** (2007), 753–762.
[2] Dědina J., Tsalev D. L.: *Hydride generation atomic absorption spectrometry.* Wiley, Chichester 1995.
[3] Pohl P.: *Trends Anal. Chem.* **23** (2004), 21–27.
[4] Matoušek T.: *Anal. Bioanal. Chem.* **388** (2007), 763–767.
[5] Matoušek T., Dědina J., Vobecký M.: *J. Anal. At. Spectrom.* **17** (2002), 52–56.
[6] Matoušek T., Sturgeon R. E.: *J. Anal. At. Spectrom.* **18** (2003), 487–494.
[7] Pena-Vázquez E., Villanueva-Alonso J., Bermejo-Barrera P.: *J. Anal. At. Spectrom.* **22** (2007), 642–649.
[8] Sun H. W., Suo R.: *Int. J. Environ. Anal. Chem.* **88** (2008), 791–801.
[9] Xu S. K., Sturgeon R. E.: *Spectrochim. Acta B* **60** (2005), 101–107.

[10] Ma H. B., Fan X. F., Zhou H. Y., Xu S. K.: *Spectrochim. Acta B* **58** (2003), 33–41.
[11] Li Z. X.: *J. Anal. At. Spectrom.* **21** (2006), 435–438.
[12] Sun H. W., Suo R., Lu Y. K.: *Anal. Chim. Acta* **457** (2002), 305–310.
[13] Matoušek T., Sturgeon R. E.: *J. Anal. At. Spectrom.* **19** (2004), 1014–1016.
[14] Zhang C., Li Y., Cui X. Y., Jiang Y., Yan X. P.: *J. Anal. At. Spectrom.* **23** (2008), 1372–1377.
[15] Feng Y. L., Sturgeon R. E., Lam J. W., D'Ulivo A.: *J. Anal. At. Spectrom.* **20** (2005), 255–265.
[16] Musil S., Kratzer J., Vobecký M., Hovorka J., Benada O., Matoušek T.: submitted to *Spectrochim. Acta B*.
[17] Luna A. S., Sturgeon R. E., de Campos R. C.: *Anal. Chem.* **72** (2000), 3523–3531.
[18] Luna A. S., Pereira H. B., Takase I., Goncalves R. A., Sturgeon R. E., de Campos R. C.: *Spectrochim. Acta B* **57** (2002), 2047–2056.
[19] Kratzer J., Dědina J.: *Anal. Bioanal. Chem.* **388** (2007), 793–800.
[20] Kratzer J., Dědina J.: *Spectrochim. Acta B* **60** (2005), 859–864.
[21] Kratzer J., Dědina J.: *J. Anal. At. Spectrom.* **21** (2006), 208–210.
[22] Kratzer J., Dědina J.: *Spectrochim. Acta B* **63** (2008), 843–849.
[23] Matoušek T., Dědina J., Selecká A.: *Spectrochim. Acta B* **57** (2002), 451–462.

Ionic Liquids – Electrolytes For Electrochemical Sensors

Martina Nádherná[a, b], František Opekar[a], Jakub Reiter[b]

[a] *Department of Analytical Chemistry, Faculty of Science, Charles University in Prague, Albertov 2030, 128 43 Prague 2, Czech Republic*
[b] *Institute of Inorganic Chemistry of the ASCR, v. v. i., 250 68 Řež near Prague, Czech Republic,* ✉ *nadherna@iic.cas.cz*

Keywords
gold minigrid
ionic liquid
nitrogen dioxide
reticulated vitreous carbon
sensor

Abstract
New ionic liquid-polymer electrolyte was successfully tested in two amperometric solid-state sensors sensitive towards nitrogen dioxide. The electrolyte consists of 1-butyl-3-methylimidazolium hexafluorophosphate and poly(ethylene glycol) methyl ether methacrylate in the ratio 57:43 mol. %. Gold minigrid or reticulated vitreous carbon were used as an indicating electrode, Pt/air as a reference and platinum as a counter electrode. The analyte, gaseous nitrogen dioxide in air, was determined using electrochemical reduction at −600 mV and −900 mV *vs.* Pt/air on gold or reticulated vitreous carbon electrode, respectively.

1. Introduction

A significant group of chemical sensors is based on the electrochemical principles. Beside numerous bio-applications, the detection of environmentally important gases is being intensively studied. The parameters of the chemical sensor are primarily determined by the type of material of the basic sensor parts and their configuration. One of important parts of the sensor is the electrolyte, which should exhibit good ionic conductivity together with chemical, thermal and electrochemical stability.

As a solid electrolyte, silver iodide [1], zirconium phosphate and phosphonate [2] and many other inorganic materials were used [3], but their low conductivity in some cases has to be solved by elevated operating temperature. Another type of sensors contain liquid phase as the electrolyte. *E. g.* the Clark type of amperometric sensor contains gas permeable membrane in contact with a liquid electrolyte [4]. These sensors give a reliable response at the room temperature, but the disadvantages are in the vaporization of the electrolyte with time and difficulties in their preparation and maintenance.

Due to these obstacles, recent development of solid-state electrolytes with good ionic conductivity is concentrated on the solid polymer electrolytes [5]. The absence of macroscopic liquid phase is important also due to the demand of the device miniaturisation. Inherent ion-conducting polymers (*e. g.* Nafion®) [6, 7] or various binary (polymer-salt) or ternary systems (polymer-solvent-salt) have been used as ion-conducting electrolytes in different electrochemical devices [8–11]. Since there is a problem with partial or complete vaporization of the present solvent from the electrolyte and due to a big influence of the humidity on the overall conductivity in case of hydrophilic polymers such as Nafion®, electrolytes without volatile solvents are highly appreciated.

In the previously developed NO_2 solid-state sensor, a ternary system polyvinylchloride (PVC), 2-nitrophenyloctyl ether (NPOE), and tetrabutylammonium hexafluorophosphate ($TBAPF_6$) served as the electrolyte [11, 12]. To maintain the advantages of the polymer gel electrolytes or solid polymer electrolytes, our interest was aimed at a combination of an ionic liquid and polymer forming together a self-standing stable electrolyte with sufficient ionic conductivity and electrochemical stability. Here, the ionic liquids employ their advantageous properties in comparison to water or non-aqueous solvents [13]. Especially for the electrochemical gas sensors their non-volatility, high thermal and electrochemical stability is appreciated [13]. The function of embedded solution of salt in a solvent is here joined in the hydrophobic ionic liquid [14].

Our recent work was focused on development and characterisation of binary polymer-ionic liquid electrolytes and their application in amperometric gas sensor for nitrogen dioxide detection. The principle of NO_2 detection is based on the measurement of current generated by the electrochemical reduction of NO_2. The generally accepted overall reaction of the NO_2 reduction [15, 16] is:

$$NO_2 + 2\,H^+ + 2\,e^- \rightarrow NO + H_2O \qquad (1)$$

2. Experimental

Several monomers or macromonomers: 2-hydroxyethyl methacrylate (HEMA, M = 130.1 g mol^{-1}), poly(ethylene glycol) methacrylate (PEGMA, M_n = 360 g mol^{-1}),

and poly(ethylene glycol) methyl ether methacrylate (PEGMEMA, M_n = 300 g mol^{-1}), all from Sigma-Aldrich), and ionic liquids: 1-butyl-3-methylimidazolium hexafluorophosphate ($BMIPF_6$), 1-butyl-3-methylimidazolium tetrafluoroborate ($BMIBF_4$) and 1-ethyl-3--methylimidazolium tetrafluoroborate ($EMIBF_4$), all prepared following literature [17–19], were combined in various molar ratios.

Polymer electrolytes were prepared by direct, thermally initiated radical polymerization (150 min at 80 °C) of the initial liquid mixture containing the monomer, ionic liquid (synthesised according to [18]), and polymerization initiator 2,2'-azo-bis(isobutyronitrile) (AIBN; Sigma-Aldrich; recrystallised from acetone). The polymerization was carried out in a cell formed of polypropylene plate, packing distance frame (silicone rubber) and glass plate.

The initial electrochemical characterization of prepared electrolytes was performed on a potentiostat PGSTAT 30 (Eco Chemie, The Netherlands) including the FRA-2 module for impedance measurements.

The sensors tested have been designed and fabricated as described previously [10, 11]. In the three-electrode arrangement, gold minigrid (Gold Mesh, 0.005 mm wire diameter, 1500 wires/inch; Goodfellow, United Kingdom) or reticulated vitreous carbon (100-S, Energy Research and Generation, USA) serves as an indicating electrode, platinum as an auxiliary and pseudoreference Pt/air electrode. The testing apparatus was described in ref. [10]. The air was pumped by a membrane pump (Cole-Palmer, USA) and divided into two streams: main and reference. A known amount of nitrogen dioxide was added to the main flow using a calibrated permeation tube (Vici AG International, USA) with NO_2 production of 148 ng min^{-1} (2%). The NO_2 concentration range (0.6–2.0 ng mL^{-1}, thus 0.3–1.1 ppm) was obtained by changing the air flow-rate along the permeation source. To humidify both air streams, two flask were included in the apparatus with salt solutions providing stable and reproducible relative humidity: LiCl (12%), $MgCl_2$ (33%), $Mg(NO_3)_2$ (54%), and NaCl (75%). The sensor was placed inside a glass through chamber with volume about 8 cm^3. All the measurements were implemented by room temperature with a gas flow rate of 1 mL s^{-1}. The potentiostat and current meter were laboratory made of the operational amplifiers.

3. Results and discussion

3.1. Preparation and optimisation of polymer-ionic liquid electrolyte

Our first step was to find compatible combination of an ionic liquid with a polymer. Various monomers and macromonomers were combined with imidazolium--based ionic liquids, see Tab. 1. This research follows the results reported previously, where the electrolyte based on poly(2-ethoxyethyl methacrylate)-ionic liquid-lithium salt contained also an aprotic solvent (propylene or ethylene carbonate) [18].

The combinations PEGMEMA-$BMIPF_6$ and PHEMA-$BMIBF_4$ form samples with suitable mechanical properties allowing both manipulation and electrochemical tests such as impedance and voltammetrical measurements. Impedance measurements showed a reasonable ionic conductivity of PEGMEMA-$BMIPF_6$ electrolyte (2.4×10^{-4} S cm^{-1} at 20 °C) and PHEMA--$BMIBF_4$ (8.2×10^{-6} S cm^{-1} at 20 °C). For other experiments was chosen electrolyte PEGMEMA-$BMIPF_6$ due to its higher conductivity.

The combination PEGMEMA-$BMIPF_6$ in the molar ratio 43:57 mol. % gives foils with suitable mechanical properties allowing both fabrication of a sensor and electrochemical tests.

3.2. Sensor with a gold minigrid electrode

Initially, a steady-state polarization curve of the reduction of nitrogen dioxide at the indication electrode at the relative humidity of 54% and the analyte concentration of 0.6 ppm. The measurement was done in the potential range from +300 to –1000 mV *vs.* Pt/air as shown on Fig. 1. The suitable potential for the NO_2

Table 1. Properties of prepared combinations of ionic liquids with polymers.

ionic liquid / polymer	$BMIPF_6$	$BMIBF_4$	$EMIBF_4$
HEMA	bad mechanical properties	75:25 (mol.%) good mechanical properties ($\sigma = 8.2\times10^{-6}$ S cm^{-1})	phase to phase separation
PEGMA	bad mechanical properties	phase to phase separation	phase to phase separation
PEGMEMA	43:57 (mol. %) good mechanical properties ($\sigma = 2.4\times10^{-4}$ S cm^{-1})	bad mechanical properties	phase to phase separation

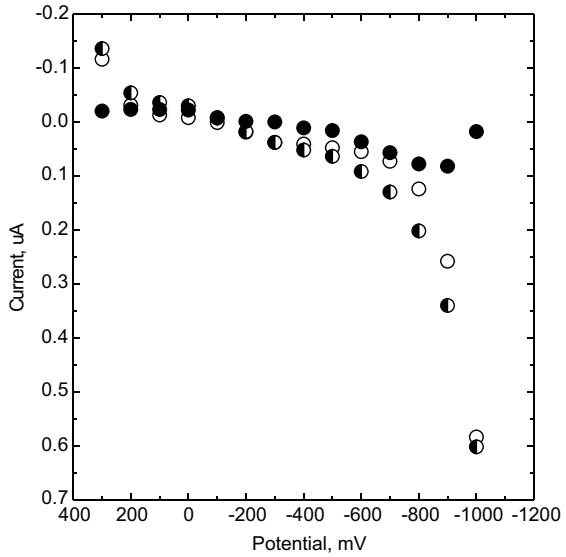

Fig. 1. Steady-state polarization curves of the sensor with gold minigrid (NO_2 concentration 0.6 ppm, flow rate 1 mL s^{-1}, relative humidity 54%) for pure air (background) – empty circle, air plus NO_2 reduction current – half full circle, NO_2 reduction current after background subtraction – full circle.

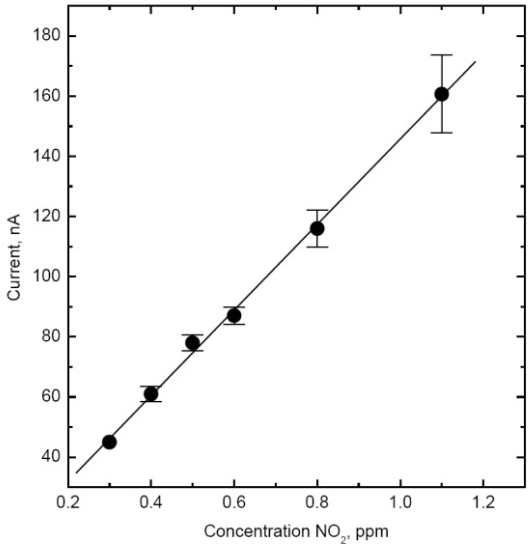

Fig. 2. Dependence of the gold minigrid sensor signal (reduction current without background) on the NO_2 concentration, (relative humidity 54%, flow rate 1 mL s^{-1}, at potential of −900 mV, NO_2 concentration range 0.3–1.1 ppm, standard deviations marked as error bars).

detection lies in the limiting current region, where the difference between the background current and the current of NO_2 reduction with background is the highest. According to this, the potential value of −900 mV *vs.* Pt/air was used in further measurements.

The dependence of the sensor response on nitrogen dioxide concentration was measured at the potential −900 mV and relative humidity 54%. The experimental data were fitted with the linear equation

$$I = 142\, c(NO_2) - 3.6 \qquad (2)$$

where I is current in nA, and $c(NO_2)$ concentration in ppm. The dependence was linear in the concentration range 0.3–1.1 ppm (Fig. 2).

Other obtained parameters are listed and compared with those for similar sensors [11, 12] in Table 2.

3.3. Sensor with a reticulated vitreous carbon electrode

A steady-state polarization curve of the reduction of nitrogen dioxide at the indication electrode at the relative humidity of 54% and the analyte concentration of 1.1 ppm was similar to the polarization curve on gold minigrid sensor. The highest difference between current obtained in pure air and reduction current of NO_2 was at the potential of −600 mV. At this potential the signal dependence on NO_2 concentration was measured, see Fig. 3. The dependence was linear in the concentration range 0.3−0.8 ppm and the regression equation is

$$I = 0.010\, c(NO_2) + 0.001 \qquad (3)$$

Analytical parameters for this sensor are reported in Tab. 3 and compared with those for similar sensor but with different electrolyte [10].

Table 2. Selected analytical parameters obtained for the sensor with Au minigrid indicating electrode in comparison with those obtained with the sensors containing Au powder [11] and Au minigrid [12] indicator electrode.

Parameter	Au minigrid	Au powder [11]	Au minigrid [12]
Electrolyte	PEGMEMA, $BMIPF_6$	PVC, NPOE, $TBAPF_6$	PVC, NPOE, $TBAPF_6$
Slope (sensitivity), nA/ppm	142 (3)	411 (22)	21.7 (0.5)
Intercept, nA	3.6 (2.2)	*n/a*	0.81
Standard error, nA	2.16	*n/a*	0.51
Correlation coefficient	0.998	0.99	0.999
Number of points	6	*n/a*	6
Working potential *vs.* Pt/Air electrode, mV	−900	−500	−300
Linear concentration range, ppm	0.3–1.1	*n/a*	0.2–5.0

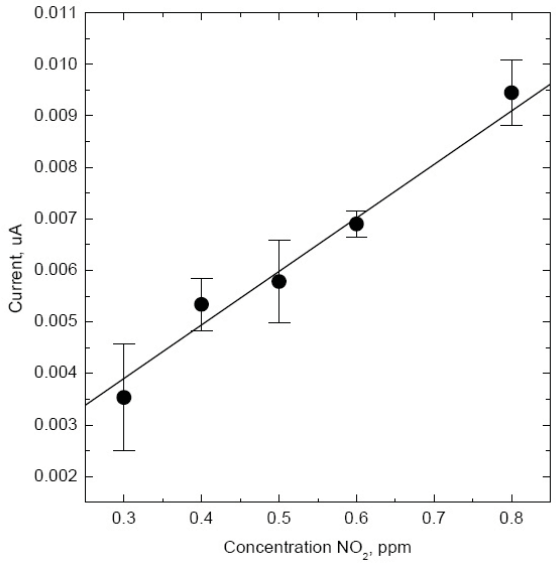

Fig. 3. Dependence of the sensor signal (reduction current without background) on the NO_2 concentration of the sensor with RVC indicating electrode, (relative humidity 54%, flow rate 1 mL s^{-1}, at potential of −600 mV, NO_2 concentration range 0.3−0.8 ppm, standard deviations marked as error bars).

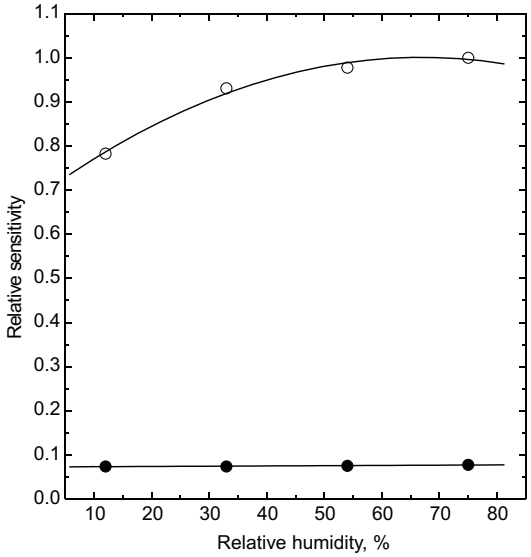

Fig. 4. Dependence of the relative sensitivity on the relative humidity for sensor with gold minigrid (empty ring), and for sensor with RVC (full ring) indicating electrode.

Table 3. Selected analytical parameters obtained for the sensor with reticulated vitreous carbon indicating electrode in comparison with those for the sensor from previous research [10].

Parameter	RVC	RVC [10]
Electrolyte	PEGMEMA, $BMIPF_6$	PVC, NPOE, $TBAPF_6$
Slope (sensitivity), nA/ppm	0.010 (0.001)	0.277 (0.009)
Intercept, nA	0.001 (0.001)	0.003 (0.007)
Standard error, nA	0.661	0.015
Correlation coefficient	0.964	0.994
Number of points	5	15
Working potential *vs.* Pt/Air electrode, mV	−600	−500
Linear concentration range, ppm	0.3–0.8	*n/a*

3.4. Influence of relative humidity on both tested sensors

The dependence of the relative sensitivity on relative humidity for both sensors is depicted on Fig. 4. Lower sensitivity and almost independency on relative humidity of sensor with RVC indicating electrode is demonstrable. In the case of gold minigrid we can see polynomial increase of signal dependency with increasing relative humidity.

The sensitivity decreased with increasing RH due to the presence of hydrophobic electrolyte both with gold minigrid and RVC indicating electrode [10, 12], while hydrophillic Nafion membrane had an opposite effect [20]. The sensor with polymer-ionic liquid electrolyte and Au minigrid electrode exhibits also increased sensitivity with increasing humidity to a certain extent. The sensitivity of the sensor with RVC electrode is practically independent on the change in RH. The explanation of the effect of the electrolyte hydrophobicity or hydrophillicity on the sensor sensitivity needs some more experiments.

Table 4. Comparison signals dependence on relative humidity for chosen sensors.

Sensor type	Sensitivity – dependence on RH
Au minigrid tested sensor	0.7% per 1% RH
Au minigrid [12]	−0.5% per 1% RH
RVC tested sensor	practically independent on RH
RVC [10]	−0.16% per 1% RH

4. Conclusions

In our recent work we demonstrated functionality of a binary polymer-ionic liquid electrolyte in the solid--state sensor for nitrogen dioxide with two different materials of indicating electrode: gold grid and reticulated vitreous carbon. Basic analytical parametrs were obtained including the effect of the relative humidity of analysed gas on the sensor functionality and sensitivity. Further research will include study of interferences and electrolytes with different ionic liquids.

Acknowledgements. *This work was supported by the Grant Agency of the Academy of Sciences of the Czech Republic (KJB200320901), the Ministry of Education, Youth and Sports (LC523 and MSM0021620857) and by the Academy of Sciences (AV0Z40320502).*

References

[1] Suzuki S., Nagashima K.: *Anal. Chim. Acta* **144** (1982) 261–266.
[2] Alberti G., Cherubini F., Palombari R.: *Sens. Actuators B* **24–25** (1995) 270–272.
[3] Alber K.S., Cox J.A., Kulesza P.J.: *Electroanalysis* **9** (1997) 97–101.
[4] Ramamoorty R., Dutta P.K., Akbar S.A.: *J. Mater. Sci.* **38** (2003) 35–44.
[5] Opekar F., Štulík K.: *Anal. Chim. Acta* **385** (1999) 151–162.
[6] Wallgren K., Sotiropoulos S.: *Electrochim. Acta* **46** (2001) 1523–1532.
[7] Mayo N., Harth R., Mor U.,Marouani D., Hayon J., Bettelheim A.: *Anal. Chim. Acta* **310** (1995) 139–144.
[8] Armand M.: *Solid State Ion.* **9–10** (1983) 745–754.
[9] Reiter J., Krejza O., Sedlaříková M.: *Sol. Energy Mater. Sol. Cells* **93** (2009) 249–255.
[10] Hrnčířová P., Opekar F., Štulík K.: *Sens. Actuators B* **69** (2000) 199–204.
[11] Hoherčáková Z., Opekar F.: *Sens. Actuators B* **97** (2004) 379–338.
[12] Langmaier J., Opekar F., Samec Z.: *Sens. Actuators B* **41** (1997) 1–6.
[13] *Electrochemical Aspects of Ionic Liquids.* Ohno H. (Ed.). New York, Wiley 2005.
[14] Wang R., Okajima T., Kitamura F., Ohsaka T.: *Electroanalysis* **16** (2004) 66–72.
[15] Sedlak J.M., Blurton K.F.: *Talanta* **23** (1976) 811–814.
[16] Bergman I.: *J. Electroanal. Chem.* **157** (1983) 59–73.
[17] Bonhote P., Dias A.P., Papageorgiou N., Kalyanasundaram K., Gratzel M.: *Inorg. Chem.* **35** (1996) 1168–1178.
[18] Reiter J., Vondrák J., Michálek J., Mička Z.: *Electrochim. Acta* **52** (2006) 1398–1408.
[19] Lewandowski A., Swiderska A.: *Solid State Ion.* **169** (2004) 21–24.
[20] Opekar F.: *Electroanalysis* **4** (1992) 133–137.

Determination of *trans*-Resveratrol on Carbon Paste Electrode

Lenka Němcová, Jiří Zima, Jiří Barek

UNESCO Laboratory of Environmental Electrochemistry, Department of Analytical Chemistry, Charles University in Prague, Albertov 6, 128 43 Prague 2, Czech Republic, ✉ *nemcova.len@seznam.cz*

Keywords
carbon paste electrode
electrochemical detection
HPLC
polyphenols
trans-resveratrol

Abstract
Trans-resveratrol (3,5,4′-trihydroxystilbene) is a polyphenolic compound present in peanuts, grapes, cranberries, buckwheat and wine which is well-known for its health protecting properties, such as anticarcinogenic, antioxidative, phytoestrogenic and cardioprotective activities. We have developed a reverse-phase high-performance liquid chromatographic method with amperometric detection to determine *trans*-resveratrol on carbon paste electrode in the concentration range from 4×10^{-8} to 1×10^{-4} M. The limit of detection was 3.5×10^{-8} M for electrochemical detection (E = +1.2 V) and 3.2×10^{-8} M for spectrophotometric detection (306 nm) in mixture of a Britton-Robinson buffer (pH = 7) with acetonitrile 1:1 (v/v).

1. Introduction

Trans-reveratrol (3,5,4′- trihydroxystilbene; Fig. 1) is a polyphenolic phytoalexin produced by plants in response to exogenous stimuli like UV light, ozone exposition, mechanical damage or fungal infection [1]. It can be found in more than 72 plants, which are often component of human diet [2], for example in wine grapes (also in red and less in white wine), peanuts, cabbage, beetroot, broccoli [3], blueberries [4], cranberries, buckwheat and many more.

Hydroxystilbenes are well known to have protective effects against reactive oxygen and nitrogen species. Resveratrol possesses diverse health-protecting properties, such as anti-inflammation, antioxidation, inhibition of platelet aggregation, chemoprevention of cancer, neuroprotective, anti-aging and protection of coronary heart disease [5–8]. *Trans*-resveratrol can undergo izomerization to the *cis* form when exposed to UV light [9–12].

Quantitative determination of *trans*-resveratrol is mainly done by HPLC with UV/VIS [13–15], MS [16, 17] and electrochemical detection [3, 18], GC/MS [19, 20] or electrophoresis [21, 22].

The aim of this work was to develop a new amperometric detection for HPLC method for the determination of trace amounts of trans-resveratrol using anodic oxidation at a carbon paste electrode (CPE) and compare it with spectrophotometric detection. The advantages of CPE [23–25] are broad potential window, low background current, possibility of chemical or biological modification of the carbon paste composition and ease of renewal of working surface of the carbon paste electrode.

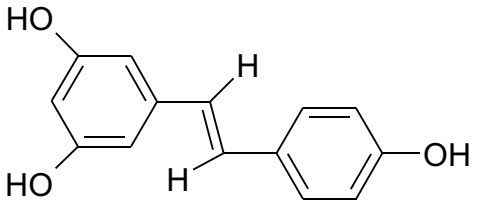

Fig. 1. Structure of *trans*-reveratrol

CPEs are very useful electrochemical sensors for the determination of organic compounds that can be anodically oxidized [26].

2. Experimental

2.1. Instruments

The HPLC system consisted of high-pressure piston pump HPP 5001 (Laboratorní přístroje, Czech Republic), injection valve D with 20 μL sample loop (Ecom, Czech Republic), spectrophotometric detector Sapphire 800 UV/VIS (Ecom, Czech Republic), electrochemical detector CHI 802B (CH Instruments Electrochemical Analysis, USA) with three-electrode system consisted of reference silver/silver chloride electrode RAE 113 (Monokrystaly, Czech Republic) filled with 3 M KCl, working CPE (3 mm in diameter) and platinum wire serving as auxiliary electrode. Column Kromasil C-18 (5 μm), 125 × 4 mm (Prochrome, India) and precolumn Gemini C-18, 4 × 3 mm (Phenomenex, USA) were used.

The mobile phase was acetonitrile-water (1:1, v/v), the flow rate was 1 mL min^{-1}. The amperometric

detector, employing electrochemical oxidation of phenolic hydroxy groups, was placed behind the UV/VIS detector operating at 306 nm. CPE was working in a wall--jet configuration. The system was operated by Clarity 2.3.0 programme (DataApex, Czech Republic) and CHI 6.26 programme (CH Instruments, USA) working in the Windows XP system (Microsoft).

An ultrasonic bath PS02000A (Powersonic, USA) was used to facilitate dissolution of the analytes. The pH of the solutions was measured with a pH meter Jenway 4330 (Jenway, UK) with a combined glass electrode. Spectrophotometer Agilent 8453 (Agilent, USA) was used to study the stability of the stock solution. All experiments were carried out at laboratory temperature.

2.2. Materials

Trans-reveratrol was purchased from Sigma-Aldrich (USA). Its stock solution (1×10^{-3} M) was prepared by dissolving an accurately weighed amount of the substance in methanol (p.a., Lach-Ner, Czech Republic) and stored away from daylight at 4 °C until used. Solutions of lower concentrations were prepared by dilution of the stock solution with methanol.

A spectrophotometric study of the stability of the stock solution demonstrated that it was stable for at least five months.

Britton-Robinson buffers were prepared in a usual way, by mixing 0.04 M phosphoric acid, 0.04 M acetic acid and 0.04 M boric acid with an appropriate amount of 0.2 M sodium hydroxide. All the chemicals used were of analytical reagent grade (Lachema, Czech Republic).

The mobile phase for HPLC contained acetonitrile for HPLC (Merck, Germany) and aqueous Britton-Robinson buffer diluted 10 times.

Carbon paste contained 250 mg of spherical microparticles of glassy carbon with a diameter 0.4–12 μm (Alpha Aesar, USA) and 90 μl of mineral oil (Fluka).

All aqueous solutions were prepared using deionized water obtained from a MilliQ Plus system (Millipore, France).

3. Results and discussion

One of the problems while determining *trans*-resveratrol is the fact, that trans-resveratrol izomerizes to *cis*-resveratrol, when exposed to UV radiation, included daylight. The mobile phase containing 50% acetonitrile and 50% of Britton-Robinson buffer allowed us to separate these two isomers in 4.5 min (with resolution of 1.6). The sample for the analysis was prepared by exposing (1×10^{-4} M in methanol) of trans-resveratrol to daylight for 20 min (Fig. 2).

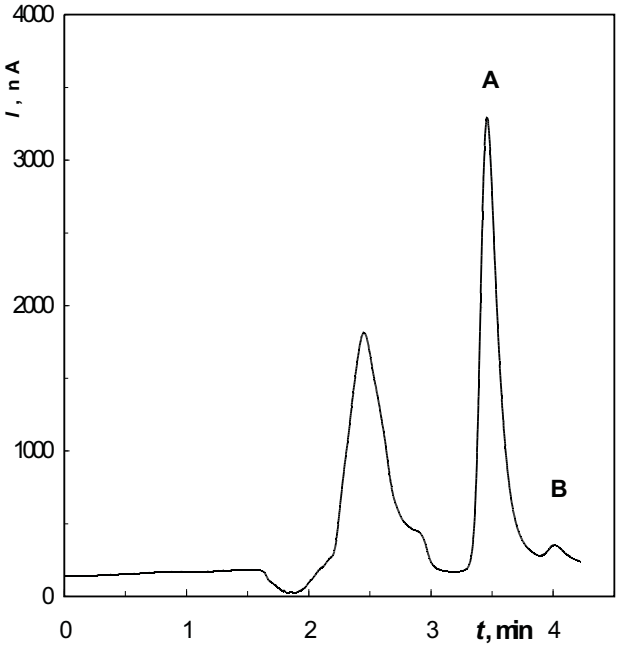

Fig. 2. HPLC-ED chromatogram of *trans*-resveratrol (injected 20 μl of 1×10^{-4} M solution) on CPE (E = + 1.2 V) after 20 minutes expositon to daylight, in the mobile phase Britton-Robinson buffer (pH = 7):acetonitrile (1:1). Peaks: *trans*-resveratrol (A), *cis*-resveratrol (B).

The separation of *trans*-resveratrol and *cis*-resveratrol was found to be independent of the pH of the mobile phase. Therefore, optimal pH was determined from hydrodynamic voltammograms from the region compatible with the used column. Hydrodynamic voltammograms in Britton-Robinson buffers of pH = 3, 5 and 7 in the potential range from 0.0 to +1.4 V are shown in Fig. 3. The highest and best developed analytical signals were obtained in Britton-Robinson buffer (pH = = 7):acetonitrile (1:1) at a potential +1.2 V.

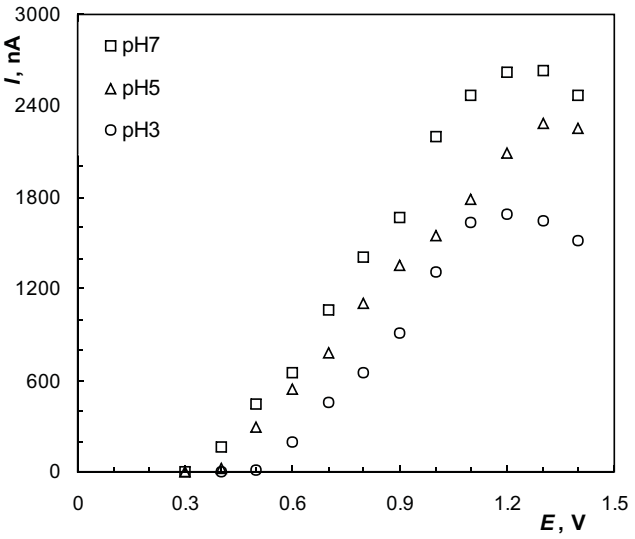

Fig. 3. Hydrodynamic voltammograms of *trans*-resveratrol (injected 20 μl of 1×10^{-4} M solution) on CPE in the mobile phase Britton-Robinson buffer (pH = 7):acetonitrile (1:1).

Table 1. Parameters of the calibration lines for HPLC-ED of *trans*-resveratrol on CPE ($E = +1.2$ V) measured in the concentration range of 4×10^{-8}–1×10^{-4} M.

Evaluated	Slope mA (*resp.* mC) M^{-1}	Intercept nA (*resp.* nC)	R^2	*LOD* 10^{-8} M
peak height	25.4	–0.86	0.9986	3.5
peak area	307.5	–13.9	0.9989	

Table 2. Parameters of the calibration lines for HPLC UV/VIS detection (306 nm) of *trans*-resveratrol measured in the concentration range of 4×10^{-8}–1×10^{-4} M.

Evaluated	Slope AU (*resp.* AU s) M^{-1}	Intercept mAU (*resp.* mAU s)	R^2	*LOD* 10^{-8} M
peak height	2457.6	–0.06	0.9993	3.2
peak area	21531	0.97	0.9991	

The calibration curves were measured in the concentration range of 4×10^{-8}–1×10^{-4} M. Calibration curves were measured in triplicate and evaluated by a linear regression method. The parameters of the measured calibration curves are summarized in Table 1 and 2. The limit of detection (*LOD*) was calculated as the amount of *trans*-resveratrol, which gave the signal three times higher than the background noise (*S*/N*)*. Calibration curve in the concentration range of 4×10^{-7}–1×10^{-6} M is shown in Fig. 4. It can be observed that the electrochemical detection on carbon paste electrode gives comparable results as the UV/VIS detection.

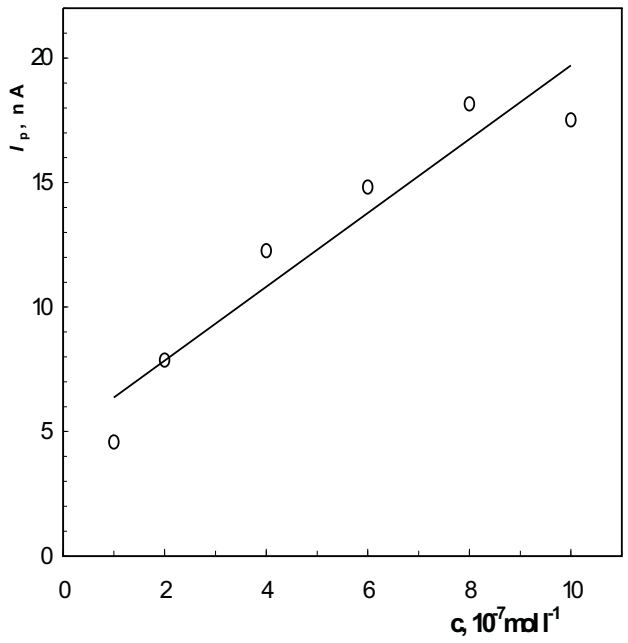

Fig. 4. HPLC-ED calibration curve of trans-resveratrol in the concentration range of 1×10^{-7}–1×10^{-6} M on CPE in the mobile phase Britton-Robinson buffer (pH = 7):acetonitrile (1:1).

4. Conclusions

The optimal conditions for the determination of *trans*--resveratrol using HPLC with spectrophotometric and electrochemical detection on the carbon paste electrode have been found. The limit of detection was 3.5×10^{-8} M for electrochemical detection (E = +1.2 V) and 3.2×10^{-8} M for spectrophotometric detection (306 nm) in a mixture of Britton-Robinson buffer (pH = 7) with acetonitrile 1:1 (v/v). It has been proved that both UV/VIS detection and electrochemical detection on carbon paste electrode is applicable in the determination of micro- and submicromolar concentrations of *trans*-resveratrol.

Acknowledgements. *This research was supported by the Ministry of Education, Youth and Sports of the Czech Republic (project LC 06035, MSM 0021620857, and RP 14/63).*

References

[1] Yu Ch., Shin Y. G., Chow A., Li Y., Kosmeder J. W., Lee Y. S., Hirschelman W. H., Pezzuto J. M., Mehta R. G., Breemen R. B.: *Pharm. Res*. **19** (2002), 1907–1914.
[2] Šmidral J., Filip V., Melzoch K., Hanzlíková I., Buckiová D., Křísa B.: *Chem. Listy* **95** (2001), 602–609.
[3] Kolouchová I., Melzoch K., Šmidrkal J., Filip V.: *Chem. Listy* **99** (2005), 492–495.
[4] Rimando A. M., Cody R.: *LC/GC North Am.* **23** (2005), 1192–1200.
[5] Huang H., Zhang J., Chen G., Lu Z., Wang X., Sha N., Shao B., Li P., Guo D.: *Biomed. Chromatogr.* **22** (2008), 421–427.
[6] Delmas D., Jannin B., Latruffe N.: *Mol. Nutr. Food Res.* **49** (2005), 377–395.
[7] Kueck A., Opipari A. W., Griffith K. A., Tan L., Choi M., Huang J., Wahl H., Liu J. R.: *Gynecol. Oncol.* **107** (2007), 450–457.
[8] Sönmez U., Sönmez A., Erbil G., Tekmen I., Baykara B.: *Neurosci. Lett.* **420** (2007), 133–137.

[9] López-Hernández J., Paseiro-Losada P., Sanches-Silva A. T., Lage-Yusty M. A.: *Eur. Food Res. Technol.* **225** (2007), 789–796.
[10] Goldberg D. M., Ng E., Karumanchiri A., Yan J., Diamandis E. P., Soleans G. J.: *J. Chromatogr. A* **708** (1995), 89–98.
[11] Wang L., Zhang Z.: *Anal. Chim. Acta* **592** (2007), 115–120.
[12] Trela B. C., Waterhouse A. L.: *J. Agric. Food Chem.* **44** (1996), 1253–1257.
[13] Souto A. A., Carneiro M. C., Seferin M., Senna M. J. H., Conz A., Gobbi K.: *J. Compos. Anal.* **14** (2001), 441–445.
[14] Zhu Z., Klironomos G., Vachereau A., Neirinck L., Goodman D. W.: *J. Chromatogr. B* **724** (1999), 389–392.
[15] Pineiro Z., Palma M., Barroso C. G.: *J. Chromatogr. A* **1110** (2006), 61–65.
[16] Stecher G., Huck Ch. W., Popp M., Bonn G. K.: *Fresenius J. Anal. Chem.* **371** (2001), 73–80.
[17] Liu R., Zhang J., Liang M., Zhang W., Yan S., Lin M.: *J. Pharm. Biomed. Anal.* **43** (2007), 1007–1012.
[18] McMurtrey K. D., Minn J., Pobanz K., Schultz T. P.: *J. Agric. Food Chem.* **42** (1994), 2077–2080.
[19] Luan T., Li G., Zhang Z.: *Anal. Chim. Acta* **424** (2000), 19–25.
[20] Flamini R., Vedova A. D.: *Rapid Commun. Mass Spectrom.* **18** (2004), 1925–1931.
[21] Gu X., Ureasy L., Kester A., Zeece M.: *J. Agric. Food Chem.* **47** (1999), 3223–3227.
[22] Peng Y., Zhang Y., Ye J.: *J. Agric. Food Chem.* **56** (2008), 1838–1844.
[23] Adams R.N.: *Anal. Chem.* **30** (1958), 1576.
[24] Švancara I., Vytřas K.: *Chem. Listy* **88** (1994), 138–146.
[25] Švancara I., Schachl K.: *Chem. Listy* **93** (1999), 490–499.
[26] Zima J., Stoica A.I., Zítová A., Barek J.: *Electroanalysis* **18** (2005), 158–162.

Conformational Changes of Polypeptides Studied by Vibrational Circular Dichroism

Pavlína Novotná[a], Marie Urbanová[b]

[a]Department of Analytical Chemistry, [b]Department of Physics and Measurements, Institute of Chemical Technology, Technická 5, 166 28 Prague 6, Czech Republic, ✉ Pavlina.Novotna@vscht.cz, ✉ Marie.Urbanova@vscht.cz

Abstract

Poly-γ-benzyl-L-glutamate (PBLG) and poly-β-benzyl-L-aspartate (PBLA) are synthetically prepared polypeptides soluble in organic solvents. Their conformations and aggregation states were studied by vibrational circular dichroism spectroscopy (VCD) under different conditions: acidity of solvent and temperature. PBLG and PBLA both exhibit the α-helical conformation in several helicogenic solvents. However, their structures have different sense of helicity. The effect of additions of trifluoroacetic acid into the solution of PBLG or PBLA in $CHCl_3$ was studied in this work. The change of the conformation from α-helical to polyproline II-like was observed. A lower stability of the α-helical conformation of PBLA than PBLG was also proven. Temperature dependent spectra of PBLG were measured in temperature region 13–50 °C. Induction of secondary conformational changes was also observed; either from α-helical to polyproline II-like or vice versa, depending on the temperature and on the amount of trifluoroacetic acid in solution.

Keywords
conformational changes
polypeptide
poly-β-benzyl-L-aspartate
poly-γ-benzyl-L-glutamate
temperature dependence
vibrational circular dichroism

1. Introduction

Polypeptides are important compounds especially due to their close relation to proteins. Their secondary and tertiary structure, besides their chemical constitution, determines unique and various characteristics of proteins. Polypeptides can then be used as model compounds for such complicated biological systems.

The synthetic polypeptides poly-γ-benzyl-L-glutamate (PBLG) and poly-β-benzyl-L-aspartate (PBLA) are both soluble in organic solvents and they show topological chirality. Their secondary structure and aggregation state depend on the solvent used, on the concentration of the solution and on the temperature. Because of this, they represent good model matrices for study of biologically important interactions in dependence on the acidity and polarity of the solvent and also on the structure of the chiral matrix used. Following of systems like PBLG or PBLA in diverse organic solvents can help understanding aggregation and conformational changes in biological systems. This is the main reason why these two polypeptides were chosen to show what structural information can be provided by vibrational circular dichroism (VCD) in the infrared (IR) region.

Chiral molecules absorb right and left circularly polarized light in slightly different extents. Circular dichroism is defined as a difference between the absorptions for the left and right circularly polarized light. The transitions between vibrational states of the molecule occur if the incoming light is from the IR region and we then measure VCD spectra [1]. The intensity of the VCD signal is approximately 4–6 grades weaker than the corresponding absorption.

The structural properties of synthetic polypeptides were characterised by various chemical and physical methods. However, VCD provides alternative view on polypeptides and proteins with advantage discussed in reviews [1, 2] over more routine electronic circular dichroism (ECD), IR spectroscopy and other structural methods. Both polypeptides have been already studied by VCD [3–8], but these studies were predominantly focused on characterization of their α-helical conformation in chloroform solution.

Both polypeptides are formed by the derivatized amino acid groups: glutamic and aspartic acid. Both amino acids are chiral but this paper follows rather chirality which is evoked by the secondary conformation of the polypeptide chain. Main difference between PBLG and PBLA issues from their side chains which are one carbon shorter for PBLA. This also causes principal differences in the stability of their conformations.

Conformation and aggregation of PBLG and PBLA is mainly influenced by the polarity and acidity of the solvent. PBLG takes the right-handed α-helix in solvents like chloroform, benzene, dioxane or nitrobenzene [9]. This conformation is stabilised by intramolecular hydrogen bonds. Besides, formation of intermolecular hydrogen bonds [10, 11] causes molecular association and formation of aggregates. Cholesteric liquid crystals may be formed at high concentrations [12].

PBLA is on the contrary very unusual synthetic homopolypeptide because it forms left handed α-helix in

common helicogenic solvents such as chloroform. This behaviour is probably induced by steric hindrance in the side chains which are shorter than for PBLG. The right handed structure is also high on entropy and then destabilised energetically [13, 14]. However, the right handed α-helix of PBLA was still observed in trimethylphosphate solution [15].

Both PBLG and PBLA take the conformation analogical to polyproline II conformation (PPII) in acidic solvents like trifluoroacetic acid (TFA) or dichloroacetic acid (DCA). Interactions between the acid and the polypeptide are of high importance in these solutions. The PPII conformation was formerly entitled as disordered random coil structure. But ECD and especially VCD studies [2, 16] prove that this secondary structure is the locally ordered left-handed helix.

The above mentioned conformations are characterised in this work by vibrational circular dichroism and IR absorption spectroscopy. Different conditions as acidity of the solvent or temperature were examined in order to induce conformational changes of the polypeptides.

2. Experimental

2.1. Chemicals

Poly-γ-benzyl-L-glutamate (Fig. 1) of the average molecular weight 69 000 g mol^{-1} (Sigma) and poly-β--benzyl-L-aspartate (Fig. 1) of the average molecular weight 26 600 g mol^{-1} (Sigma) were used in this work. Chloroform (Lachner) and trifluoroacetic acid (Penta) were used for preparations of the polypeptide solutions.

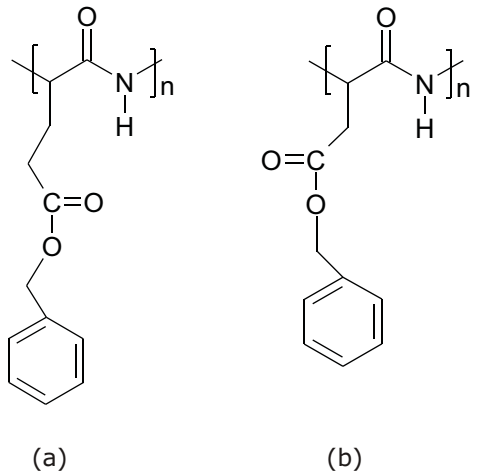

Fig. 1. Structural formula of poly-γ-benzyl-L-glutamate (a), and poly-β-benzyl-L-aspartate (b)

2.2. Instrumentation, experimental conditions

The VCD spectra were recorded in two IR regions: the first being 1800–1400 cm^{-1} (region I), the second being 3800–2000 cm^{-1} (region II). Fourier transform spectrometer IFS-66/S (Bruker, Germany) equipped with a VCD/IRRAS module PMA 37 (Bruker, Germany), a BaF_2 polarizer, a ZnSe photoelastic modulator (Hinds Instruments) and a MCT (InfraRed Associates) detector was used in region I. Fourier transform spectrometer Tensor 27 (Bruker, Germany) equipped with a VCD/IR-RAS module PMA 50 (Bruker, Germany), a BaF_2 polarizer, a ZnSe photoelastic modulator (Hinds Instruments) and a LN-InSb (InfraRed Associates) detector was used in region II.

The absorption and VCD spectra were recorded simultaneously with a resolution 8 cm^{-1} using methods described earlier [17, 18]. Each spectrum is an average of six blocks, each measured for 20 minutes. Only the temperature dependent spectra were measured as six 10 minutes blocks. A baseline correction was made because of the weak VCD signal. The baseline was obtained as the spectrum of the solvent measured at same conditions as the spectrum of the sample. The IR absorption spectra are also corrected for the solvent absorption.

The liquid samples were placed in an A145 demountable cell (Bruker) constructed of the CaF_2 or infrasil windows separated by 0.05 mm teflon spacers. The temperature dependent spectra were measured in a demountable electric heated cell P/N20500 (Specac, UK) constructed of the CaF_2 windows separated by a 0.05 mm teflon spacer. The heated jacket controller 3000 series (Specac, UK) adjusted the temperature.

2.3. Solution preparation

PBLG solutions in $CHCl_3$ and in the mixed solvent $CHCl_3$/TFA were prepared for concentration of $\rho = 30$ g L^{-1}. The volume fractions of TFA in $CHCl_3$ were 0.05, 0.1, 0.15, and 0.20.

Solutions of PBLA in $CHCl_3$ and in mixed solvent system $CHCl_3$/TFA were prepared for the same concentration of $\rho = 30$ g L^{-1}. The volume fractions of TFA in $CHCl_3$ were 0.01, 0.02, 0.05, and 0.20.

3. Results and discussion

3.1 Effect of the amount of TFA in $CHCl_3$/TFA solutions on the structure of PBLG

Figures 2 and 3 show the spectra of PBLG dissolved in $CHCl_3$ and in $CHCl_3$/TFA with various volume fractions of TFA for the regions I and II, respectively. The VCD

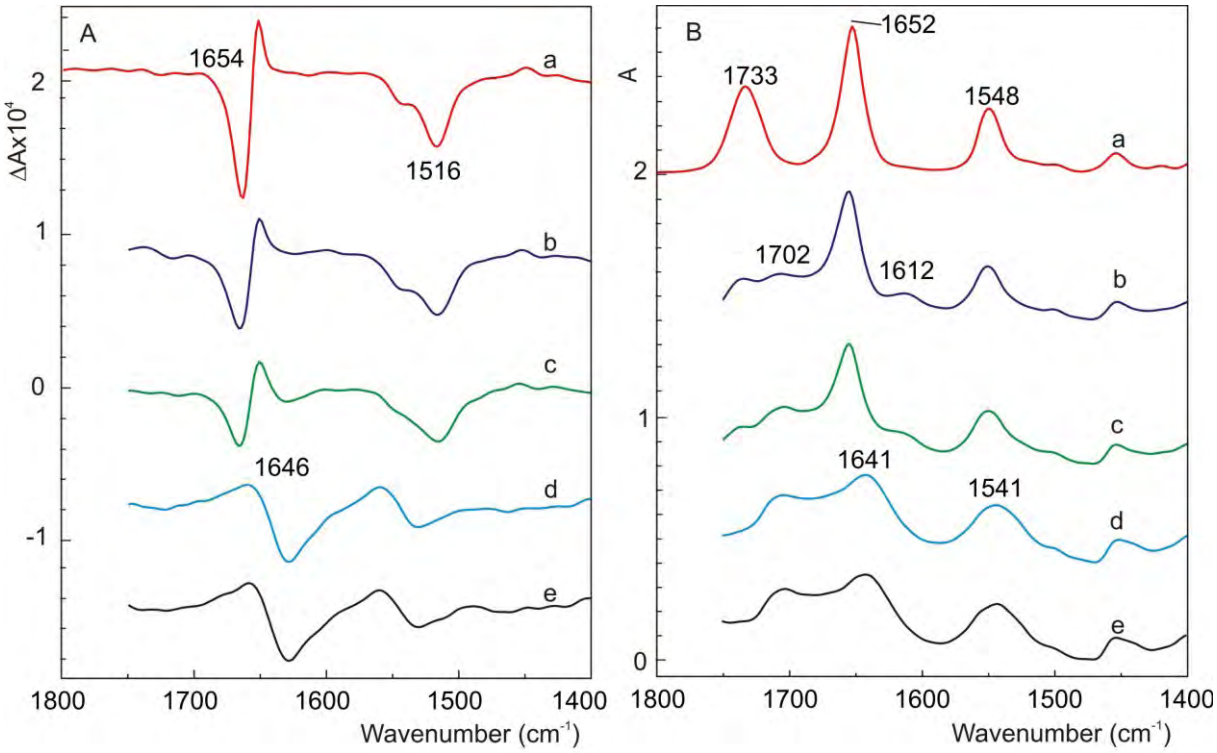

Fig. 2. Vibrational circular dichroism (A) and absorption (B) spectra of PBLG in $CHCl_3$ (a) and in $CHCl_3$/TFA for volume fractions of TFA: (b) 5 vol.%, (c) 10 vol.%, (d) 15 vol.%, and (e) 20 vol.% in the region I. Some spectral regions were omitted because of a high absorption of TFA.

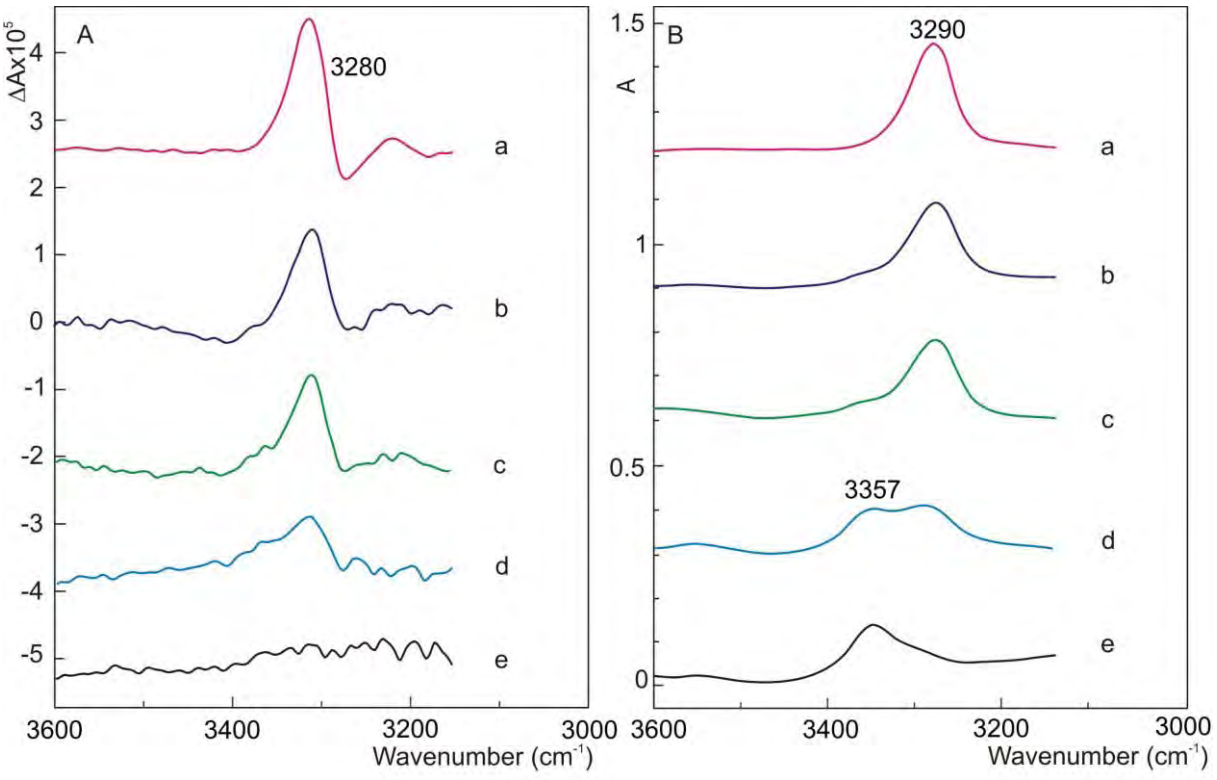

Fig. 3. Vibrational circular dichroism (A) and absorption (B) spectra of PBLG in $CHCl_3$ (a) and in $CHCl_3$/TFA for volume fractions of TFA: (b) 5 vol.%, (c) 10 vol.%, (d) 15 vol.%, and (e) 20 vol.% in the region II. Some spectral regions were omitted because of a high absorption of TFA.

spectrum of PBLG in $CHCl_3$ in region I is characterised by a positive VCD couplet in the amide I at 1664(–)/1650(+) cm^{-1} and by a negative VCD signal in amide II at 1516 cm^{-1}. A positive VCD couplet is a pair of reversed VCD signals, the positive one being at lower wavenumbers. These spectral characteristics are typical for right-handed α-helix [19]. In region II, three signals (+)/(–)/(+) are observed in amide A.

As the amount of TFA increases, changes in the VCD and absorption spectra occur in the both regions I and II.

In region I the following changes are observed. The intensity of the absorption signal at 1733 cm^{-1} decreases and the intensity of the signal at 1702 cm^{-1} increases simultaneously. With the first addition of the acid, a new signal at 1612 cm^{-1} appears and intensity of the amide I is moderately lowered. More pronounced changes are observed in the VCD spectra. When the amount of TFA in $CHCl_3$ increases up to 10 vol.%, the intensities of the positive and negative signals of the amide I couplet become more balanced and the intensity of the amide II negative signal at 1516 cm^{-1} slightly decreases. For solution with 15 vol.% of TFA in $CHCl_3$, the signs of the amide I couplet changes and the position shifts to lower wavenumbers: from 1654 to 1646 cm^{-1}. Simultaneously, the absorption signal is shifted from 1652 to 1641 cm^{-1}. Between 10 and 15 vol.% of TFA, the shape of the VCD signal of amide II changes from the clear negative signal to a new negative couplet and the corresponding absorption is shifted from 1548 to 1541 cm^{-1}. In the region II the following changes were observed. With increasing amount of the acid, the absorption signal of the amide A shifts from 3290 to 3357 cm^{-1}. VCD signal at 3280 cm^{-1} gradually weakens.

The changes of absorption signal intensities at 1733 and 1702 cm^{-1} may be explained subsequently. In both cases these signals correspond to the vibrations of the C=O ester groups in the side chains of the polypeptide. These groups interact with TFA via hydrogen bonds which results in the shift of the peak position [20].

The new signal at 1612 cm^{-1} and the moderate decrease of the signal intensity of amide I are results of the hydrogen bonds formation between TFA and C=O groups in the main chain. TFA does not interact with all C=O groups but only with a few accessible, especially terminal groups of the polypeptide [20]. This is the reason for the small intensity of the signal.

The equalizing of the amide I couplet intensity and the decrease of the intensity of amide II signal may be related to a decrease of the PBLG aggregation. TFA, the polar and acidic solvent, prevents aggregation because it interacts with PBLG itself and competes intermolecular hydrogen bonds between PBLG molecules. This interpretation corresponds to the change of the sample viscosity. The change of the signs of the amide I couplet and its shift occurs at higher amounts of TFA in the solution: 15 and 20 vol.%. This can be due to the change of conformation from right-handed α-helical to PPII-like, which is characterized as locally left-handed helix [16]. Because the sense of the helix locally changes, the signs of the couplet change as well. The shift of the couplet is connected with the change of the conformation and also with the hydrogen bonds between TFA and C=O groups of the main chain.

The changes in VCD spectra also occur in amide II. Between 10 and 15 vol.% of TFA in the solution, the shape of the VCD signal transforms. Simultaneously the absorption signal shifts. These changes are probably results of a formation of hydrogen bonds between TFA and the C=O groups of the main chain [20]. The observation is also connected with the change of the conformation; it takes place together with the transformation to the PPII-like structure.

Changes in the amide A region are closely connected with the amide II region. Both signals in the absorption spectrum show the change of the hydrogen bond character in dependence on the amount of TFA in the solution. Intermolecular bonds disrupt with additions of the acid and the acid interacts with C=O groups of PBLG itself. These changes can be observed in the absorption spectra in the both regions. The amide II position shifts from 1548 to 1541 cm^{-1} and the amide A position from 3290 to 3357 cm^{-1}. For 5 and 10 vol.%, the intensity of the negative amide II signal decreases but then the shape of the signal transforms and the influence of the hydrogen bonds is not clear. The triple amide A VCD signal gradually decreases in intensity and is nearly not notable at 20 vol.% of TFA in the solution. The conformational change can not be observed in this region. Hydrogen bonds between TFA and the N-H group of the main chain must also be considered. But in the case of their existence the frequencies of amide A and II would be probably lower [20, 21].

VCD spectra of amide I and II remain nearly the same for solutions with 15 and 20 vol.% of the acid so probably no other conformational changes take place.

Around 10 vol.% of TFA in the solution, the helices cease to aggregate and this is accompanied by the decrease of the solution viscosity. Distinctive change of the conformation from α-helix to PPII-like occurs between 10 and 15 vol.% of the acid. Next addition of the acid to 20 vol.% probably does not cause any conformational changes. These changes go along with the changes of hydrogen bonds in the system. At the beginning, the intermolecular hydrogen bonds between PBLG molecules weaken and the C=O groups of the side chains interact with TFA which destabilizes the α-helical conformation. This is the same for the C=O groups of the

main chain. The interaction with TFA does not support the α-helical conformation and the structure changes to PPII-like.

3.2 Effect of the amount of TFA in $CHCl_3$/TFA solutions on the structure of PBLA

Figures 4 and 5 show spectra of PBLA dissolved in $CHCl_3$ and in $CHCl_3$/TFA with various volume fractions of TFA in the regions I and II, respectively. The VCD spectrum of PBLA in $CHCl_3$ in region I is characterised by a negative VCD couplet in amide I at 1671(+)/ /1659(–) cm^{-1} and a positive VCD signal in amide II at 1547 cm^{-1}. These spectral characteristics are typical for left-handed α-helix [19]. In region II three signals in amide A at 3329(–)/3284(+)/3232(–) cm^{-1} are observed.

When the amount of TFA increases, several changes both in VCD and in absorption spectra occur. In region I the following changes were observed. With the first additions of the acid, the negative couplet in amide I weakens. At 5 vol.% of TFA in the solution, the couplet widens and shifts to lower wavenumbers to 1662 cm^{-1}. With the amount of 2 vol.% of TFA in the solution, the positive signal in amide II changes to mostly negative signal. Besides, a negative couplet at 1740 cm^{-1} can be observed for solution of PBLA in $CHCl_3$. It probably shifts to 1712 cm^{-1} and grades to positive signal with additions of the acid.

Changes also occur in the absorption spectra. Amide I signal at 1667 cm^{-1} firstly decreases in intensity and a new signal forms at 1637 cm^{-1}. Then at 5 vol.% of the acid in the solution, the signal at 1667 cm^{-1} shifts to 1653 cm^{-1}. Signal at 1734 cm^{-1} shifts to 1724 cm^{-1}. Signal at 1558 cm^{-1} widens and shifts to lower wavenumbers to 1540 cm^{-1}.

No changes of the VCD spectra were observed for the first addition of the acid in region II. However, at the amounts of 5 and 20 vol.% of the acid, the three signals (–)/(+)/(–) fade away and a new positive signal at 3374 cm^{-1} forms. Simultaneously the absorption signal at 3300 cm^{-1} shifts to 3340 cm^{-1}.

The influences of TFA on the structure of a polypeptide were discussed earlier for PBLG. Yet, they are slightly different for PBLA. Possible reasons for this are one carbon shorter side chains in PBLA than in PBLG. The ester groups of the side chains then lie closer to the main chain and stronger interactions can be expected.

First consequence of this structural difference is a weak negative couplet at 1745(+)/1723(–) cm^{-1} in the VCD spectra of PBLA in $CHCl_3$ solution. It probably forms as a result of the chiral organization of the main chain into helix which induces the C=O groups of the side chains esters to be organized as well. This results into the new observed couplet in the VCD spectra.

The differences between the spectra of PBLG and PBLA are well demonstrated in the Fig. 6. Different signs of the amide I and amide II signals are observed because of different handedness of their helices in $CHCl_3$ solution. We can also observe how strongly the main chain of PBLA influences the C=O groups of the side chains by observation of the new couplet at 1740 cm^{-1}.

It is also evident that the negative couplet of the α-helical PBLA is stronger than the positive one in the PBLG spectra for the same value of absorbance. Therefore it is probable that the percent content of α-helical conformation for PBLA is higher than for PBLG. On the contrary, the signal corresponding to PPII-like conformation of PBLG at 20 vol.% of TFA in solution is stronger than for PBLA. Consequently it is likely that PBLG has higher percent content of PPII-like conformation than PBLA.

VCD spectrum of PBLA in the amide A region differs from that of PBLG just in the signs of the signals as a consequence of different helix handedness.

Above mentioned changes occur with additions of the acid into the solution of PBLA in $CHCl_3$. The reason for a slight decrease of the absorption signal of amide I and formation of a new signal with smaller additions of the acid (1 and 2 vol.%) is the same as in the case of PBLG; the interaction between TFA and C=O groups of the main chain. A newly formed weak absorption signal at 1637 cm^{-1} can be then assigned to C=O groups which interact with TFA via hydrogen bonds. This signal is stronger than in the case of PBLG which means that more C=O groups interact with TFA in spite of using lower amounts of the acid. On the other hand the signal can be found at higher wavenumbers which means that hydrogen bonds are probably weaker. The most probable reason for these differences is again the one carbon shorter side chain of PBLA. This possibly facilitates more C=O groups of the main chain to interact with TFA but it sterically hinders stronger bonds.

The influence of TFA additions on the C=O groups of the side chains can be observed as well as in the case of PBLG. Absorption signal at 1734 cm^{-1} decreases in intensity and a new signal at 1724 cm^{-1} forms. These changes can be also followed in the VCD spectra. Initial negative couplet at 1740 cm^{-1}, which is connected with these groups, decreases in intensity at 1 vol.% of the acid in solution and then it disappears completely. Unfortunately observation of this signal is strongly influenced by high absorption of TFA in this region. A new positive VCD signal at 1712 cm^{-1} forms with additions of the acid above 1 vol.%. It is probably also closely connected with the C=O groups of the side chains of PBLA. However, in this case the groups interact with TFA via hydrogen bonds. Due to that, the intensity of this signal increases with the first additions of the acid.

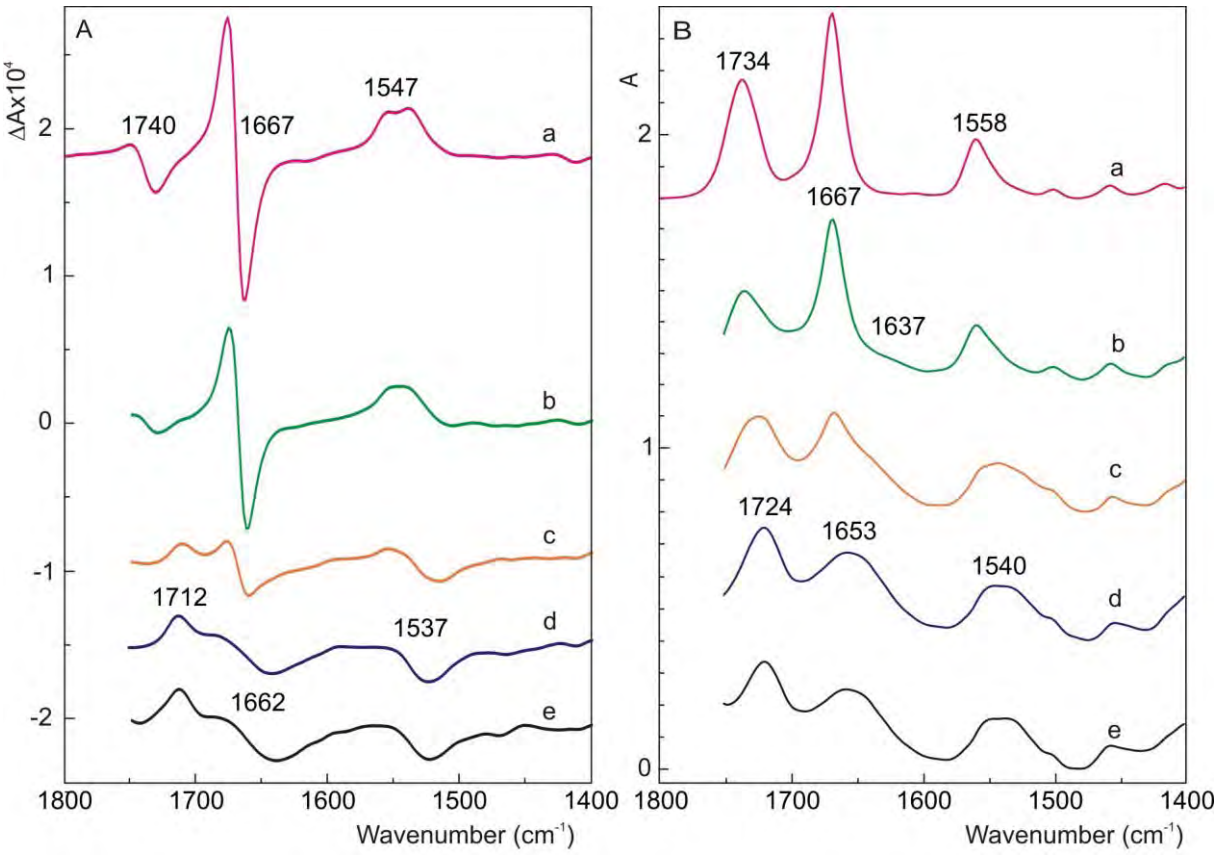

Fig. 4. Vibrational circular dichroism (A) and absorption (B) spectra of PBLA in $CHCl_3$ (a) and in $CHCl_3$/TFA for volume fractions of TFA: (b) 1 vol.%, (c) 2 vol.%, (d) 5 vol.%, and (e) 20 vol.% in the region I. Some spectral regions were omitted because of a high absorption of TFA.

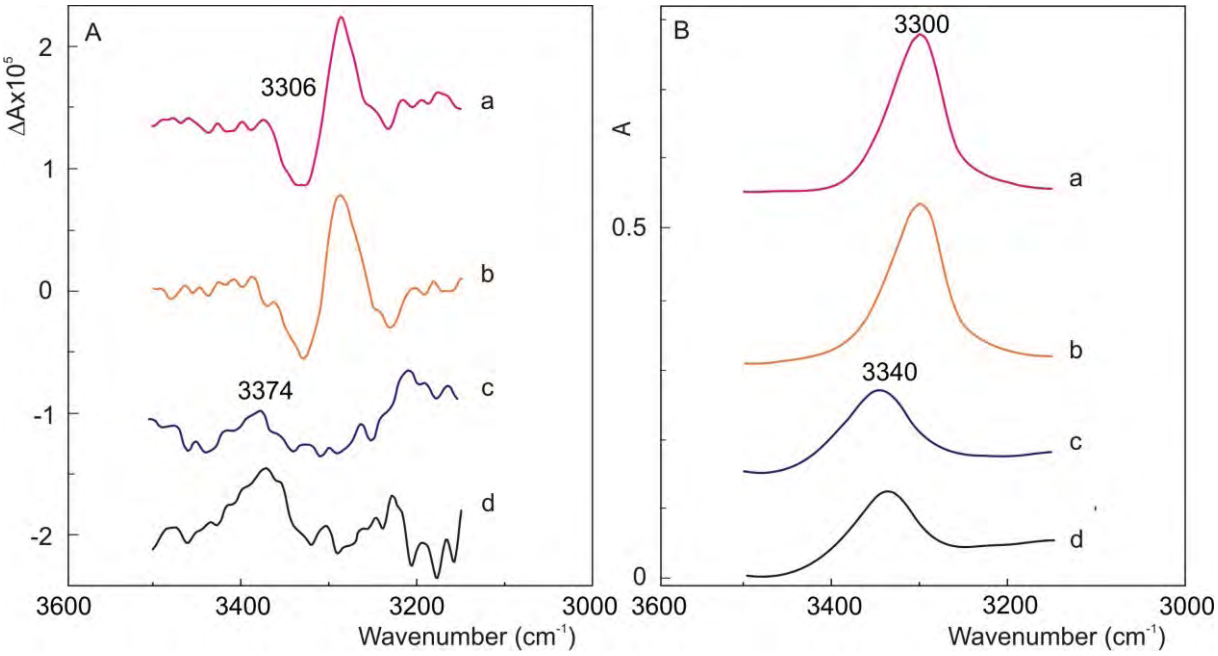

Fig. 5. Vibrational circular dichroism (A) and absorption (B) spectra of PBLA in $CHCl_3$ (a) and in $CHCl_3$/TFA for volume fractions of TFA: (b) 1 vol.%, (c) 2 vol.%, (d) 5 vol.%, and (e) 20 vol.% in the region I. Some spectral regions were omitted because of a high absorption of TFA.

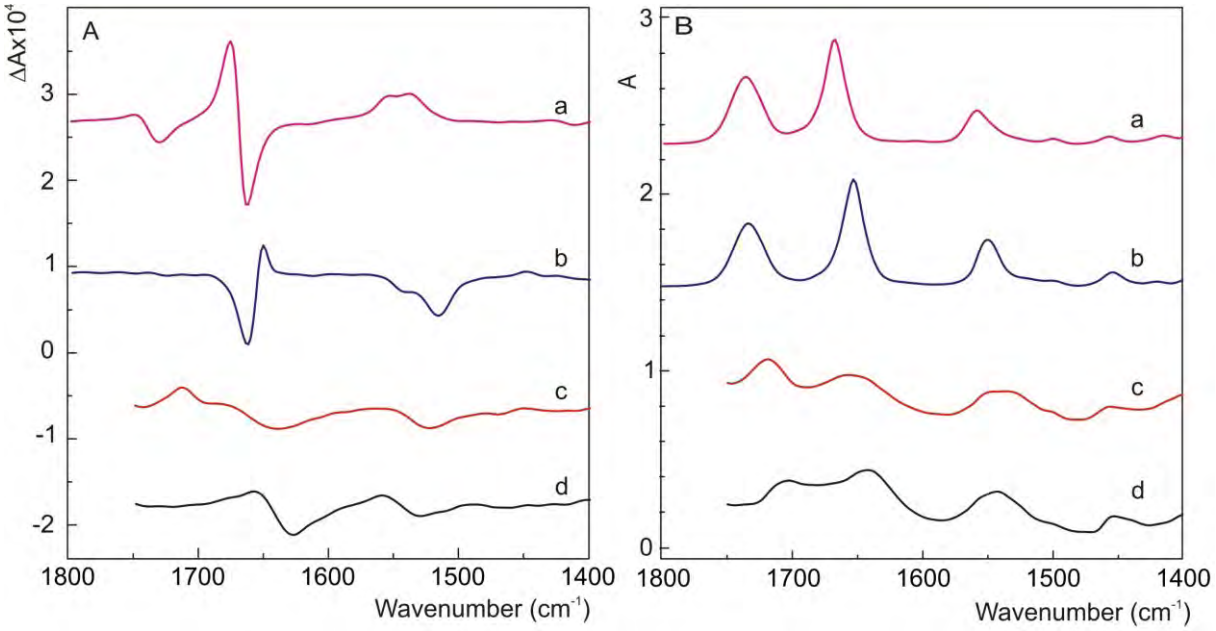

Fig. 6. Vibrational circular dichroism (A) and absorption (B) spectra of PBLA in $CHCl_3$ (a), PBLG in $CHCl_3$ (b), PBLA in $CHCl_3$/TFA for 20 vol.% of TFA (c) and PBLG in $CHCl_3$/TFA solution for 20 vol.% of TFA (d) in the region I.

A pronounced decrease of the amide I couplet was observed at the 1 and 2 vol.% additions of the acid. The intensity of the couplet reduces respectively to 72% and 25% with regard to the intensity in $CHCl_3$ solution. We did not observe any couplet intensity equilibration as in the case of PBLG because the intensity of the couplet signals for PBLA is approximately balanced in all spectra. So, maybe because of shorter side chains of PBLA, its helix is more available for TFA and it transforms to other secondary structure. However, with the addition of the acid to 5 vol.% we observed the shift of the whole couplet and its broadening. The amide I couplet is now very similar to that observed for PBLG. The shift and broadening of the amide I absorption signal also corresponds to this observation. So the left handed α-helix changes into locally left-handed helix of PPII. This transformation is hence not accompanied by the signs change as in the case of PBLG.

Amide II also changes with TFA additions. Initially positive VCD signal gradually decreases and a new mostly negative signal forms at lower wavenumbers. Amide II absorption signal broadens similarly as in the case of PBLG. These changes are connected rather with hydrogen bonds between TFA and the C=O groups of the main chain than with the change of conformation to PPII-like. This is because they can be observed at smaller amounts of the acid in the solution when the α-helical conformation still prevails over PPII-like. The shape of amide II for PPII-like conformation is again similar to that of PBLG.

The changes in amide A should be again closely connected with the amide II. However, no gradual change in the amide A absorption spectra was observed for PBLA. The shift of the signal to higher wavenumbers is spontaneous and it indicates that in PBLA solution hydrogen bonds between C=O groups of the main chain and TFA influence C–N bonds and this can be observed in amide II. They probably do not affect N–H bonds and we can not see any gradual changes with an increasing amount of hydrogen bonds in the amide A region. On the contrary, the spontaneous shift of the absorption signal can be explained as a result of the conformational change of PBLA which occurs at 5 vol.% of TFA in $CHCl_3$ solution. The intensity of amide A VCD signal also does not decrease gradually but the signal completely transforms to new positive signal at 3374 cm^{-1} which was not observed in PBLG solutions.

It is very likely that conformation of PBLA differs from that of PBLG. It can be particularly influenced by shorter side chains of PBLA. Rather bulky ester groups are then closer to the main chains.

The α-helical conformation of PBLA is also less stable than that of PBLG. Only 5 vol.% of TFA in the solution are enough to disrupt the α-helical conformation while it was 15 vol.% for PBLG.

3.3 Effect of temperature on the structure of PBLG

The effect of temperature was studied in five different solutions of PBLG. However, we did not observe any structural changes at all available temperatures for PBLG solution in $CHCl_3$ and in mixed solvent of $CHCl_3$/TFA with 5 and 20 vol.% of TFA. On the other hand we observed very interesting changes in solutions of PBLG

in $CHCl_3$/TFA with 10 and 15 vol.% of TFA. These dependences on temperature are shown in the Fig. 7 and Fig. 8.

Temperature dependent spectra of PBLG in $CHCl_3$/TFA solution with volume fraction of TFA 10 vol.% are shown in the Fig. 7. This temperature dependence was measured firstly for laboratory temperature 25 °C. Then the temperature was lowered to 20 °C, then to 15 °C and lastly to 13 °C and then it was again increased to 15 °C, 20 °C, 25 °C, 30 °C, 35 °C, 40 °C and 50 °C. So VCD spectra at several temperatures were measured twice. The second measurement is shown chained-dotted.

Especially interesting changes were observed when lowering the temperature. The spectrum measured at 25°C shows positive VCD couplet in the amide I which is characteristic for the α-helical conformation. At 20 °C, the couplet becomes rather negative and at 15 and 13 °C it shows nearly the same shape as was observed for PPII-like conformation. Then when increasing the temperature, the negative couplet again changes to positive above 20 °C. Then no other changes occur up to 50 °C. The change is obviously reversible. The VCD signal of amide II also changes. We observed a negative signal at 25 °C which changes to negative couplet when lowering the temperature.The spectral pattern doesn't change for temperatures from 25–50 °C.

Both amides I and II also change in the absorption spectra. At 25 °C there is just one peak in amide I at 1652 cm^{-1}. At 20 °C intensity of this signal decreases and a new signal at 1641 cm^{-1} forms. At 15 and 13 °C the first signal disappears and the signal at 1641 cm^{-1} predominates. The absorption signal of amide II widens and moves slightly to lower wavenumbers when lowering the temperature. No other changes occur in the absorption spectra from 25 to 50 °C.

In the Fig. 8 we report the temperature dependent spectra of PBLG in $CHCl_3$/TFA solution with volume fraction of TFA 15 vol.%. The temperature dependence measurement was started at 20 °C, and then the

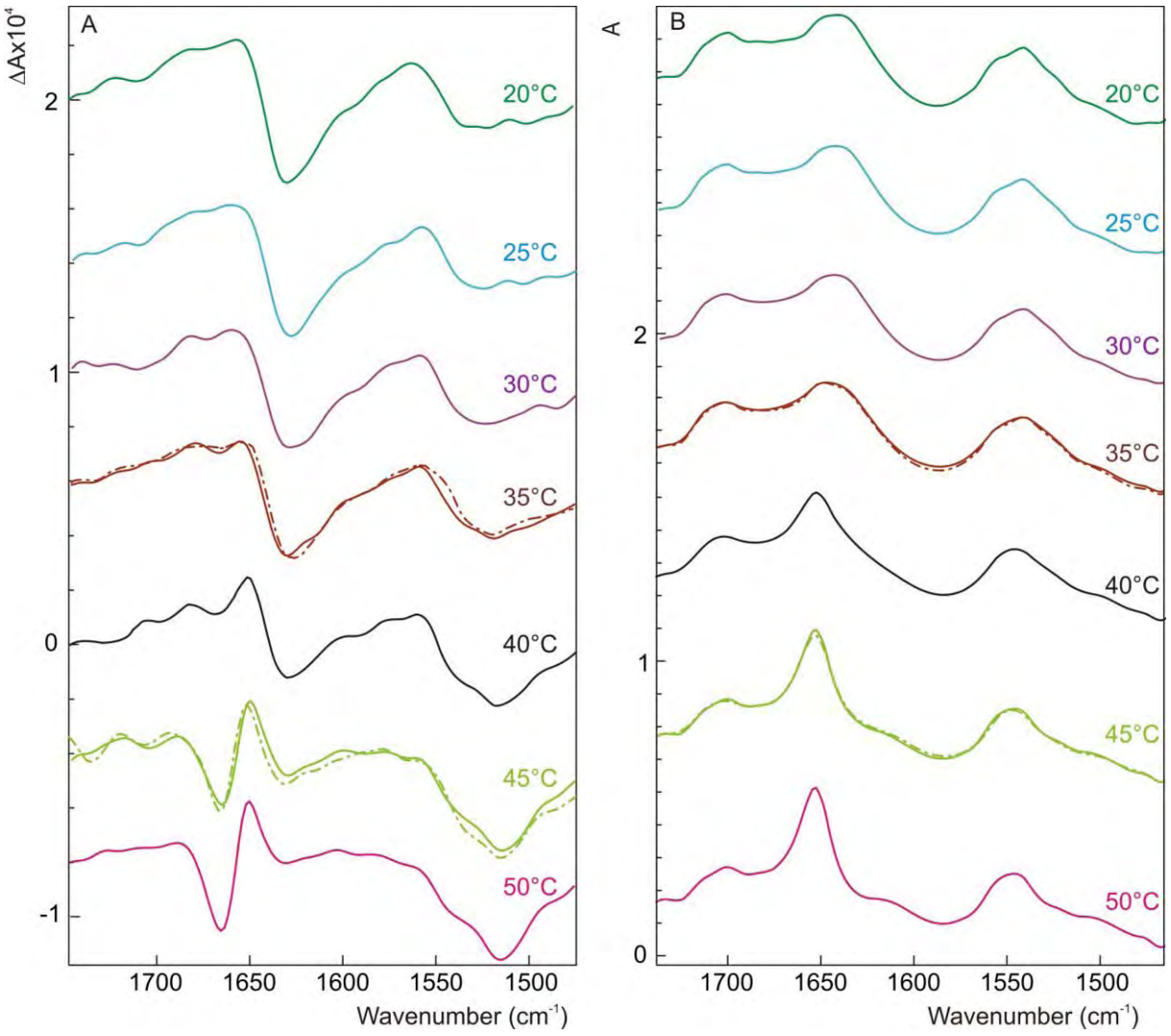

Fig. 7. Vibrational circular dichroism (A) and absorption (B) temperature dependent spectra of PBLG in $CHCl_3$/TFA solution for 10 vol.% TFA in the region I. Some spectral regions were omitted because of a high absorption of TFA.

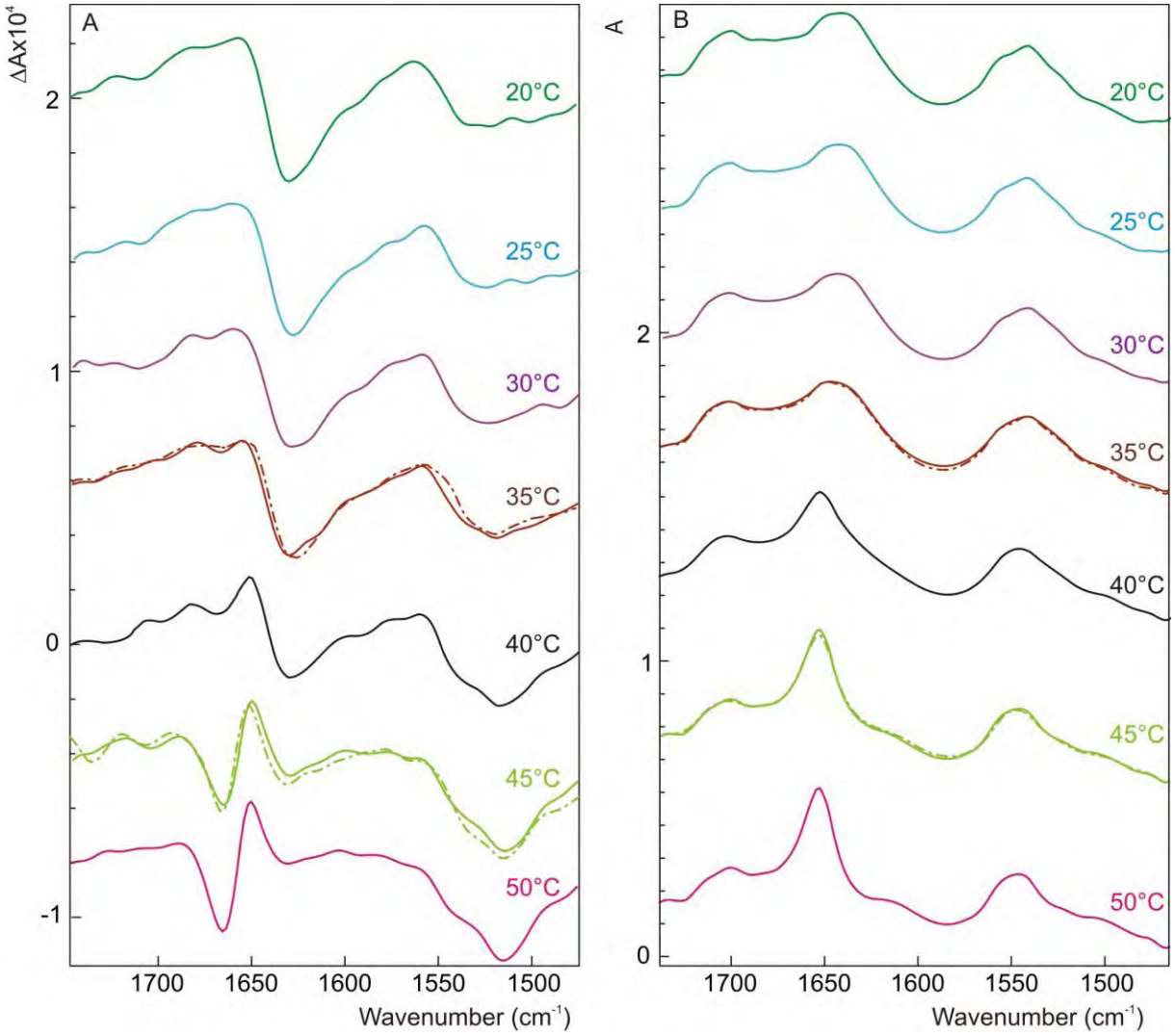

Fig. 8. Vibrational circular dichroism (A) and absorption (B) temperature dependent spectra of PBLG in $CHCl_3$/TFA solution for volume fraction of TFA 15 vol.% of TFA in the region I. Some spectral regions were omitted because of a high absorption of TFA.

temperature was increased to 25, 30, 35, 40, 45, and 50 °C. Then it was again lowered to 45 and 35 °C. So VCD spectra at several temperatures were again measured twice. The second measurement is shown chained-dotted. Especially interesting changes were observed when increasing the temperature. The spectra measured at 20, 25, 30, 35 and 40 °C show negative VCD couplet in the amide I which is characteristic for the PPII-like conformation. But already at 45 °C the couplet becomes positive as well as at 50 °C. That is characteristic for the α-helical conformation. Then, when decreasing the temperature bellow 45 °C, the positive couplet again changes to negative. Then no other changes occur down to 20 °C.

The VCD signal of amide II also changes. We observed negative couplet at 25 °C (also at 30, 35 and 40 °C) but then it changes to negative signal when increasing the temperature up to 45 and 50 °C. The changes can be followed also in the absorption spectra. From 20 to 35 °C, there is just one peak at 1641 cm^{-1}. At 40 °C this peak decreases in intensity and a new peak at 1652 cm^{-1} forms. At 45 and 50 °C the peak at 1641 cm^{-1} disappears and the one at 1652 cm^{-1} prevails. As lowering the temperature from 50 °C down to 20 °C the opposite changes occur. The absorption signal of amide II moves slightly to higher wavenumbers as increasing the temperature.

The changes observed in the both cases lead to following interpretation. Especially the changes in the VCD spectra of amide I are very significant because VCD is very sensitive method and very well reflects secondary conformation. In the first case of the solution of PBLG in 10 vol.% of TFA in $CHCl_3$, the change from positive to negative couplet between 25 and 15 °C indicates the change of conformation. Not only amide I but also amide II shows this effect of temperature. While the spectral features at 25 °C are characteristic for α-helical conformation, at 15 °C they are more characteristic for PPII-like conformation. So it seems to us that

lowering the temperature evokes this conformational change which occurs probably close to 20 °C where the characteristics for both conformations can be observed in the absorption spectra. VCD spectrum is also not so clearly distinguished at this temperature.

Very similar behaviour can be observed with second solution of PBLG in 15 vol.% of TFA in $CHCl_3$. The change from negative to positive amide I couplet between 35 and 45 °C also indicates the change of conformation. Spectral characteristics in all regions, not just amide I, are at 25 °C (also at 20, 30, and 35 °C) typical for PPII-like conformation. On the other hand at 45 °C they are characteristic for α-helix. In this case, increasing the temperature evokes the conformational change around 40 °C where the VCD spectrum is still more characteristic for PPII but the absorption spectrum is not so explicit.

When the effect of TFA on the structure of PBLG was studied, it was noticed that the change of conformation from α-helix to PPII-like occurred between molar fractions of 10–15 vol.% of TFA. For 10 vol.% of TFA and 25 °C, the VCD signal indicated the α-helical conformation, but at 15 °C the conformation changed to PPII-like. So it seems that lower temperature supports the PPII-like conformation and the effect of the acid. On the other hand, the effect of temperature is probably not so strong because any change of conformation was not observed for solution of 5 vol.% of TFA in $CHCl_3$. Temperature probably influences the acidity constant of TFA. As it decreases with decreasing temperature, more –COOH groups are non-dissociated and can interact with PBLG via hydrogen bonds and destabilize the α-helical conformation. This theory is supported by the second temperature dependency measurement with solution of 15 vol.% of TFA. At 25 °C, its VCD signal indicated the PPII-like conformation, but at 45 °C the conformation changed to α-helix. The PPII-like conformation was again observed for lower temperature and only the increase of the temperature changed it to α-helix. With increasing temperature more –COOH groups are dissociated and can not interact with PBLG via hydrogen bonds which again stabilizes the α-helical conformation and probably restores intermolecular hydrogen bonds between PBLG molecules. However, similar dependence was measured with solution of 20 vol.% of TFA and no conformational change was observed in available region of temperatures. So probably there was so much of the acid in the solution that temperature was not able to induce the conformational change.

Similar dependence was measured with PBLA in the solutions with these volume fractions of TFA in $CHCl_3$: 0, 1, 2, 3, and 5 vol.% but the induction of conformation was not successful.

4. Conclusions

It was shown that the structure of PBLG and PBLA depends on the volume fraction of TFA in $CHCl_3$. The conformational variation was induced in the both cases. The α-helical conformation changed to PPII-like. The α-helix of PBLA was shown to be less stable than that of PBLG. It changed to PPII-like with the addition of only 5 vol.% of TFA to the solution, while 15 vol.% was needed for PBLG. The temperature variation also inducts the conformation changes in solutions of PBLG with 10 and 15 vol.% of TFA in $CHCl_3$. This conformational change was shown to be reversible.

Acknowledgement. *The work was supported by the Grant agency of the Czech Republic (GACR 203/07/1335).*

References

[1] Urbanová M., Maloň P. In: *Analytical methods in Supramolecular Chemistry.* Weinheim, Wiley 2007.
[2] Berova N., Nakanishi K., Woody R.W.: *Circular Dichroism. Principles and Applications.* 2nd ed. New York, Wiley 2000.
[3] Freedman T. B., Nafie L. A., Keiderling T. A.: *Biopolymers* **37** (1995) 265–279.
[4] Lal B. B., Nafie L. A.: *Biopolymers* **21** (1982) 2161–2183.
[5] Lipp E. D., Nafie L. A.: *Biopolymers* **24** (1985) 799–812.
[6] Malon P., Kobrinskaya R., Keiderling T. A.: *Biopolymers* **27** (1988) 733–746.
[7] Sen A. C., Keiderling T. A.: *Biopolymers* **23** (1984) 1519–1532.
[8] Singh R. D., Keiderling T. A.: *Biopolymers* **20** (1981) 237–240.
[9] Balik C. M., Hopfinger A. J.: *J. Colloid Interfac. Sci.* **67** (1978) 118–126.
[10] Chakrabarti S., Miller W. G.: *Biopolymers* **23** (1984) 719–734.
[11] Torii T., Yamashita T., Horie K.: *Eur. Polym. J.* **29** (1993) 1265–1270.
[12] Patel D. L., Dupre D. B.: *Mol. Cryst. Liq. Cryst.* **53** (1979) 323–334.
[13] Bradbury E. M., Downie A. R., Elliott A., Hanby W. E.: *Proc. R. Soc. London, Ser. A* **259** (1960) 110–128.
[14] de Ilarduya A. M., Aleman C., Garcia-Alvarez M., Lopez-Carrasquero F., Munoz-Guerra S.: *Macromolecules* **32** (1999) 3257–3263.
[15] Giancotti V., Crescenzi V., Quadrifoglio F.: *J. Am. Chem. Soc.* **94** (1972) 297.
[16] Dukor R. K., Keiderling T. A.: *Biopolymers* **31** (1991) 1747–1761.
[17] Urbanova M., Setnicka V., Volka K.: *Chirality* **12** (2000) 199–203.
[18] Julínek O.: *Diplomová práce.* Praha, Vysoká škola chemicko-technologická v Praze 2006.
[19] Yasui S. C., Keiderling T. A.: *Biopolymers* **25** (1986) 5–15.
[20] Combelas P., Garrigou-Lagrange C., Lascombe J.: *Biopolymers* **13** (1974) 577–589.
[21] Socrates G.: *Infrared and Raman Characteristic Group Frequencies: Tables and Charts.* Chichester, Wiley 2001.

Investigation of Cryogenic Trapping for Arsenic Speciation Analysis by Hydride Generation – Atomic Absorption Spectrometry

Milan Svoboda[a, b], Jan Kratzer[b], Miloslav Vobecký[a], Petr Rychlovský[a], Jiří Dědina[b]

[a] *Department of Analytical Chemistry, Faculty of Science, Charles University in Prague, Albertov 6, 128 43 Prague 2, Czech Republic*
[b] *Institute of Analytical Chemistry, Academy of Sciences of the Czech Republic, v. v. i. Vídeňská 1083, 142 20 Prague 4, Czech Republic,* ✉ *svoboda750@biomed.cas.cz*

Abstract

The general aim of this work was to contribute to further improvement of the method for complete speciation analysis of trivalent and pentavalent human metabolites of arsenic in complex biological matrices.

The method combines selective hydride generation (based on the pre-reduction of pentavalent arsenic forms by L-cysteine) with the generation of substituted arsines followed by hydride trapping in a cryogenic trap (cooled by liquid nitrogen, packed with Chromosorb). After the preconcentration step, the trap is heated and collected arsines are separated according to their boiling points and released into a quartz multiatomizer. The detection is performed by an atomic absorption spectrometer.

The main target of this work was to investigate processes during the cryotrapping procedure. The arsine collection and volatilization efficiency were determined employing ^{73}As radioactive indicator. 100% efficiency was found for both collection and volatilization step. In addition, spatial distribution of arsine in the cryogenic trap was studied by image plate autoradiography. Collected arsine was proved to be located in a small spot at the upstream part of the U-shaped cryogenic trap.

A way to achieve lower concentration detection limits is to increase the sample volume. Then a trap blockage by frozen water vapour presents a serious problem. The amount of water vapour can be reduced to a tolerable extent when using a nafion tube dryer with optimized nitrogen dryer gas flow rate.

Another possibility of further improvement of detection limits is to replace atomic absorption detector by atomic fluorescence one. Preliminary comparison of detection limits obtained for arsine, methylarsine and dimethylarsine by the both detection methods will be presented and discussed.

Miniaturization of cryogenic trap by replacing quartz U-tube (i. d. 2 mm) (packed with chromosorb) by a quartz capillary (i. d. 0.53 mm) was tested. Relevant parameters (carrier gas flow rate, trapping temperature, column length) were optimized for arsine trapping. Employing the ^{73}As radioactive indicator; 94% trapping and 100% volatilization efficiency, respectively, were found. A nafion tube dryer with optimized nitrogen dryer gas flow rate was used to prevent the blockage of the capillary by frozen water vapour. Also the position of the capillary in vessel with liquid nitrogen was optimized to minimize retention of water vapour.

Advantages and disadvantages of the proposed miniaturized design in comparison to the conventional U-tube will be discussed.

Keywords
arsenic speciation
atomic absorption spectrometry
atomic fluorescence spectrometry
cryogenic trapping
hydride generation

1. Introduction

Realgar, orpiment and other arsenic minerals were already known to the Greeks of Aristotle's time (about 300 BC), even though the element itself was not known. Arsenic was first described by Albertus Magnus in the thirteenth century. It was widely used as poison and in folk remedies. The element found more and more application in agriculture and industry in the twentieth century. Nowadays, the biological and environmental effects of arsenic are studied in detail since serious pollution and numerous cases of poisoning from arsenic in drinking water have been found in the last decades. Many cases occur in poor countries that lack the necessary infrastructure to be able react promptly. Even though regulations still focus on total arsenic concentrations, the effect of arsenic is dependent on the physical and chemical properties, toxicity, mobility and biotransformation of arsenic species [1]. As a consequence arsenic speciation analysis rather than

determination of total arsenic content is required nowadays in environmental, industrial and clinical analysis.

Inorganic As (iAs) is the prevalent form of As in the environment. Human metabolism of iAs involves reduction of As(V) to As(III) and the oxidative methylation of As(III)-species that yields methylated arsenicals containing either As (III) or As(V) [2]. Toxicity of tri- and pentavalent iAs and methylated arsenicals differ significantly [3]. Therefore, method development for oxidation state specific speciation analysis of As in biological matrices has become a key issue for As toxicology and analytical chemistry. Although the iAs(III)/iAs(V) analysis is very common, the reports on the oxidation state specific speciation analysis of methylated species – methylarsonite (MAs(III)), dimethylarsinite (DMAs(III)), methylarsonate (MAs(V)) dimethylarsinate (DMAs(V)) and trimethylarsine oxide (TMAs(V)O) – remain very scarce [4].

One of the approaches to arsenic speciation analysis combines selective hydride generation with atomic absorption spectrometry. One aliquot is pre-reduced by L-cysteine in order to determine total arsenic as the sum of trivalent and pentavalent arsenic forms. Another sample aliquot is not treated by L-cysteine. Thus, only trivalent arsenic forms are determined. The pentavalent forms are calculated from the difference. TRIS buffer was found to be the most suitable reaction medium yielding the highest generation efficiency for arsenic species. The pH of the buffer must be kept around 6 since it is crucial for reaching 100% hydride generation efficiency. In collection step, iAs and their methylated forms are converted to arsines and methylated forms and retained in the cryogenic trap cooled by liquid nitrogen. The cryogenic trap is heated in volatilization step to release collected arsenic species stepwise according to their boiling points to the multiatomizer. The whole procedure can be automated [5].

The general aim of this work was to contribute to further improvement of the cryogenic trap system. The targets were to search for new possibilities of miniaturization and further simplification of the system as well as to investigate the collection and volatilization processes and to test atomic fluorescence spectrometry as an alternative detection method to atomic absorption spectrometry.

2. Experimental

2.1. Instrumentation

The detection was performed by atomic absorption spectrometer Perkin Elmer Aanalyst 800 (Norwalk, USA) equipped with FIAS 400 flow injection accessory (FIAS). The arsenic EDL lamp System II (Perkin Elmer) operated at 376 mA with deuterium background correction was used. The slit width was set to 0.7 nm. A multiplemicroflame quartz tube atomizer (multiatomizer) heated rheostaticly to 900°C and supplied with 35 mL min^{-1} of air as outer gas was employed as an atomizer.

The in-house designed research grade atomic fluorescence spectrometer equipped with As EDL lamp System II (Perkin Elmer) operating at 340 mA and accommodated with flame-in-gas shield (FIGS) atomizer was employed as an alternative detector.

2.2. Standards and reagents

A stock solution of 1000 μg As L^{-1} was prepared for each of other arsenic species in water using following compounds: As_2O_3, Lachema, Czech Republic (iAs(III)); $Na_2CH_3AsO_3.6H_2O$, Chem. Service, West Chester, USA (MAs(V)); $H(CH_3)_2AsO_2$, Strem Chemicals, USA (DMAs(V)). Working standards were prepared for individual species by serial dilution of the stock solutions in water. Mixed standards prepared by mixing the solutions of individual species during the last dilution, *i. e.* at the ng mL^{-1} level. For trivalent species, water for standard preparation was deaerated by purging with nitrogen for at least one hour. If stored in the fridge at 4 °C, standard solutions were stable for several weeks. It was found that the As content in methylated species can differ from the expected value by as much as 20%. Thus standardization of the solutions was necessary. The total As content was determined in approximately 100 μg L^{-1} solutions of individual species by liquid sampling graphite furnace-AAS, using a Perkin-Elmer Analyst 800 instrument with graphite furnace atomizer. End-capped transversely heated tubes permanently modified by 4 μg of Ir were used conditions recommended by the WinLab program ver. 6.5 Perkin Elmer manufacturer. Assuming that the sensitivity for individual As forms are identical in the graphite furnace--AAS, the values found was taken as the reference.

Deionized water (<0.2 μS cm^{-1}, ULTRAPURE, Watrex) was used for preparation of all solutions. The reductant solution containing 1% $NaBH_4$ (Fluka, Buchs, Switzerland) in 0.1% (m/v) KOH (p. a., Lachema, Brno, Czech Rep.) was prepared daily. A 0.75 M Tris(hydroxymethyl)aminomethane (TRIS)HCl buffer (pH = 6) was prepared from a reagent grade Trizma® hydrochloride (Sigma) and pH adjusted to 6 by NaOH. Other reagents included HCl (p. a., Merck, Darmstadt, Germany) and a biochemistry grade L-cysteine hydrochloride monohydrate (Merck).

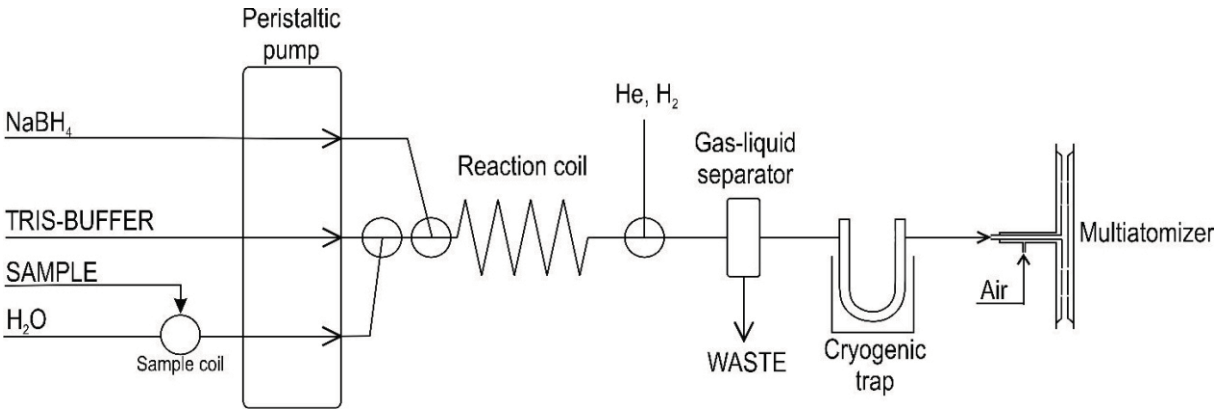

Fig. 1. Experimental setup of hydride generator with cryogenic trap for AAS

2.3. Hydride generator and cryogenic trap

A scheme of the HG-CT-AAS system, built around the Perkin-Elmer FIAS 400 unit, is shown in Fig. 1. All gas flows were controlled by mass flow controllers (FMA-2400 or 2600 Series, Omega Engineering, USA). The sampling coil of 500 µL was used. The manifold was built using PTFE T-pieces (0.75 mm bore) and 1/4–28 threaded connectors. The PTFE tubing was used as follows: 1/16″ o. d./0.75 mm i. d. for the liquid leads, 1/16″ o. d./0.5 mm i. d. for the He/H_2 inlet; 1/16″ o. d./-1 mm i. d. for the reaction coil (1 mL), respectively; 1/8″o. d./ 1/16″ i. d. for GLS to U-tube and U-tube to atomizer connections (150 in lenght mm each). GLS with forced outlet was used as it can handle overpressure caused by the resistance of the packed U tube (typically 20 PSI). The plastic GLS was a polypropylene 50 mL screw-cup vial with a custom made acrylic lid with two 1/16″ and one 1/8″ inlets. The PTFE tubing was secured by 1/4–28 Rheodyne RheFlex flat bottom flangeless fittings. The mixture from reaction coil is led into half of the vial's height by a tube through the lid, so that it enters near tangentially close to the wall and does not strike the wall to minimize aerosol production. The waste outlet starts at the cone-shaped bottom. Gas outlet tube opening is located in the free volume at approximately 3/4 of vial's height. The GLS can accommodate up to 20 mL of liquid, which corresponds to 5 mL of sample volume in a single generation cycle (since appart from the sample flow there are equal flows of sample/carrier, buffer and reductant solution).

Two different cryogenic systems were investigated: the first on based on a U-tube packed with Chromosorb, the second one based on a bare quartz capillary. A glass U-tube 2 mm i. d. and 50 cm long was packed with 0.8 g of Chromosorb WAW-DCMS 45/60 (15% OV-3). After packing, the U-tubes were treated with 50 µl Rejuv-8 silylating reagent (Sigma) and flushed with helium for 5 hours. To heat the U-tube it was evenly wrapped with a Ni80/Cr20 wire (0.51 mm diameter/5.275 $\Omega\ m^{-1}$, Omega Engineering, USA) providing a total resistance of 15 Ω, for broad and narrow U-tube, covering the entire Chromosorb column. Heating current of 2.2 A was applied to the wire in the volatilization step of the procedure (see below) to heat the cryogenic trap to 150 °C (power source EA-PS 3065-10B, Elektro-Automatik, China). The U-tube was immersed into 3-liter Dewar flask (11 cm i. d.), filled with liquid nitrogen. Liquid nitrogen was maintained in 3/4 of the U-tube height.

The miniaturizer cryogenic trap was realized by a non polar fused silica capillary 0.53 mm i. d. (Supelco, USA) covered with polyimide: 20 cm of the capillary was inserted into teflon tube 0.75 mm i. d. as a protection against mechanical damage. Both ends of the capillary were sealed in a teflon tube 0.53 mm i. d. and connected with the hydride generator by Rheodyne RheFlex flat bottom flangeless fittings. The nafion membrane (MD-110-12FP, Perma Pure, USA, with 2 L min^{-1} N_2) connected with GLS was employed through the analysis to remove water vapour and prevent capillary blockage by frozen water. The capillary was immersed in the same Dewar flask as the U-tube, but with polyethylen foam lid on the top. Heating was carried out by ambient temperature in the volatilization step (see section 2.5.). The hydride generator system was the same as the system connected with U-tube.

The hydride generator system with a U-tube as a cryogenic trap was coupled to atomic fluorescence spectrometer as an alternative detection method. The system of hydride generator had several modifications in gas supplies made mainly to meet requirements neccessary for flame in gas shield atomizer (FIGS), Fig. 2 (*see next page*). Moreover, it was neccessary to attach the syringe filter (FP 30/0.2 CA, 30 mm diameter, 0.2 µm pore size cellulose acetate membrane, WhatmanSchleicher & Schuell) to the downstream end of the U-tube to prevent water vapour and spray transport into the FIGS atomizer.

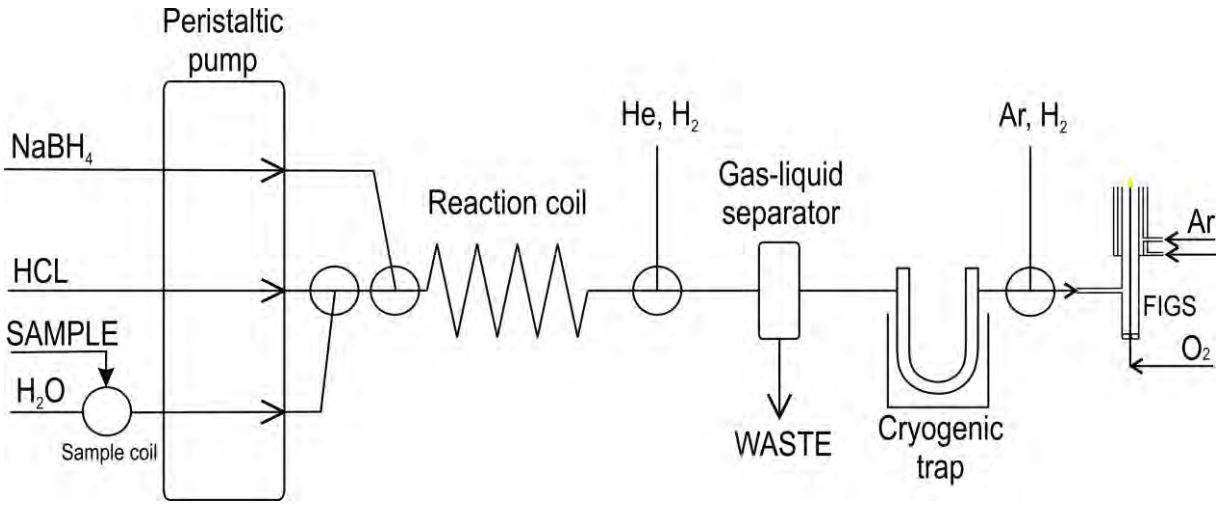

Fig. 2. Experimental setup of hydride generator with cryogenic trap for AFS

2.4. Atomizers

The multiatomizer for atomic absorption measurement was identical to that described previously (model MM5 in Ref. [6]). The inner tube of the optical arm of the atomizer used in this study was 120 mm long with 7 mm i. d. and fourteen orifices having diameter between 0.1 and 1 mm [6]. The atomizer was heated to 900 °C by the FIAS heating device. 35 mL min^{-1} of air was used as outer gas for the atomizer.

The flame-in-gas shield atomizer (FIGS), that makes use of highly fuel-rich hydrogen-oxygen microflame shielded by Ar flow, was used for atomic fluorescence investigation. The core of the atomizer is identical to the miniature DF: it is a quartz tube with the inlet of the mixture of hydrogen in argon containing the hydride. In contrast to the miniature DF, there is a capillary centered inside the quartz tube. It serves to introduce very small flow rates of oxygen. Oxygen burns at the end of the capillary in the excess of hydrogen to form the microflame. This is the substantial difference to miniature DF where hydrogen is burning in the excess of oxygen of ambient atmosphere. The microflame must be protected from the ambient atmosphere by a laminar flow of argon. The argon shield is produced by a simple glass shielding unit [7, 8].

2.5. Cryotrapping procedure

2.5.1. Collection step

Firstly, sampling loop is loaded by the sample solution at the flow rate of 2.5 mL min^{-1}. Simultaneously, there are three reagent flows pumped at the same flow rate of 1.0 mL min^{-1}: water to the Carrier channel, the TRIS buffer solution to the Acid/Buffer channel and the reducing solution to the Reductant channel. Pump for waste (not displayed in the Fig. 1) is also switched on. After this step the sample is injected to the flow of carrier water. Pump for waste is switched off so that reaction mixture is not removed from the GLS. After this step 90 s waiting time is applied to ensure complete generation of arsines and their transport into the cryogenic trap; reaction mixture is retained in the GLS. In the course of all these steps, cryogenic trap is immersed in liquid nitrogen and the heating is off. The gas flow rates are follows: 75 mL min^{-1} helium (for U-tube); 35 mL min^{-1} (for capillary) and 15 mL min^{-1} hydrogen which is not neccessary for collection step but it is neccessary for next volatilization step and its flow is not switched off in the collection step just for the sake of simplicity.

2.5.2. Volatilization step

In the volatilization step, the cryogenic trap is taken out from dewar flask with liquid nitrogen and trap heating starts. Trap is heated either resistively (in case of U-tube) or by ambient atmosphere (as in case of the capillary). Then a 58 s long reading period (the longest possible allowed by the spectrometer software) is initiated. As the cryogenic trap warms up, hydrides (arsines) evaporate according to their boiling points and are separated and enter the atomizer. Afterwards, the cryogenic trap is further heated up to approximately 150 °C to remove all the moisture. At the end of the cycle the pump for waste is switched on to remove waste from GLS and then the cryogenic trap is immersed in liquid nitrogen to let cool down for next run. The gases flow rates are the same as in collection step. Hydrogen presence is neccessary for efficient atomization of arsines because there is not hydrogen production from hydride generation.

2.6. Radiotracer experiments

$^{73, 74}$As radioactive indicators were produced at U 120 M cyclotron (Nuclear Physics Institute of the ASCR, v.v.i., Řež near Prague, Czech Republic) by bombardment of GeO_2 target by protons (energy 36 MeV, current 4 μA) according to the reaction:

$$Ge_{nat}(p, x\,n)\,^{73,74}As \quad (1)$$

Further chemical separation and isolation of radioarsenic (being further indicating as ^{73}As radioactive indicator according to the isotope with longest half-life) of high specific activity was carried out in our laboratory. Half life values ($T_{1/2}$) of the isolated As radioisotopes are 80.3 days and 17.8 days, respectively for ^{73}As and ^{74}As. Also ^{71}As radioisotope with $T_{1/2}$ = 2.7 day is present in the mixture. The stock solution of ^{73}As radioactive indicator was prepared in 7 M HCl. All three radioisotopes are gamma emitters and their corresponding lines are 53 and 596 keV, respectively, for ^{73}As and ^{74}As. To detect the lines of both isotopes two energy windows (from 30 to 200 keV and from 30 to 1300 keV) were scanned using the auto-gamma counting system.

An auto-gamma counting system equipped with scintillation NaI(Tl) well-type detector (Minaxi 5000, Packard) with 1 min counting time was employed to quantify the activity of ^{73}As radioactive indicator retained in different parts of apparatus.

The spatial distribution of the ^{73}As radioactive indicator activity in the cryogenic trap was investigated by image plate autoradiography. A laser scanner (Fuji BAS 5000) was employed to measure phosphorence induced by radioactivity present in the sample. Images were further evaluated using the Aida software (Raytest, Germany).

Typical activity of the radioactive indicator taken for a single experiment was ca 5 kBq. Since the prepared ^{73}As radiotracer was of high specific activity a non-radioactive iAs standard solution (carrier) was added to working radiolabeled solutions. Thus, the trapped analyte mass was the same in all radiotracer and AAS experiments and the results from radiotracer study are fully comparable with those received by AAS. Calculated mass of the radiotracer having activity of 1 kBq was found to be ca 10^{-13} g kBq^{-1}. Since the trapped analyte mass is typically in 10 ng in our experiments the contribution of radiotracer to the mass that is ca 10^{-3} ng is negligible and carrier must be added.

The working radiotracer solutions at the specific activity of 10 kBq mL^{-1} were prepared in 1 M HCl containing 2 ppb non-radioactive iAsIII. The working radiolabeled solution was prereduced before use by adding L-cysteine to reach its final 2 % (m/v) content in the solution. 0.5 mL of radiolabeled solution was used for a single experiment.

Radiotracer experiments were carried out following the procedure described in section 2.5. However, several changes were made. The multiatomizer was replaced by 4 cm long column packed with 2 g of active carbon in the collection step. After the collection step the column with active carbon was replaced by a new one and volatilization step was processed as described in section 2.5. The activity retained in different parts of apparatus was compared to the activity taken for the individual experiment as a reference value. Thus, collection and volatilization efficiencies can be estimated as described below and also reported in one of our previous studies [9].

At the beginning of each experiment, the radioactivity of the batch generator with the sample was counted (A_{input}). This was taken as 100 %. The same hydride generator containing the waste (mixture of acidified sample and $NaBH_4$) was measured after the experiment (A_{waste}). Thus, the fraction of analyte remaining in the generator ($E_{non\text{-}gen}$) was estimated. It can be thus quantified according to the equation:

$$E_{non\text{-}gen} = 100\,(A_{waste})/(A_{input}) \quad (2)$$

$E_{non\text{-}gen}$ was in all experiments lower than 10 % for both analytes.

The quantification of the trapping and volatilization efficiency, respectively is always related only to the activity of analyte converted to the gaseous phase (A_{gen}), which was taken as 100 %. Obviously, following equation holds:

$$A_{gen} = A_{input} - A_{waste} \quad (3)$$

The analyte fraction retained in any part of apparatus ($E_{apparatus}$) is defined as the ratio of the activity found in any part of apparatus ($A_{apparatus}$) after the experiment (trap, column with activated carbon, tubings, *etc.*) to the activity of analyte converted to the gaseous phase (A_{gen}):

$$E_{apparatus} = 100\,(A_{apparatus})/(A_{gen}) \quad (4)$$

It was verified that the geometric effect on the sensitivity and accuracy of the measurements was negligible. All the radiotracer experiments were carried out in the exhaust hood of a radiochemical laboratory.

Experiments dealing with image plate autoradiography to study spatial distribution of arsenic in the U-tube were carried out following the procedure described in section 2.5. Only the tubular shaped dewar flask was replaced by cuboidal PE container. The image plate was attached to the outer wall of the PE container and the U-tube was fixed to the inner wall. Then the

U-tube was connected to the hydride generator system and collection step was proceed. During the collection the column filled with active carbon was connected to the downstream end of the U-tube. After collection step the hydride generator was disconnected and the another column with active carbon was connected to the U-tube upstream end. Exposition time was 5 hours and the PE container was regularly filled up with liquid nitrogen so that the U-tube was cooled all the time. The image plate was removed from the PE container wall and the image was evaluated using Fuji BAS 5000 laser scanner (see above). A new actived carbon column was attached to the downstream end of the cryogenic trap which was still immersed in liquid nitrogen. The upstream end of the cryogenic trap was connected to the hydride generator but only gases were switched on whereas the pump was switched off. Subsequently the trap was removed from liquid nitrogen and heated resistively to the volatilization temperature.

3. Results and discussion

3.1. Applicability of atomic fluorescence spectrometry

The possibility of coupling HG-CT to an atomic fluorescence detector was investigated. It was found that the L-cysteine is not suitable pre-reductant because the signal of arsenic forms is overlayed by the nonspecific signal related to L-cysteine. The interference is probably caused by dispersion of radiation on sulphur particles rising from L-cysteine. This assumption is supported by the observation of increased amount of solid particles in the inlet arm of the multiatomizer after many measurements with atomic absorption spectrometry. As a consequence, it was neccessary to find another pre-reductant or change hydride generation conditions. The simpliest way appeared to replace the TRIS buffer/L-cysteine system by hydrochloric acid medium. The results demonstrated hydrochloric acid as a suitable reagent, however, it was not possible to carry out the arsenic speciation analysis of tri- and pentavalent forms because each arsenic form in both trivalent and pentavalent form is generated. Thus it is not posssible to generate trivalent or pentavalent forms separately by 1 M hydrochloric acid. This implies that another approach for arsenic speciation of tri- and pentavalent forms by hydride generation must be found in this case. However, it was demonstrated the possibility of HG-CT-AFS connection by application of hydrochloric acid medium (Fig. 3B). Moreover lower detection limits can be reached employing atomic fluorescence spectrometry (see Table 1) since the baseline noise in AFS is lower than in AAS (compare Fig. 3).

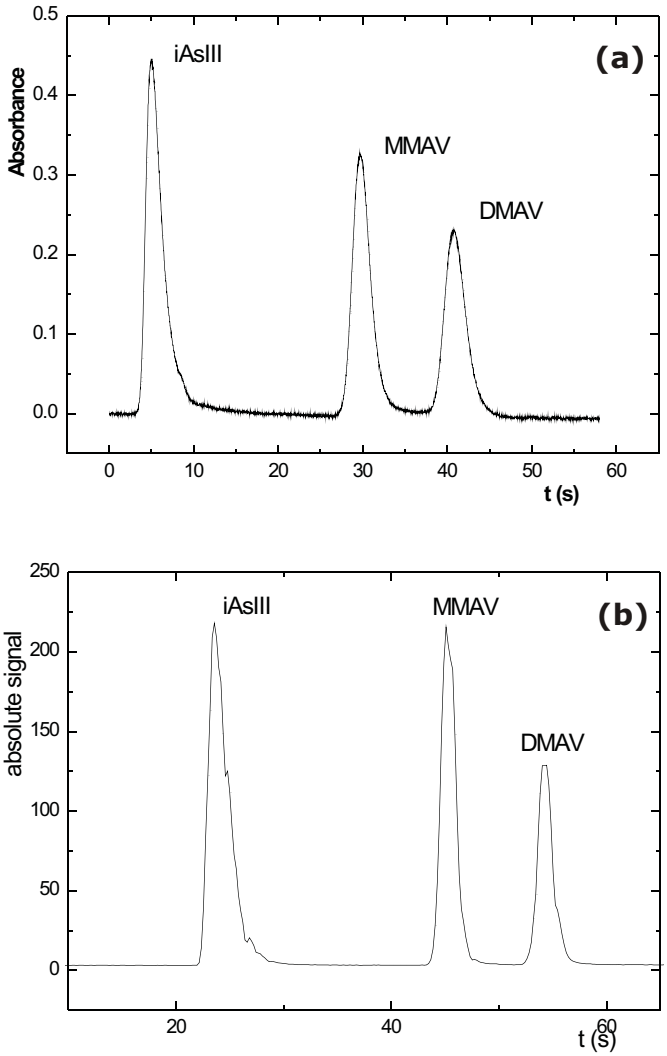

Fig. 3. Chromatograms of mixed standards of As species: 1.00 ng As each form detection by AAS (A) 0.25 ng each form detection by AFS (B)

Table 1. Comparison of detection limits of arsenic species for atomic absorption spectrometry and atomic fluorescence spectrometry.

	LOD (ppt)	
As species	AAS	AFS
iAsIII	5	6
MMAV	6	2
DMAV	10	2

3.2. Trapping investigation

^{73}As radioactive indicator was employed to visualize spatial distribution of analyte in the U-tube trap as well as to estimate trapping and volatilization efficiency of inorganic arsenic in both cryogenic systems tested.

Spatial distribution of trapped inorganic arsenic was studied by image plate autoradiography in the U-tube cryogenic trap only. It was found that most of analyte is

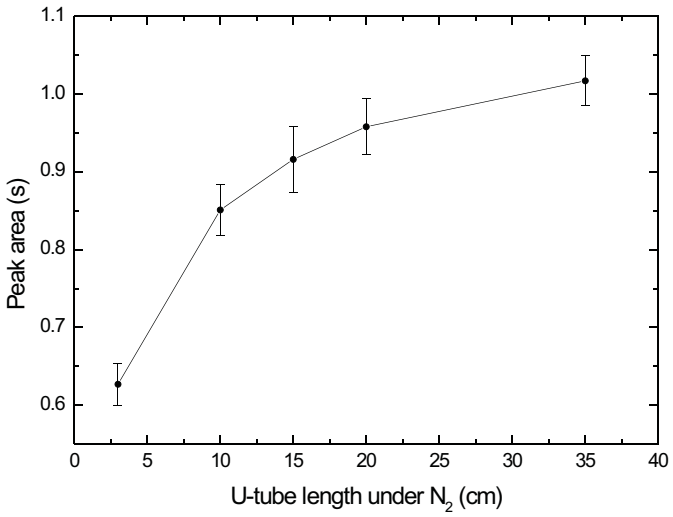

Fig. 4. Influence of U-tube length (immersed into liquid nitrogen) on peak area of 2 ppb iAsIII; peak area 1.00 corresponds approximately to 100% efficiency.

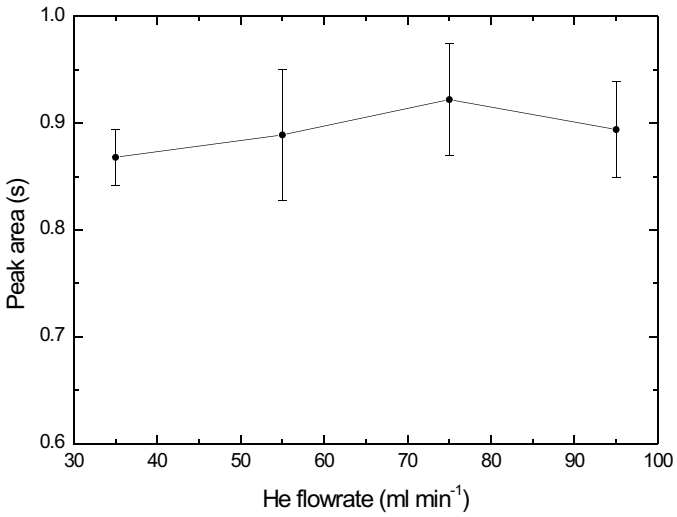

Fig. 5. Influence of helium flowrate on peak area of 2 ppb iAsIII

trapped on a Chromosorb filling in a small spot ca 3 cm in an upstream part of the U-tube.

Effect of U-tube length immersed in liquid nitrogen on peak area of inorganic arsenic was studied using a non-radioactive As standard and AAS detection. According to this experiment the minimum neccessary length of U-tube immersed in liquid nitrogen is 20 cm (see Fig 4).

Trapping and volatilization efficiencies found by radiotracer technique for both cryogenic traps: U-tube packed with Chromosorb and miniaturized quartz capillary are summarized in Tab. 2. Complete collection and volatilization is reached in the trap based on U-tube. 94% collection efficiency followed by complete volatilization was observed in the capillary. It should be highlighted that the encouraging results obtained for the capillary were found under the conditions found previously to be optimum for the U-tube. There was no attempt to optimize the conditions (carrier gas flow rate, *etc.*) for the miniaturized capillary system. Collection efficiency in the capillary might be further improved.

Table 2. Comparison of collection and volatilization efficiency for packed U-tube and capillary cryogenic traps

	U-tube	Capillary
Collection efficiency (%)	99.9 ± 0.1	94.3 ± 0.2
Volatilization efficiency (%)	100.0 ± 0.8	100.0 ± 0.1

3.3. Miniaturized cryogenic trap design

The U-tube design of the cryogenic trap, which is usually employed for arsenic speciation, needs large dewar flask and consumes a lot of liquid nitrogen to be cooled down. Consequently, automated system such as described by Matousek *et al.* [5] recently, requires supervision by the operator and liquid nitrogen has to be filled up quite often. On the contrary, the U-tube can be miniaturized but not significantly as is indicated in Fig. 4 (the 20 cm U-tube length under liquid nitrogen is needed). Therefore the capillary design was found as a promising design of cryogenic trap. The capillary has several important advantages. The capillary does not contain any filling thus overpressure in the system of hydride generator is lower. The simple and fast changing of the capillary after damage is also advantage. The capillary cryogenic trap does not require any treatment before analysis (no REJUV – silylating reagent). Last but not least the consumption of liquid nitrogen within this system is lower.

On the other hand capillary is much more sensitive to blockage by freezed water. This problem can be partly overcome using a polyethylene foam lid that is placed on the dewar flask ca 2 cm above the level of liquid nitrogen. The capillary goes through this lid. A zone of cold air is formed above the level of liquid nitrogen in the volume covered by the lid. Under these conditions there is a less steep temperature gradient in the capillary. Thus water vapour is freezed on larger area along the capillary wall and the risk of ice lid leading to the blockage of the capillary is minimized.

The water vapour amount transported to the trap was minimized by using a nafion tube dryer placed between GLS and cryogenic trap. However, this nafion tube dryer is not sufficient if sample volume is higher than 2 mL.

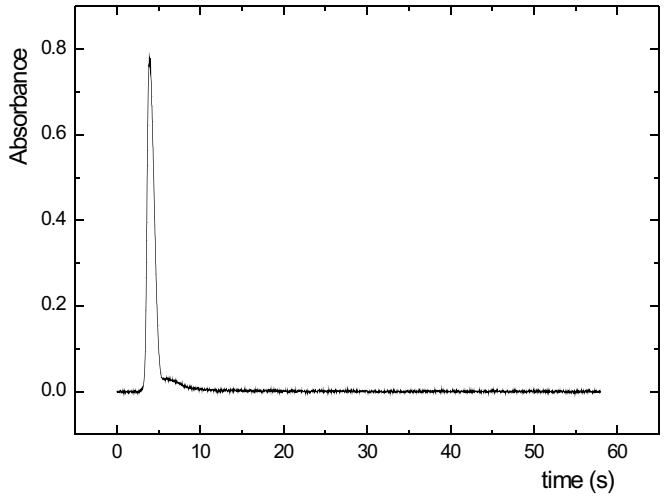

Fig. 6. The typical chromatogram of 2 ppb iAsIII from the capillary cryogenic trap.

After two minutes the capillary is blocked by freezed water even if the nafion tube dryer is supplied with maximum flowrate of N_2 (dryer gas). Thus, the other technique of water prevention must be found for higher sample volumes.

It was found that 35 mL min^{-1} helium is the optimum carrier gas flowrate for collection step resulting in the lowest standard deviation as depicted in Fig. 5. Only 3 cm of capillary length was under liguid nitrogen, the same length as in case of radiotracer experiments.

There is an evidence that 3 cm of capillary length under liquid nitrogen during the collection step is sufficient. The 50 cm long capillary was immersed in liquid nitrogen gradually increasing its length subnerged into liquid nitrogen and the variations in iAsIII peak area were not observed.

iAsIII standard was used as a model arsenic specie to optimize trapping conditions in this miniaturized trap. Narrower and higher peaks were observed in this arrangement compared to U-tube cryogenic trap system (Fig. 6). The full width at half maximum is approximately 1 s in the novel design (compare with 3 s for U-tube) and peak height is approximately 0.8 (0.4 for U-tube).

Preliminary experiments were performed employing resistive heating of the capillary in the volatilization step. However, it was found that heating by ambient temperature is sufficient for 100% volatilization efficiency and satisfactory peak profile (see Fig. 5). Negligible peak tailing which does not influence peak area evaluation is observed using heating by ambient atmosphere. Nevertheless, resistive heating might be used in future in an automated cryogenic system based on capillary trap.

4. Conclusions

It was proved the possibility of connection of hydride generation-cryogenic trapping approach (HG-CT) with atomic fluorescence spectrometry (AFS) as a detection method for arsenic determination. Probably the -SH group in L-cysteine caused the imposibility to use as a pre-reductant agent therefore is not possible to carry out arsenic speciation with this approach. The hydrochloric acid was employed only for demonstration of possible HG-CT and AFS connection. Nevertheless the detection limits were lower for all arsenic species.

Inorganic As radiotracers utilization for trapping and volatilization studies demonstrated that the quartz capillary is a possible new cryogenic trap. The approach miniaturize whole system of cryogenic trap and could work automatically similarly to automated cryogenic trap system designed by T. Matoušek *et al.* [8]. Nevertheless it is necessary to find the optimal behaviour for trapping of methylated arsenic forms. Afterwards the new trap could be connected with separtion method like a gas chromatography.

Acknowledgements. *This work was supported by the GA ASCR (grant No. A400310507), GA CR (grant No. 203/09/1783), GA UK (Project No. 133008); MŠMT no. MSM0021620857; Gillings Innovation Labs project (PI: M. Stýblo) and Institute of Analytical Chemistry of the ASCR, v.v.i. (project no. AV0Z40310501).*

References

[1] Cornelis R.: *Handbook of Elemental Speciation II*. Wiley, Chichester 2005.
[2] Devesa V., Del Razo L.M., Adair B., Drobná Z., Waters S.B., Hughes M.F., Stýblo M., Thomas D.J.: *J. Anal. At. Spectrom.* **19** (2004), 1460–1467.
[3] Stýblo M., Del Razo L.M., Vega L., Germolec D.R., Le Cluyse E.L., Hamilton G.A., Reed W., Wang C., Cullen W.R., Thomas D.J.: *Arch. Toxicol.* **74** (2000), 289–299.
[4] Francesconi K.A., Kuehnelt D.: *Analyst* **129** (2004), 373–395.
[5] Matoušek T., Hernandéz-Zavala A., Svoboda M., Langerová L., Adair B. M., Drobná Z., Thomas D. J., Stýblo M., Dědina J.: *Spectrochimica Acta Part B* **63** (2008), 396–406.
[6] Matoušek T., Dědina J., Selecká A.: *Spectrochim. Acta Part B* **57** (2002), 451–462.
[7] Dědina J., D' Ulivo A.: *Spectrochim. Acta B* **52** (1997), 1737–1746.
[8] Dědina, J.: *Spectrochim. Acta B* **62** (2007), 846–872.
[9] Kratzer J., Vobecký M., Dědina J.: *J. Anal. Atom. Spectrom.*, in press

Polystyrene Based Capillary Monolithic Columns: Preparation and Characterization

Adéla Svobodová[a], Tomáš Křížek[a], Pavel Coufal[a], Eva Tesařová[b]

[a] *Department of Analytical Chemistry,* [b] *Department of Physical and Macromolecular Chemistry, Faculty of Science, Charles University in Prague, Albertov 2030, 128 43 Prague 2, Czech Republic,* ✉ *adelka.svoboda@seznam.cz*

Abstract

In this work, polystyrene-based capillary monolithic columns were prepared in fused silica capillaries by a single step radical copolymerization reaction of styrene, divinylbenzene and methacrylic acid monomers in presence of toluene and isooctane as porogen solvents and azobisisobutyronitrile as the initiator. The influence of incorporation of methacrylic acid into the polymerization mixture on the separation behaviour and column efficiency was investigated by the capillary liquid chromatography and capillary electrochromatography. The dependence of the bed morphology on polymerization conditions was characterized by means of mercury intrusion porosimetry and nitrogen adsorption/desorption method. Finally, chromatographic behaviour of the prepared monolithic columns was tested and characterized with compounds of various polarities.

Keywords

capillary electrochromatography
capillary liquid chromatography
methacrylic acid
polystyrene-based monolithic stationary phase

1. Introduction

In recent years, a new type of separation media, monolithic stationary phases, has attracted attention in separation techniques. In the early 90s, Švec and Fréchet [1] introduced a stationary phase based on rigid macroporous organic polymer monoliths. Since that time, they have become, because of their excellent properties, one of the widely developing stationary phases for liquid chromatography and electrochromatography.

Monoliths are separation media that can be described as a single large "particle" of porous material. This porous material is often characterized by bimodal pore size distribution [2]. Two main types of pores in the structure of continuous bed are flow-through pores, enabling an easy flow of the mobile phase, and a group of mesopores and micropores which are filled with stagnant mobile phase where the solute molecules diffuse to access the adsorption sites. The structure of stationary phases, especially monolithic stationary phases, plays a very important role in their subsequent chromatographic behavior. The pore characteristics and their distribution, total porosity and specific surface area are major factors affecting separation process and, above all, separation efficiency. Mercury intrusion porosimetry and nitrogen adsorption using Brunauer, Emmet, Teller equation are the most common methods for determination of the porous properties.

Technology of monolithic columns overcomes some difficulties associated with common packed capillary columns [3] – monoliths fill the column volume completely without interparticular voids. As a result, all the mobile phase must flow through the stationary phase accelerating the rate of mass transfer. In contrast to diffusion, which is the main driving force for mass transfer in particulate stationary phase during chromatographic separation, this convective flow through the pores enables considerable increase in speed of the separation of large molecules such as proteins. Liapis [4] has recently described a complete theoretical treatment of mass transfer within monolithic materials. Fig. 1 shows structural characteristics of packed and monolithic chromatographic beds. The main advantages are the simplicity of their preparation and no need of retaining frits which are often responsible for bubbles formation during analysis. In addition to this, the functionality and morphology of monolithic column can easily be tuned by the composition of polymerization mixture and the polymerization conditions. Monoliths are

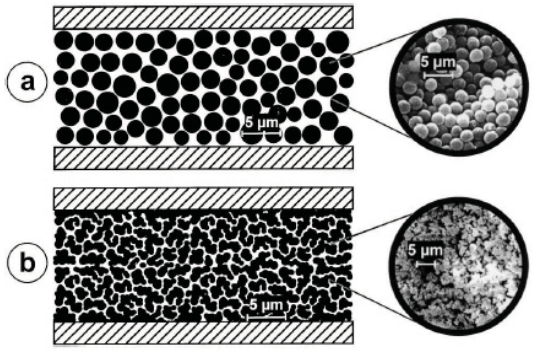

Fig. 1. Structural characteristics of (a) packed and (b) monolithic chromatographic beds [13].

polymerized in situ within a tube such as chromatographic column or capillary in which they remain after the preparation is completed. The polymerization mixture contains a functional monomer which is responsible for the resultant polarity of the monolithic separation medium, a monomer with two or more double bonds (crosslinking agent), initiator of polymerization reaction and porogenic solvent determining pore size distribution. Monoliths based on polyacrylamide (highly polar) [5, 6], polystyrene (strongly hydrophobic) [7, 8], polymethacrylate (medium polar) [9, 10] and polynorbornene (non-polar) [11] were prepared as stationary phases. The possibility of synthesis of monoliths with broad range of chemical properties and functionalities enables their application to many different analytes, *e. g.* peptides and proteins [12], nucleic acids [13] or low molecular mass compounds [14]. The concept of monolithic stationary phases is especially favorable for the fabrication of capillary columns which bring many advantages such as low consumption of mobile and stationary phase as well as decreased amounts of samples necessary for injection.

This work is focused on polystyrene-based capillary monolithic columns which are prepared by copolymerization of styrene or its derivatives with divinylbenzene as the crosslinking agent. Polystyrene monolithic columns can directly be used for reversed-phase chromatography due to the hydrophobicity of monomers. For capillary electrochromatography and other chromatographic modes, a chemical modification is necessary. Several ways of chemical modification are possible [15, 16]. One of them is a change of the monomer mixture composition. Incorporation of methacrylic acid to the polymerization mixture implements charged moieties to the monolith which can generate electroosmotic flow when a voltage is implied on the column therefore they can be use for capillary electrochromatography.

The aim of this study was to investigate the influence of addition of methacrylic acid to the polymerization mixture on the separation behavior and separation efficiency of prepared monolithic columns. The selectivity and the efficiency of capillary liquid chromatography and capillary electrochromatography separations of a test mixture were compared. The dependence of the bed morphology on polymerization time was studied as well.

2. Experimental

2.1. Chemicals

Styrene (for synthesis), divinylbenzene (for synthesis), toluene (extra pure) and α,α'-azobisisobutyronitrile (98%) were purchased from Merck. Isooctane (p.a.) was bought from Lach-Ner (Czech Republic). 3-(trimethoxysilyl)-propyl-methacrylate (99%) and ethylbenzene (p.a.) were provided by Fluka. Sodium hydroxide (p.a.) was purchased from Lachema (Czech Republic). Thiourea as dead time marker, phenol (99%), aniline (98%), benzene (99%), propylbenzene (99%) and butylbenzene (98%) were provided by Sigma Aldrich. Acetonitrile and methanol (gradient-grade for liquid chromatography) were supplied by Merck. The water used in this work was purified with Milli-Q water purification system (Millipore, USA).

2.2. Equipment and materials

The capillary monolithic columns were prepared within polyimide-coated fused silica capillaries of 100 and 320 μm i.d. provided by Supelco. An oven UL 400 Memmert (Germany) was used for thermostating the capillaries during pretreatment and polymerization. An ISCO syringe pump model 100 DM, a Valco International injection valve with a 100 nL internal loop (Schenkon, Switzerland) and a LINEAR UVIS-205 absorbance detector (USA) were used for chromatographic measure-ments. The column inlet was installed in the injection valve using a PEEK sleeve and finger--tight fitting. The monolithic column was connected by a piece of PTFE tubing to a 100 μm i.d. fused silica capillary with a detection window positioned 80 mm from the separa-tion column outlet. The 100 μm i.d. capillary with burnt detection window was placed in the absorbance detector operated at two parallel wavelengths of 214 and 254 nm. Chromatograms were recorded and evaluated using Clarity computer software by DataApex (Czech Republic). The monolithic columns prepared were tested under flow rates from 0.5 to 5.0 μL min^{-1} at ambient temperature. Electrochromatographic measurements were performed on a CE3D instrument (Agilent Technologies, Germany). The monolithic column with burnt detection window (procedure is described in section 2.4.) was placed in the CE instrument. Capillary cassette temperature was maintained at 25 °C by air-cooling system, separation voltage was set to 15 kV and a pressure of 350 kPa was applied to both ends of the column. Samples were electrokinetically injected into the capillary for 5 s at a voltage of 5 kV. The diode array detector collected data within range of 200–400 nm and a 200 nm wavelength, exhibiting the highest sensitivity, was used for data evaluation. Mobile phase 65 % acetonitrile in 10 mM phosphate buffer, pH = 7.0, was used for all experiments. Electrochromatograms were recorded and evaluated using Agilent Chem Station (Germany). All samples were prepared dissolving test solutes in mobile phase.

2.3. Capillary pretreatment

Before polymerization, the capillary was pretreated with the following procedure [17]. The inner wall of the fused silica capillary was modified by sodium hydroxide and silanization solution to improve the adhesion of the monolithic bed to the capillary wall. Capillary was flushed and filled with 1 M aqueous NaOH. Both ends were plugged with rubber stoppers (pieces of GC injector septa) and the capillary was left in an oven for 3 hours at 120 ºC. Subsequently, the capillary was rinsed with deionized water followed by acetone. Next, the capillary was dried in the stream of nitrogen for 10 min and then dried in an oven for another 1 h at 120 ºC. After that, the silanization mixture containing 10% (v/v) 3-(trimethoxysilyl)-propylmethacrylate in toluene was introduced. The silanization solution was degassed in the stream of nitrogen and filled into the capillary. The capillary ends were closed with rubber stoppers and left to react for 2 h at room temperature. The silanization mixture was then washed out by toluene and the capillary was dried in the stream of nitrogen. Thereby Si-O-Si-C bonds were formed between the capillary wall and the reactive methacryloyl groups, which are available for consequent attachment of monolith to the capillary wall during the polymerization.

2.4. Column preparation

The monolithic column was prepared by polymerization of mixture, consisting of styrene as a function monomer, divinylbenzene as a crosslinking monomer, methacrylic acid as a charge bearing monomer, toluene and isooctane as porogens, using azobisisobutyronitrile as an initiator (1% with respect to the monomers). The polymerization mixture was sonicated for 20 min to obtain a homogenous solution and then degassed in the stream of nitrogen for 10 min. After, the pretreated capillary was completely filled with the polymerization mixture, both ends were sealed by rubber stoppers and left to react in an oven for 1.5–24 h at 70 ºC. The prepared columns, without visible contraction of monolith, were cut at both ends and connected to the injection valve and flushed with methanol to remove unreacted monomers and porogens. Afterwards, the detection window for capillary electrochromatography columns was created in the capillary by burning off a segment of the outer polyimide coating and pyrrolyzing a part of the monolith inside. During the creation of detection window, capillaries were flushed with deionized water, applying a pressure of up to 15 MPa. The ashes produced during pyrrolyzation were removed by flushing with methanol. Prior to chromatographic measurements, both types of columns (for capillary electrochromatography and capillary liquid chromatography) were washed with mobile phase. Samples for characterization of the polymer morphology were prepared in plastic vials in the same way as columns (polymerization time 1.5–12 h), rinsed with acetonitrile and dried under the vacuum at 60 °C overnight. The polymeric monoliths produced in vials and in the capillary may not exactly be identical. Nevertheless, the data obtained from vials can be considered as an important reference points for the monolith prepared within the capillary.

3. Results and discussion

The preparation procedure for polystyrene-based monolithic capillary columns of 100 μm i.d. published by Jin *et al.* [16] used in capillary electrochromatography was adopted in several points. Polymerization mixture was composed of 50 μl of styrene, 100 μl of divinylbenzene, 50 μl of methacrylic acid, 300 μl of toluene and 300 μl of isooctane. A set of capillary electrochromatography columns and samples for morphology measurements differing in polymerization time was prepared. The same polymerization mixture was also used for preparation of 320 μm i.d capillary columns for capillary liquid chromatography mode. As poly(styrene--*co*-divinylbenzene-*co*-methacrylic acid) monolith was used for the first time as the stationary phase in capillary liquid chromatography, the effect of polymerization conditions on the morphology of the monolith and on the capillary liquid chromatography separation was studied. At first, the polymerization conditions such as polymerization temperature and polymerization time were examined. The morphology of the monolithic column remained relatively unaffected if the polymerization temperature was changed between 60 and 70 ºC, whereas if the polymerization temperature was lower than 60 ºC, a considerable bed inhomogeneity was observed. As a result, the polymerization temperature was maintained at 70 ºC in order to achieve reproducible monolithic columns. From morphology measurements, it was obvious that polymerization time significantly altered the quality of continuous bed. The most frequent pore radius increased with the extending polymerization time. Furthermore, an increase in reaction time caused a decrease in the specific surface area produced by the polystyrene-based monolith. Fig. 2 (*see next page*) shows both dependences on the increasing polymerization reaction time.

Simultaneously with morphologic measurements, the effect of polymerization time on separation behavior of the eight analytes was investigated by capillary liquid chromatography. Acetonitrile/water 65:35 % (v/v) was chosen as the mobile phase for separation of set of

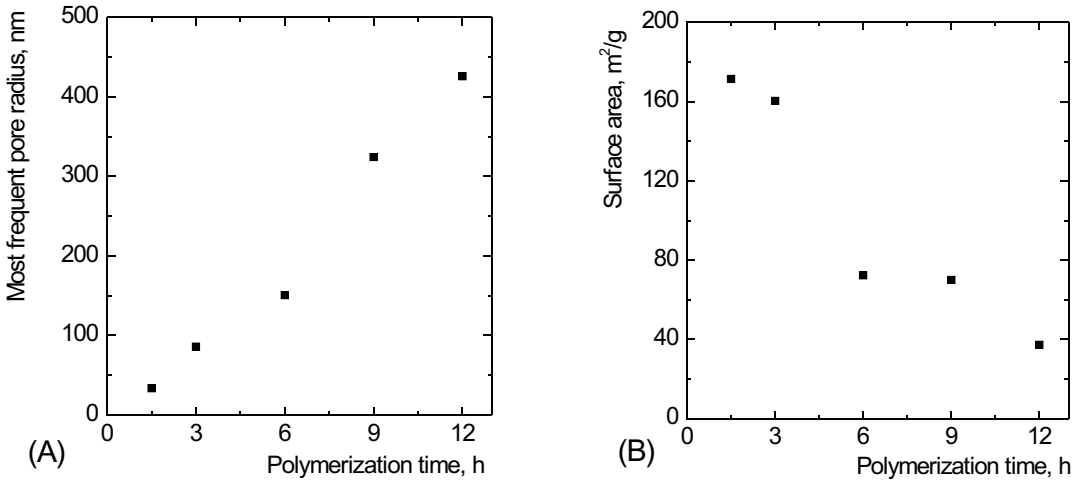

Fig. 2. Dependence of the most frequent pore radius (A) and the specific surface area (B) on the polymerization time.

eight compounds differing in their polarities. The test mixture was composed of thiourea used as the dead retention time marker, phenol, aniline, benzene, toluene, ethylbenzene, propylbenzene and butylbenzene. All the columns prepared provided baseline separation of all eight test analytes. However, the duration of polymerization reaction affected the permeability of the columns significantly. In accordance with the morphological measurements, the higher polymerization time, the higher permeability of the monolith. It was observed that the separation efficiency increased with the reaction time. Furthermore, the monolithic column prepared by a longer polymerization reaction provided more reproducible retention behavior for the test mixture. Subsequently, a polymerization time of 12 h was chosen as the optimal on in this study. Figs. 3 and 4 show the optimized capillary electrochromatography and capillary liquid chromatography separations of the studied compounds. To assess the effect of incorporation of charge-bearing monomer (methacrylic acid) to the polymerization mixture, a batch of columns without methacrylic acid was prepared. For fabrication of these columns, the

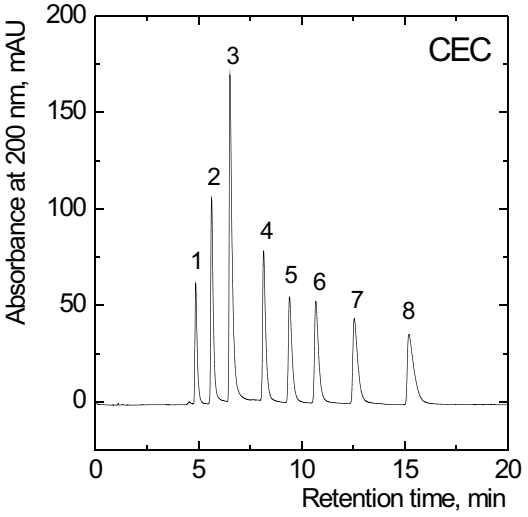

Fig. 3. The capillary electrochromatography separation of test mixture containing: (1) thiourea, (2) phenol, (3) aniline, (4) benzene, (5) toluene, (6) ethylbenzene, (7) propylbenzene, and (8) butylbenzene on the poly(styrene-*co*-divinylbenzene-*co*-methacrylic acid) monolithic column. Effective column length: 24 cm; eluent: 10 mM phosphate buffer containing 65% acetonitrile; applied voltage: 15 kV; electrokinetic injection: 5 kV for 5 s; detection: 200 nm.

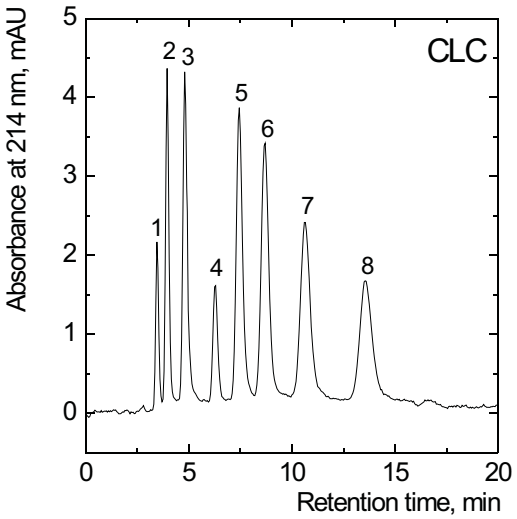

Fig. 4. The capillary liquid chromatography separation of test mixture containing: (1) thiourea, (2) phenol, (3) aniline, (4) benzene, (5) toluene, (6) ethylbenzene, (7) propylbenzene, and (8) butylbenzene on the poly(styrene-*co*-divinylbenzene-*co*-methacrylic acid) monolithic column. Effective column length: 18 cm; eluent: acetonitrile-water (65:35, v/v); flow rate: 4 μL min^{-1}; injection: 100 nL; detection: 214 nm.

Table 1. The comparison of capillary liquid chromatography (CLC) and capillary electrochromatography (CEC) methods.

Analyte	Retention		Resolution		Efficiency [N m^{-1}]	
	CLC	CEC	CLC	CEC	CLC	CEC
Thiourea	0.00	0.00	–	–	15600	46800
Phenol	0.14	0.16	1.87	3.96	15800	50900
Aniline	0.39	0.34	2.63	4.08	13800	52600
Benzene	0.81	0.68	3.73	6.76	18000	71400
Toluene	1.14	0.93	2.44	4.52	15100	63100
Ethylbenzene	1.50	1.20	2.08	3.92	14300	64500
Propylbenzene	2.06	1.58	2.61	4.91	12600	60900
Butylbenzene	2.89	2.12	3.06	5.39	13400	48000

proportion of styrene in the polymerization mixture was increased by the amount of methacrylic acid missing. The columns polymerized without methacrylic acid were only able to separate polar compounds (thiourea, phenol, aniline) from non-polar ones (benzene and its alkylderivatives).

Similar chromatographic conditions were employed for testing of the capillary electrochromatography columns. To assure electric conductivity, 10 mM phosphate buffer, pH = 7.0, was used instead of water to prepare the mobile phase. A baseline separation of all the test analytes was achieved in less than 17 minutes. The analysis time and selectivity of both methods are therefore comparable. The retention factors, resolution and separation efficiency for the test analytes are displayed in Table 1. Although the capillary electrochromatography method offers at least threefold higher separation efficiency, it requires rather laborious and time-consuming conditioning and complicated experimental setup which hinders eventual automation of the method.

4. Conclusions

Monolithic beds based on the poly(styrene-*co*-divinylbenzene-*co*-methacrylic acid) copolymer were prepared and characterized as the stationary phases for capillary liquid chromatography and capillary electrochromatography. Morphological properties of the stationary phases were studied and their chromatographic behavior in both methods was compared. The optimized stationary phase prepared has offered efficient separation of compounds of various polarities in both, capillary electrochromatography and capillary liquid chromatography modes. There were no previous capillary liquid chromatography applications of the studied copolymer published in the literature. This method seems to be more suitable for testing and characterization of stationary phases in general because of its simplicity. Although the most publications consider methacrylic acid only as a charge-bearing agent for generation of electroosmotic flow, this work reveals the essential influence of this agent on the separation selectivity of the monoliths.

Acknowledgements. *The project No. 203/07/0392 of the Grant Agency of the Czech Republic and the research project MSM 0021620857 of the Ministry of Education, Youth and Sports of the Czech Republic are highly acknowledged for the financial support.*

References

[1] Švec F., Frechet J. M. J.: *Anal. Chem.* **54** (1992), 820–822.
[2] Urban J., Eeltink S., Jandera P., Schoenmakers P. J.: *J. Chromatogr. A* **1182** (2008), 161–168.
[3] Švec F.: *J. Sep. Sci.* **27** (2004), 1419–1430.
[4] Meyers J. J., Liapis A. I.: *J. Chromatogr. A* **852** (1999), 3–23.
[5] Palm A., Novotný M. V.: *Anal. Chem.* **69** (1997), 4499–4507.
[6] Fujimoto Ch., Kino J., Sawada H.: *J. Chromatogr. A* **716** (1995), 107–113.
[7] Gusev I., Huang X., Horváth C.: *J. Chromatogr. A* **855** (1999), 273–290.
[8] Petro M., Švec F., Gitsov I., Fréchet J. M. J.: *Anal. Chem.* **68** (1996), 315–321.
[9] Grafnetter J., Coufal P., Tesařová E., Suchánková J., Bosáková Z., Ševčík J.: *J. Chromatogr. A* **1049** (2004), 43–49.
[10] Buszewski B., Szumski M.: *Chromatographia* **60** (2004), 261–267.
[11] Mayr B., Hölzl G., Eder K., Buchmeise M. R., Huber C. G.: *Anal. Chem.* **74** (2002), 6080–6087.
[12] Bandilla D., Skinner C. D.: *J. Chromatogr. A* **858** (1999), 91–101.
[13] Oberacher H., Huber C. G.: *Trends Anal. Chem.* **21** (2002), 166–174.
[14] Ericson Ch., Liao J.-L., Nakazato K., Hjérten S.: *J. Chromatogr. A* **767** (1997), 33–41.
[15] Kučerová Z., Szumski M., Buszewski B., Jandera P.: *J. Sep. Sci.* **30** (2007), 3018–3026.
[16] Jin W. H., Fu H. J., Huang X. D., Xiao H., Zou H. F.: *Electrophoresis* **24** (2003), 3172–3180.
[17] Courtois J., Szumski M., Byström E., Iwasiewicz A., Shchukarev A., Irgum K.: *J.Sep. Sci.* **29** (2006), 14–24.

Organic Dyes and Their Identification

Eva Svobodová[a], Martina Ohlídalová[b], Miroslava Novotná[b], Zuzana Bosáková[a], Věra Pacáková[a]

[a] *Department of Analytical Chemistry, Faculty of Science, Charles University in Prague, Albertov 6, 128 43 Prague 2, Czech Republic,* ✉ *svobod15@natur.cuni.cz*
[b] *Laboratory of Molecular Spectroscopy, Central Laboratories, Institute of Chemical Technology Prague, Technická 5, 166 28 Prague 6, Czech Republic*

Abstract

This work deals with red organic dyes identification using molecular spectroscopic method. The infrared spectroscopy in reflectance mode (wavenumber between 650–4000 cm^{-1}) has been optimized for identification of nine selected red dyes (*i. e.*, akaroid, brazil, dragon blood, kamala, logwood, cochinea, kraplak, lac and santal). The spectra of individual dyes and their main dyeing components were measured. The significant absorption bands of individual dyes were found and used for identification and differentiation of studied dyes. Further the model samples of dyed textile fibres were prepared. The wool and viscose fibres were mordanted by three types of mordants (namely potassium aluminium sulphate, ferrous sulphate and cupric sulphate) and dyed with seven dyes. The spectra of dyed textile fibres were measured both before and after an accelerated ageing by emission in visible and near infrared area. The ageing had no influence on the dyes, but the fibres were degraded. The possibilities of identification and differentiation of selected dyes bound on fibres are discussed.

Keywords
accelerated ageing
identification
infrared spectroscopy
organic dyes
textile fibres

1. Introduction

Natural organic dyes are produced by plants or animals, especially by insects. Their main components are quinones, flavones, indols, and their derivatives. The most of natural dyes belong to mordant dyes requiring the modification of substrate, namely textile, leader or paper [1, 2]. Natural dyes have been used for dying of different materials since the ancient cultures in Greece, Roma, Egypt and Chine. Later the natural dyes had been applied over the world until the first synthetic dye has been produced (in second half of the nineteenth century) [3–5].

The vast majority of natural organic colouring material belong to the chemical classes of flavonoids (yellow), indigoids (blue) and anthraquinones (red). Flavonoid and anthraquinone dyestuffs, soluble in water, are found in paintings in a manufactured insoluble form called lake [2]. To natural red organic dyes belong akaroid, alkana, brazil, dragon blood, durra, harmala, kamala, logwood, kermes, cochinea, kraplak, lac, orchil, purpur, saflor, sandarak, santal and gale [5, 6].

Akaroid is resin dye used to prepare varnish layer on the painting. Cochinea, containing carminic acid, is produced by *Coccus* and was for the first time exported into Europe in the year 1516. The carminic acid is soluble in water and at present is still used as food dyestuff. The *Coccus lacca* living in tropical part of Asia produces a colouring matter called lac. Lac contains mainly laccaic acid in five different forms (forms A–E). Lac was imported into Europe during 13th century and is still used for textile dying and as furniture varnish [4, 5].

Several red organic dyes are produced by plants and used in paintings and/or as textile dyes. Brazilein made from trees *Caesalpinia crista* and *C. brasiliensis* in India and Brazil, is the main colouring compound of dye called brazil wood. This dyestuff has used in Europe from 9th century in book paintings, to textile dying and as ink. To textile dying and as furniture varnish the dye santal has used since 19th century when it was imported to Europe. It contents colouring compound santalin A and santalin B, which belong to group of pyrrole derivatives. Other pyrrole derivatives dracorubin and dracorhodin are contained in colour named dragon blood. This dyestuff has been using in book paintings and as furniture varnish, too. For textile dying and in aquarelle kamala and logwood are used also. Kamala's red pigmentation is due to rottlerin and isorottlerin produced by plant *Rottleria tinctoria.* The plant *Haematoxylon campechianum* is a producer of haematein, main compound of logwood, which originates by oxidation of haematoxylin. The most used dyestuff is kraplak well known as madder. The composition of this dye is very various in dependence on plants species. It can content carmine, purpurin, pseudopurpurin, tubuadin, mujnistin, alizarin and anthragallol-dimethylether. The kraplak has been used in paintings, aquarrele and to carpet and textile dying until 1868 when the first synthetic dyes alizarin and carmine were manufactured [4, 5].

Natural organic dyes suffer from degradation during the time. The works of art need to be restored or conserved and the identification of dyes used is important. The development of analytical methods for the dye identification is of great interest.

For identification of organic dyes colorimetric tests, electroanalysis, separation methods and spectroscopic methods have been used. Colorimetric tests are useful for differentiation of natural/synthetic dyes and in routine analysis [6, 7]. To identify anthraquinone, naphtoquinone and flavonoid dyes the paper and thin-layer chromatography [8] are mostly employed because of their low cost and simplicity. More efficient separation methods are reversed-phase high performance chromatography [9–14] and electromigration techniques [8, 9], namely capillary zone electrophoresis and micellar electrokinetic chromatography. These methods are used to identify and quantify quinone and flavonoid derivatives. Disadvantage of separation methods is their destructive character. Non-destructive methods, such as electroanalysis and especially spectroscopic techniques are in front of interest of restorers. The voltametry was used for identification of anthraquinone dyes, namely alizarin, purpurin and their impurities, in inorganic matrix [15]. Among spectroscopic methods, microscopy with emission in visible and ultraviolet area, electron microscopy, X-ray fluorescence and diffraction [16] and molecular absorption spectroscopy [11, 17–19] were employed. The Raman spectroscopy is useful only for certain organic dyes because the most of them cause high fluorescence and the background of spectra is too high. For reduction of high background the surface-enhanced Raman spectroscopy [20–25] and the surface-enhanced resonance Raman spectroscopy [26–29] have been recommended. The most suitable method for identification of natural or synthetic dyes is infrared spectroscopy [5, 30], often using Fourier transform [31, 32] or ATR crystal [33]. The infrared spectroscopy is especially useful in connection with microscope using reflectance mode which does not destruct the sample.

This work deals with the identification of red organic dyes, *i. e.*, akaroid, brazil, dragon blood, kamala, logwood, cochinea, kraplak, lac and santal, using infrared spectroscopy in reflectance mode (wavenumber between 650–4000 cm^{-1}) and studies their ageing when bound of fibres.

2. Experimental

2.1. Chemicals

The dyes akaroid, kamala and kraplak were obtained from Kremer Pigmente, Germany. The colouring dyestuffs dragon blood, cochinea (dried abdomens of *coccus*) and santal were obtained from Sandragon, Czech. Other dyes brazil wood, logwood and lac were donated by Department of Chemical Technology of Monuments Conservation, ICT Prague. Standards of colouring main compounds of dyes, carmine, carminic acid, laccaic acid, haematein and rottlerin were obtained from Sigma-Aldrich, Germany, and purpurin was obtained from Fluka, Germany. The alizarin was isolated at the Institute of Microbiology of the Academy of Sciences of Czech Republic.

Chloroform (Sigma-Aldrich) was used for cleaning the steel plates. Potassium aluminium sulphate, ferrous sulphate and cupric sulphate were used as mordants in preparation of model samples of colouring textile wool and viscose. Fibres were pigmented with studied dyes, with the exception of akaroid and dragon blood, in colouring baths according to origin recipes described by Schweppe [1]. Other chemicals used were methanol (Sigma-Aldrich), $KAl(SO_4)_2 \cdot 12H_2O$, Na_2CO_3 (both Lachema, Czech Republic) and acetic acid (Penta, Czech Republic). Distilled water was used in the measurement.

2.2. Instruments

The infrared spectroscpic measurements in reflectance mode have been carried out on spectrometers Bruker IFS 66v with IR microscope Hyperion (Bruker Optics, Germany) and FTIR spectrometer Nicolet 6700 with microscope Continuum (Thermo-Nicolet, USA). The infrared spectrum of each analyte was measured in reflactance mode in the range of wave numbers between 650–4000 cm^{-1} and with spectral resolution of 4 cm^{-1}.

The accelerating ageing of model samples of colouring textile fibres has been carried out in a fluorescent tube Philips TL20W/09N at National Archive in Prague. The textile fibres were exposed to visible and near ultraviolet light (300 to 450 nm) for 300 hours at temperature of 25±2 °C.

3. Results and discussion

The identification of historic natural organic dyes in real samples by spectroscopic techniques has been based on their specific absorption bands. Dyes contain a wide spectrum of compounds (resins, sugars, proteins, *etc.*) but their pigmentation is given by the main colouring dyestuffs. For dyes identification, the absorption bands corresponding to characteristic structure bond vibration of main colouring dyestuffs are needed. Only those are specific and unique for their identification. At first the spectroscopic behaviour of available main colouring dyestuffs, namely alizarin (dye kraplak), purpurin (dye

kraplak), carmine (dye kraplak), carminic acid (dye cochinea), laccaic acid (dye lac), haematein (dye logwood) and rottlerin (dye kamala), has been investigated.

All available main colouring dyestuffs except of rottlerin and haematein are anthraquinone derivatives with different type of substituents and their location. Their absorption bands belong to vibration of the following bonds [34]: conjugated multiple bonds (~1600 cm^{-1}, ~1660–1580 cm^{-1} in the presence of carbonyl, ~1625 cm^{-1} in the presence of aromatic circle, ~1550 cm^{-1} in case of substituted anthracene, ~1415–1380 cm^{-1} for ring vibration and ~900––650 cm^{-1}); hydroxy groups (~3600–3450 cm^{-1} in the presence of hydrogen bonding, ~3610–3645 cm^{-1} in case of –OH groups bound by alifatic carbon, ~1440––1260 cm^{-1} for deformation vibration and ~1170––1130 cm^{-1} for C–O vibration); quinoid oxygen atoms and oxygen atoms bound in ether or ketone (at ~1690––1655 cm^{-1} two bands, ~1650 cm^{-1} in the presence of hydroxy group, ~1740 cm^{-1} for ketone and ~1630 cm^{-1} for C=O bound in COO^-); groups of C–H bonds (~3000–2800 cm^{-1} for aromates, ~1470–1400 cm^{-1} for $–CH_3$ and $–CH_2–$ asymmetric deformation vibration and ~1380 cm^{-1} for $–CH_2–$ and $–CH_3$ symmetric deformation vibration).

Carminic acid and laccaic acid both contain carboxy groups and in the structure of laccaic acid, nitrogen atom is presented (vibration bands at ~1665–1645 cm^{-1} for group $R_2C=N–R$). Carminic acid contents in its structure glucose (at ~3340 cm^{-1} for hydroxy groups, at ~2900 cm^{-1} for C–H bonds, at ~1460–1200 cm^{-1} and at ~1160–1000 cm^{-1} for C–O bonds and at ~980–730 cm^{-1} for C–H bonds deformation vibration). The absorption bands corresponding to vibration of glucose are not significant for the identification of dyestuffs.

The natural dyes studied in this work are extracts from plants (except cochinea) in a form of pigment. They are precipitated on an inorganic substrate, often on sulphate or other salts. The strong or medium strong absorption bands below 900 cm^{-1} prove the presence of inorganic salts. Particular spectra of red organic dyes with spectra of their main colouring dyestuffs are shown in Fig. 1–9 (*see the Annexe)*. There are two strong absorption bands for wave numbers 1648 cm^{-1} and 1548 cm^{-1} in the spectrum of cochinea (Fig. 5; *see the Annexe*). These bands are typical for proteins and correspond to bands called amide I and amide II. The band amide I corresponds to vibration of C=O bond and the band amide II corresponds to vibration of N–H and C–N bond [34]. These bands represent the proteins from *coccus* bodies and complicate the identification of colouring matter. The significant bands of saccharide in the range of wave number 1100–1000 cm^{-1} indicate the presence of carminic acid.

Table 1. The wavenumbers of the significant absorption bands of the studied dyes. The bold letters of the wavenumbers represent specific spectral bands.

Dye	Wavenumber, cm^{-1}
brazil wood	1497; **1424**; 1363; 1250; 1113; 1047
santal	1737; 1506; 1424; 1327; **1226**; 1155; 1032
akaroid	1513; 1204; 1161; 835
dragon blood	1511; 1205; 1171; 954; 835
kamala	**1551**; 1346; 1167; **1130**
logwood	**1503; 1476; 1293; 1209; 1056**
kraplak	1669; **1411**; 1146; **1022**; **996**
lac	**1715**; 1378; 1309; 834; **812**; **774**

Positions of the absorption bands of each dye spectrum are very similar due to similar chemical structure of main colouring compounds of dyes. To identify and differentiate the dyes it is necessary to find absorption bands that are specific for each dye. Infrared spectra of all dyes were compared and the significant absorption bands have been found which differ from each other. The wave-numbers of the significant spectral bands for studied dyes are presented in the Table 1. The absorption bands in bold letters shown in Table 1 are specific for each dye. Akaroid and dragon blood belong to group of resin dyes and it is impossible to distinguished them from each other using the infrared spectroscopic method. None of the significant absorption bands have been found for cochinea dye.

Model samples of dyed textile fibres were prepared for the verification of identification and differentiation of studied dyes. The wool and viscose fibres were at first mordanted using three types of mordants, namely potassium aluminium sulphate, ferrous sulphate and cupric sulphate. Then the fibres were dyed by cochinea, kraplak, santal, brazil wood, logwood, kamala and lac (according to recipes by Schweppe [1]). The infrared spectra of individual brown-state mordanted fibres were measured. The spectrum of wool fibres contains strong absorption bands in the range of ~2800–3600 cm^{-1} which correspond to vibration of OH, N–H and C–H groups, and two very strong protein bands amide I and amide II close to 1600 cm^{-1}. These absorption bands complicate dyes identification.

On contrary, very strong bands close to 1000 cm^{-1}, corresponding to saccharide units of fibres, are present in spectra of the viscose fibres. However, the viscose fibres are difficult to dye using mordating dyes due to absence of amide bonds.

Effect of dyes ageing has been studied. The infrared spectra of dyed fibres have been measured before and after the accelerated ageing (*i. e.*, the exposition to visible and near ultraviolet light (300 to 450 nm) for 300 hours at temperature of 25 ± 2 °C). A comparison of the infrared spectrum of kamala, its main colouring

dyestuff rottlerin, a brown-state wool fibre mordanted by potassium aluminium sulphate and the same mordated fibres dyed with kamala is presented in Fig 10 (*see the Annexe*). The spectrum of coloured wool fibres contrasts from the brown-state fibres spectrum at wavenumbes 1738, 1167 and 1130 cm^{-1}. The bands at 1167 and 1130 cm^{-1} are specific significant bands for dye kamala (see Table 1). Other significant bands of kamala (at 1551 and 1346 cm^{-1}) are overlapped by amide bands.

During to the accelerated ageing the colour tone of aged fibres has changed to the darker tone due to the photochemical degradation of wool fibres. The degradation has not changed the position of absorption bands in infrared spectrum of aged wool fibres dyed by kamala but changed the intensity of the bands (*see* Fig. 11 *in the Annexe*). The decrease in the intensity of the absorption bands at wavenumbers below 1200 cm^{-1} is caused by the decreased number of hydroxy groups in the structure of aged fibres. In the spectrum of aged fibres the absorption band at wavenumber 1152 cm^{-1} is overlapped by absorption band at 1238 cm^{-1} and the absorption band at 1121 cm^{-1} is three times lower compared to absorption band in the dye spectrum before the accelerated ageing. Nevertheless this specific band of kamala at wavenumber 1121 cm^{-1} is still useful for its identification.

4. Conclusions

The infrared spectroscopy in reflectance mode in range of wavenumbers between 650–4000 cm^{-1} has been optimised for the identification of selected natural red organic dyes, *i. e.*, akaroid, brazil wood, dragon blood, kamala, logwood, cochinea, kraplak, lac and santal. The specific absorption bands in the absorption spectra of the dyes and their main colouring dyestuffs have been found. They can be used for reliable identification of seven studied dyes. Akaroid and dragon blood have not been distinguished using the infrared spectroscopy. For the dye cochinea any significant absorption bands were not found. The mathematical operations, such as bands separation, differential spectra and Fourier deconvolution of spectrum, could improve the identification of dyes. The optimised method was verified for identification of studied dyes bound on textile fibres before and after accelerated ageing.

Acknowledgements. *This work was supported by the Ministry of Education, Youth and Physical Training of the Czech Republic, Project MSM 0021620857 and by the Grant Agency of the Charles University in Prague, Project 69807.*

References

[1] Schweppe H.: *Handbuch der Naturfarbstoffe. Vorkommmen. Verwendung. Nachweis.* Landsberg/Lach, Ecomed 1992.
[2] Wyplosz N.: *Laser Desorption Mass Spectrometric Studies of Artists' Organic Pigments.* Amsterdam, MolArt 2003.
[3] Čopíková J., Uher M., Lapčík O., Moravcová J., Drašar P.: *Chem. Listy* **99** (2005), 802–816.
[4] Šimůnková E., Bayerová T.: *Pigmenty.* Praha, STOP 1999.
[5] Hřebíčková B. A.: *Recepty starých mistrů aneb Malířské postupy středověku.* Brno, Computer Press 2006.
[6] Hofenk de Graaff J. H., Roelofs W. G. Th., Van Bommel M. R.: *The Colourful Past: Origins, Chemistry and Identification of Natural Dyestuffs.* Abegg-Stiftung and Archetype Publications 2004.
[7] Karsbeek N.: *Studies in Conservation* **50** (2005), 205–229.
[8] Watanabe T., Terabe S.: *J. Chromatogr. A* **880** (2000), 311–322.
[9] Puchalska M., Orlińska M., Ackacha M. A., Połeć-Pawlak K., Jarosz M.: *J. Mass Spectrom.* **38** (2003), 1252–1258.
[10] Sanyova J.: *Microchim. Acta* **162** (2008), 361–370.
[11] Karapanagiotis I., Lakka A., Valianou L., Chryssoulakis Y.: *Michrochim. Acta* **160** (2008), 477–483.
[12] Clementi C., Nowik W., Romani A., Cibin F., Favaro G.: *Anal. Chim. Acta* **596** (2007), 46–54.
[13] Novotná P., Pacáková V., Bosáková Z., Štulík K.: *J. Chromatogr. A* **863** (1999), 235–241.
[14] Bosáková Z., Peršl J., Jegorov A.: *J. High Resolut. Chrom.* **23** (2000), 600–602.
[15] Grygar T., Kučková Š., Hradil D., Hradilová J.: *J. Solid State Electrochem.* **7** (2003), 706–713.
[16] Algra R. E., Graswinckel W. S., Enckevort W. J. P. van, Vlieg E.: *J. Crystal Growth* **285** (2005), 168–177.
[17] Murcia-Mascaros S., Domingo C., Sanchez-Cortes S., Canamares M. V., Garcia-Ramos J. V.: *J. Raman Spectrosc.* **36** (2005), 420–426.
[18] Kandelbauer A., Kessler W., Kessler R. W.: *Anal. Bioanal. Chem.* **390** (2008), 1303–1315.
[19] Bettinger C., Zimmermann H. W.: *Histochemistry* **95** (1991), 279–288.
[20] Canamares M. V., Barcia-Ramos J. V., Gomez-Varga J. D., Domingo C., Sanchez-Cortes S.: *Langmuir* **23** (2007), 5210–5215.
[21] Whitney A. V., Casadio F., Van Duyne R. P.: *Appl. Spectrosc.* **61** (2007), 994–1000.
[22] Chen K., Leona M., Vo-Dinh K. C., Yan F., Wabuyele M. B., Vo-Dinh T.: *J. Raman Spectrosc.* **37** (2006), 520–527.
[23] Leona M., Stenger J., Ferloni E.: *J. Raman Spectrosc.* **37** (2006), 981–992.
[24] Whitney A. V., Van Duyne R. P., Casadio F.: *J. Raman Spectrosc.* **37** (2006), 993–1002.
[25] Doherty B., Miliani C., Berghe I. V., Sgamellotti A., Brunetti B. G.: *J. Raman Spectrosc.* **39** (2008), 638–645.
[26] Peica N., Kiefer W.: *J. Raman Spectrosc.* **39** (2008), 47–60.
[27] Shadi I. T., Chowdhry B. Z., Snowden M. J., Withnall R.: *Spectrochim. Acta A* **59** (2003), 2201–2206.
[28] Shadi I. T., Chowdhry B. Z., Snowden M. J., Withnall R.: *J. Raman Spectrosc.* **35** (2004), 800–807.
[29] Shoute L. C. T., Loppnow G. R.: *J. Chem. Phys.* **117** (2002), 842–850.
[30] Kučková Š., Němec I., Hynek R., Hradilová J., Grygar T.: *Anal. Bioanal. Chem.* **382** (2005), 275–282.
[31] Valla V., Bakola-Christianopoulou M., Kojic V., Bogdanovic G.: *Synth. React. Inorg. Met. Org. Nano. Met. Chem.* **37** (2007), 41–51.
[32] Holmgren A., Wu L. M., Forsling W.: *Spectrochim. Acta A* **55** (1999), 1724–1730.
[33] Marengo E., Liparota M. C., Robotti E., Bobba M.: *Anal. Chim. Acta* **553** (2005), 111–122.
[34] Sokrates G.: *Infrared and Raman Characteristic Group Frequencies.* London, Wiley 2001.

Annexe

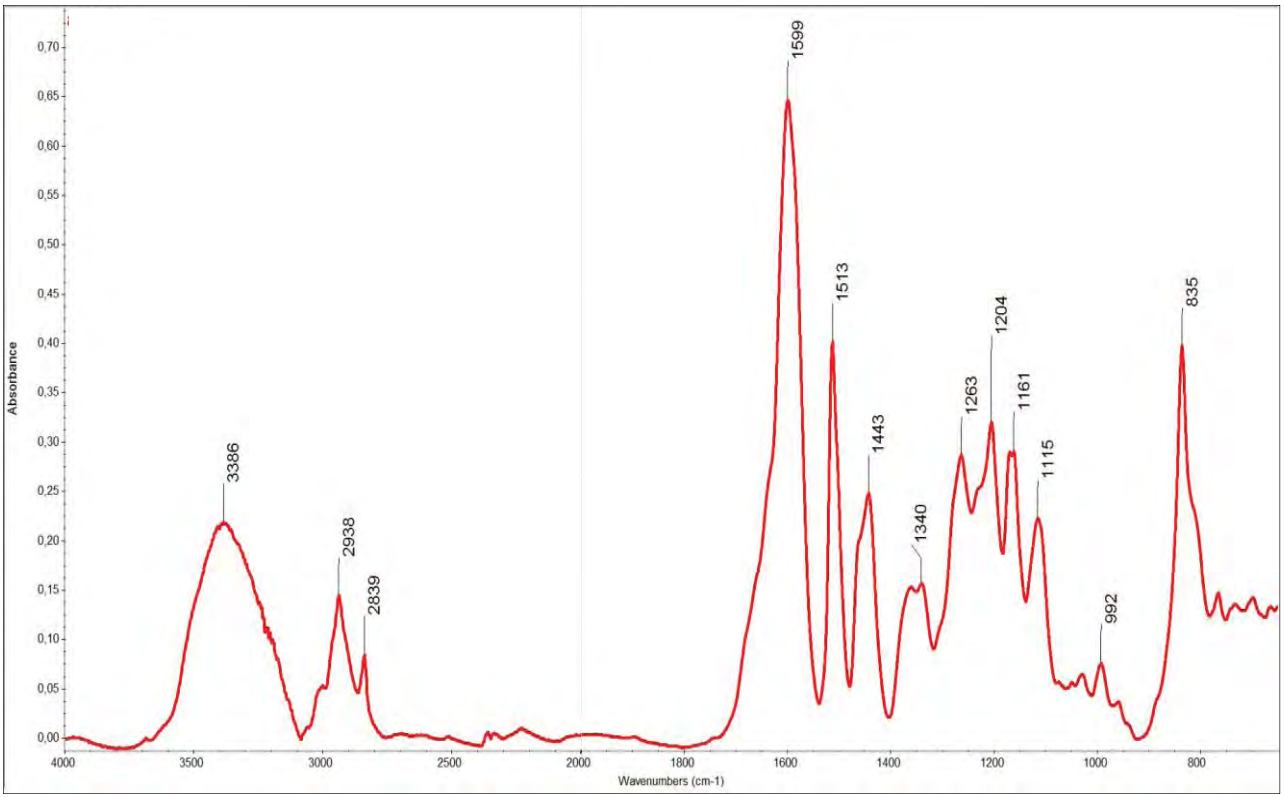

Fig. 1. Infrared spectrum of the dye akaroid.

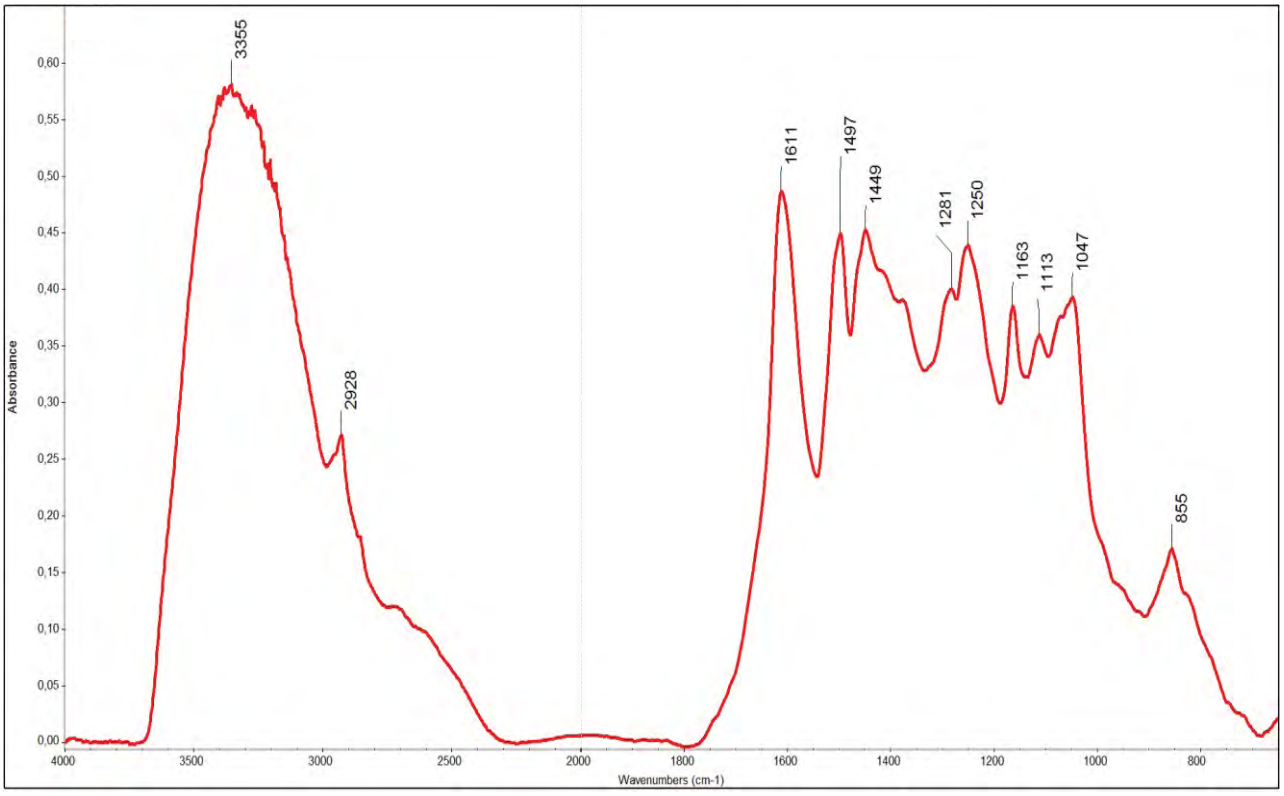

Fig. 2. Infrared spectrum of the dye brazil wood.

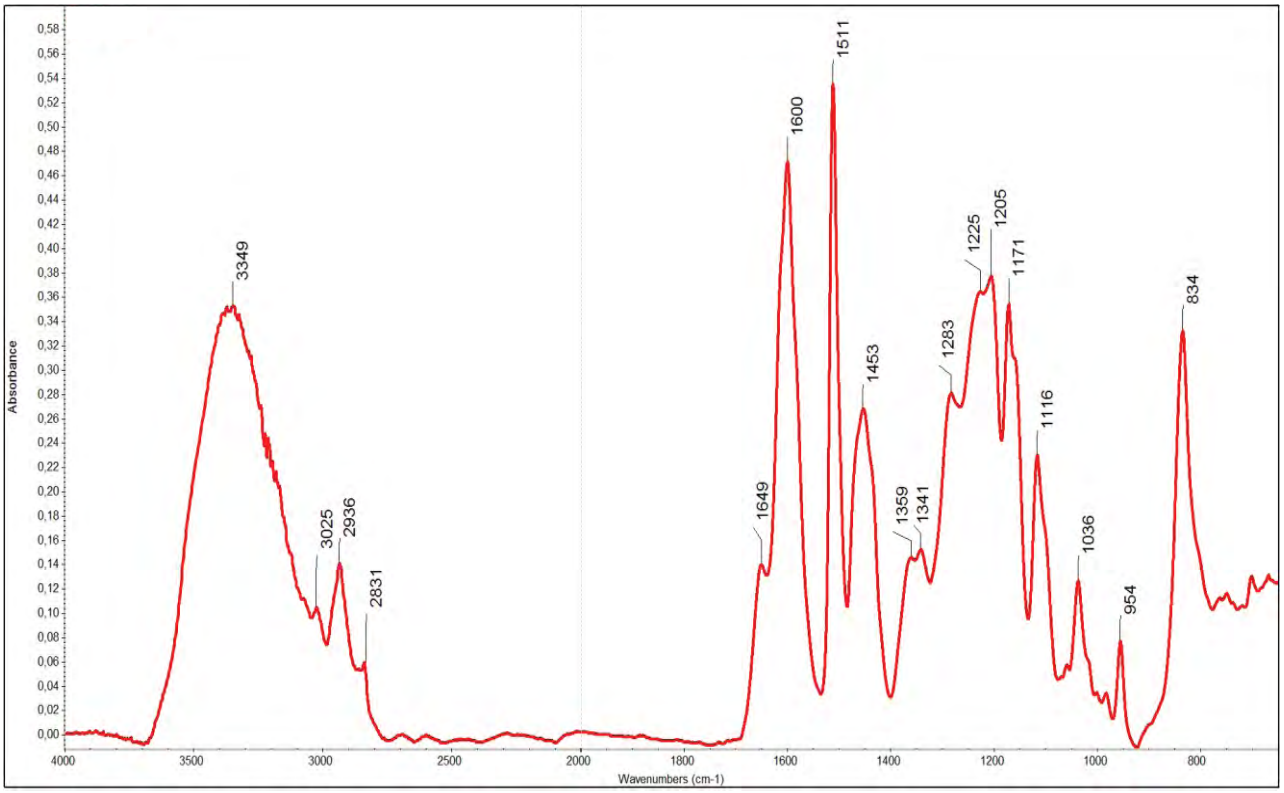

Fig. 3. Infrared spectrum of the dye dragon blood.

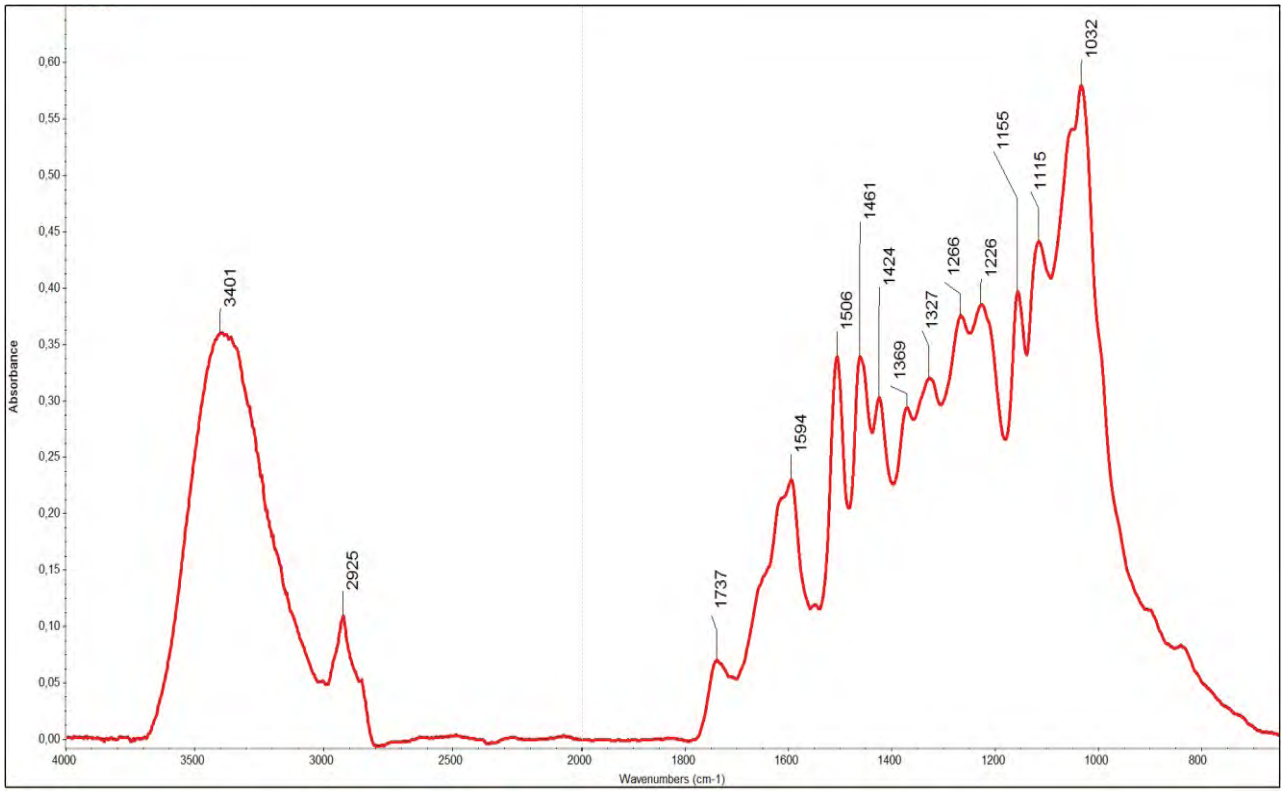

Fig. 4. Infrared spectrum of the dye santal.

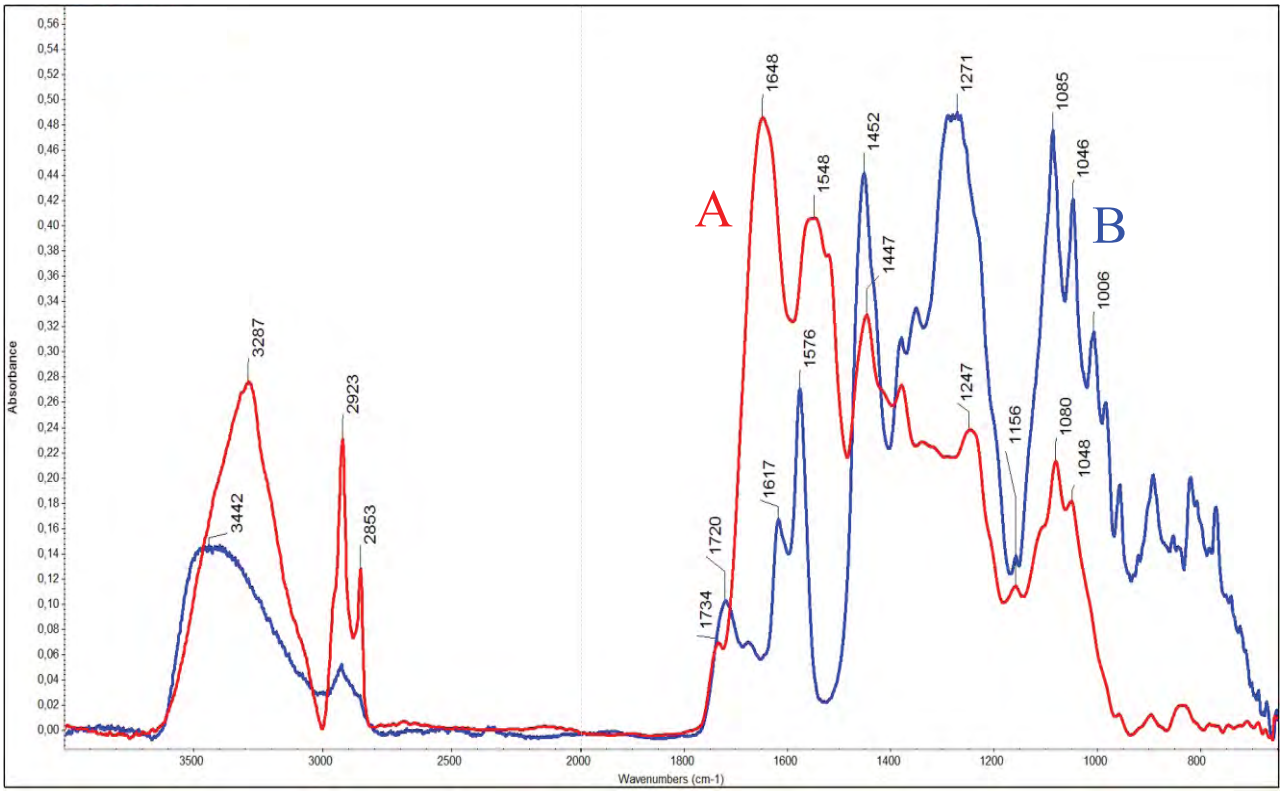

Fig. 5. Infrared spectrum of the cochinea (from *coccus* bodies) (A) and its main colouring compound carminic acid (B).

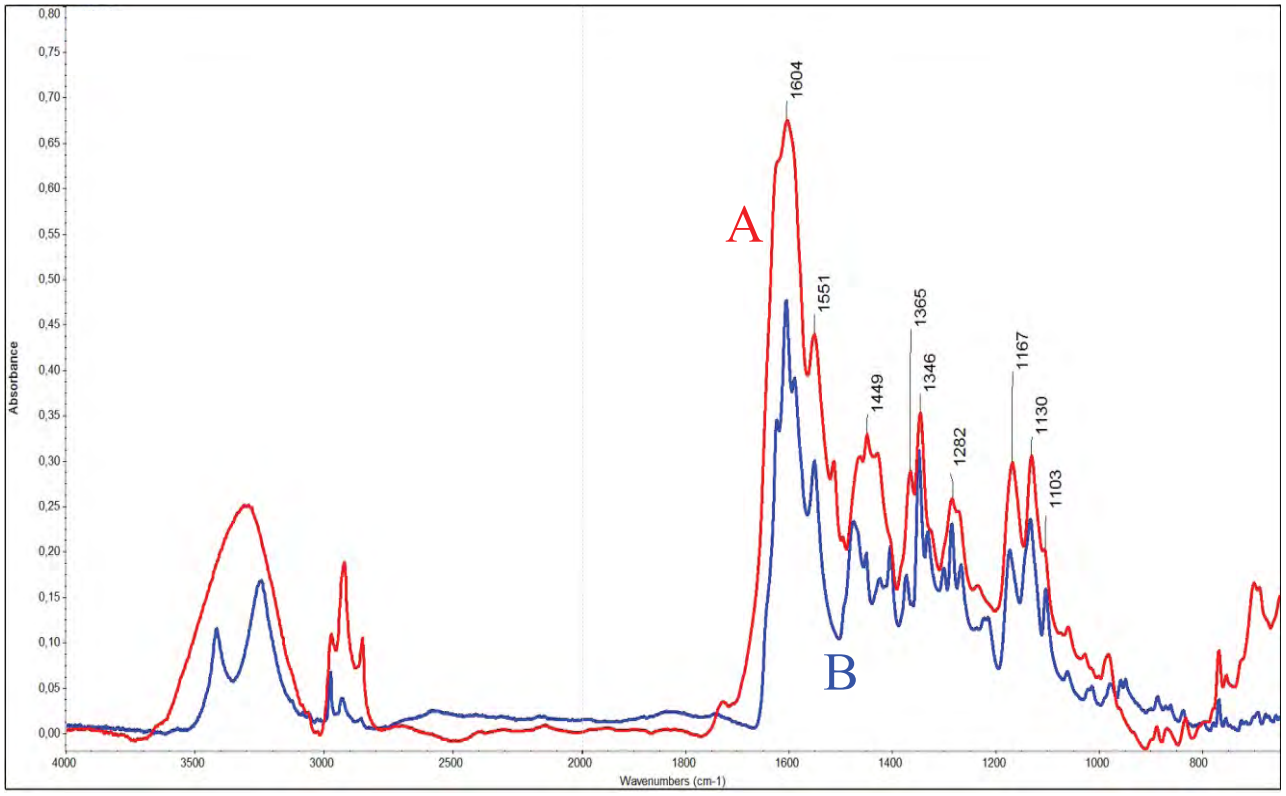

Fig. 6. Infrared spectrum of the dye kamala (A) and its main colouring compound rottlerin (B).

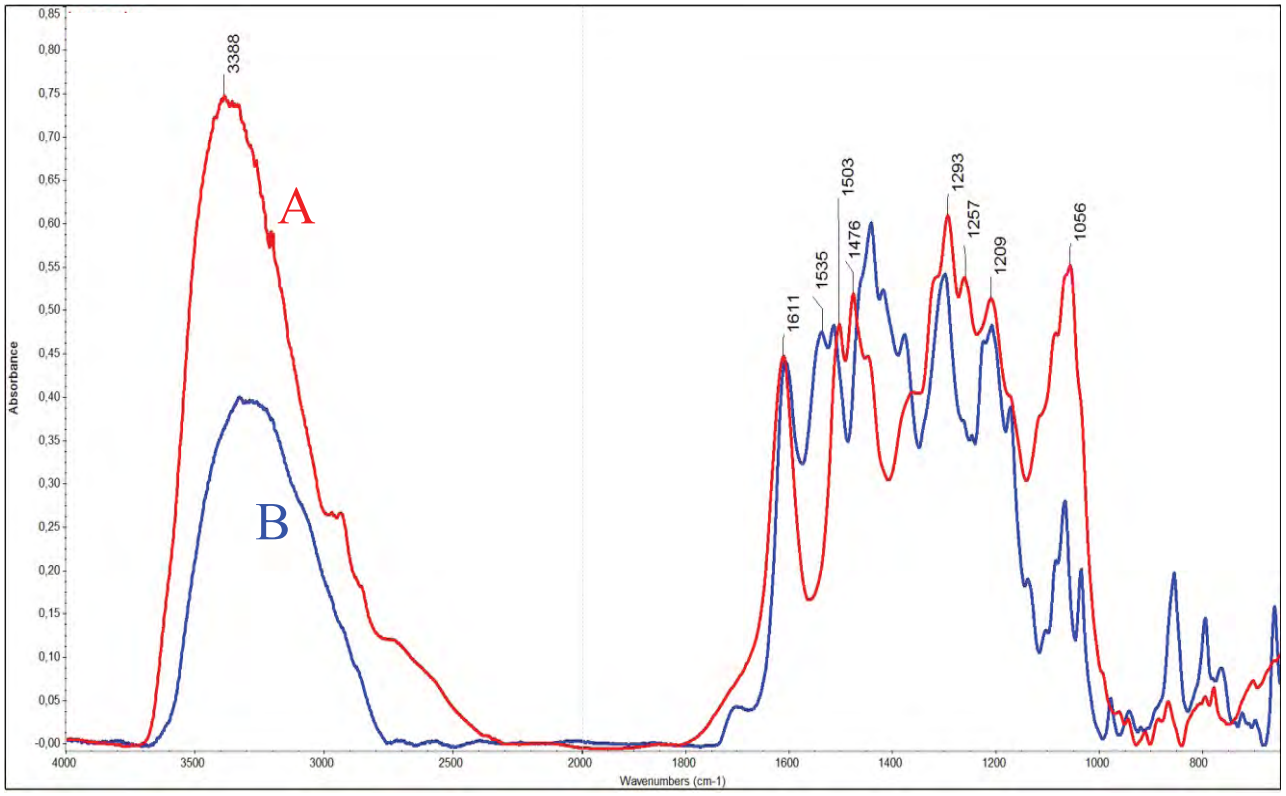

Fig. 7. Infrared spectrum of the dye logwood (A) and its main colouring compound haematein (B).

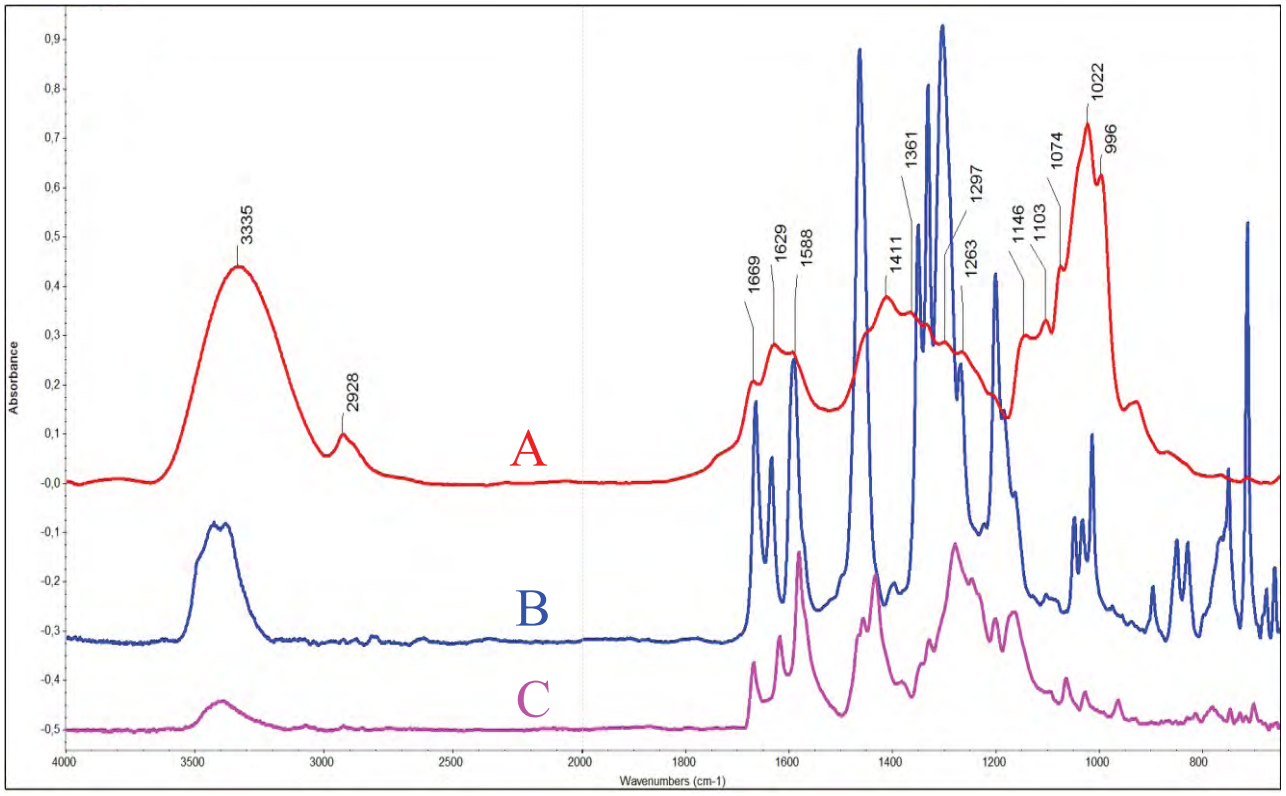

Fig. 8. Infrared spectrum of the dye kraplak (A) and its main colouring compounds alizarin (B) and purpurin (C).

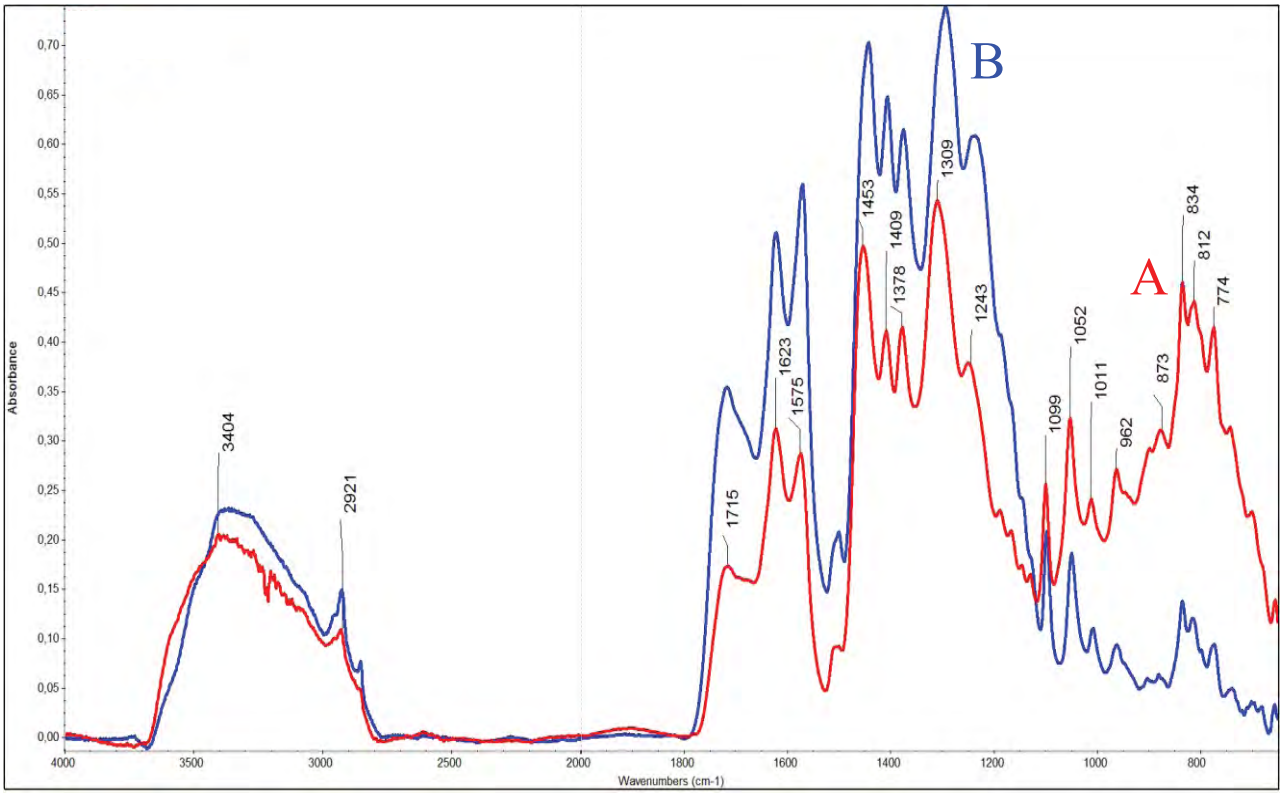

Fig. 9. Infrared spectrum of the dye lac (A) and its main colouring compound laccaic acid (B).

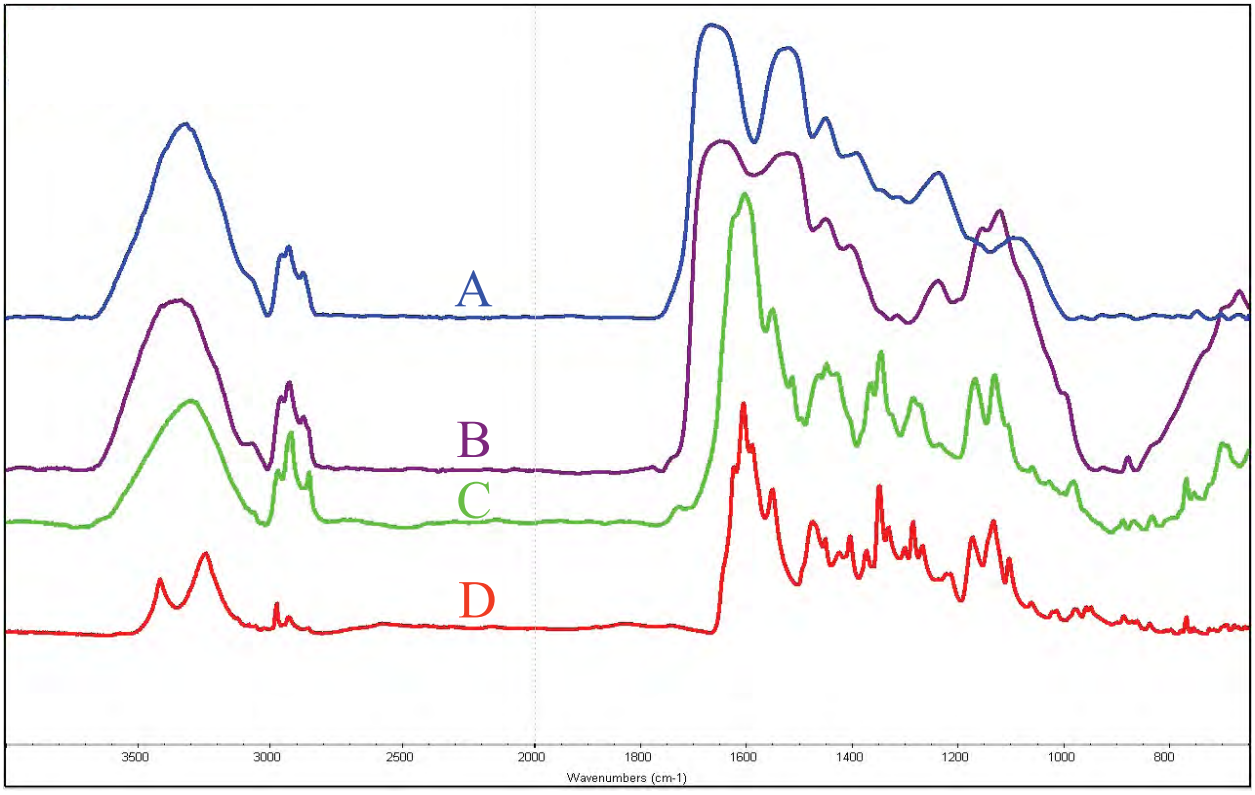

Fig. 10. Infrared spectra of (A) brown-state wool fibres mordanted by potassium aluminium sulphate and (B) the same mordated wool fibres dyed by kamala, (C) dye kamala and (D) its main colouring dyestuff rottlerin.

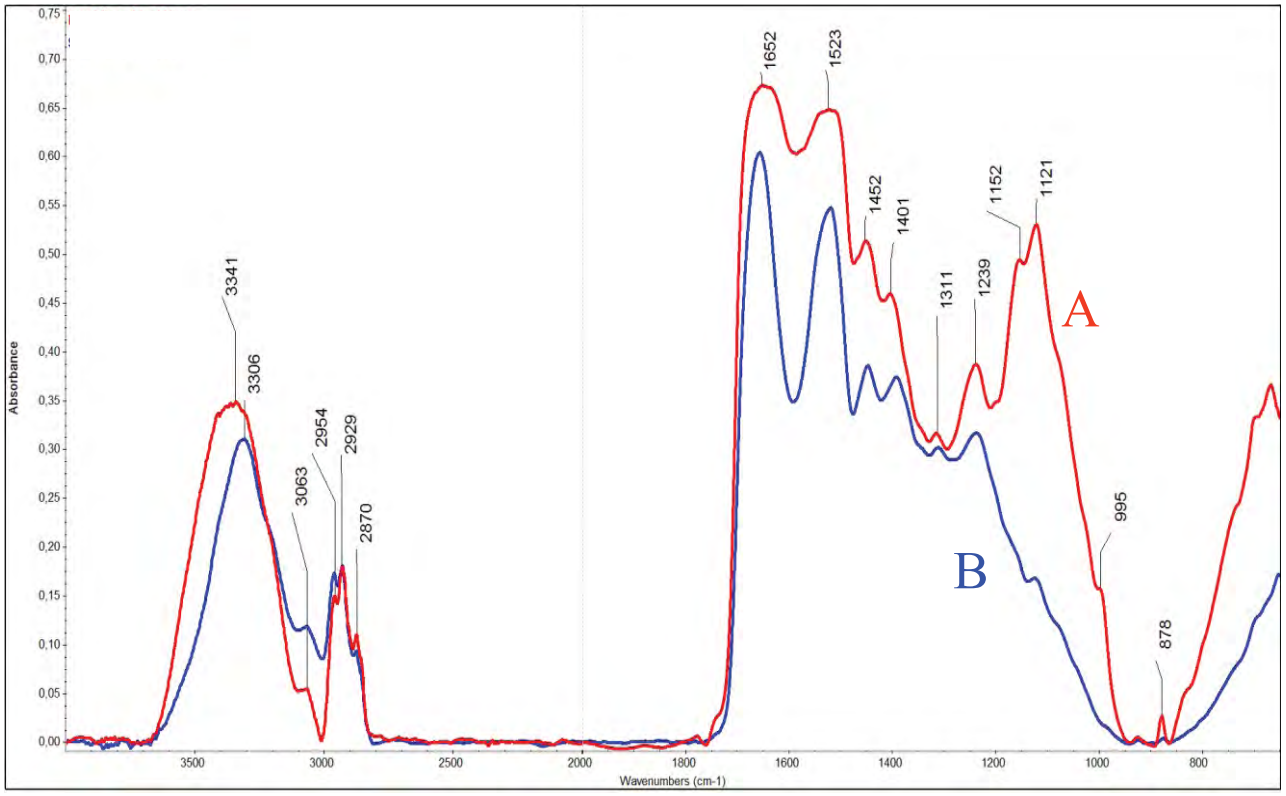

Fig. 11. Infrared spectra of wool fibres dyed by kamala (mordanted by potassium aluminium sulphate) before (A) and after (B) accelerated ageing.

New Capillary Monolithic Columns Designed for Separation of Phenolic Acids by HILIC

Veronika Škeříková, Romana Kubíčková, Jiří Urban, Marcela Pospíšilová, Pavel Jandera

Department of Analytical Chemistry, Faculty of Chemical Technology, University of Pardubice, Studentská 573, 532 10 Pardubice, Czech Republic, ✉ *Veronika.Skerikova@upce.cz*

Abstract

This work is considered to the preparation and testing of monolithic capillary columns designed for the separation of phenolic acids. The polymerization mixture with defined amount of [2-(methacryloyloxy)ethyl]-dimethyl-(3-sulfopropyl)-ammonium hydroxide (MEDSA) was used for the preparation of these columns. MEDSA contains Zwitterionic Sulfobetaine group in his molecular structure and stationary phases prepared by his polymerization are suitable for the separation of polar compounds by Hydrophilic Interaction Liquid Chromatography (HILIC). Ten monolithic columns for HILIC were prepared by radical copolymerization of MEDSA and ethylene dimethacrylate. Retention of phenol, toluene, uracil and thiourea in acetonitrile with water and of phenolic acids in acetonitril with aqueous 10 mM ammonium acetate was investigated. Experimentally obtained data were compared with mathematical model for dual RP-HILIC mechanism.

Keywords
capillary columns
HILIC
monolithic columns
phenolic acids
RP-HPLC
Zwitterionic Sulfobetaine group

1. Introduction

Hydrophilic Interaction Liquid Chromatography (HILIC) is known about 30 years, but the interest of this technique and the number of scientific publications increased in the 90th, when new stationary phases were developed for separation of polar compounds and it is useful technique for separation of strongly polar compounds that are poorly retained in the reversed-phase mode. HILIC is Normal-Phase Liquid Chromatography employing aqueous-organic mobile phases and polar stationary phases [1–9].

The mobile phase is similar to the polar mobile phases used in Reversed-Phase Liquid Chromatography, consisting of a polar organic solvent as acetonitrile or methanol with a low concentration of water (1–10%), which is very important for hydrophilic interaction mechanism. Water in mobile phase (1–2%) creates a thin diffuse layer between the stationary and mobile phase.

In reversed-phase systems with binary aqueous--organic mobile phases the retention decreases as the concentration of the organic solvent in the mobile phase increases, whereas in normal-phase non-aqueous chromatography the retention decreases with increasing concentration of the more polar of the organic solvents. The effects of the concentration, volume fraction φ, of organic solvent in a binary mobile phase on the retention factor, k, can be described by a semi-empirical Eq. (1) in reverse-phased system [10–12] and by a semi-empirical Eq. (2) in normal-phase system [12–14]:

$$\log k = \log k_0 - m_1 \varphi = a - m_1 \varphi \quad (1)$$

$$\log k = \log k_B - m_2 \log \varphi = a' - m_1 \log \varphi \quad (2)$$

In the presence of a dual HILIC-RP mechanism, Eq. (1) and Eq. (2) can be combined to describe the effects of the concentration of water $\varphi(H_2O)$ as the stronger elution solvent on the retention factors k over a broad composition range of aqueous-organic mobile phase:

$$\log k = a_1 + m_1 \varphi(H_2O) - m_2 \log \varphi(H_2O) \quad (3)$$

The parameter m_1 characterizes the effect of increasing concentration of water in the mobile phase on increasing contribution of RP mechanism to the retention, the parameter m_2 is a measure of decreasing HILIC contribution to the retention in highly organic mobile phases and a_1 is an empirical constant without special physical meaning. All these parameters can be determined by non-linear regression of the experimental retention factors measured at varying volume fractions of water in the mobile phase.

Jin *et al.* [15] showed that Eq. (3) is more suitable for accurate calculation of the HILIC retention than polynomial empirical equations. However, it should be noted that the Eq. (3) fails at very low concentrations of water, lower than 2% ($\varphi(H_2O) < 0.02$).

As a polar stationary phase, silica gel or silica modified with bonded amino-, amido-, cyano-, carbamate-, diol-, and polyol- ligands or recently

introduced zwitterionic sulfobetaine groups have been used. Polar stationary phases strongly adsorb water by hydrogen bonding and the bulk layer of water is creating (water-solvated stationary phase). Analytes are distributed between the mobile phase and water-solvated stationary phase on the base of partition mechanism. Due to potential interactions with polar functional groups and positive or negative charges of stationary phase, the retention of analytes may be also affected by adsorption and ion-exchange mechanism [16]. The retention increases with increasing polarity of compounds. The elution order of compounds is generally opposite to the retention in Reversed-Phase mode.

Zwitterionic columns (ZIC) are commercially available under the trade marks ZIC-HILIC (on silica gel support) and ZIC-pHILIC (on polymer support). Zwitterionic columns HILIC column was used for separation of small organic ionic and proteins and pH, salt concentration, and concentration ratio of acetonitrile to water was used to adjust the chromatographic selectivity suitable for particular separation problems [7]. The active layer grafted on wide-pore silica gel or polymer support contains both strongly acidic sulphonic acid groups and strongly basic quaternary ammonium groups separated by a short alkyl spacer.

Only few HILIC applications for polar compounds on capillary monolithic columns have been reported [17–21]. The reason for late introduction of organic--polymer monolithic phases in HILIC may be the lack of commercially available polar monomers for the preparation of polar organic-polymer monoliths and limited solubility of very polar monomers in most commonly used porogens, which requires polymerization in new porogen solvent mixtures with relatively high concentration of water [17–18].

Holdšvendová *et al.* [17] prepared capillary hydroxymethyl methacrylate-based monolithic columns for separation of mixed-sequence oligonucleotides in the HILIC mode using the gradient of acetonitrile in 100 mM aqueous triethylamine acetate and evaluated the influence of the steepness of the gradient on the separation of oligonucleotides.

A porous monolithic poly-(SPE-*co*-ethylene dimethacrylate) capillary column prepared by thermo-initiated *co*-polymerization of N,N-dimethyl-N-methacryloxyethyl-N-(3-sulfopropyl)ammonium betaine and ethylene dimethacrylate (EDMA) were prepared [18]. These capillary columns showed good selectivity for neutral, basic and acidic polar analytes in the HILIC mode.

Hence, the chromatographic properties of zwitterionic materials significantly differ from other HILIC phases.

2. Experimental

2.1. Materials

Ethylene dimethacrylate (EDMA), [2-(methacryloyloxy)ethyl]-dimethyl-(3-sulfopropyl)-ammonium hydroxide (MEDSA), 3-(trimethoxysilyl)propyl methacrylate, 1-propanol, and uracil were purchased from Sigma-Aldrich. 1,4-butanediol, hydrochloric acid, toluene, acetic acid, phenol and radical polymerization initiator azobisisobutyronitrile (AIBN) were obtained from Fluka. Thiourea was purchased from Lachema (Czech Republic). Gallic (GAL), protocatechuic (PRO), 4-hydroxybenzoic (PHB), 4-hydroxyphenylacetic (HPA), vanillic (VAN), ferulic (FER), syringic (SYR) and sinapic (SIN) acids were obtained from Fluka. Caffeic acid (CAF) was purchased from Sigma-Aldrich. The structures are shown in Table 1 (*see next page*).

A commercial ZIC-HILIC column, 5 µm, 4.6 × 150 mm with sulfobetaine stationary phase chemically bonded to silica gel support (SeQuant, Sweden) was used in conventional LC. Polyimide-coated 320 µm i.d. fused silica capillaries (J & W, Folsom, USA) were used to prepare monolithic polymethacrylate HILIC columns.

Acetonitrile for HPLC (LiChrosolv, gradient grade) was obtained from Merck, ammonium acetate (TraceSelect, 99.995%) from Fluka and formic acid (98%) from Riedel-de Haën. Distilled water was purified in a Demiwa 5ROI station (Watek, Czech Republic).

2.2. Capillary liquid chromatography

A modular micro liquid chromatograph was assembled from two LC10ADvp pumps (Shimadzu) with a high--pressure gradient controller; a micro valve injector with a 60 nL inner sampling loop (Valco, USA) controlled using a pneumatic actuator and an electronic time switcher for injection of sample volumes < 60 nL; a restrictor capillary inserted as a mobile phase flow splitter before the injector; a variable wavelength LCD 2083 UV-detector adapted for capillary chromatogrphy with a fused silica capillary flow-through cell, 50 µm i. d. (ECOM, Czech Republic), operated at 254 nm; and a personal computer with a chromatographic CSW Data Station for Windows, version 1.5 (Data Apex, Czech Republic). Fused silica capillary monolithic columns were fitted directly into the body of a micro valve injector on one side and connected to the detector on the other using a zero-volume fitting.

Table 1. Chemical structures of samples and components of polymerization mixture.

Compound	Short name	Structure
[2-(methacryloyloxy)ethyl]- -dimethyl-(3-sulfopropyl)- -ammonium hydroxide	MEDSA	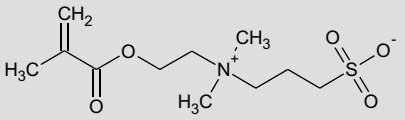
Ethylene dimethacrylate	EDMA	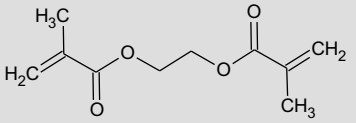
Azobisisobutyronitrile	AIBN	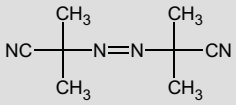
Sinapic acid	SIN	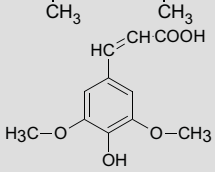
Ferulic acid	FER	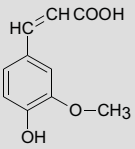
Syringic acid	SYR	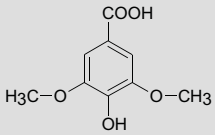
Vanilic acid	VAN	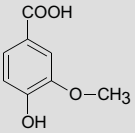
4-hydroxyphenylacetic acid	HPA	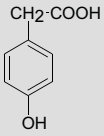
p-hydroxybenzoic acid	PHB	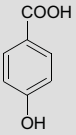
Caffeic acid	CAF	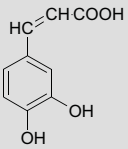
Protocatechuic acid	PRO	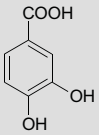
Gallic acid	GAL	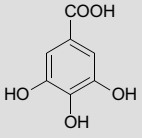

2.3. Conventional liquid chromatography

A modular liquid chromatograph used for the work with the conventional ZIC-HILIC column was assembled from a low-pressure gradient pump, LCP 4100, a manual sample valve injector with a 10 μL sampling loop, a column thermostat compartment LCO 101, operated at 40 °C, and a variable wavelength UV-detector, LCD 2084, set at 254 nm (all from ECOM, Czech Republic). The detector signal was processed via a personal computer with a chromatographic CSW Data Station for Windows, version 1.5 (Data Apex, Czech Republic).

2.4. "In-situ" preparation of capillary columns

Before polymerization, the inner wall surface of a polyimide-coated fused silica capillary was modified to improve the adhesion of the monolith bed to the capillary walls, as recommended by Lee *et al.* [30]: 320 μm i. d. capillaries were first rinsed with acetone and water, activated by flushing with a 0.2 M sodium hydroxide solution for 30 min at 0.25 μL min^{-1}, and subsequently washed with water, 0.2 M HCl for 30 min (0.25 μL min^{-1}), and finally with ethanol. A 20% solution of 3-(trimethoxysilyl)propyl methacrylate in 95% ethanol (pH adjusted to 5 with acetic acid) was then pumped through the capillary at 0.25 μL min^{-1} using a syringe pump (KD Scientific, USA) for 1 h. The modified capillary was washed with ethanol, dried with a stream of nitrogen, and kept at ambient temperature for 24 h before polymerization.

Monolithic stationary phases were prepared in silica capillaries by in-situ (*co*)polymerization of MEDSA and EDMA as the monomer and cross-linker in various porogen binary and ternary solvent mixtures, containing ethanol, 1-propanol, 1,4-butanediol and water (Table 2). 2,2′-azo-bis-isobutyronitrile (AIBN) was used as the initiator of the polymerization reaction and was added to all polymerization mixtures at a constant concentration (1% w/w, relative to the sum of monomers). As AIBN was the only component whose concentration was kept constant during preparation of various monolithic columns, the composition of the polymerization mixtures is given before the addition of AIBN throughout this work for the sake of simplicity.

The polymerization mixtures were pushed into fused-silica capillaries with modified internal walls using a micro-syringe. Both ends of the filled capillary were sealed with rubber stoppers and the capillary was placed in a circulated-air thermostat. The polymerization reaction was performed at 60 °C for 20 hours. Then, both ends of the capillary were cut and the monolithic column was washed with mobile phase.

2.5. Chromatographic methods

For isocratic separations of non-ionic compounds on capillary monolithic columns, mobile phases were prepared by mixing appropriate volumes of acetonitrile and water. For isocratic and gradient separations of phenolic acids, mixtures of acetonitrile and aqueous buffer containing 10 mM CH_3COONH_4 adjusted with formic acid to pH = 3 were used as the mobile phase. This buffer provided more stable gradient baseline and more reproducible retention times than acetate/acetic acid, or formate/formic acid buffers. In the HILIC mode, gradients were run with increasing concentrations of aqueous buffer (solvent B) in acetonitrile (solvent A), whereas in the RP mode the concentration of acetonitrile (in this case solvent B) increased in the buffer used as the solvent A. Before use, all mobile phases were filtered over a Millipore 0.45 μm filter and degassed by ultrasonication.

Sample solutions were prepared in the mobile phase at concentrations yielding adequate detector response. The column hold-up volumes were determined from the

Table 2. Composition of polymerization mixtures used for the preparation of capillary monolithic columns, % (w/w).

Column	% MEDSA	% EDMA	% BUT	% PROP	% H_2O	% ETOH
MON 1	15.05	19.09	–	–	17.11	48.75
MON 2	14.95	20.05	–	49.69	15.31	–
MON 3	14.99	19.99	16.79	41.46	6.77	–
MON 4	14.91	19.89	15.23	34.65	15.33	–
MON 5	14.98	19.96	10.04	39.72	15.30	–
MON 6	20.05	15.03	15.09	34.89	14.94	–
MON 7	17.42	17.66	14.91	35.04	14.97	–
MON 8	19.83	15.38	10.03	39.66	15.11	–
MON 9	19.99	14.95	19.98	30.10	14.97	–
MON 10	19.98	15.01	24.97	25.13	14.91	–

Table 3. Characteristics of the capillary monolithic columns, i. d. = 320 μm. Abbreviations: L – column length, V_M – hold-up volume measured with toluene in 98% acetonitrile (HILIC mode) and with uracil in 50% acetonitrile (RP mode), ε_T – total porosity in the HILIC and in the RP modes, K_F – permeability, N – number of theoretical plates for toluene (TO), uracil (UR), thiourea (TU), and phenol (PH).

Column	L, mm	V_M^{TO}, μL	V_M^{UR}, μL	ε_T^{TO}	ε_T^{UR}	K_F, 10^{10} cm^2	N, m^{-1} (95% ACN)			
		HILIC	RP	HILIC	RP		TO	UR	TU	PH
MON 1	197	11.80	10.94	0.745	0.690	15.70	658	90	1147	167
MON 2	198	12.58	12.00	0.790	0.754	6.66	1214	360	725	1106
MON 3	193	12.40	13.38	0.799	0.862	10.70	1104	460	1295	847
MON 4	185	11.84	11.76	0.796	0.790	10.10	940	837	2611	837
MON 5	201	13.55	13.02	0.838	0.806	8.70	1352	1317	1317	1417
MON 6	194	11.68	10.81	0.749	0.693	4.24	3585	981	3389	3252
MON 7	184	11.71	11.43	0.791	0.772	7.03	694	867	1346	753
MON 8	206	11.40	12.36	0.688	0.746	4.21	3173	1422	3658	3331
MON 9	125	7.45	7.67	0.741	0.763	3.36	3755	4248	11144	4289
MON 10	191	11.67	12.59	0.759	0.819	4.85	1505	2232	7031	1781

elution volumes of uracil as non-retained marker in the RP-mode (in 50% acetonitrile) and of toluene in HILIC-mode (in 98% acetonitrile), *see* Table 3.

In capillary HPLC, sample volumes of 60 nL or lower were injected and the flow-rate of the mobile phase was adjusted in the range between 3 and 25 μL min^{-1}. The actual flow rate was measured using a stop-watch and a calibrated 100 μL microburette, connected to the detector outlet. All separations were performed at ambient temperature.

The column hold-up volume of the ZIC-HILIC column (1.54 mL) was measured as the elution volume of toluene in 98% acetonitrile in the HILIC-mode. The flow-rate was set to 0.5 mL min^{-1} and the actual flow-rate was controlled using a stop-watch and a burette. All separations were run at 40 °C.

The retention times and the bandwidths at the half peak height were evaluated using the standard CSW data evaluation software (Data Apex, Czech Republic). All experiments were repeated in triplicate and the mean values of the retention data were used for column characterisation.

3. Results and discussion

The composition of the polymerization mixtures was varied to prepare monolithic columns with different porosities, efficiencies, selectivities and permeabilities (Table 3). Various polar porogen solvents as ethanol, 1-propanol, 1,4-butanediol and their mixtures with water were used for preparation of monolithic columns for HILIC with different chromato-graphic properties. Also, the ratio of monomer (MEDSA) to cross-linker (EDMA) was varied (Table 2). Therefore, the ratio of monomer mixture (monomer + cross-linker) to porogen solvent mixture was kept constant (35% to 65%).

Aqueous ethanol for column MON 1 and aqueous propanol for column MON 2 were used as binary porogen solvent mixture. Further, eight capillary monolithic columns with four different ratios of MEDSA to EDMA dissolved in ternary porogen solvent mixtures (varying proportion of 1,4-butanediol, 1-propanol and water) were prepared (columns MON 3–10). Even 6.8% of water is enough to prepare a homogenous polymerization mixture, which we used to prepare the column MON 3. For all other columns (MON 4–10), a higher concentration of water in the polymerization mixture (14.9–15.3%) were used.

Table 3 lists the dimension of the columns, their hold--up volumes, porosities and permeabilities, K_F, characterizing the hydrodynamic flow resistance [22]:

$$K_F = \frac{F_m \eta L}{\Delta P \pi r^2} \quad (4)$$

where F_m is the flow rate (mL min^{-1}), η is the mobile phase viscosity, P is the pressure drop across the column, L is the column length and r is the column inner radius (both in cm). The column hold-up volumes, V_M, were determined from the elution volumes of non-retained compounds (RP-mode: uracil in 50% ACN, HILIC--mode: toluene in 98% acetonitrile). The porosities of the columns were calculated from the column hold-up volumes and the geometrical volumes of the empty columns V_C

$$\varepsilon_T = V_M / V_C \quad (5)$$

The retention of four non-ionic compounds (toluene, uracil, thiourea and phenol) was measured on the capillary monolithic columns MON 1–10 in water rich (40–60%) and in highly organic (2–20% water) mobile phases. The experimental log k were plotted versus $\varphi(H_2O)$ for four monolithic columns (MON 4, MON 6, MON 7 and MON 10). The regression parameters a_1, m_1 and m_2 based on Eq. (3) and determined as the best-fit multiple non-linear regression parameters were calculated using statistical software ADSTAT (Trilobyte, Czech Republic). The minimum of the plot log k versus $\varphi(H_2O)$, the concentration of water, at which the HILIC--mechanism changes to the RP-mechanism, were calculated according

$$\varphi_{min} = m_2 / (2.301\, m_1) \quad (6)$$

The results show that the dual mechanism controls the retention of phenol on all prepared monolithic capillary columns. The columns MON 4 and MON 7 show retention minima of toluene in 91–93% acetonitrile. However, for the other monolithic columns, the dual mode equation, Eq. (3), is not suitable for the description of the retention of non-polar toluene. Because the reversed-phase mechanism controls the retention over the whole mobile phase composition range and the retention grows continuously at increasing concentration of water, Eq. (1) was used for calculation of parameters a and m.

The chromatograms in Fig. 1 and Fig. 2 illustrate changes in the separation selectivity and in the elution order of thiourea, uracil, phenol and toluene at changing concentration of acetonitrile in the mobile phase for the monolithic columns MON 6 and MON 10. In the mobile phases containing 40% or less acetonitrile, the analytes elute in the order of decreasing polarities, as usual in the reversed-phase mode (uracil < thiourea < phenol < < toluene). Thiourea is retained more strongly than uracil and the retention of the two compounds increases significantly with the increasing concentration of acetonitrile. In mobile phases containing more than 80–90% acetonitrile, toluene elutes before phenol and both compounds are very weakly retained on all monolithic columns. These results show that uracil and thiourea cannot be used as column hold-up volume markers in HILIC mode.

Retention behaviour of nine phenolic acids, which are difficult to separate by reversed-phase HPLC, was investigated on four monolithic capillary columns (MON 4, MON 6, MON 7 and MON 10). The main criteria for choosing of columns were high values of φ_{min} and parameter m_2 of Eq. (6), suggesting relatively high retention in HILIC mobile phases with high concentrations of acetonitrile. To suppress the retention of weak phenolic acids, aqueous buffer (10 mM CH_3COONH_4 adjusted with formic acid to pH = 3) was used instead of water in mixed aqueous-organic mobile phases.

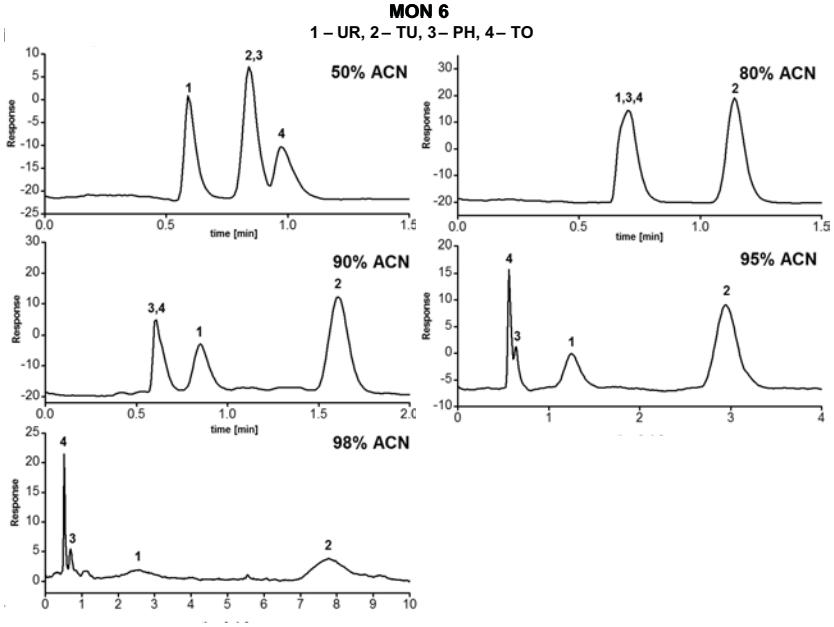

Fig. 1. Chromatograms of toluene (TO), uracil (UR), thiourea (TU) and phenol (PH) on the monolithic columns MON 6 in aqueous acetonitrile. Flow-rate: 18 μL min^{-1} (50% and 80% ACN), and 21 μL min^{-1} (90%, 95% and 98% ACN), UV-detection (λ = = 220 nm), laboratory temperature.

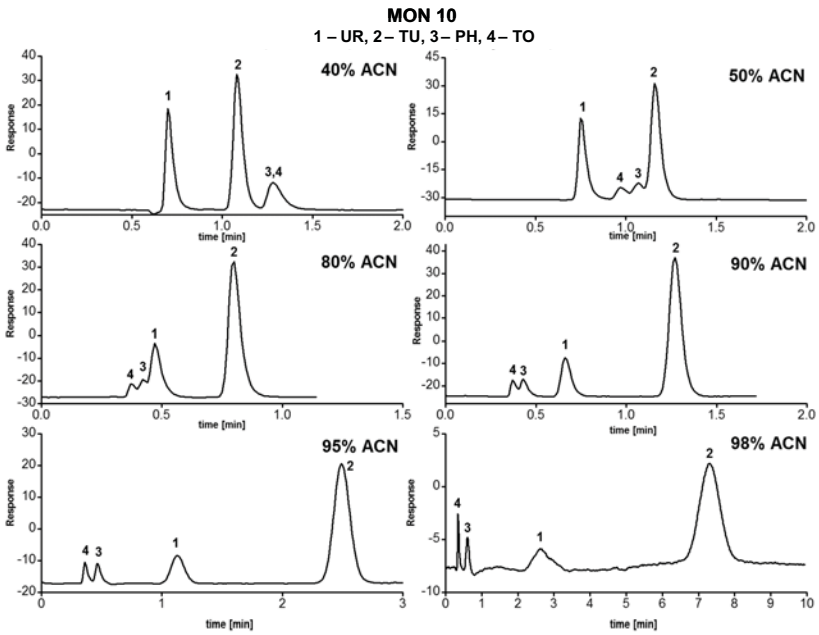

Fig. 2. Chromatograms of toluene (TO), uracil (UR), thiourea (TU) and phenol (PH) on the monolithic columns MON 10 in aqueous acetonitrile. Flow-rate: 17 μL min^{-1} (40%, 60% and 80% ACN), and 30 μL min^{-1} (90%, 95% and 98% ACN), UV-detection (λ = = 220 nm), laboratory temperature.

Retention data of nine phenolic acids on the four selected capillary columns were measured in mobile phases with various concentration of acetonitrile (2–90%). The plots of log *k* versus *φ*(buffer) show typical "U-turn" shape retention behaviour for all acids. The retention decrease with increasing concentration of buffer up to 20–30% in the mobile phase (HILIC-mode) and then increase with increasing buffer concentration (reversed-phase mode). The (U-turn) volume fractions of buffer, φ_{min}, (Eq. (6)) depend on the type of the acid and seems to increase with increasing number of phenolic groups, from ~0.2 for monohydroxy derivatives of cinnamic acid (sinapic and ferulic acids) to 0.32–0.34 for trihydroxybenzoic (gallic) acid, but are less affected by the type of the monolithic phase. The parameters a_1, m_1 and m_2 of Eq. (3) were calculated using non-linear regression. In the low range of buffer concentrations, the results may by affected by some experimental deviations. However, the model can be used to estimate the effects of the mobile phase on the retention in dual HILIC-RP mode.

Separations of phenolic acids on capillary monolithic columns were compared with separations on a commercial available conventional ZIC-HILIC column with sulfo-betaine stationary phase bonded on silica gel particles. Fig. 3 (*see next page*) shows the separation of mixtures of phenolic acids on the MON 10 capillary monolithic column in the HILIC mode using isocratic elution (95% acetonitrile) and gradient elution (97–80% acetonitrile in 20 min). The column shows sufficient selectivity for separation of six of the test acids, except couples: syringic / vanillic and hydroxy phenyl acetic / *p*-hydroxybenzoic acids. The ZIC-HILIC column shows good isocratic (96.5% acetonitrile) and gradient (100–90% acetonitrile in 15 min) separation (Fig. 4; *see next page*). The elution order of six acids is the same as using monolithic column, but better separation efficiency (especially for less retained compounds) was achieved. Further, lower efficiency of the monolithic columns can be attributed to the contribution of the extra-column band broadening, which is much more significant in the capillary than in the conventional column format. Anyway, the comparison shows that the approach described in this work can be used to prepare capillary columns with useful performance in HILIC mode.

We also compared the separation of the nine phenolic acids on the monolithic and commercial particulate HILIC columns in the reversed-phase mode. As expected, the elution order was significantly different in the RP mode. The retention is much higher on the monolithic column than on the ZIC-HILIC column. Pure aqueous buffer was used to accomplish the separation on ZIC-HILIC column shown in Fig. 5 (*see page 108*), with poor or no resolution of syringic, hydroxy phenylacetic, sinapic and vanillic acids. These four acids could be well resolved on the MON 10 column using gradient elution with increasing concentration of acetonitrile in the buffered aqueous-organic mobile phase. Contrary to the expected RP behaviour, the retention of caffeic and protocatechuic acids with two phenolic groups and gallic acid with three phenolic groups is higher than the

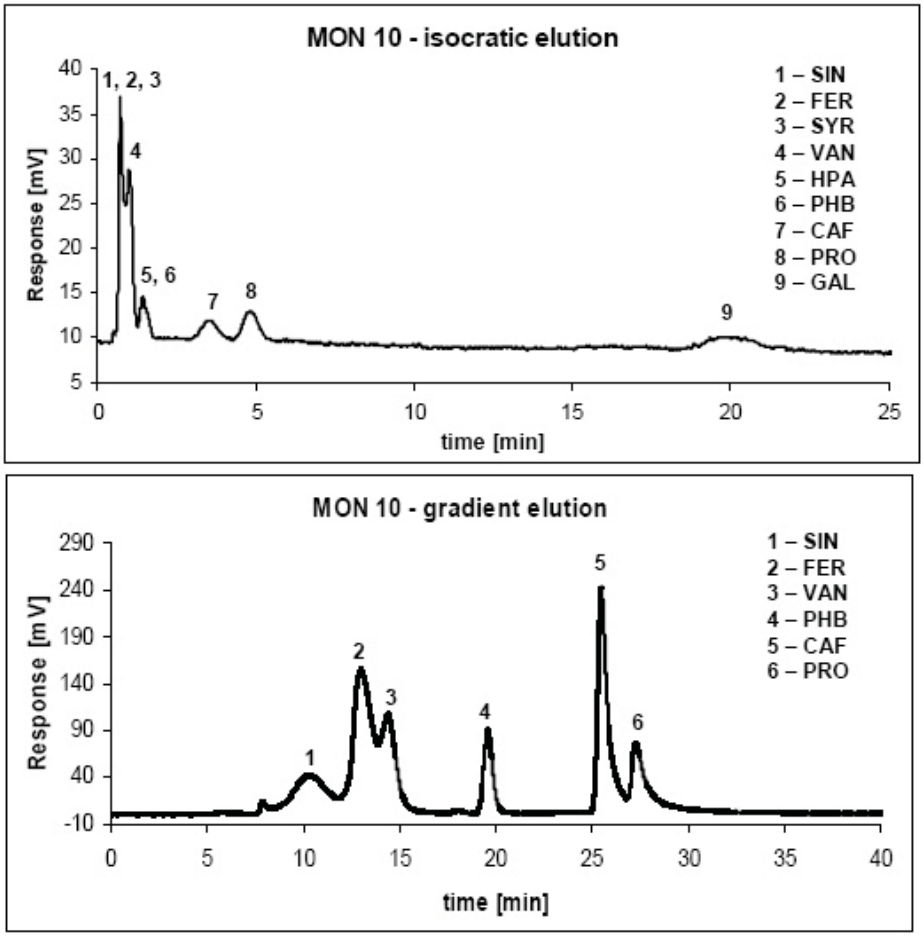

Fig. 3. Isocratic and gradient elution of phenolic acids using HILIC on monolithic column MON 10.

Isocratic elution: MF: 5% 10 mM ammonium acetate in water (pH ~ 3) + 95% acetonitrile, flow-rate: 18.5 μL min^{-1}, UV-detection: 220 nm, laboratory temperature.

Gradient elution: MF (A): 10 mM ammonium acetate in water (pH ~ 3), MF (B): acetonitrile. Gradient: 0–5 min: 3% MF (A), 5–10 min: 3–5% MF (A), 10–15 min: 5–10% MF (A), 15–20 min: 10–20% MF (A). Flow-rate: 3.0 μL min^{-1}, UV-detection: 280 nm, laboratory temperature.

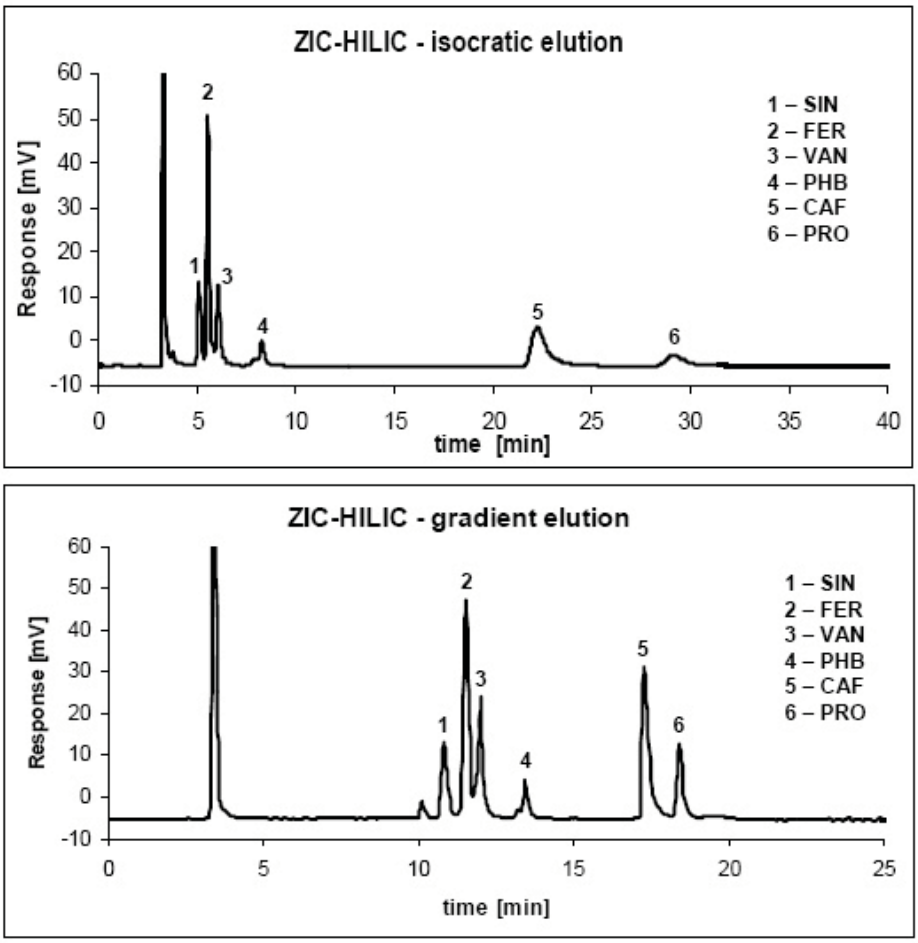

Fig. 4. Isocratic and gradient elution of phenolic acids using HILIC on convential column ZIC-HILIC.

Isocratic elution: MF: 3.5% water + 96.5% acetonitrile, flow-rate: 0.5 μL min^{-1}, UV-detection: 254 nm, 40 °C, injected volume: 10 μL.

Gradient elution: MF (A): water, MF (B): acetonitrile. Gradient: 0–15 min: 0–10% MF (A), 15–30 min: 10% MF (A). Flow-rate: 0.5 mL min^{-1}, UV-detection: 254 nm, 40 °C, injected volume: 10 μL.

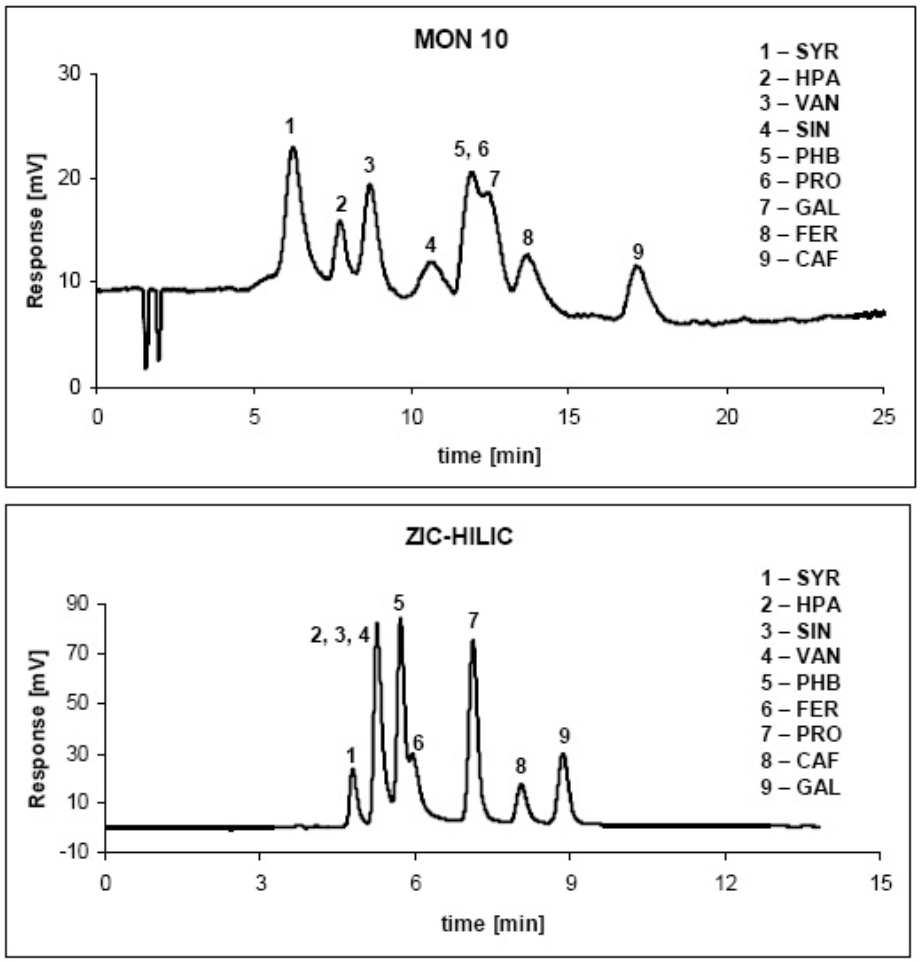

Fig. 5. Gradient elution of phenolic acids using RP-HPLC on monolithic column MON 10 (MF (A): 10 mM ammonium acetate in water (pH ~ 3), MF (B): acetonitrile. Gradient: 0–30 min: 15–40% MF (B), Flow-rate: 5.263 μL min^{-1}, UV-detection: 220 nm, laboratory temperature.

Isocratic elution of phenolic acids using RP-HPLC on convential column ZIC-HILIC (MF: 10 mM ammonium acetate in water (pH ~ 3). Flow-rate: 0.5 mL min^{-1}, UV-detection: 254 nm, 40 °C, injected volume: 10 μL.

retention of less polar phenolic acids with a single phenolic group on the two sulfobetaine columns (except for ferulic acid on the monolithic column). This retention behaviour probably indicates some effect of ion-exchange mechanism. The selectivity of the monolithic column for these acids differs from the ZIC-HILIC column, where the most polar gallic acid is more strongly retained. Hence, the monolithic sulfobetaine columns are more suitable to perform separation of polar compounds in both HILIC and RP modes in comparison to the ZIC-HILIC column, which shows rather limited performance in low-organic mobile phases, due to low retention. This could be attributed rather to ion-exchange than to RP mechanism.

4. Conclusions

Polymethacrylate monolithic capillary columns with zwitterionic sulfobetaine groups were prepared using binary or ternary porogen solvent mixtures containing water. Porosity, permeability, selectivity and retention characteristics of prepared columns depend on the composition of the polymerization mixture. The main factors affecting the selectivity of monolithic stationary phase are the concentration of MEDSA and the composition of the porogen solvents in the polymerization mixture. Uracil and thiourea show HILIC retention behaviour, their retention increased proportionally to the concentration of acetonitrile. Due to, these compounds cannot be used as the column hold-up time markers in HILIC mode. However, toluene in 98% acetonitrile is well suited for this purpose. The retention of phenol and phenolic acids on the monolithic columns shows dual RP-HILIC separation mechanism depending on the concentration of acetonitrile in the mobile phase. The monolithic sulfobetaine columns show similar separation selectivity for phenolic acids as the commercial column with sulfobetaine stationary phase chemically bonded on silica gel particles in the HILIC--mode at high concentrations of acetonitrile in the mobile phase, but show significantly higher retention and separation selectivity than the silica-based column in the reversed-phase mode in highly aqueous mobile phases.

Acknowledgements. *This work was supported by the Ministry of Education, Youth and Sports of the Czech Republic under the project MSM 0021627502 and by the Grant Agency of Czech Republic under the project No. 203/07/0641.*

References

[1] Alpert A.J.: *J. Chromatogr.* **499** (1990), 177–196.

[2] El Rassi, Z.: Reversed phase and hydrophobic interaction chromatography of carbohydrates and glycoconjugates. *In: Carbohydrate Analysis: High Performance Liquid Chromatography and Capillary Electrophoresis.* El Rassi Z. (edits.). Amsterdam, Elsevier 1995, p. 41–102.

[3] Yoshida T.: *Anal. Chem.* **69** (1997), 3038–3043.

[4] Zhu B.-Y., Mant C.T., Hodges R.S.: *J. Chromatogr.* **548** (1991), 13–24.

[5] Hemström P., Irgum K.: *J. Sep. Sci.* **29** (2006), 1784–1821.

[6] Jandera P.: *J. Sep. Sci.* **31** (2008), 1421–1437.

[7] Jiang W., Irgum K.: *Anal. Chem.* **71** (1999), 333–344.

[8] Ikegami T., Horie K., Saad N., Hosoya K., Fiehn O., Tanaka N.: *Anal. Bioanal. Chem.* **391** (2008), 253–32542.

[9] Núñez O., Nakanishi K., Tanaka N.: *J. Chromatogr. A* **1191** (2008), 231–252.

[10] Snyder L.R., Dolan J.W., Gant J.R.: *J. Chromatogr.* **165** (1979), 3–30.

[11] Jandera P., Churáček J., Svoboda L.: *J. Chromatogr.* **174** (1979), 35–50.

[12] Jandera P., Churáček J.: *J. Chromatogr.* **91** (1974), 207–221.

[13] Snyder L.R.: *Anal. Chem.* **46** (1974), 1384–1393.

[14] Snyder L.R., Poppe H.: *J. Chromatogr.* **184** (1980), 363–413.

[15] Jin G., Guo Z., Zhang F., Xue X., Jin Y., Liang X.: *Talanta* **76** (2008), 522–527.

[16] Guo Y., Gaiki S.: *J. Chromatogr. A* **1074** (2005), 71–80.

[17] Holdšvendová P., Suchánková J., Bunček M., Bačkovská V., Coufal P.: *J. Biochem. Bioph. Methods* **70** (2007), 23– 29.

[18] Jiang Z., Smith N.W., Ferguson P.D., Tailor M.R.: *Anal. Chem.* **79** (2007), 1243–1250.

[19] Smith N.W., Jiang Z.: *J. Chromatogr. A* **1184** (2008), 416–440.

[20] Lin J., Wu X., Lin X., Xie Z.: *J. Chromatogr. A* **1169** (2007), 220–227.

[21] Wang Z., Lü H., Lin X., Xie Z.: *J. Chromatogr. A* **1190** (2008), 365–371.

[22] Carman P.: *Flow of Gases Through Porous Media.* London, Butterworth 1956.

Utilization of Calix[4]arenes for the Preparation of Electrochemical Biosensors

Barbora Šustrová[a, b], Vladimír Mareček[b], Karel Štulík[a]

[a] *Department of Analytical Chemistry, Faculty of Science, Charles University in Prague, Albertov 6, 128 43 Prague 2, Czech Republic*
[b] *J. Heyrovský Institute of Physical Chemistry, v.v.i., Academy of Sciences of the Czech Republic, Dolejškova 3, 182 23 Prague 8, Czech Republic,* ✉ *barbora.sustrova@jh-inst.cas.cz*

Abstract

Electrochemical measuring techniques belong among the most important methods used to study biological membrane processes. The present work deals with the development of an electrochemical biosensor, operating on the principle of a specific complex reaction between the ligand and the ions studied. The ligand is covalently bonded, through a sulfur atom, to the surface of a gold electrode.

The modified calix[4]arene molecule, with four sulfur-containing groups located at the lower rim, is used as the ligand. The calix[4]arene molecules form a self-assembled monolayer (SAM) at the electrode surface and specifically modify it. The electrode properties are thus altered and the interactions of the ions studied with the modifying monolayer can be monitored primarily through changes in the electrode potential and in the capacitance of the electric double-layer.

Preliminary electrochemical measurements by cyclic voltammetry determined the potential window of the modified electrode, from –0.5 V to –1.1 V in an ethanol-aqueous solution of 0.1 M NaOH. It seems that calix[4]arenes are more easily adsorbed from chloroform solutions, without applying any potential to the electrode, but this assumption has not yet been verified. To describe the SAM structure, further measuring techniques, such as electron microscopy, must be used. Electrochemical impedance spectroscopic measurements have demonstrated that the SAM-covered electrode has an impedance different from that of the bare electrode. This method will be used to study the conditions of ion transport and the modified electrode selectivity toward various ions.

Keywords
calix[4]arenes
cyclic voltammetry
electrochemical impedance spectroscopy
gold electrode
ion transport
self-assembled monolayers

1. Introduction

Artificial models of biological membrane systems are necessary to understand, explain and simulate mechanisms of transport processes occurring at the cells of living organisms (plants, animals and humans).

Phospholipid bilayers are composed of two amphiphilic layers of lipids, which are oriented by their nonpolar tails into a two-layered sheet (a bilayer), whereas the hydrophilic heads stay oriented into either extracellular, or intracellular aqueous solutions. The phospholipid bilayer centre contains almost no water and this fact also prevents larger and polar molecules from being transported across it.

The transport of charged or uncharged particles across the phospholipid bilayers can be realized in various ways: by passive diffusion processes or by facilitated motion, through ion channels, by ion pumps, by endocytose or exocytose, *etc.* To facilitate the transport, a chemical compound (an ionophore) can bind the ion to be transported, shield its charge from the surrounding environment and thus permit its crossing of the hydrophobic interior of the phospholipid bilayer. The ion transport processes play a very important role in living cells. Therefore, it is very desirable to study and to understand the principles and parameters of the transporting processes. Many of these properties have been studied with the use of artificial "model" monolayers produced in a lab.

The utilization of electrochemical methods, *e. g.*, cyclic voltammetry (CV), or electrochemical impedance spectroscopy (EIS), as a tool for observation of transport processes seems to be very advantageous, easy, fast and relatively cheap [1–3], in comparison with other techniques.

In the centre of our interest is the complexation reaction, through which the transported molecule is bound to the ligand modifying the surface of a gold electrode. As the specific ligand, we use synthetic organic macrocyclic compounds, calix[4]arenes. The molecule of a bare calix[4]arene consists of a central annulus, a wider hydrophobic upper rim and a narrower hydrophilic lower rim with four OH groups, creating the hydrophobic cavity [4]. Calix[4]arenes can adopt four different conformations, namely, a cone, partial cone, 1,2-alternate and 1,3-alternate. The bare molecule is

most stable in the cone conformation, but this does not hold for calix[4]arene derivatives, where some other conformations are more frequent [5] and the type of conformation depends on the substitution in the upper, lower or both of the rims. The conformation of the ligand molecule is very important in the complexation studies, because different stable conformers of calix[4]arenes have different capabilities for recognition of ions and molecules [6].

In our work, the calix[4]arenes used have all the four OH groups substituted by the thiol groups and through them the molecule is covalently bonded to the surface of a gold electrode. This method of electrode modification is based on the formation of a self-assembled monolayer (SAM) of calix[4]arene molecules, resulting in a change of the electrode properties.

For utilization of a new modified electrode in practical measurements, it is necessary to describe in detail and explain the electrode behaviour and its properties during the measurement. To characterize the modified electrode, we use electrochemical techniques, cyclic voltammetry (CV) and electrochemical impedance spectroscopy (EIS), and in the future we would like to employ other physico-chemical methods, such as electron microscopy, to describe the structure of the SAM of bonded calix[4]arenes.

2. Experimental

The properties of the modified gold disk electrode (1 mm in diameter) were determined using cyclic voltammetry and electrochemical impedance spectroscopy, in the base electrolyte of 0.1 M NaOH dissolved in a 1:1 mixture of ethanol and water. The reference electrode was the saturated calomel electrode. The measurements were performed using an Electrochemical Workstation CHI660C (IJ Cambria Scientific, UK). The conditions of the EIS measurements: A sine-wave signal with 5 mV perturbation was applied within the $0.01–1\times10^5$ Hz frequency range. The obtained data were analyzed using a CHI660 software.

The SAM of substituted calix[4]arenes on the electrode was prepared: *i)* without any applied potential, by placing a cleaned, activated electrode into a solution of calix[4]arenes (5 mM in DMF or 5 mM in chloroform) for 20 min, or *ii)* by electrochemical deposition on a cleaned, activated electrode at an applied potential of –0.5 V for 5 min.

The gold electrode was mechanically polished with suspensions of 1.00 μm and then 0.05 μm alumina particles and electrochemically activated by applied potential cycling in 0.1 M H_2SO_4 within an interval from +1.4 to –0.4 V (0.5 V s^{-1} scan rate), prior to each measurement.

3. Results and discussion

The potential window of the modified electrode in the base electrolyte was determined first using cyclic voltammetry. Close to –0.5 V, calix[4]arenes are oxidized on the surface of a gold electrode, the reduction peak of the adsorbed calix[4]arenes is close to –1.15 V. The potential window of the electrode in 0.1 M NaOH is from –0.5 V to –1.1 V.

The dependence of the calix[4]arene reduction peak area on the bulk concentration of the compound in the base electrolyte was determined, obtaining the Langmuir adsorption isotherm given in Fig. 1. It can be seen that the dependence corresponds to a Langmuir isotherm equation.

The area on the gold electrode surface, covered by a single calix[4]arene molecule on completion of the self-assembling process was calculated from the charge on the electrode. The areas obtained for potential--controlled deposition and for adsorption in the absence of applied potential are given in Table 1.

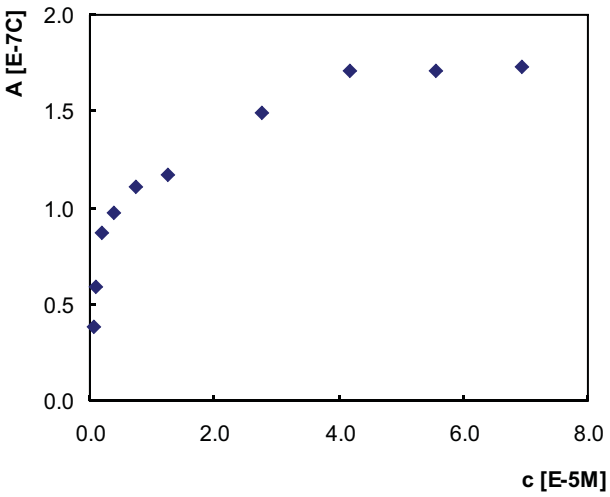

Fig. 1. Langmuir adsorption isotherm of calix[4]arenes electrochemically deposited on the gold electrode. Adsorption: $E = –0.5$ V; t = 300 s; base electrolyte: 0.1 M NaOH in a 1:1 ethanol-water solution, measured over two orders of calix[4]arene concentration (10^{-7} to 10^{-5} M).

Table 1. The electrode surface areas covered by a single calix[4]arene molecule obtained for electrochemically controlled deposition and for adsorption in the absence of applied potential from two different solutions (DMF – dimethylformamide).

	Solution	Surface covered by a single molecule [nm^2]
Electrochemical adsorption	DMF	0.342
Adsorption in the absence of potential applied	DMF	0.505
	Chloroform	0.647

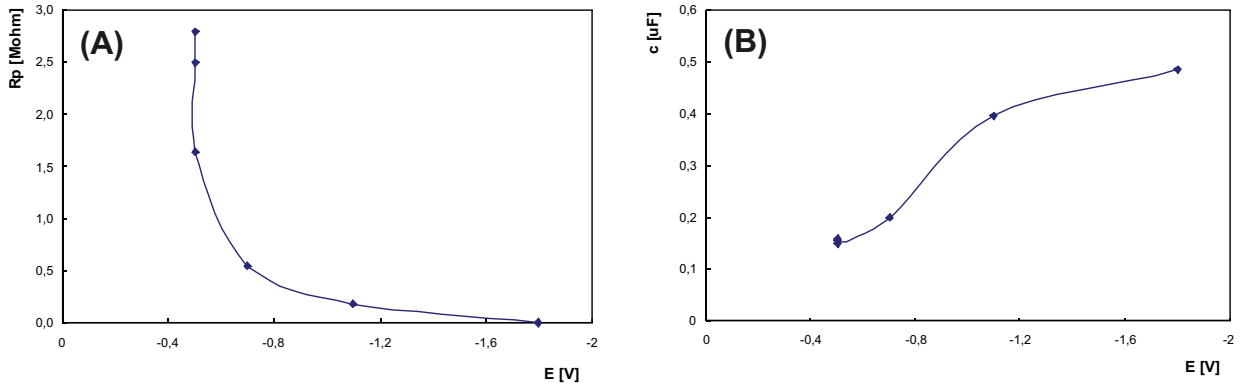

Fig. 2. Changes in (A) resistance and (B) capacitance of a modified electrode depending on the electrode potential.

Table 1 demonstrates that the adsorption conditions influence the resultant self-assembled layer. The area occupied by a single molecule after adsorption without any applied potential was greater for adsorption from chloroform than that for adsorption from DMF. Under an applied potential, the area occupied was smallest. The reason for this may be either a different kind of bonding of the molecule to the electrode surface, or the formation of a multilayer in the case of the smallest area occupied. In the future, we would like to employ electron microscopy to describe the structure and bonding of the SAM of adsorbed calix[4]arenes in a greater detail.

In the second step, EIS measurements were used to determine the changes in the capacitance of the modified electrode during the adsorption process. From preliminary measurements it can be concluded that the calix[4]arene SAM changes the electrode impedance, compared to the bare electrode (Fig 2).

The electrode resistance (Fig 2A) was highest at the adsorption potential, –0.5 V, around 3.0 MΩ, the capacitance (Fig 2B) was, on the contrary, the lowest, 0.15 μF. At a potential of –1.8 V, the results were opposite. The resistance rapidly decreased, the capacitance increased to 0.50 μF and the results became identical with those for a bare electrode. Consequently, at a potential of -1.8 V, the SAM of calix[4]arenes desorbs from the electrode surface.

4. Conclusions

The above preliminary experiments suggest that calix[4]arenes should be suitable for modification of gold electrode surfaces in the study of ion-to-ligand interactions underlying biological membrane processes. Further study is now required to provide a better understanding of these complex systems in developing practically useful sensors.

Acknowledgements. *The authors gratefully acknowledge the financial support from the Grant Agency of the Academy of Sciences of the Czech Republic (Project No. IAA400400806), and from the Ministry of Education, Youth and Sports of the Czech Republic, project No. MSM0021620857.*

References

[1] Becucci L., Innocenti M., Salvietti E., Rindi A., Pasquini I., Vassalli M., Foresti M. L., Guidelli R.: *Electrochim. Acta* **53** (2008), 6372–6379.
[2] Janchenova H., Stulik K., Maeda K., Marecek V.: *J. Electroanal. Chem.* **632** (2009), 55–58.
[3] Koryta J., Brezina M., Hofmanova A., Homolka D., Hung L. Q., Khalil W., Marecek V., Samec Z., Sen S. K., Vanysek P., Weber J.: *Bioelectrochem. Bioenerg.* **7** (1980), 61–68.
[4] Chawla H. M., Singh S. P., Sahu S. N., Upreti S.: *Tetrahedron* **62** (2006), 7854–7865.
[5] Hong J., Ham S.: *Tetrahedron Lett.* **49** (2008), 2393–2396.
[6] Halouani H., Dumazet-Bonnamour I., Duchamp C., Bavoux C., Ehlinger N., Perrin M., Lamartine R.: *Eur. J. Org. Chem.* (2002), 4202–4210.

Detailed Study of Free Molecular Radicals $FCO_2^•$ and $FSO_3^•$

Juraj Varga[a], Lucie Kolesniková[a], Lucie Nová Stříteská[a], Helmut Beckers[b], Patrik Kania[a], Helge Willner[b], Pavel Veis[c], Štěpán Urban[a]

[a] *Institute of Chemical Technology, Department of Analytical Chemistry, Technická 5, 166 28 Prague 6, Czech Republic,* ✉ *juraj.varga@vscht.cz*
[b] *Bergische Universität Wuppertal, FB 9, Anorganische Chemie, Gaußstr. 20, 42097 Wuppertal, Germany*
[c] *Comenius University, Faculty of Mathematics, Physics and Informatics, Department of Experimental Physics, Mlynská dolina, F2, 84248 Bratislava, Slovakia*

Abstract

Rotational spectra of fluoroformyloxyl ($FCO_2^•$) and fluorosulfate ($FSO_3^•$) molecular free radicals in their vibronic ground state were measured in the millimeter wave region using the Prague microwave high resolution spectrometer. The measured data were analyzed using matrix elements of rotational, centrifugal distortion, fine and hyperfine terms of the corresponding effective Hamiltonians. More than 160 new hyperfine components of rotational transitions of the $FCO_2^•$ radical were observed. These new transition frequencies were analyzed together with previously measured ones and a set of precise values of rotational, centrifugal distortion, magnetic hyperfine and fine parameters were derived. The microwave spectra of the $FSO_3^•$ free radical were measured, identified and analyzed for the first time. More then 250 rotational transitions with resolved fine structures were unambiguously assigned. The corresponding set of precise rotational, centrifugal distortion and fine structures parameters was derived and the molecular symmetry of the vibronic ground state was definitely confirmed to be C_{3v}. In addition to those, a measurable A_1–A_2 splitting of the $K = 3$ levels in the fluorosulfate radical rotational spectra was observed.

Keywords
fine and hyperfine structure
free radicals
microwave spectroscopy
rotational spectra
Zeeman effect

1. Introduction

Molecular free radicals are transient molecular species that have a short lifetime in the gaseous phase under ordinary laboratory conditions. The free molecular radicals are usually very reactive. According to the quantum chemistry, the molecular radicals have one or more unpaired electrons and thus such molecular species has a nonzero electron spin.

A participation of the free radicals in atmospheric processes, combustion products, and photochemical processes as well as in an interstellar chemistry is well known. The radicals frequently constitute important intermediates in many chemical reactions and detailed knowledge of their spectroscopic properties is crucial for the atmospheric and combustion chemistry since molecular microwave spectra are an adequate tool for the chemical analysis and monitoring of the radical species. Besides this, the microwave data are also extremely useful to derive precise molecular parameters such as rotational constants, centrifugal distortion and "fine and hyperfine structure" parameters.

Both the $FCO_2^•$ and $FSO_3^•$ radicals are of an atmospherical interest. The $FCO_2^•$ radical may be produced by stratospheric degradations of HCFCs and HFCs [1, 2] and $FSO_3^•$ radical is, in principle, considered as a trace atmospheric pollutant. It can act as a strong oxidizer and fluorinating agent [3, 4] and its presence in interstellar medium is also probable. Both the radicals contain one unpaired electron that causes, above all, the fine splitting of the rotational levels into two sublevels. Beside this, there are hyperfine interactions due to ^{19}F nucleus that make possible an additional hyperfine doubling of rotational levels.

Francisco *et al.* [5, 6] made first theoretical consideration of existence of fluoroformyloxyl radical $FCO_2^•$. In 1993 Maricq *et al.* [7] recorded an absorption spectrum in the visible region with the origin at 760 nm which was assigned as the $B^2A_1 \leftarrow X^2B_2$ transition of the $FCO_2^•$ radical. Following measurements of the photoelectron spectra of the anion FCO_2^- [8] and infrared spectra of the matrix isolated $FCO_2^•$ [9] led to confirmation of this assignment and all six fundamental vibrational states on the basis of C_{2v} symmetry were assigned.

First report of the absorption spectrum of equilibrium mixtures of $F_2S_2O_6 \leftrightarrow FSO_3^•$ in the range of 200–800 nm was made by Castellano *et al.* [10]. More systematic spectroscopic studies of this radical were published by

King *et al.* [11–13]. They identified three absorption systems: two in near infrared region and one stronger in visible region and the assignments were made by assuming C_{3v} symmetry. The first millimeter wave high resolution spectra were performed by Kolesnikova *et al.* [14] and this study confirmed the C_{3v} symmetry.

2. Energy levels and Hamiltonian matrix elements

Both the radicals are open-shell molecular species with one unpaired electron. The nonzero total electronic angular momentum causes a fine splitting of rotational levels (electron spin-rotational interaction). Further hyperfine splitting of the J into the F levels results, likewise, from two possible orientations of the fluorine nuclear spin angular momentum ($m_F = ½$ or $–½$), and the mutual magnetic interaction of the electron and nuclear spins (dipolar and Fermi contact terms). An additional contribution to the fluorine hyperfine splittings is due to the nuclear spin-rotational interaction.

The coupling scheme, $\boldsymbol{J} = \boldsymbol{N} + \boldsymbol{S}$ and $\boldsymbol{F} = \boldsymbol{J} + \boldsymbol{I_F}$, of the rotational $\boldsymbol{N}$, electron spin $\boldsymbol{S}$ and ^{19}F nuclear spin $\boldsymbol{I}_F$ angular momentum is used in this analysis. Since the spin quantum number of the unpaired electron is $S = ½$, all the rotational levels except the $N = 0$ level, are split into doublets (fine structure) with J quantum numbers $J = N + ½$ and $J = N – ½$ and each of these levels is further split into two sublevels (hyperfine structure) with F quantum numbers $F = J + ½$ and $F = J – ½$ due to the two ^{19}F nuclear spin orientations ($m_F = \pm ½$). As a result all the rotational levels (except $N = 0$) are split into quadruplets.

The radical $FCO_2^{\bullet}$ is an oblate asymmetric rotor ($\kappa = +0.45$) with a C_{2v} molecular symmetry that indicates the two identical oxygen nuclei. Since the ^{16}O nucleus is a boson ($I_O = 0$), the total internal wave functions of the molecule must be symmetric with respect to the oxygen nuclei permutation to comply with the Pauli principle. Since the ground vibronic wavefunction is of B_2 symmetry and the nuclear spin wavefunction of the two bosons is always totally symmetric, only the rotational states of B_1 or B_2 symmetries (odd K_a) are allowed in the vibronic ground state and the rotational levels (rovibronic states) with the even K_a are excluded by the Pauli principle. Only rotational states with the odd K_a are allowed.

The radical $FSO_3^{\bullet}$ is a symmetric rotor with a C_{3v} molecular symmetry that indicates the three identical nuclei. Due to the Pauli principle, the total internal wave functions of the molecule must be again symmetric with respect to the oxygen nuclei permutation. Since the ground vibronic wavefunction is of A_2 symmetry and the nuclear spin wavefunction of the two bosons is always totally symmetric, only the rotational states with $K = 0, 3, 6$ *etc.* with the A_1 or A_2 symmetries are allowed in the vibronic ground state. The rotational states with $K = 1, 2, \ldots$ *etc.* are forbidden.

A standard rotational Hamiltonian for an open-shell asymmetric top molecule can be written:

$$\mathbf{H} = \mathbf{H}_{rot} + \mathbf{H}_{fs} + \mathbf{H}_{hfs} \qquad (1)$$

where $\mathbf{H}_{rot}$ is an A – reduced or symmetric top rotational Hamiltonian for the $FCO_2^{\bullet}$ or $FSO_3^{\bullet}$ radical, respectively. Both the Hamiltonians are described in the excelent Watson paper [15] together with corresponding matrix elements. The fine structure Hamiltonian $\mathbf{H}_{fs}$ and its matrix elements are discussed in the Brown and Sears paper [16] and in the Hirota's book [17]. The hyperfine splitting was analyzed in the $FCO_2^{\bullet}$ radical only. The corresponding magnetic hyperfine Hamiltonian $\mathbf{H}_{hfs}$ includes the ^{19}F nuclear spin-rotational interaction term $\mathbf{H}_{nsr}$ and the nuclear spin-electron spin Hamiltonians $\mathbf{H}_{dip}$ (dipolar) and $\mathbf{H}_F$ (Fermi contact term) [18, 19].

We used the Pickett's programs SPFIT and SPCAT [20] to determine molecular parameters that are parameters of the above mentioned Hamiltonian matrix elements.

3. A_1–A_2 splitting in the $FSO_3^{\bullet}$ radical rotational spectra

A special splitting of $K = 3$ rotational levels was observed in the $FSO_3^{\bullet}$ radical rotational spectrum (Fig. 1). This so called, the A_1–A_2 splitting is caused by quartic and sextic centrifugal distortion Hamiltonian terms [14, 15]:

$$\mathbf{H}_{split} = \varepsilon \{\boldsymbol{N}_z (\boldsymbol{N}_+^3 + \boldsymbol{N}_-^3) + (\boldsymbol{N}_+^3 + \boldsymbol{N}_-^3)\boldsymbol{N}_z\} + \\ + h_3' (\boldsymbol{N}_+^6 + \boldsymbol{N}_-^6) \qquad (2)$$

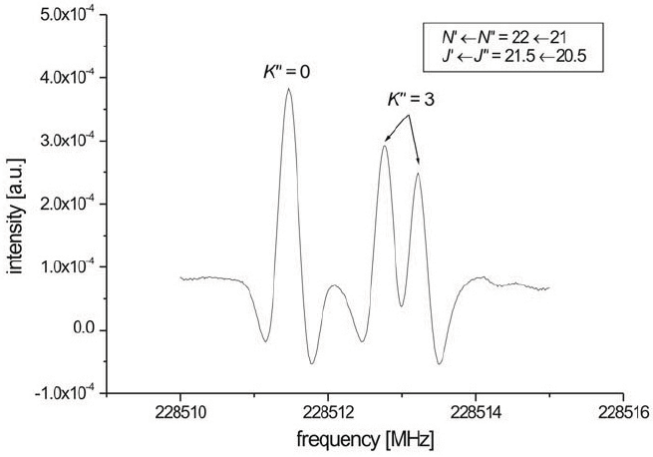

Fig. 1. $N' \leftarrow N'' = 21 \leftarrow 20$ rotational transition of the $FSO_3^{\bullet}$ radical with the $K = 3$ splitting.

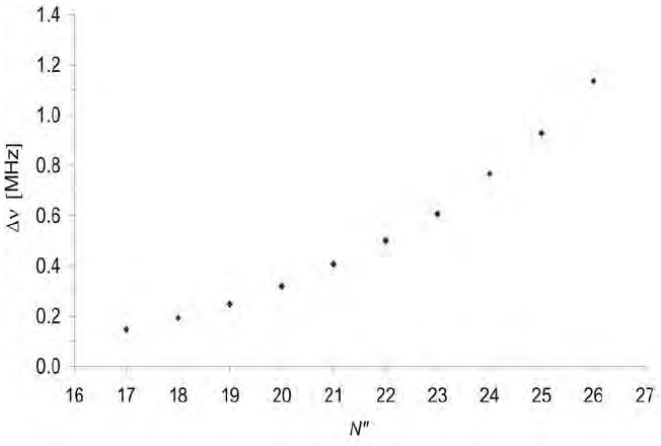

Fig. 2. N – dependence of A_1–A_2 splitting of fine component.

which provide offdiagonal matrix elements. In the symmetrised wavefunctions $|N, K^{\pm}\rangle = 2^{-1/2}\,[|N, k\rangle \pm \pm |N, -k\rangle]$ the $\Delta k = 6$ matrix element is diagonal for $K = 3$, which together with the quartic term splits the $K = 3$ levels. The experimental splittings exhibit a significant dependence on the rotational quantum number N as it can be seen on Fig. 2. This dependence corresponds with a simple expression which can be derived from matrix elements of the $\mathbf{H}_{\text{split}}$ operator:

$$\Delta E_3 = {}^4\Delta E_3 + {}^6\Delta E_3 = h_3 \frac{(N+3)!}{(N-3)!} \tag{3}$$

4. Experimental details

Rotational spectra of both the $FCO_2^{\bullet}$ and the $FSO_3^{\bullet}$ radicals were measured with the Prague microwave spectrometer [14, 19, 21] (Fig. 3) at sample pressures (the sample pressure is related to the equilibrium mixtures described by Eq. 4 and 5) about 30 μbar and 10 μbar, respectively. The very sensitive frequency modulation of the generated microwave radiation was used in all experiments. The modulated signal was detected in the second harmonic (approximately the second derivative of the signal) by the Perkin-Elmer lock-in amplifier. The optical pathlength of the 200 cm long glass cell was doubled using a roof top mirror to increase measurement sensitivity.

Since the radicals are generally short-lived species, it is desirable to generate them inside the cell during spectroscopic measurements. In our experiment, the radicals were produced by a low pressure pyrolysis of suitable precursors: bis(fluoroformyl)peroxide – $FCO_2^{\bullet}$ and bis(fluorosulfuryl)peroxide – $FSO_3^{\bullet}$ at temperatures about 570 K and 440 K, respectively. Both the pyrolysis reactions can be described by the following equilibriums:

$$FC(O)O–OC(O)F \leftrightarrow 2\,FCO_2^{\bullet} \tag{4}$$

$$FSO_2O–OSO_2F \leftrightarrow 2\,FSO_3^{\bullet} \tag{5}$$

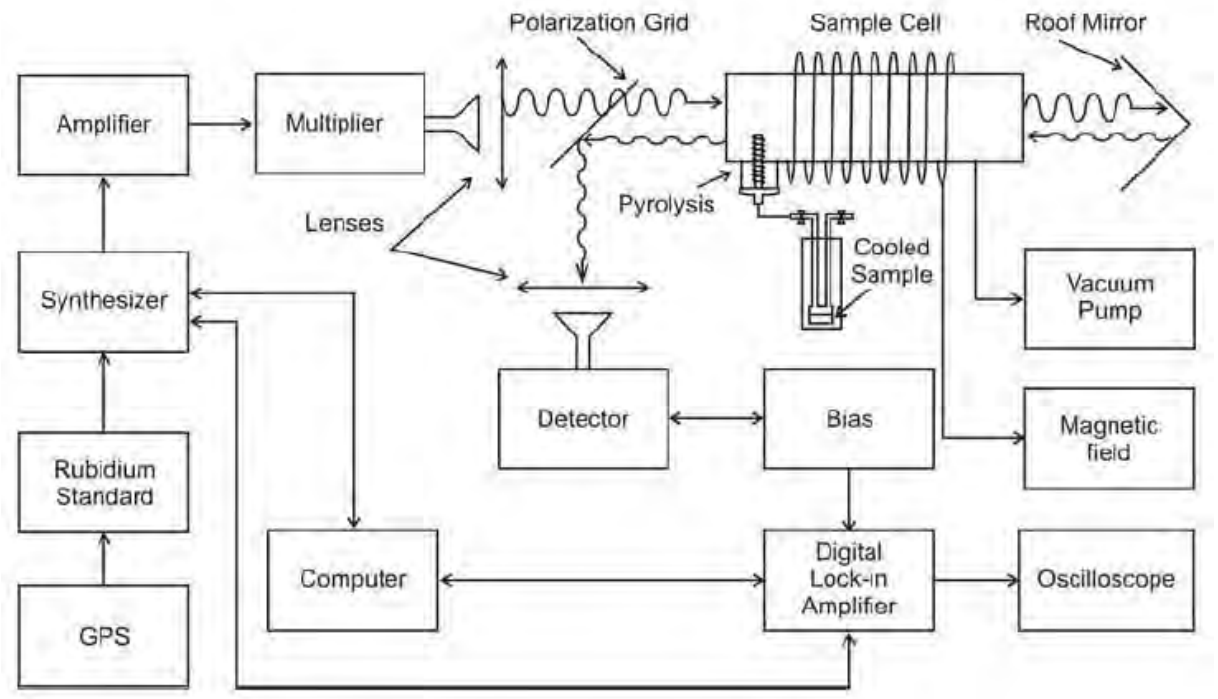

Fig. 3. Prague microwave spectrometer set-up with pyrolysis device for radical measurements.

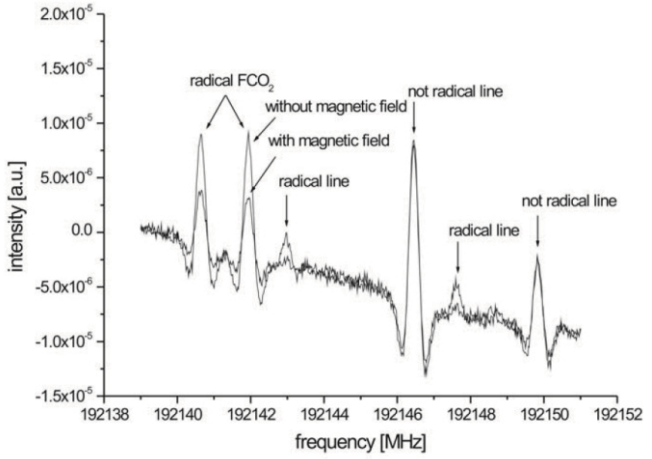

Fig. 4. Two traces of measured spectra with and without magnetic field. The radical lines are broadened and lowered because of the molecular Zeeman Effect.

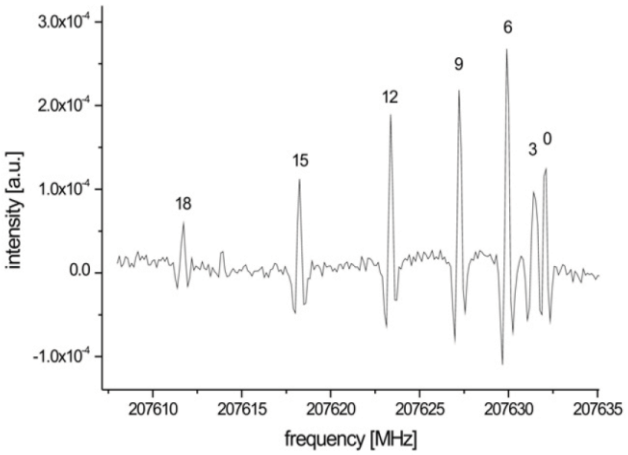

Fig. 5. The rotational sequence for N" = 19 for the lower fine component (J = 19.5) of the fluorosulfate ($FSO_3^{\bullet}$) radical with rotational transitions with K = 0, 3 6, … 18. The K = 3 line is broadened because of the A_1–A_2 splitting (see text).

The precursors were cooled with an ethanol-dry ice bath at 195 K. A special cell for radical measurements including pyrolysis device was developed.

The equilibrium radical reactions in Eq. 4 and 5 are not the only one being in progress during the pyrolysis. In our measured spectra, a lot of unknown transition lines appeared. A simple experimental technique was used to distinguish between the transition lines belonging to the radical open shell molecules and transitions belonging to standard closed shell molecules. We coiled absorption cell by a copper wire to generate a magnetic field inside the cell. The magnetic field splits rotational energy levels belonging to the free radicals due to the molecular Zeeman Effect while the energy levels of the close shell molecules are unaffected. The radicals carrying a nonzero magnetic dipole moment lose space degeneracy and the rotational levels are slightly split into $2N + 1$ sublevels (N is the rotational quantum number). Since the magnetic field is weak, the corresponding splitting is not sufficiently resolved and causes a broadening of the radical lines only. Then in the experimental spectrum with the second harmonic lock-in detection, the peak heights of the corresponding radical lines are measurably decreased while nonradical lines are unaffected by applied magnetic field (Fig. 4).

The $FCO_2^{\bullet}$ radical spectra were measured in the frequency region of 130–242 GHz where the transition $\Delta N = \Delta J = \Delta F = +1$ were observed only. The $FSO_3^{\bullet}$ radical spectra were measured in the frequency region of 93–280 GHz and again only $\Delta N = \Delta J = \Delta F = +1$ transitions were observed.

5. Results

Rotational spectra of fluoroformyloxyl ($FCO_2^{\bullet}$) and fluorosulfate ($FSO_3^{\bullet}$) radicals were measured using the Prague semiconductor microwave spectrometer in the spectral range of 93–280 GHz.

The measured rotational spectra with resolved fine and, in the case of the fluoroformyloxyl radical, hyperfine structures were analyzed in terms of matrix elements of rotational, centrifugal distortion, fine and hyperfine effective Hamiltonians. The parameters of the corresponding Hamiltonian matrix elements are given in Tables 1 and 2 (*see next page*).

Spectral features observed for both the radical can serve as a textbook example of the spin statistic and the Pauli Exclusion Principle. From this point of view, the additional measurements of rotational transitions are extremely interesting in excited vibrational states of B_1 or B_2 and E symmetries for $FCO_2^{\bullet}$ and $FCO_3^{\bullet}$, respectively, since the transitions excluded in the ground state are allowed in these excited states and vice versa, the observed ground state transitions are forbidden in these upper states.

While the analysis of the $FCO_2^{\bullet}$ radical frequencies enabled us to determine a set of precise rotational, centrifugal distortion, fine and hyperfine parameters where the hyperfine part involves parameters of the ^{19}F nuclear spin-rotational and nuclear spin-electron spin (dipolar as well as Fermi contact term) magnetic interactions, in the case of the fluorosulfate radical the ^{19}F hyperfine effects are small and the corresponding hyperfine parameters were not straightforwardly determined.

The microwave measurements, assignments and analysis of the fluorosulfate radical ($FSO_3^{\bullet}$) spectra were

Table 1. Ground state molecular parameters of the $FC^{16}O_2^{\bullet}$ radical (all data are in MHz; numbers in parentheses are standard deviations in units of the last decimal digit).

Parameter	Previous study [22]	Prague (130–242 GHz)	Prague + Lille (130–380 GHz)
A	13752.2758 (63)	13752.22400 (235)	13752.22368 (176)
B	11310.2307 (55)	11310.31990 (133)	11310.31805 (117)
C	6192.80035 (58)	6192.79960 (32)	6192.799622 (202)
$\Delta_N \times 10^3$	7.691 (18)	7.8221 (48)	7.8164 (43)
$\Delta_{NK} \times 10^3$	–	−0.3127 (214)	−0.2912 (181)
Δ_K	0.015682 (156)	0.0155102 (217)	0.0155045 (186)
$\delta_N \times 10^3$	3.3119 (92)	3.37941 (248)	3.37625 (216)
δ_K	0.010690 (34)	0.0107414 (67)	0.0107461 (49)
ε_{aa}	−80.233 (211)	−83.442 (110)	−83.386 (81)
ε_{bb}	−789.868 (87)	−794.682 (73)	−794.630 (59)
ε_{cc}	−44.2597 (227)	−44.1607 (96)	−44.1657 (70)
$\Delta^S_N \times 10^3$	−0.0923 (297)	4.232 (111)	4.160 (100)
$\Delta^S_{NK} \times 10^3$	−1.64 (45)	−20.48 (48)	−20.32 (44)
Δ^S_K	–	0.01676 (65)	0.01640 (51)
$\delta^S_N \times 10^3$	−3.80 (38)	2.045 (56)	2.014 (51)
$\delta^S_K \times 10^3$	–	−2.507 (258)	−2.785 (187)
a_F	−243.7 (79)	−77.28 (93)	−77.75 (77)
1.5 T_{aa}	−27.16 (90)	−85.767 (201)	−85.780 (199)
¼($T_{bb} - T_{cc}$)	6.008 (131)	39.910 (37)	39.930 (37)
C_{aa}	12.990 (159)	–	–
¼($C_{bb} - C_{cc}$)	−0.3830 (115)	–	–
s*	–	0.0287	0.0509

* The symbol s denotes a standard deviation of the fit given in MHz.

Table 2. Ground state molecular parameters of the $FSO_3^{\bullet}$ radical (numbers in parentheses are standard deviations in units of the last decimal digit).

Parameter	Value [MHz]
A*	5447.9
B	5195.528309 (269)
$D_N \times 10^3$	3.76280 (62)
$D_{NK} \times 10^3$	−1.28189 (130)
$H_N \times 10^9$	−6.83 (45)
$H_{NK} \times 10^6$	0.18823 (126)
$H_{KN} \times 10^6$	−0.34641 (195)
$h_3 \times 10^9$	6.716 (112)
ε_{aa}	−37.369 (58)
ε_{bb}	−271.9171 (191)
$D^S_N \times 10^3$	−0.9934 (76)
D^S_{NK}	−0.0702 (189)
D^S_{KN}	0.0731 (190)
$D^S_K \times 10^3$	−1.619 (277)
s**	0.016

* Fixed value based on a semiempirical estimation, for details see [14, 23].

** The symbol s denotes a standard deviation of the fit given in MHz.

improved comparing to previous study [14]. The new parameter set includes the rotational constant A which enhances reliability of the extrapolation to higher N and the plausibility of the parameter h_3 of the $\Delta k = 6$ off-diagonal matrix element (see Tab. 2.).

Acknowledgements. *The work was supported through the Grant Agency of the Czech Academy of Sciences (grants IAA400400504 and 1ET400400410), the Ministry of Education, Youth and Sports of the Czech Republic (research programs MSM6046137307 and LC06071) and by the COST project OC 110. Collaborations with the Bergische Universität Wuppertal were facilitated by the European Commission through contract No. MRTN-CT-2004-512202 QUASAAR, and the DAAD (PPP-Tschechien). H. B. and H. W. acknowledge support from the Deutsche Forschungsgemeinschaft (DFG). We acknowledge also Prof. Sarka help for his reading the manuscript.*

References

[1] MS. von Ahsen, H. Willner, G. A. Arguello: *Journal of Fluorine Chemistry* **125** (2004), 1057.
[2] J. S. Francisco *et al.*: *Journal of Physical Chemistry* **94** (1990), 4791.
[3] H. Herrman: *Chemical Reviews* **103** (2003), 4691.
[4] S. T. Arnold, T. M. Miller, A. A. Viggiano: *Journal of Physical Chemistry A* **106** (2002), 9900.
[5] J. S. Francisco, A. N. Goldstein: *Chemical Physics* **127** (1988), 73.
[6] J. S. Francisco, A. Ostafin: *Molecular Physics* **68** (1989), 255.
[7] M. M. Maricq *et al.*: *Journal of Chemical Physics* **98** (1993), 784.
[8] D. W. Arnold *et al.*: *Journal of Chemical Physics* **102** (1995), 3493.
[9] G. A. Arguello *et al.*: *Journal of Physical Chemistry* **99** (1995), 17525.
[10] E. Castellano *et al.*: *Zeitschrift Fur Physikalische Chemie-Frankfurt* **42** (1964), 174.
[11] G. W. King, D. P. Santry, C. H. Warren: *Journal of Molecular Spectroscopy* **32** (1969), 108.
[12] G. W. King, C. H. Warren: *Journal of Molecular Spectroscopy* **32** (1969), 121.
[13] G. W. King, C. H. Warren: *Journal of Molecular Spectroscopy* **32** (1969), 138.
[14] L. Kolesnikova *et al.*: *The Journal of Chemical Physics* **130** (2009), 184309.
[15] J. K. G. Watson. In: *Vibrational Spectra and Structure: A Series of Advances*. J. R. Durig (Ed.). New York, Elsevier 1977.
[16] J. M. Brown, T. J. Sears: *Journal of Molecular Spectroscopy* **75** (1979), 111.
[17] E. Hirota: *High-Resolution Spectroscopy of Transient Molecules*. Berlin, Springer 1985.
[18] A. Carrington, J. M. Brown: *Rotational Spectroscopy of Diatomic Molecules*. Cambridge, Cambridge University Press 2003.
[19] L. Kolesnikova *et al.*: *Journal of Chemical Physics* **128** (2008), 224302.
[20] H. M. Pickett: *Journal of Molecular Spectroscopy* **148** (1991), 371.
[21] P. Kania *et al.*: *Journal of Molecular Structure* **795** (2006), 209.
[22] Z. Zelinger *et al.*: *Journal of Molecular Spectroscopy* **243** (2007), 292.
[23] G. Cazzoli *et al.*: *Journal of Molecular Spectroscopy* **162** (1993), 467.

Detection of the Damage Caused to DNA by 2-Nitrofluorene Using an Electrochemical DNA Biosensor

Vlastimil Vyskočil[a], Ján Labuda[b], Jiří Barek[a]

[a] *UNESCO Laboratory of Environmental Electrochemistry, Department of Analytical Chemistry, Faculty of Science, Charles University in Prague, Hlavova 2030/8, 128 43 Prague 2, Czech Republic,* ✉ *vyskoci1@natur.cuni.cz*
[b] *Institute of Analytical Chemistry, Faculty of Chemical and Food Technology, Slovak University of Technology in Bratislava, Radlinského 9, 812 37 Bratislava, Slovak Republic,* ✉ *jan.labuda@stuba.sk*

Keywords
DNA biosensor
DNA damage
Electrochemical detection
2-Nitrofluorene
Screen printed carbon paste electrode

Abstract
An electrochemical DNA biosensor based on the screen printed carbon paste electrode (SPCPE) has been used for investigation of the interaction between genotoxic 2-nitrofluorene and calf thymus DNA. Two types of DNA damage have been investigated and electrochemically detected at the DNA/SPCPE biosensor: the DNA damage caused by short-living radicals generated by the electrochemical reduction of nitro group and the damage caused by the direct interaction with 2-nitrofluorene.

1. Introduction

The emissions of gasoline and diesel engines contribute significantly to ever increasing pollution of living environment. A specific part of exhaust gases is composed of nitrated polycyclic aromatic hydrocarbons (NPAHs). Nitrated polycyclic aromatic hydrocarbons belong in environment to substances which are causally connected with increasing rate of cancer disease [1]. Presence of these compounds in environment threatens natural biological functions of ecosystem and healthy organism growth [2]. In the eighties and the nineties of the last century, L. Möller studied influences of NPAHs and their *in vivo* metabolites on living organisms and their DNA [3]; carcinogenic 2-nitrofluorene was chosen as a NPAHs model marker [4, 5]. 2-Nitrofluorene is proven to be carcinogenic to rats and thus possibly carcinogenic to humans (IARC class 2B) [4, 6], and its presence is demonstrably proven in vehicle exhaust gases, too [7, 8].

In our work *in vitro*, an electrochemical DNA biosensor [9] based on the screen printed carbon paste electrode (SPCPE) has been used for investigation of the interaction between 2-nitrofluorene and calf thymus DNA. Two types of DNA damage have been investigated and electrochemically detected at the DNA/SPCPE biosensor: the DNA damage caused by short-living radicals generated by the electrochemical reduction of nitro group, previously described by Abreu [10], and the damage caused by the direct interaction with the studied compound, previously described in references [11–13]. The type of direct interaction between 2-nitrofluorene and DNA has been characterized using previously tested DNA intercalators: cobalt(III) and copper(II) complexes of 1,10-phenanthroline [14].

2. Results and discussion

The 2-nitrofluoreneDNA interaction was investigated using the DNA-biosensor prepared by immobilizing DNA onto the SPCPE surface (representative cyclic voltammograms of the ferrocyanide redox system at bare SPCPE is depicted in Fig. 1). The DNA gel on the

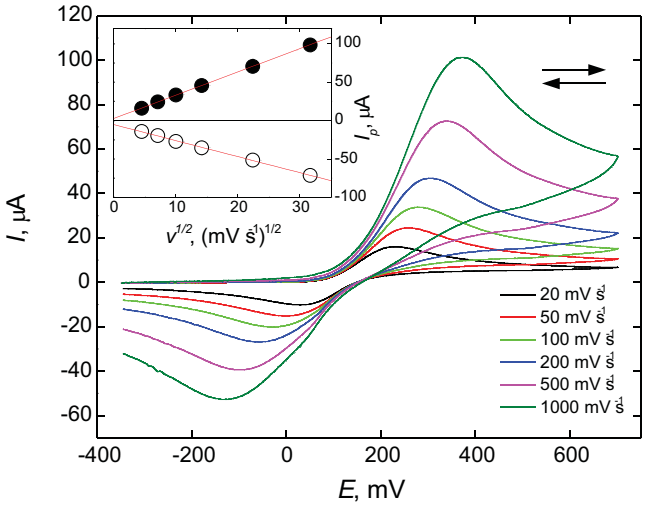

Fig. 1. Cyclic voltammograms of 1×10^{-4} M $K_4[Fe(CN)_6]$ in 0.1 M KCl (aq) measured at SPCPE (pretreated by applying a potential of +1600 mV for 120 s and +1800 mV for 60 s in 10 mL of AcB); scan rates (mV s^{-1}): 20, 50, 100, 200, 500 and 1000. The dependence of anodic (●) and cathodic (○) ferrocyanide/ferricyanide peak currents on the square root of the scan rate is in the inset.

electrode surface enables the accumulation of the analyte on the biopolymer matrix. The electrochemical reduction of 2-nitrofluorene (during the first 4-electron reduction step of nitro group reduction to hydroxylamino group) generates short-living radicals that interact with DNA causing damage [15]. This interaction was detected by electrochemical sensing of the oxidation of the DNA purine bases [16] using differential pulse voltammetry (DPV). We have tested two ways of reduction of 2-nitrofluorene (in 0.25 M acetate buffer with 10 mM KCl pH = 4.75 (AcB)–methanol (99:1) medium; concentration of 2-nitrofluorene was 1×10^{-5} M) successive cathodic/anodic cycling, from 0 to –1000 mV (15 scans), and reduction at fixed potential of –900 mV (10 minutes). Furthermore, the solution was stirred or not during the reduction, and the solution was tempered at room temperature 25 °C or at human body temperature 36 °C. However, under these conditions only (AcB--methanol (99:1) stirred medium tempered at 36 °C and using reduction by successive cathodic/anodic cycling, from 0 to –1000 mV (15 scans)), the appearance of guanosine (E_p ~ +800 mV) and adenosine (E_p ~ ~ +1100 mV) peaks (Fig. 2) demonstrates clearly that the damage by the radicals caused distortion of the double helix and exposure of the bases that can be oxidized.

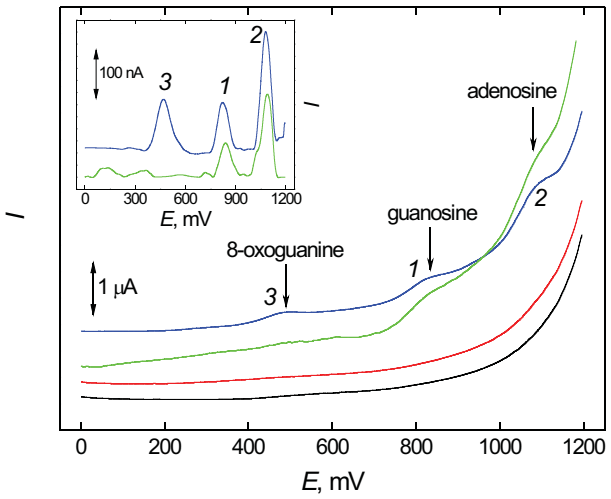

Fig. 2. Oxidation DPV peaks of DNA immobilized onto the SPCPE electrode surface measured in AcB–methanol (99:1) medium; scan rate: 20 mV s^{-1}, E_{step} = 5 mV, $E_{amplitude}$ = 50 mV, pulse width: 80 ms, t = 36 °C. DP voltammograms obtained at bare SPCPE in AcB (black line), at bare SPCPE after successive cathodic/anodic cycling, from 0 to –1000 mV (15 scans), in solution of 2-nitrofluorene (c = = 1×10^{-5} M) in AcB–methanol (99:1) (red line), at DNA/SPCPE in AcB (green line) and at DNA/SPCPE after successive cathodic/anodic cycling, from 0 to 1000 mV (15 scans), in solution of 2-nitrofluorene (c = 1×10^{-5} M) in AcB–methanol (99:1) (blue line); oxidation peaks of guanosine (1), adenosine (2) and 8-oxoguanine (3) are observable at distorted double helix. DP voltammograms obtained at DNA/SPCPE biosensor (green and blue line) after baseline correction are depicted in the inset.

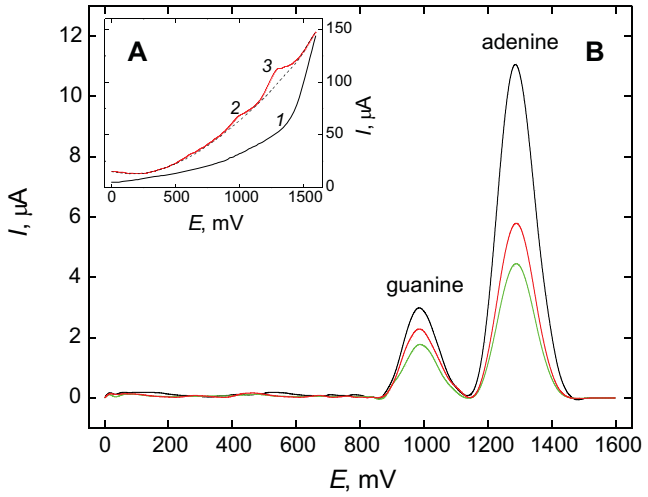

Fig. 3. Oxidation SWV peaks of DNA immobilized onto the SPCPE electrode surface measured in AcB medium; scan rate: 3000 mV s^{-1}, E_{step} = 15 mV, $E_{amplitude}$ = 40 mV, frequency = 200 Hz. (A) Baseline control scan performed to monitor the cleaning stage of the carbon paste working electrode (1), SW voltammogram of guanine (2) and adenine (3) with displayed baseline (dashed line). (B) SWV scan of guanine and adenine after baseline correction; DNA/SPCPE biosensor incubated 2 minutes in AcB–methanol (99:1); concentration of 2-nitrofluorene in incubate solution (M): 0 (black line), 5×10^{-6} (red line) and 1×10^{-5} (green line).

The oxidation peak of 8-oxoguanine, a product of guanine oxidation (E_p ~ +450 mV) [16] could also be identified (Fig. 2).

The investigation of the damage caused to DNA by the direct interaction with 2-nitrofluorene, general procedure of experiment consists of five main steps: pretreatment, DNA immobilization, blank or sample interaction, flushing and measurement. The electrode surface was pretreated by applying a potential of +1600 mV for 120 s and +1800 mV for 60 s in 10 mL of AcB, under stirred conditions; this procedure was necessary to oxidize all contaminants present on the graphite surface and to activate the electrode surface [13] and make it susceptible to the following DNA immobilization. After the first step the baseline control scan was performed to monitor the cleaning stage of the carbon paste working electrode (Fig. 3-A). Then the biosensor was developed by immobilizing DNA (5 µL of 0.1 mg mL^{-1} calf thymus DNA) onto the screen-printed electrode surface. The square-wave voltammetric (SWV) scan of immobilized DNA was performed for a few electrodes to evaluate the oxidation of guanine ($I_{p,G}$) and adenine peak height ($I_{p,A}$) (at about +1000 mV and +1300 mV *vs.* Ag pseudo-reference screen printed electrode for guanine and adenine, respectively) as a blank (relative value of $I_{p,G}$ and $I_{p,A}$ ~ 100.0%). For the rest of the electrodes an interaction step was performed by immersing the DNA/SPCPE in a stirred solution containing 2-nitrofluorene (AcB–methanol (99:1)

medium). After 2 minutes of incubation the sensor was washed by dipping the electrode in a clean acetate buffer solution under open-circuit condition for 10 s and after that SWV scan was carried out in fresh AcB (Fig. 3). Obtained results show the decrease of $I_{p,G}$ and $I_{p,A}$ from 100.0% in average (n = 3) to 77.3% and 52.1% (in the case of direct interaction of DNA with 2-nitrofluorene in concentration 5×10^{-6} M), and to 60.3% and 40.6% (in the case of direct interaction of DNA with 2-nitrofluorene in concentration 1×10^{-5} M), respectively (Fig. 3-B).

From these facts it results that 2-nitrfluorene interacts with DNA, immobilized at SPCPE surface, concentration-dependently. The type of interaction was investigated voltammetrically (using DPV) by binding reactions of cobalt(III) and copper(II) complexes of 1,10-phenanthroline with calf thymus DNA [14]. Obtained results indicate a transition in the interaction mode between the metal species and DNA from dominantly electrostatic to dominantly intercalative with the increase in ionic strength (detailed results presented in [17]).

Acknowledgements. *This work was financially supported by the Ministry of Education, Youth and Sports of the Czech Republic (projects LC 06035, MSM 0021620857 and RP 14/63) and by the European Union Lifelong Learning Programme (Erasmus). J. L. thanks to the Grant Agency VEGA (project 1/0852/08) of the Ministry of Education of the Slovak Republic and Slovak Academy of Sciences for financial support.*

References

[1] Jacob J., Karcher W., Belliardo J. J., Dumler R., Boenke A.: *Fresenius. J. Anal. Chem.* **340** (1991), 755–767.
[2] Moreira J. C., Barek J.: *Quim. Nova* **18** (1995), 362–367.
[3] Moller L.: *Environ. Health Perspect.* **102** (1994), 139–146.
[4] Moller L., Rafter J., Gustafsson J. A.: *Carcinogenesis* **8** (1987), 637–645.
[5] Edenharder R., Tang X.: *Food Chem. Toxicol.* **35** (1997), 357–372.
[6] Ueda O., Kitamura S., Kubo R., Yano Y., Kanzaki Y., Fujimoto T., Tatsumi K., Ohta S.: *Xenobiotica* **31** (2001), 33–49.
[7] Schuetzle D.: *Environ. Health Perspect.* **47** (1983), 65–80.
[8] Albinet A., Leoz-Garziandia E., Budzinski H., ViIlenave E.: *Sci. Total Environ.* **384** (2007), 280–292.
[9] Diculescu V. C., Paquim A. M. C., Brett A. M. O.: *Sensors* **5** (2005), 377–393.
[10] Abreu F. C., Goulart M. O. F., Brett A. M. O.: *Biosens. Bioelectron.* **17** (2002), 913–919.
[11] Lucarelli F., Palchetti I., Marrazza G., Mascini M.: *Talanta* **56** (2002), 949–957.
[12] Bagni G., Hernandez S., Mascini M., Sturchio E., Boccia P., Marconi S.: *Sensors* **5** (2005), 394–410.
[13] Szpakowska I., Krassowska-Swiebocka B., Maciejewska D., Kazmierczak P., Jemielita W., Konrad M., Trykowska J., Maj-Zurawska M.: *Electroanalysis* **18** (2005), 1422–1430.
[14] Labuda J., Bučková M., Vaníčková M., Mattusch J., Wennrich R.: *Electroanalysis* **11** (1999), 101–107.
[15] Tocher J. H.: *Gen. Pharmacol.* **28** (1997), 485–487.
[16] Oliveira-Brett A. M., Serrano S. H. P., Piedade A. J. P.: Electrochemistry of DNA. In: *Comprehensive Chemical Kinetics, Vol. 37.* Compton R. G., Hancock G. (edits.). Amsterdam, Elsevier 1999, p. 91–119.
[17] Vyskočil V., Labuda J., Barek J.: *Euroanalysis 2009, Innsbruck, Austria.* Analytical Chemistry of the EuCheMS 2009. Book of Abstracts, P023-A1.

Speciation of Mercury in Biological Material by Using of AMA 254 and HPLC-ICP-MS

Kateřina Wranová[a, b], Věra Spěváčková[b], Lucie Kašparová[b], Mája Čejchanová[b]

[a] *Department of Analytical Chemistry, Faculty of Science, Charles University in Prague, Albertov 6, 128 43 Prague 2, Czech Republic*
[b] *The National Institute of Public Health in Prague, Šrobárova 48, 100 04, Prague 10, Czech Republic,* ✉ *wranova@szu.cz*

Abstract

On the request of the Czech Science Committee for Foodstuffs a project for mapping the exposure of the Czech population with mercury and especially methylmercury ($MeHg^+$) has been started.

Hair has been chosen as a suitable biomarker for $MeHg^+$ exposure in human because concentration of this mercury species once bonded in hair is stable. The procedure was based on the verified analytical method (extraction and AMA-254 detection) described previously [1]. Various factors (sampling procedure, storage conditions, and sources of contamination) were studied. The verification of the analytical method included all steps of the procedure (cleaning of utensils, calibration, yield of the separation step, *etc.*). The repeatability, internal reproducibility, distance from the scalp and other parameters were tested on control samples, the accuracy was proved by using a control reference material. The results confirmed the suitability of the method, which ought to be further used for different studies including biological monitoring.

In the second part of this work a possibility of the determination of mercury species in fish tissue (CRM) has been studied. HPLC technique coupled with ICP-MS led to the development of the method for the determination of mercury species in biological materials. [2] Liquid extraction of mercury by 2-mercaptoethanol was followed by separation of mercury species on reversed phase HPLC connected to ICP-MS. The method was validated by analyses of certified reference materials with declared concentration of total mercury and $MeHg^+$. Results of pilot study confirmed the suitability of the proposed method for determination of mercury species in biological materials.

Keywords
AAS
fish
hair
HPLC
ICP-MS
mercury
methylmercury
population groups
speciation

1. Introduction

It is well known that mercury is one of the most hazardous pollutants in the environment. The most monitored species generally found in biological samples are the inorganic mercury (Hg^{2+}) and monomethylmercury ($MeHg^+$). The mercury species are different in their bioavailability and toxicity. These differences are necessary to take into account by the development of a high sensitive and accurate method for simultaneous determination of mercury species in biological samples [2].

Health risks of exposure to mercury and its compounds are well described in literature [3–11]. From these publications it follows that urine, blood and hair are the most used biomarkers of mercury body burden (with some limitations). Urine is considered to be the best indicator of body burden from long-term exposure to elemental and inorganic mercury (Hg_{in}). Blood is a good biomarker of short-term exposures and hair is well suited as a biomarker for the $MeHg^+$ endogenous exposure. The advantage of using hair as a biomarker for the $MeHg^+$ is the stability of the concentration of this species once bonded in hair [12].

The most important source of non-professionally human exposure to Hg is dietary intake of $MeHg^+$ in fish and fish products [13, 14]. Indeed, in connection with changes of the dietary habits of Czech population (higher frequency of fish consumption in the last years), The Scientific Committee for Foodstuffs in the Czech Republic decided in 2004 that a study of body burden of $MeHg^+$ is necessary even that the fish consumption is still low in comparison with coastal states (<5 kg per reference man per year with seafood accounting for 63% of this amount) [3, 15]. Results from this study will serve as a starting point for future biological monitoring studies. For this purpose we used a rapid and very simple validated method using the one-purpose atomic spectrometer AMA-254 which was described previously [1, 16] and is used for routine analyses. Into the boat of AMA-254 instrument, liquid and solid samples are introduced directly without any pre-treatment.

The other methods commonly applied for mercury analyses and speciation are based on the use of gas

chromatography (GC) or liquid chromatography (HPLC) connected to element-specific detection. Gas chromatography is normally preferred for non-polar volatile species. High performance liquid chromatography techniques are more suited for the separation of polar species (organomercury and inorganic mercury speciation). To compare these techniques, sample treatment for HPLC could be easier, and the derivatization step could be eliminated [17].

Mercury compounds have a strong affinity to sulphanyl groups (–SH) and reagents with these groups are commonly used as extraction solutions or for preparing of mobile phases (L-cysteine, dithizone, thiourea, 2-mercaptoethanol *etc.*) [17, 18].

One of the most attractive detection systems for elemental speciation in HPLC-based method is ICP-MS. An excellent detection limit, a multi-element capability, a wide linear dynamic range and in some cases its ability to measure isotope ratio belong to the advantages of this system. The coupling of HPLC to ICP-MS is technically very simple and consists of the connecting the exit of the chromatographic column to the nebuliser but with some limitations. Mobile phases generally contain salts in buffer solutions, organic solvents and/or ion pairing reagents, which can lead to the blockage of cones and to the signal degradation over time [17, 19, 20].

The AMA-254 method is commonly used at our laboratory for the determination of total mercury and in combination with the extraction method for the determination of its species. Validation and some results were published previously [1] and in this report a brief summary is made.

The possibility of using of the HPLC technique connected to ICP-MS led us to the development of other method for the determination of mercury species in fish tissues and also in human hair. In this study the pilot results are published.

2. Experimental

2.1. Instrumentation

The first part of measurements were performed on a single-purpose spectrometer AMA-254 (Altec Prague, Czech Republic) by the cold vapour atomic absorption spectroscopy (CV AAS) technique with a previous combustion of the sample in oxygen atmosphere and amalgamation preconcentration [21].

The second part of results was obtained by using of HPLC-ICP-MS system. The high performance liquid chromatography system used for the separation of methylmercury and inorganic mercury consisted of a Perkin Elmer Series 200 Pump (Perkin Elmer), Series 200 Peltier Oven (DBS Strumenti Scientifici, Italy), Rheodyne LLC injector with a 200 µL sample loop and a reverse phase column (Spheri RP18 column, 220 mm × 4.6 mm × 10 µm, Perkin Elmer). The mobile phase flow rate was 1.5 mL per min. The outlet of the column was directly connected to the PFA concentric nebuliser of an ICP-MS system by PEEK tubing.

The determination of mercury was carried out on a Perkin Elmer ICP-MS Elan DRC-e (Perkin ElmerSCIEX Instrument, Canada) through all the experiment. The conditions of the instrument were controlled daily by a performance solution of 10 µg L^{-1} Be, Mg, Co, Rh, In, Ce, Ba and Pb. The optimisation of the lens voltage and the nebuliser gas flow was done daily by using of a solution of 10 µg L^{-1} Hg.

The optimal operation conditions of the HPLC-ICP--MS system are given in Table 1.

2.2. Reagents, Materials and Vessels

For AMA analyses nitric acid (Suprapur®, Merck), concentrated and 2 M hydrochloric acid (Suprapur grade, Merck), standard solution of 1000 mg Hg L^{-1} for AAS (Merck) was used. The methylmercury chloride (CH_3HgCl) was supplied by Riedel-de Haën and oxygen of medical purity (Linde,Czech Republic) was used. Working standards of mercury were prepared from the standard solution and stabilized by 1 % (v/v) HNO_3 and 0.01 % (w/v) potassium dichromate (reagent grade, Lachema, Czech Republic). Demineralised water

Table 1. The instrumental HPLC-ICP-MS conditions used during the study.

Elan Drc-e ICP-MS	
RF power (W)	1300
Gas flow (L min^{-1})	plasma 15, auxiliary 1.2, nebuliser 0.9–1.2 (10 µg L^{-1} Hg)
Interface	PFA concentric nebuliser, cooled cyclonic spray chamber (5 °C)
Lens voltage (V)	10–12.5 (10 µg L^{-1} Hg)
Dwell time (ms)	250
Isotope monitored (*m*/*z*)	^{202}Hg
HPLC	
Pump	Series 200 LC PUMP
Mobile phase	5 % (v/v) methanol, 0.1 % (v/v) 2-mercaptoethanol, 0.06 M ammonium acetate at 1.5 mL min^{-1}
Injector	Rheodyne all PEEK with 200 µL PEEK injection loop
Pre-column	C8 33 mm (Perkin Elmer)
Column	Spheri RP18 column, 220 mm × × 4.6 mm × 10 µm (Perkin Elmer) at 25 °C
Sample volume (µL)	100

(18.2 MΩ cm^{-1}) from a Milli-Q water purification system (Millipore, France) was used.

For HPLC analyses the hydrochloric acid (Suprapur®), HPLC grade methanol (LiChrosolv®), potassium chloride (p.a.) and ammonium acetate (Suprapur®) were obtained from Merck. The guaranteed grade 2-mercaptoethanol was supplied by Merck.

The HPLC mobile phase containing 5 % (v/v) methanol, 0.1 % (v/v) 2-mercaptoethanol and 0.06 Mammonium acetate was used [2].

Several certified reference materials (CRMs) including CRM GBW 07601 (human hair, total mercury), IAEA 085 (methylmercury), NRCC DORM 2 (dogfish muscle) and NRCC DOLT 2 (dogfish liver) were used for validation and verification of the method.

Before use, glass vessels and tubes used for AMA analyses were washed to avoid the contamination as described previously [1].

2.3. Analytical Procedures

To determine the total Hg, Hg_{in} and $MeHg^+$ levels in human hair, scalp hair samples (about 0.2 g) taken from the occipital area were cut on pieces of about 5 mm long, homogenized, washed by the procedure recommended by WHO/IAEA (acetone, 3 times demineralised water, acetone) and dried at about 50 °C in drying oven.

Total mercury concentration was determined directly without mineralization. About 10 mg of the sample was directly weighed into the boat of AMA-254 analyser, dried, combusted, and decomposed in a stream of oxygen on a catalytic column. After quantitative mercury trapping on the surface of gold amalgamator, the mercury was completely evaporated at 900 °C into the optical cell and measured at 253.7 nm. Methylmercury was extracted from the subsample of hair by hydrochloric acid (2 M, v/w = 40 mL g^{-1}) for 4 h. After centrifugation, 100 µL of the solution was pipetted into AMA 254 boat and measured by the same way as total mercury. The content of inorganic bound mercury was calculated as a difference between total Hg and $MeHg^+$.

The procedure of preparation samples for AMA analyses is shown in Fig. 1. Fig. 2 shows the instrument of AMA 254.

To determine mercury species by HPLC separation, about 100 mg of the sample (CRM of fish tissue, human hair) was weighted into a PP centrifuge tube. Consequently, 5 mL of the extraction solution which consists of 0.1 % (v/v) hydrochloric acid, 0.1 % (v/v) 2-mercaptoethanol and 0.15 % (w/v) potassium chloride were added. The mixture solution was put into a shaker and shaken overnight (about 14 hrs) at room temperature. Afterwards, the centrifugation at 5000 rpm for about 10 min was used for separation of the supernatant. Extraction was repeated by another 2.5 mL of the extraction solution for about 1 min. After, fractions were mixed together and filtered through a 0.45 µm Nylon filter prior to analysis.

Blanks were prepared in the same way as the samples in each batch [2].

3. Results and discussion

3.1. Determination of mercury species by AMA-254

The validated method was used for the determination of mercury species in various groups of Czech population.

Groups of dentist, workers in fish industry and professionally non-exposed adults (altogether sixty persons) were included in our study. Filled-in questionnaires included the number of amalgam fillings, frequency of fish consumption, gender, age, smoking habits and informed consent. Descriptive data are reported in the study published previously [12].

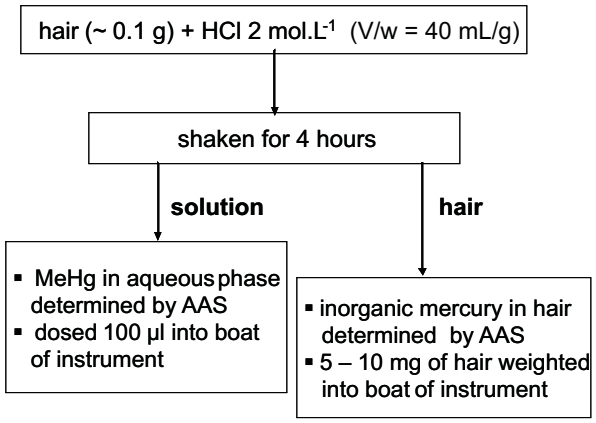

Fig. 1. Preparation of samples (human hair) for AMA-254 analyses, description of the method.

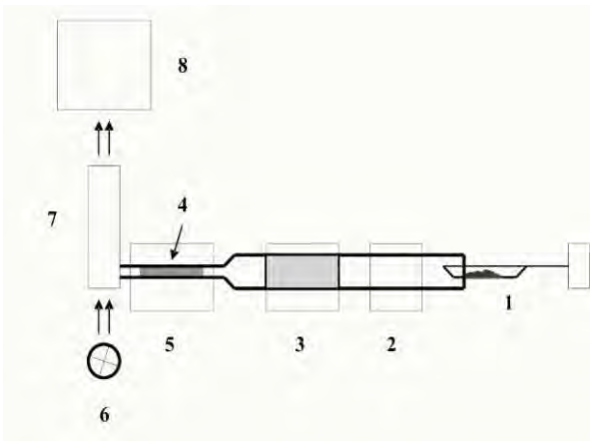

Fig. 2. Scheme of an AMA-254 instrument: boat (1), ashing oven (2), amalgamator (3)catalyst (4), releasing oven (5), Hg lamp (6), optical system with cells (7), detector (8).

Table 2. Determined levels of mercury species in certified reference materials of human hair

Certified reference material	Hg [μg g^{-1}]	
	Certified level	Measured level (SD)
GBW 07 601 (total Hg)	0.36±0.05	0.36±0.01
IAEA 085 ($MeHg^+$)	21.9–23.9	22.4±2.00

3.1.1. Validation, QA and QC

All validation parameters used in described analytical method have been published previously [1]. The limit of detection for mercury was 0.7 ng g^{-1}, limit of quantification was 1.4 ng g^{-1}. Uncertainty was about 7 % for Hg_{in} and 10 % for $MeHg^+$. The accuracy of the method was confirmed by the analysis of certified reference materials of hair: IAEA 085 and GBW 07 601. Determined values for both certified reference materials are shown in Table 2. The control sample analysed with every set of samples throughout the study was used to ensure the accuracy and compatibility of the results.

3.1.2. Sampling of Hair

It was found out that used technique of hair sampling is useful for our purpose. All steps of collecting samples (treatment, stability, possibility of external contamination) have to be under control.

To test the distribution of mercury on various sampling points on the head we collected samples of hair from two volunteers from four different sampling points: samples from an occipital area, which is usually recommended [22], samples from left and right temple and samples collected above forehead. The significant differences in ratios of mercury species were not found. The measured values are shown in Table 3.

3.1.3. Statistical Evaluation

The results obtained for $MeHg^+$ and Hg_{in} in the groups of dentists, workers in "freshwater" fish industry and professionally non-exposed adults (about 20 persons in each group) were statistically evaluated by ANOVA and QC Expert, and Student's *t*-test at the level $\alpha \geq 0.95$ [23].

All results had log-normal distribution and therefore before statistical evaluation, the data were modified by logarithmic transformation. Calculated critical value of the determination coefficient (R^2) at the level $\alpha = 0.95$ equals to 0.102 (higher values signalised significance of parameter).

In the evaluation, smoking habits were omitted because of the very low number of smokers (< 10 % from all participants). The results on the hair concentration of mercury species are summarised in Table 4.

3.1.4. Discussion to the AMA-254 Study

Influences of various mutually independent parameters (age, number of amalgam fillings, dietary habits, professional exposure and gender) on methylmercury and inorganic bound mercury species were studied.

Table 3. Measured levels (μg g^{-1}) of total mercury and methylmercury in hair collected in different sampling point. The abundance of $MeHg^+$ is mentioned in brackets.

Sampling point	Volunteer I		Volunteer II	
	Total Hg	$MeHg^+$	Total Hg	$MeHg^+$
Occipital area	0.34	0.26 (75 %)	0.14	0.09 (61 %)
Left temple	0.46	0.34 (75 %)	0.09	0.06 (67 %)
Right temple	0.58	0.45 (77 %)	0.10	0.08 (80 %)
Above forehead	0.26	0.17 (67 %)	0.10	0.09 (89 %)

Table 4. Results of hair mercury species (μg g^{-1}) in groups of dentists and professional non-exposed population.

		Total Hg	$MeHg^+$	Hg_{in}
Non-exposed population groups	Median	0.33	0.20	0.10
	Max	2.38	1.56	0.90
	Min	0.07	0.04	0.01
	Percentile 0.9	1.00	0.72	0.26
Dentists group	Median	0.51	0.29	0.23
	Max	5.69	1.60	4.45
	Min	0.28	0.07	0.11
	Percentile 0.9	4.17	1.00	2.60

Mercury species in human hair were determined in groups of dentists, workers in "freshwater" fish industry and professionally non-exposed adults with different dietary habits.

We found that differences among groups of workers in "freshwater" fish industry, other professionally non-exposed adults and celiatics (different dietary habits) in all parameters under study were statistically non significant and these groups were henceforth taken as one "non-exposed" group. Dentists were treated as a professionally exposed group.

In all groups no significant influence of age and gender was found for both species.

A significant difference between non-exposed groups and dentists was found for inorganic mercury form. At dentists, the total mercury concentration > 1 μg g^{-1} (the median for total Hg 0.51 μg g^{-1}) was found for 5 persons (*i.e.*, 29%) and median of abundance of Hg_{in} was about 60% while median of abundance of Hg_{in} in "non--exposed" group was about 30%. Four dentists had the concentration of Hgin > 1 μg g^{-1}. This fact can be explicated by the exogenous contamination of dentist's hair by inorganic form of mercury presented in the atmosphere of the working place. All non-dependent parameters seemed to be statistically non-significant in the group of dentists but differences could be covered up by the higher mercury content.

In the professionally non-exposed group we found that the median of total Hg was 0.33 μg g^{-1}, the median of abundance of $MeHg^+$ was 70%. Two persons, having concentration of $MeHg^+$ higher than 1 μg g^{-1} (1.5 and 1.2 μg g^{-1} respectively), consumed fish more than 3 times per week. Four persons have a concentration of total Hg > 1 μg g^{-1}. The influence of amalgam fillings was non-significant for $MeHg^+$ (determination coefficient 0.019) but significant for inorganic Hg (determination coefficient 0.193). The influence of fish consumption was significant for both $MeHg^+$ (determination coefficient 0.533) and Hg_{in} (determination coefficient 0.189). Described influences are shown in Figs. 3 and 4.

Table 5. Limits of detection and limits of quantification HPLC-IC-MS method.

	$MeHg^+$	Hg^{2+}
LOD [μg L^{-1}]	0.20	0.25
LOQ [μg L^{-1}]	0.50	0.65

3.2. HPLC-ICP-MS Pilot Study

3.2.1. Validation

Validation parameters of the method used in pilot study has been confirmed by using of standard solution of monitored species and certified reference materials. Selectivity and specificity are described by retention time of mercury species and by mass detection of ICP-MS.

The limit of detection and limit of quantification were determined by repeated measurements of blank solution and counted as three times, respectively ten times of a standard deviation (SD) and their values are shown in Table 5.

The accuracy and the precision of the method were confirmed by the analysis of certified reference material of fish tissue NRCC DORM 2 (Dogfish Muscle Certified reference Material, National Research Council of Canada). The declared values are 4.64±0.26 μg g^{-1} for total Hg and 4.47±0.32 μg g^{-1} for $MeHg^+$. The value of Hg^{2+} was obtained as a difference between total mercury and $MeHg^+$. Our recovery in pilot measurements was about 95% for $MeHg^+$ and 105% for Hg^{2+}. The higher recovery of Hg^{2+} could be explained by a possible external contamination of samples and lower abundance of Hg^{2+} in reference material. In routine analyses,

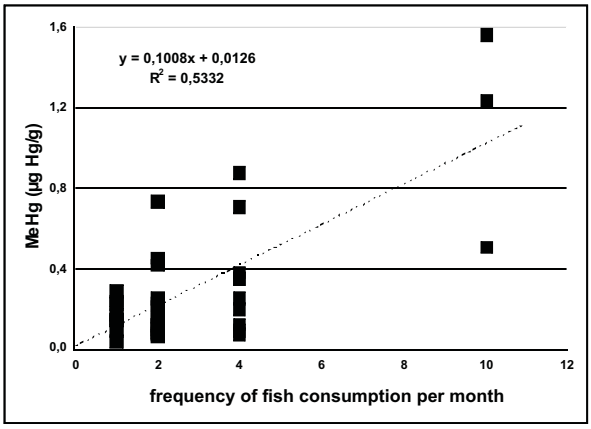

Fig. 3. Dependence of the methylmercury concentration in hair on the frequency of fish consumption (without dentists).

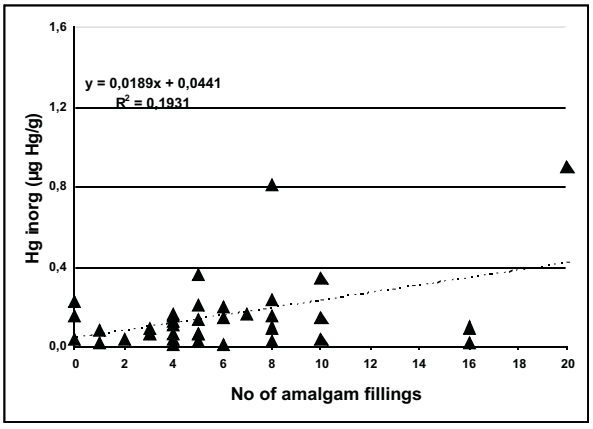

Fig. 4. Dependence of the inorganic bound mercury concentration in hair on the frequency of number of amalgam fillings (without dentists).

recovery near to 100% for $MeHg^+$ was not reached and its value was about 80%.

The repeatability was confirmed by repeated analyses of standard solution of both species (25 μg L^{-1}). We found values 0.5% for $MeHg^+$ and 5.1% for Hg^{2+}.

3.2.2. Monitored Species, Retention Time and Calibration

The described method was used for determination of mercury species, especially $MeHg^+$ and Hg^{2+} in fish tissues and in some real samples of hair. The results showed that the method is suitable for this purpose.

The chromatogram of individual mercury species is reported in the Fig. 5. It is shown that the retention times are about 12 min for $MeHg^+$ and 15 min for Hg^{2+}.

To control the linearity, long calibration in range 5–500 μg L^{-1} was checked. The Fig. 6 presents chromatograms of these analyses and shows good repeatability in retention times of both species. Good linearity was proved by the calculation of correlation coefficients which were 0.999997 for $MeHg^+$ and 0.999994 for Hg^{2+}. For routine analyses a calibration in range 25–100 μg L^{-1} was commonly used.

3.2.3. Effect of Column Temperature on Analyses

The whole procedure of HPLC separation is very time consuming for routine analyses of large series of samples. To short the time of procedure an effect of column temperature on retention times of monitored species and whole process was studied. Different column temperatures were chosen (20, 25 and 30 °C) and used for analyses. Obtained chromatograms are shown in Fig. 7. It is well seen that with higher temperature of the column both species are eluated earlier with the stable resolution. Similarly, it was found that pressure on column was lower.

In our study temperature of the column 25 °C was used, but in future we are going to use higher temperature.

3.2.4. CRMs and Real Samples

The described method was used for determination of mercury species in biological materials – in certified reference materials of fish tissues and hair and in real samples of human hair.

In reference materials two mercury species, inorganic and methylmercury are detected.

Recovery of our determination of Hg^{2+} and $MeHg^+$ in DORM 2 was good (to see in discussion in Validation part). The chromatogram of analyses of DORM 2 is reported in Fig. 8. In DOLT 2 (certified values: total Hg: 2.14±0.28 mg kg^{-1}; $MeHg^+$: 0.693±0.053 mg kg^{-1}) we obtained about 110% of certified value for $MeHg^+$ and 95% of declared value for Hg^{2+}.

However, in IAEA 085 (certified value: total Hg: 23.2±0.8 mg kg^{-1}; $MeHg^+$: 22.9±0.053 mg kg^{-1}) we noticed some problems with recovery which was only

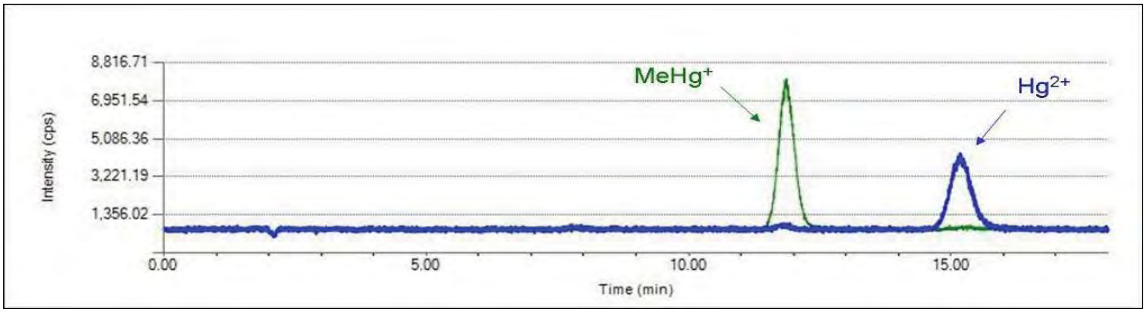

Fig. 5. Chromatogram of standard solution of $MeHg^+$ and Hg^{2+} (20 μg L^{-1}), retention times of monitored species.

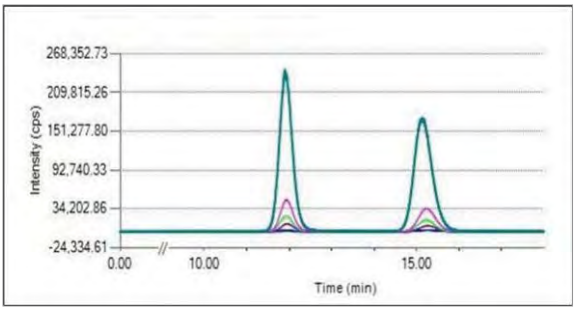

Fig. 6. Chromatogram of calibration range 5–500 μg L^{-1}.

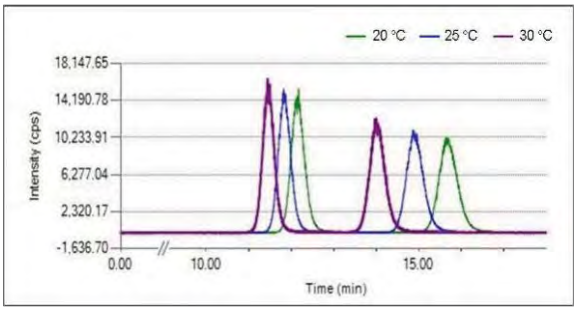

Fig. 7. Effect of column temperature on retention times of species (standard solution, 50 μg L^{-1}).

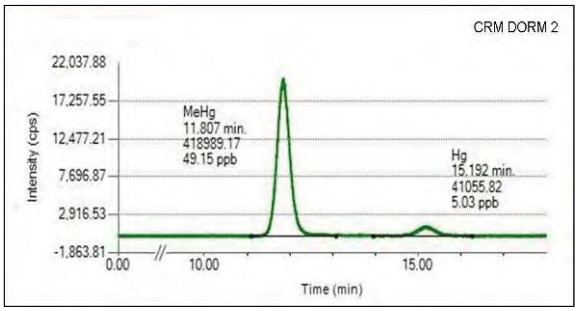

Fig. 8. CRM DORM 2; 0.1 g in 7.5 mL of supernatant.

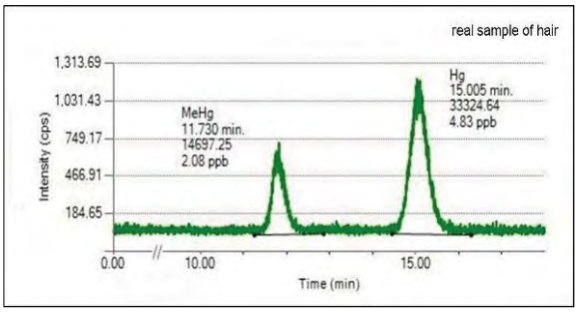

Fig. 9. Real sample of hair; 0.1 g in 7.5 mL of supernatant.

60% for $MeHg^+$, on the other hand obtained value of inorganic mercury was very high. As the concentration level of Hg^{2+} is very low we can ascribe it to the external contamination. In future, we have to look into this problem in detail.

The recovery of total mercury in reference material of human hair GBW 07 601 (certified value: total mercury: 0.36±0.05 mg kg^{-1}) was about 90%.

The method of HPLC-ICP-MS was used as an alternative to AMA-254 method for analyses of human hair. We expected that peaks of Hg species will be not registered because of low concentration of both species in human hair. Our hypothesis was not confirmed (Fig. 9).

Recovery obtained for this technique was worse and more variable than for AMA-254. This fact could be explained by variability of real samples or by problem of contamination. These problems ought to be studied in the future.

4. Conclusions

In the first part of this study results obtained by simple validated method using AMA-254 were presented. From these results we can conclude that this method is very simple and accurate. This method was used for the determination of mercury and its species in different population groups. We found that concentration values for non-exposed population are in agreement with non-exposed population in countries with similar dietary habits. The number of amalgam fillings was significant for Hg_{in}; the significant influence of fish consumption on the Hg_{in} and especially on the $MeHg^+$ levels was found although the consumption of fish in Czech Republic is rather low. The levels of mercury, obtained in the group of dentists, represent both endogenous and exogenous exposure. The higher inorganic mercury level in their hair can be ascribed to the work with amalgams and contaminated area of the surgery.

In the second part, a mild extraction method followed by HPLC-ICP-MS for determination of mercury species in fish tissues and human hair has been studied and validated. Parameters and results obtained in pilot study confirmed its suitability for our purpose. On the other hand problems with recovery, blank values and contamination (Hg^{2+}) were noticed. The lower value of recovery could be ascribed to various factors and have to be solved in the future.

We can conclude that using of "AMA-254" method is better for speciation of mercury in human hair than described extraction method connected with HPLC-ICP--MS. Disadvantages of HPLC-ICP-MS method are *e. g.* lower recovery and time-consuming process of whole procedure. Improving of method recovery, modification of HPLC condition and measurements of other real samples have to be done.

Acknowledgements. *The work was supported by the IGA grant NR 8955-3/2006 and by the EU through its Sixth Framework Programme for RTD, PHIME (contracts no FOOD-CT-2006-016253).*

References

[1] Čejchanová M., Spěváčková V., Kratzer K., Wranová K., Spěváček V. and Beneš B.: *Biol. Trace. Elem. Res*. **121** (2008), 97–105.

[2] Wang Meng *et al.: Talanta* **71** (2007), 2034–2039.

[3] Knobeloch L., Gliori G., Anderson HA.: *Environ. Res.* **103** (2007), 205–210.

[4] International Programme on Chemical Safety. Mercury environmental aspects. *Environmental Health Criteria* **86**. Geneva: WHO (1989).

[5] International Programme on Chemical Safety. Methylmercury. *Environmental Health Criteria* **101**. Geneva: WHO (1990).

[6] Horvat M., Gibičar D.: Speciation of mercury, Environment, food, clinical, and occupational health. In: *Handbook of Elemental Speciation II.* Cornelis R. (Ed.). Chichester, Wiley 2005, p. 281–304.

[7] Tuček M.: *České pracovní lékařství* **1** (2006), 26–37.

[8] Bencko V., Cikrt M., Lener J.: *Toxické kovy v životním a pracovním prostředí člověka*. Praha, GradaPublishing 1995, str. 235–254.

[9] Knobeloch L., Anderson H.A., Imm P., Peters D., Smith A.: *Environ. Res.* **97** (2005), 220–227.

[10] Valentino L., Torregrossa M.V., Saliba L.J.: *Water. Sci. Technol.* **32** (1995), 41–47.

[11] Elinder C. G., Friberg L., Nordberg G. F., Kjellstrom T., Oberdoerster G.: *Biological Monitoring of Metals*. Chemical safety monographs. WHO/EHG/94.2. Geneva, WHO 1994.

[12] Wranová K., Čejchanová M., Spěváčková V., Korunová V., Vobecký M. and Spěváček V.: *Centr. Eur. J. Public. Health.* **17** (2009), 36–40.

[13] Hight S. C., Cheng J.: *Anal. Chim. Acta* **567** (2006), 160–172.

[14] Vallant B., Kadnar R and Goessler W.: *J. Anal. At. Spectrom*. **22** (2007), 322–325.

[15] Ruprich J.: *Consumer's Foodstuff Basket for the Czech Republic*. Prague, National Institute of Public Health 2000.

[16] Kratzer K., Beneš P., Spěváčková V., Kolihová D., Žilková J.: *J. Anal. At. Spectrom.* **9** (1994), 303–306.

[17] Castillo A., Roig-Navarro A. F. and Pozo O. J.: *Anal. Chim. Acta* **577** (2006), 18–25.

[18] Shade Ch. W. and Hudson R. J. M.: *Environ. Sci. technol.* **39** (2005), 4974–4982

[19] Nelms S. M.: *Inductively Coupled Plasma Mass Spectrometry Handbook.* Blackwell Publishing 2005.

[20] Szpunar J. and Łobiński: *Hyphentaed Techniques in Speciation Analysis*. The Royal Society of Chemisty 2003.

[21] Spěváčková V., Korunová V., Čejchanová M., Vobecký M.: *Anal. Bioanal. Chem.* **380** (2004), 346–350.

[22] Chatt A., Katz S. A.: *Hair Analysis, Application in the Biomedical and Environmental Sciences.* VCH Publisher, 1988.

[23] Meloun M. and Militký J.: *Compendium of Statistic Data Processing*. Praha, Academia 2002.

Determination of Rosiglitazone and Metformin in Plasma by Capillary Electrophoresis with Mass Spectrometry

Joanna Znaleziona, Vítězslav Maier, Václav Ranc, Juraj Ševčík

Department of Analytical Chemistry, Palacký University in Olomouc, Tř. 17 Listopadu 12, 771 46 Olomouc, Czech Republic, ✉ jznaleziona@gmail.com

Keywords
capillary electrophoresis
mass spectrometry
metformin
methylbenzylamine
rosiglitazone

Abstract
This work presents capillary electrophoresis coupled with mass spectrometry for determination of antidiabetic drugs metformin and rosiglitazone. The aim of the work was optimization of analytical separation procedure and its utilization for the determination of antidiabetic drugs, mentioned above, in plasma samples. Special care was taken about parameters, such as positioning of the CE capillary and the detection mode. The developed electrophoretical method allowed the drugs separation within 10 minutes with quantification limit (*LOQ*) 10.21 ng mL^{-1} for rosiglitazone and 5.66 ng mL^{-1} for metformin.

1. Introduction

The International Diabetes Federation estimates that more than 250 million people around the world suffer from a diabetes (where 90–95% of that population are II type diabets) [1] and this number is still getting higher. Thus, diabetes can be regarded as a pandemic and all pharmaceutical investigations, biomedical studies, therapeutic drug monitoring or pharmacokinetics studies concerning this disease are essential.

Rosiglitazone is in a class of medications called thiazolidinediones and could be used alone or in combination with other anti-diabetic drugs such as metformin to treat type II diabetes. It works by increasing body's sensitivity to insulin, while metformin decreases glucose production and its absorption in entrails [2]. Structures of both medications are shown on Fig. 1.

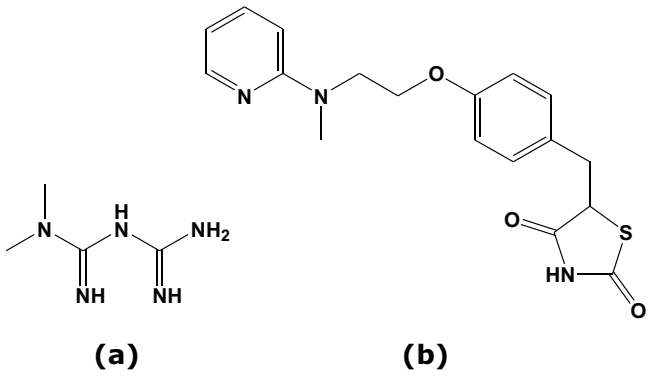

Fig. 1. Chemical structures of studied drugs (a) metformin, (b) rosiglitazone.

Several methods were developed for individual measurement of rosiglitazone and metformin in biological samples and pharmaceutical formulations. Analytical procedures include voltammetric determination, capillary electrophoresis (CE), micellar electrokinetic chromatography, high performance liquid chromatography method (differ with respect to the mode: ion-exchange, ion-pair or reverse phase) with fluorescence, UV or MS detection. The five reports concerning the determination of both drugs were published in years 2004–2007 [3–7]. Capillary electrophoresis was employed only for determination of studied drugs in pharmaceutical preparation [6], however could be an interesting alternative to HPLC method for monitoring drug level in plasma samples, especially when hyphenated with mass spectrometry.

2. Experimental

2.1. Apparatus

The CE measurements were carried out using the CE instrument HP ^{3D}CE, (Agilent Technologies) equipped with diode array detector and connected to an Agilent G6130 single quadrupole mass-selective detector. Uncoated fused-silica capillaries (MicroSolv Technology Corporation, USA) of 50 μm i. d. with 21.5 cm of the effective length was used. The capillary was rinsed 20 min with 0.1 M sodium hydroxide, 15 min with deionised water and then 5 min with running electrolyte at the beginning of each working day. The capillary was

rinsed between individual runs with background electrolyte for 5 min. Injection was performed by pressure of 50 mbar for 5 s. The applied voltage was +20 kV for all experiments. During the measurements the capillary was thermostated at 25 °C. All of the measurements were performed five times unless stated otherwise.

2.2. Chemicals

Acetic acid, formic acid, metformin and sodium hydroxide were obtained from Sigma. Methanol and methylebenzylamin (used as an internal standard) was purchased from Fluka. Rosiglitazone standard was obtained from Alexis Biochemicals. Water for LC-MS was purchased from Honeywell (Burdick and Jackson, USA) and it was used for the preparation of stock and working solutions, respectively as well as the background electrolyte for CE. All solvents and reagents were of analytical grade.

3. Results and discussion

3.1. Optimisation of Separation Conditions

To conduct the electrophoretic separation acetic and formic one were chosen. Their concentration was changing from 2.5–100 mM, when the current and efficiency of the separation with particular attention to the rosiglitazone peak intensity (due to its low doses applied in therapy) was monitored. The best results were obtained for 50 mM formic acid as a background electrolyte.

The influence of the composition of sheath liquid, its flow rate, drying gas temperature and potential on spraying capillary on effective ionisation of rosiglitazone and metformin were studied. The composition of sheath liquid plays the key role due to its influence on sample ionization, spray stability and the MS signal intensity. The percentage of protonization agent such as formic or acetic acid was optimised as well as the content of methanol. The best results were obtained when the 50% : 50% v/v mixture of methanol water was used with addition of 0.5% (v/v) formic acid. Other important parameter like temperature of drying gas was optimised in the range of 100–250 °C, and the 160 °C was determined as optimal. The voltage applied on the spraying capillary was scanned within 3.5–4.75 kV range. The best results were measured when +4.25 kV was applied on the capillary.

The MS detector was working either in scanning mode (TIC) to obtain MS spectrum or in the selected ion monitoring mode (SIM) to monitor $[M+H]^+$ with $m/z = 358$ for rosiglitazone and $m/z = 130$ for metformin. The final separation conditions are summarized in Table 1 (*see next page*) and Fig 2. show the model mixture separation of rosiglitazone and metformin with methylbenzylamine as internal standard.

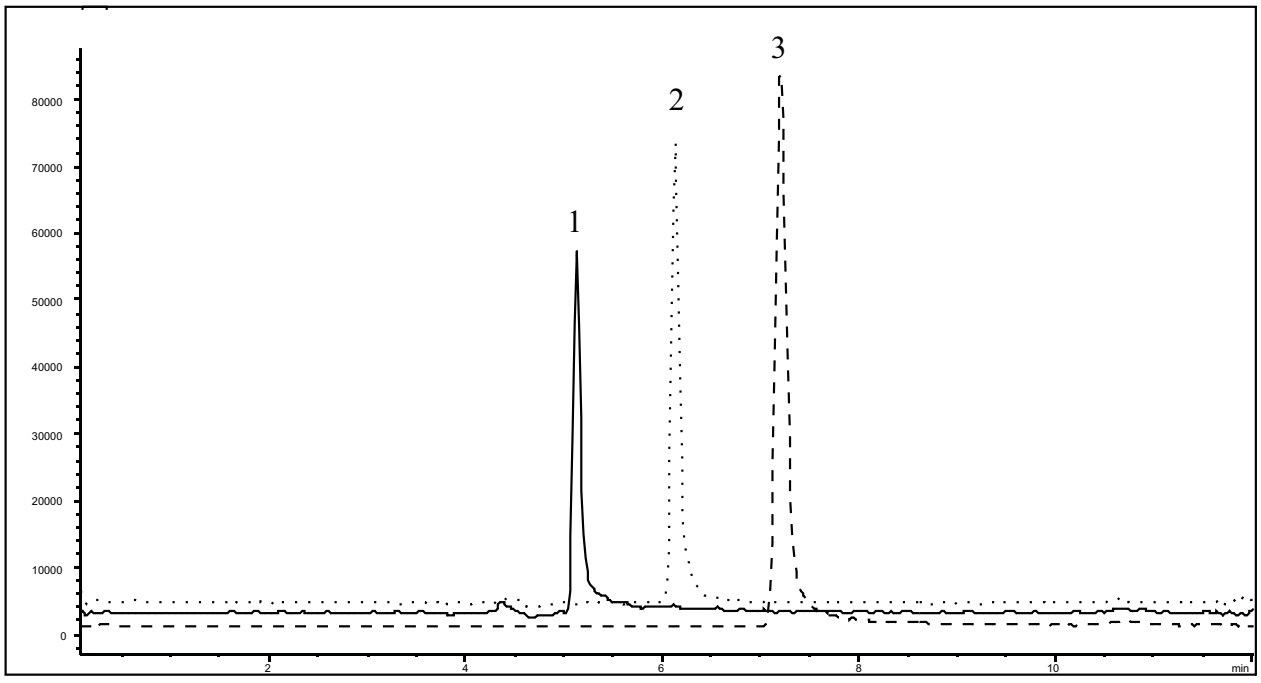

Fig. 2. Model mixture separation at final conditions (1) metformin, (2) methylbenzylamine (internal standard), (3) rosiglitazone (rosiglitazone concentration at level of 500 ng mL^{-1}).

Table 1. Optimal separation conditions for CZE-ESI-MS.

Sheath liquid composition	MeOH:H_2O = 50:50 + 0.5% (v/v) formic acid
Sheath liquid flow rate	4 μL min^{-1}
Drying gas flow rate	10 L min^{-1}
Drying gas temperature	160 °C
Nebulizer gas pressure	10 psi
Potential on spraying capillary	4250 V
ESI mode	Positive
background electrolyte	50 mM HCOOH

3.2. Statistical Parameters

The calibration curves were prepared in the range 10–1000 ng mL^{-1} for rosiglitazone and 2–400 ng mL^{-1} for metformin and were linear in the whole range. Characteristic of calibration curves is shown in Table 2.

Comparing limit of detection (LOD) with those found in patients plasma samples after single oral administration of 4 mg rosiglitazone tablet there is no need to introducing additional analytical step such as preconcentration or special sample treatment to the protocol. The mean C_{max} of rosiglitazone as reported Kim *et al.* [8] was 340 ng mL^{-1}.

Repeatability of the CE-MS method was performed by five replicate analyses of the samples containing rosiglitazone at 20 ng mL^{-1} and the results obtained are: 3.4% for the peak area and 2.5% for the peak height. Relative standard deviations for migration time obtained in the runs were within 0.62% to 2.15% for metformin and from 0.78% to 2.85% for rosiglitazone.

4. Conclusions

The proposed method CE-ESI-MS allowed the separation and determination of antidiabetic drugs rosiglitazone and metformin. It seems that it could be a good alternative for HPLC procedure due to small sample volume, short run time, good reproducibility and sensitivity. The method will be applied on the real patients' plasma samples after optimization of the sample preparation step.

Table 2. Calibration parameters of metformin and rosiglitazone.

	Rosiglitazone	Metformin
Conc. range, ng mL^{-1}	10–1000 (7 points)	2–400 (8 points)
R^2	0.996	0.998
Linear equation	$y = 0.001\,x - 0.022$	$y = 0.001\,x + 0.003$
LOD[a]	3.37	1.87
LOQ[a]	10.21	5.66

[a] Based on the standard deviation of the response and the slope [9].

Acknowledgements. *The financial support by the Research Project MSM6198959216 of the Ministry of Education of the Czech Republic and Research Project of the Grant Agency of the Czech Republic GACR No. 203/07/P233 is gratefully acknowledged.*

References

[1] International Diabetes Federation*: Diabetes. Atlas. Third edition.* 2007. IDF website: http://www.idf.org (20.08.2009).
[2] Chou C.C., Lee M.R., Cheng F.C, Yang D.Y.: *J. Chromatogr. A* **1097** (2005), 74–83.
[3] Yardımcı C., Ozaltın N.: *Chromatographia* **66** (2007), 589–593.
[4] Zhang L., Tian Y., Zhang Z., Chen Y.: *J. Chromatogr. B* **854** (2007), 91–98.
[5] Yardımcı C., Ozaltın N., Gurlek A.: *Talanta* **72** (2007), 1416–1422.
[6] Yardımcı C., Ozaltın N.: *Anal. Chim. Acta* **549** (2005), 88–95.
[7] Kolte B.L., Raut B.B., Deo A.A., Bagool M.A., Shinde D.B.: *J. Chromatogr. Sci.* **42** (2004), 70–73.
[8] Kim K.B, Lee D.J., Yeo C.W., Shin J.G., Bae S.K.: *J. Chromatogr. B* **877** (2009), 1951–1956.
[9] ICH Harmonised Tripartite Guideline: *Validation of Analytical Methods: Definitions and. Terminology.* ICH Topic Q2A. page. 3. CPMP/ICH/281/95.

Keywords Index

Author Index

Proceedings of the 5th International Students Conference
Modern Analytical Chemistry

Edited by Karel Nesměrák.
Published by Charles University in Prague, Faculty of Science.
Prague 2009.
1st edition – vi, 135 pages – Number of copies: 80.

ISBN 978-80-86561-41-7